LEABHARLANN CHOLÁISTE NA TRÍONÓIDE, BAILE ÁTHA CLIATH | TRINITY COLLEGE LIBRARY DUBLIN
Ollscoil Átha Cliath | The University of Dublin

Terms and Conditions of Use of Digitised Theses from Trinity College Library Dublin

Copyright statement

All material supplied by Trinity College Library is protected by copyright (under the Copyright and Related Rights Act, 2000 as amended) and other relevant Intellectual Property Rights. By accessing and using a Digitised Thesis from Trinity College Library you acknowledge that all Intellectual Property Rights in any Works supplied are the sole and exclusive property of the copyright and/or other IPR holder. Specific copyright holders may not be explicitly identified. Use of materials from other sources within a thesis should not be construed as a claim over them.

A non-exclusive, non-transferable licence is hereby granted to those using or reproducing, in whole or in part, the material for valid purposes, providing the copyright owners are acknowledged using the normal conventions. Where specific permission to use material is required, this is identified and such permission must be sought from the copyright holder or agency cited.

Liability statement

By using a Digitised Thesis, I accept that Trinity College Dublin bears no legal responsibility for the accuracy, legality or comprehensiveness of materials contained within the thesis, and that Trinity College Dublin accepts no liability for indirect, consequential, or incidental, damages or losses arising from use of the thesis for whatever reason. Information located in a thesis may be subject to specific use constraints, details of which may not be explicitly described. It is the responsibility of potential and actual users to be aware of such constraints and to abide by them. By making use of material from a digitised thesis, you accept these copyright and disclaimer provisions. Where it is brought to the attention of Trinity College Library that there may be a breach of copyright or other restraint, it is the policy to withdraw or take down access to a thesis while the issue is being resolved.

Access Agreement

By using a Digitised Thesis from Trinity College Library you are bound by the following Terms & Conditions. Please read them carefully.

I have read and I understand the following statement: All material supplied via a Digitised Thesis from Trinity College Library is protected by copyright and other intellectual property rights, and duplication or sale of all or part of any of a thesis is not permitted, except that material may be duplicated by you for your research use or for educational purposes in electronic or print form providing the copyright owners are acknowledged using the normal conventions. You must obtain permission for any other use. Electronic or print copies may not be offered, whether for sale or otherwise to anyone. This copy has been supplied on the understanding that it is copyright material and that no quotation from the thesis may be published without proper acknowledgement.

Cenozoic flexural uplift in northwestern Ireland and sedimentation in the northeastern Irish Rockall Basin.

Thesis submitted to the University of Dublin (Trinity College) for the degree of Doctor of Philosophy.

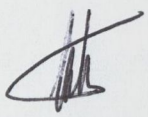
February 2002

Cristina Solla Hach

Declaration

This thesis is entirely my own work (except otherwise stated) and has not previously been submitted to this or any other university. All references are duly acknowledged.

The library of Trinity College Dublin may lend this thesis on request.



Cristina Solla Hach

To my family

Abstract

This study brings together for the first time in northwestern Ireland the onshore and offshore evolution of a passive margin during North Atlantic rifting and tries to contribute to a better understanding of the relationship between onshore and basin margin denudation, and basin deposition using a flexural model. Geomorphological observations in northwestern Ireland, including fluvial knickpoints, morphometric measures and analysis of digital geology and elevation data, are consistent with possible Cenozoic displacements on several mainly northeast-trending faults. Offshore, up to three km of Cenozoic sediments have been deposited west of Ireland in the northeastern Rockall Basin. Five regional Tertiary unconformities were mapped across the northeastern Irish Rockall Basin using offshore two-dimensional seismic reflection data. The data set includes 16 seismic surveys and offshore wells 132/15-1, 12/13-1a, 19/5-1, 13/3-1 and 27/13-1. Isochron maps of the sedimentary packages between these unconformities were depth converted and decompacted using the limited well data. During the Palaeocene a major depocentre developed north and south of the Hebrides Terrace with averaged accumulation rates of 93 m/My. This compares with denudation rates of only 9 m/My in northwestern Ireland. During the Eocene a northwest-directed sand progradation of unknown environment with accumulation rates of 38 m/My, together with high denudation rates in northwestern Ireland (16 m/My) estimated from apatite fission track modelling suggests a local Irish source for at least some of the sediment in the northeastern Irish Rockall Basin. Seismic reflectors of ?Oligocene age generally onlap onto an erosive unconformity, but sedimentary depocentres adjacent to and downslope of the basin margin locally show progradation of unknown environment, again suggesting some sediment input from the Irish continental margin. In the ?Oligocene accumulation rates of 22 m/My in the Irish Rockall Basin compare with denudation rates of only 8 m/My in northwestern Ireland. Estimated ?Miocene accumulation rates of 14 m/My are the lowest encountered during the Cenozoic. In the Plio-Pleistocene an increase on the accumulation rates of 51 m/My is related to a deltaic progradation with a sedimentary source located mainly in Scotland. Palaeocene to early Eocene extension caused offsets of the base Tertiary reflection of up to 800 ms and was related to a rift phase pre-dating oceanic spreading in the North Atlantic. Late Eocene to early Oligocene transpression with local folding was coeval with oceanic ridge push. The effects of Cenzoic offshore depositional loading and onshore erosional unloading on the continental margin were modelled assuming an elastic lithosphere of various rigidities overlying a viscous fluid. Cenozoic flexure gave rise to to rock uplift in the Irish Shelf and onshore northwestern Ireland of 700 m using a T_e of 30 km and up to 1000 m using a T_e of 3 km.

Acknowledgements

This thesis was sponsored by TotalFinaElf, Aberdeen, UK. I would like to thank Anne Schwab, Philip Newman, Chris Stephenson and the exploration department in TotalFinaElf, Aberdeen for helping me during my three months stay. Thanks to Geotrack for providing offshore Apatite Fission Track data and to TGS-Nopec, Western-Geco and Veritas DGC Limited for letting me include seismic data in this work.

Special thanks to Dr. Alexander Densmore, for supervising with patience and energy this thesis and for correcting my numerous mistakes. Without him this thesis would not exist. Thanks Alex and Melissa for dinners, cakes and Friday meetings with croassaints and geological discussions.

I would also like to thank Dr. Adrian Philips for suggesting ideas during this project. Thanks to Prof. Philip Allen for allowing me to use onshore Apatite Fission Track data. Thanks to Dr. Kerry Gallagher for providing Apatite Fission Track modelling software. Thanks to Dr. Peter Coxon for doing the palynology dating. Thanks to Dr. Peter Burgess for introducing me to a new dimension on flexural modelling. A thousand thanks to Dr. Michael Cunningham and Stuart Bennett for providing motivation and help during this project. Thanks to all staff and postgrads in the Department of Geology, Trinity College, particularly Jamie Quin, Gerry McCaughan, Declan Burke, Sarah Taylor, Louise and Peter Hildebrand, Zoe Shipton, David Chew, Neil Kearney, David Jordan, Jacqui Connolly, Niamh Connolly, Becky Gould, Phonsie Hevey, John Malone, John Murray, Ric Pascalli and Rory Dumphy, for providing both technical support and entertainment. Thanks to all my family for psychological support.

List of contents

Chapter 1 Introduction 1

1.1 Aim of this thesis 1
1.2 Rationale 1
1.3 Methods 2
1.4 Why northwestern Ireland? 2
1.5 Regional setting of the study area 4
1.6 Structure of the thesis 5

Chapter 2 A review of the geology of the northwestern Irish continental margin 7

2.1 Introduction 7
2.2 The crust 7
2.3 Archean and Proterozoic 8
2.4 The Palaeozoic 9
2.5 The Mesozoic 10
2.6 The Cenozoic 11
2.7 Summary of known Variscan and Caledonide faults 13
2.8 Summary 15

Chapter 3 Tectonic geomorphology of northwestern Ireland 17

3.1 Introduction 17
3.1.1 Was northwestern Ireland tectonically active in the Cenozoic? 17
3.1.2 Why is northwestern Ireland high? 18
3.1.3 Structure of this chapter 20
3.2 Previous work 21
3.3 Data and methods 22
3.4 Morphometric analysis 24
3.5 Lithology and topography 29
3.6 River longitudinal profiles 31
3.6.1 Data and methods 34
3.7 Relations within individual mountain ranges 34
3.7.1 Northeastern Donegal 35
3.7.2. Northwestern Donegal 36
3.7.3 Southern Donegal 38
3.7.4. Croaghgorm or Blue Stack Mountains 39
3.7.5. Sligo Mountains 42
3.7.6. The Ox Mountains 44
3.7.7 Nephin Beg Mountains 47
3.7.8. Southern County Mayo 52
3.8 Summary of suggested Cenozoic active faults 53

3.9 Fluvio-glacial terraces on the Owenmore River, Bangor, County Mayo 55
3.9.1 Introduction 55
3.9.2 Strath terraces 56
3.9.3 Sand and gravel deposits 57
3.9.4 Palynological analyses 58
3.9.5 Palynological results 58
3.10 Conclusions 59

Chapter 4 The Cenozoic of the northeastern Irish Rockall Basin 61

4.1 Introduction 61
4.2 Previous work and geological history of each basin 63
4.2.1 The Rockall Basin 63
4.2.2 The Slyne Basin 66
4.2.3 The Erris Basin 67
4.2.4 The Donegal Basin 67
4.3 Data and methods 68
4.4 Cenozoic stratigraphy 70
4.4.1 Introduction 70
4.4.2 Seismic interpretation 71
4.4.3 The Cenozoic section 73
4.4.4 Base Palaeocene and Palaeocene section 74
4.4.4.1 Characteristics of the unconformity and geology 74
4.4.4.2 Seismic facies 75
4.4.4.3 Isochron map description 75
4.4.4.4 Seismic characteristics in different parts of the study area 76
4.4.4.5 Interpretation 76
4.4.4.6 Summary 77
4.4.5 Base Eocene unconformity and Eocene section 77
4.4.5.1 Characteristics of the unconformity and geology 77
4.4.5.2 Seismic facies 78
4.4.5.3 Isochron map description 78
4.4.5.4 Seismic characteristics in different parts of the study area 78
4.4.5.5 Interpretation 80
4.4.5.6 Summary 80
4.4.6 Post-late Eocene unconformity and ?Oligocene section 81
4.4.6.1 Characteristics of the unconformity and geology 81
4.4.6.2 Seismic facies 82
4.4.6.3 Isochron map description 82
4.4.6.4 Seismic characteristics in different parts of the study area 82
4.4.6.5 Interpretation 83
4.4.6.6 Summary 84
4.4.7 ?Lower Miocene unconformity and ?Miocene section 84
4.4.7.1 Characteristics of the unconformity and geology 84
4.4.7.2 Isochron map description 85
4.4.7.3 Seismic facies 85

4.4.7.4 Interpretation *85*
4.4.7.5 Summary *86*
4.4.8 ?Lower Pliocene and Plio-Pleistocene section 86
4.4.8.1 Characteristics of the unconformity and geology *86*
4.4.8.2 Isochron map description *87*
4.4.8.3 Seismic facies *87*
4.4.8.4 Interpretation *88*
4.4.8.5 Summary *88*
4.4.9 Depth conversion 88
4.4.9.1 Introduction *88*
4.4.9.2 Cenozoic *90*
4.4.9.3 Palaeocene *90*
4.4.9.4 Eocene *91*
4.4.9.5 Late Eocene to seabed *92*
4.4.9.6 Isopach maps *92*
4.4.10. Decompaction 93
4.4.10.1 Decompaction of well 132/15-1 ..... *94*
4.4.10.2 Decompaction of the northeastern Irish Rockall Basin *97*
4.4.11 Accumulation rates and summary 97
4.5 Structure of the Rockall Basin 99
4.5.1 Introduction 99
4.5.2 Structural history of the Rockall Basin 100
4.5.3 Pre-Tertiary structural elements of the study area 101
4.5.4 Cenozoic tectonics in the northeast Rockall Basin 102
4.5.4.1 Introduction *102*
4.5.4.2 Palaeocene to early Eocene *103*
4.5.4.3 Middle to late Eocene to present *105*
4.5.4.4 Summary of tectonic structures *108*
4.6 Conclusions 108

Chapter 5 Denudation, deposition and flexure on the northwestern Irish margin during the Cenozoic 111

5.1 Introduction 111
5.2 Apatite fission track analysis 113
5.2.1 Introduction 113
5.2.2 Previous Cenozoic apatite fission track studies in Ireland 115
5.2.3 Database and methods 116
5.2.4 Modelling of well samples 118
5.2.4.1 Well 19/5-1 ..... *119*
5.2.4.2 Well 12/13-1a *121*
5.2.4.3 Well 132/15-1 ..... *122*
5.2.4.4 Well 27/13-1 ..... *123*
5.2.5 Summary 124
5.3 Denudation estimated from apatite fission track modelling 124
5.3.1 Methods 125

5.3.2 Contouring method 126
5.3.2.1 Cenozoic denudation *127*
5.3.2.1 Palaeocene denudation *127*
5.3.2.2 Eocene denudation *128*
5.3.2.3 Oligocene denudation *129*
5.3.2.4 Miocene to present denudation *129*
5.3.4 Uncertainties of denudation maps 129
5.4 Denudation versus deposition 130
5.4.1 Cenozoic denudation and deposition 130
5.4.2 Palaeocene denudation and deposition 131
5.4.3 Eocene denudation and deposition 132
5.4.4 Oligocene denudation and deposition 132
5.4.5 Miocene to present denudation and deposition 133
5.5 Flexure 134
5.5.1 Introduction 134
5.5.2 Methods 136
5.5.3 Flexural response in the northwestern Irish margin 138
5.5.3.1 Model results: flexural subsidence *138*
5.5.3.2 Model results: flexural uplift *141*
5.5.3.3 Model results: uplift and subsidence rates *142*
5.6 Conclusions 142

Chapter 6 Conclusions and discussion 144

6.1 Conclusions 144
6.2 Discussion 147
6.3 Future work 151

Appendixes 152

Appendix 1 Procedure for preparation of sediment samples for pollen analysis 152
Appendix 2 Matlab program on decompaction of well 132/15-1 155
Appendix 3 Matlab program on decompaction of the Cenozoic of the Rockall Basin 156
Appendix 4 Matlab program on flexure of the Rockall Basin 158

References 159

List of Figures

1.1 Study area
1.2 Regional setting

2.1 Geology of northern Ireland and Irish Rockall Basin
2.2 Quaternary deposits and ice movement

3.1 Tertiary stresses
3.2 Elevation of northwestern Ireland
3.3 General geology overlaid on topographic hillshade on northwestern Ireland
3.4 Slope map
3.5 Relief map
3.6 Relationships between elevation, relief and slope
3.7 Denudation estimates derived form relief
3.8 Dendation estimate derived from apatite fission track analysis
3.9 Geology of northwestern Ireland
3.10 Location of main mountain ranges in northwestern Ireland
3.11 Generation of river knickpoints
3.12 Topography, river knickpoints and faults in northeastern Donegal
3.13 Geological cross sections across the Leannan fault
3.14 Geology of northeastern Donegal and river knickpoints
3.15 River profiles across the Leannan fault
3.16 Topography, river knickpoints and faults in northwestern Donegal
3.17 Geology of northwestern Donegal and river knickpoints
3.18 River profiles in northwestern Donegal
3.19 Southwestern Donegal river knickpoints and faults
3.20 Geology of southwestern Donegal and river knickpoints
3.21 Elevation distribution within the same formation north of the study area
3.22 River profiles in southwestern Donegal
3.23 Topography, river knickpoints and faults in the Blue Stack Mountains
3.24 Geology of the Blue Stack Mountains
3.25 River profiles in the Blue Stack Mountains
3.26 Topography, river knickpoints and faults in the Sligo Mountains
3.27 Geology of the Sligo Mountains
3.28 River profiles in the Sligo Mountains
3.29 Topography, river knickpoints and faults in the Ox Mountains
3.30 Slope map of the Ox Mountains
3.31 Elevation distributions within the Ox Mountains Granodiorite
3.32 Geology of the Ox Mountains
3.33 River profiles in the Ox Mountains
3.34 Main mountain peaks in the Nephin Beg Mountains
3.35 Topography, river knickpoints and faults in the Nephin Beg Mountains
3.36 Geology of the Nephin Beg Mountains
3.37 Elevation distributions within the Nephin Beg Mountains

3.38 Relations between rock resistance and elevation in the Nephin Beg Mountains
3.39 River profiles in the Nephin Beg Mountains
3.40 Slope map of the Nephin Beg Mountains
3.41 Topography, river knickpoints and faults of southern Mayo
3.42 Geology of southern Mayo
3.43 Elevation distributions in southern Mayo
3.44 River profiles in southern Mayo
3.45 Cenozoic faults: evidence derived from river knickpoints and morphometric anlaysis
3.46 Owenmore River and fluvio-glacial terraces
3.47 Profile of the Owenmore River with plotted strath terraces.

4.1 Bathymetry of the Rockall Basin and adjacent areas
4.2 Location of regional seismic lines across the Rockall Basin
4.3 Wide angle seismic model for the RAPIDS from Shannon *et al.* (1995)
4.4 Section of WIRE 1 and 3 from Klemperer *et al.* (1991)
4.5 Structural framework from Naylor *et al.* (1999)
4.6 Stratigraphy from well logs northwest of Ireland
4.7 Location of 2D seismic reflection lines used in this work
4.8a Squematic cross section in the study area
4.8b Simplified geological cross section across the study area
4.9 Seismic lines showing the nature of the Cenozoic unconformities
4.10 Map of 2D seismic lines referred to the text
4.11 Cenozoic isochron
4.12 Palaeocene isochron
4.13 Eocene isochron
4.14 Seismic line with Eocene and Plio-Pleistocene progradations
4.15 Plan view of progradational events in the Cenozoic
4.16 ?Oligocene isochron
4.17 ?Miocene isochron
4.18 Plio-Pleistocene isochron
4.19 Depth conversion function for the Cenozoic
4.20 Depth conversion function for the Palaeocene
4.21 Depth conversion function for the Eocene
4.22 Depth conversion function for the post-Eocene
4.23 Isopach maps in the Cenozoic
4.24 Porosity-depth curve from well 132/15-1
4.25 Decompacted Cenozoic subsidence history for well 132/15-1
4.26 Tectonic subsidence for well 132/15-1
4.27 Decompacted isopach maps in the Cenozoic
4.28 Tertiary structural framework from Pharaoh (1996)
4.29 Palaeocene structural map in the northeastern Irish Rockall Basin
4.30 Eocene structural map in the northeastern Irish Rockall Basin
4.31 Compressional structure in Palaeocene and Eocene sediments
4.32 Palaocene normal fault and late Eocene anticline
4.33 Gigantic slump in Eocene sediments

4.34 Anticline deforming upper Eocene sediments
4.35 Anticline adjacent to basin boundary fault deforming the upper Eocene

5.1 Composite well log 19/15-1 and position of AFT samples
5.2 Individual fission track forward modelling run for sample GC651-12
5.3 Modelled thermal history for well 19/5-1
5.4 Composite well log 12/13-1a and position of AFT samples
5.5 Individual fission track forward modelling run for sample GC942-13
5.6 Modelled thermal history for well 12/13-1a
5.7 Composite well log 132/15-1 and position of AFT samples
5.8 Individual fission track forward modelling run for sample GC564-10
5.9 Modelled thermal history for well 132/15-1
5.10 Composite well log 27/13-1 and position of AFT samples
5.11 Individual fission track forward modelling run for sample GC375-2
5.12 Modelled thermal history for well 27/13-1
5.13 Total Cenozoic denudation derived from AFT modelling
5.14 Palaeocene denudation derived from AFT modelling
5.15 Eocene denudation derived from AFT modelling
5.16 Oligocene denudation derived from AFT modelling
5.17 Miocene to present denudation derived from AFT modelling
5.18 Mosaic of denudation and deposition in the Cenozoic
5.19 Mosaic of denudation and deposition in the Palaeocene
5.20 Mosaic of denudation and deposition in the Eocene
5.21 Mosaic of denudation and deposition in the Oligocene
5.22 Mosaic of denudation and deposition in the Miocene to present
5.23 Schematic diagram for flexural model
5.24 Flexural response in the Cenozoic along three profiles
5.25 Flexural response using T_e of 10 km and position of unconformities
5.26 Flexural response using T_e of 3 km and position of unconformities
5.27 Flexural response in the Palaeocene along three profiles
5.28 Flexural response in the Eocene along three profiles
5.29 Flexural response in the Oligocene along three profiles
5.30 Flexural response in the Miocene to present along three profiles

List of Plates

3.1 Owenmore River and gravel terrace
3.2 Gravel terrace in northern shore of Owenmore River
3.3 Gravel and sand terrace lying on bedrock
3.4 Stepped strath terrace
3.5 Strath terrace forming cascades
3.6 Two generations of gravel terraces
3.7 Two generations of gravel terraces
3.8 Internal sedimentary structure of sands and gravel terraces
3.9 Parallel and cross lamination in coarse sands
3.10 Erosive surface within gravels and sands
3.11 Clasts broken by frost shattering previous to deposition
3.12 Clasts broken by frost shattering posterior to deposition
3.13 Decalcified and weathered fossil
3.14 Decalcified crinoid within gravel deposit

List of Tables

3.1 Sample type and pollen content

4.1 Exploration wells in the study area
4.2 Other well data controlling the Cenozoic stratigraphy
4.3 2D seismic reflection surveys used in this study
4.4 Cenozoic regional seismic reflections in the Rockall Basin by previous authors
4.5 Well data for depth conversion
4.6 Cenozoic section in metres and seconds
4.7 Palaeocene section in metres and seconds
4.8 Eocene section in metres and seconds
4.9 Post-Eocene section in metres and seconds
4.10 Summary of velocity values and functions in the Cenozoic
4.11 Depth from sea bed to unconformities in well 132/15-1
4.12 Decompacted depth in metres in well 132/15-1
4.13 Backstripped porosity from well 132/15-1
4.14 Calculated bulk density
4.15 Backstripped tectonic subsidence
4.16 Spatially-averaged accumulation rates in the northeaster Irish Rockall Basin

5.1 Cenozoic thermal histories by other authors
5.2 AFT sample information from Allen *et al.* (in press)
5.3 AFT sample information from offshore wells
5.4 Reconstruction of initial thermal history using the stratigraphy of well 19/5-1
5.5 Summarized maximum palaeo-temperatures reached for each sample in well 19/5-1
5.6 Reconstruction of initial thermal history using the stratigraphy of well 12/13-1a
5.7 Summarized maximum palaeo-temperatures reached for each sample in well 12/13-1a
5.8 Reconstruction of initial thermal history using the stratigraphy of well 132/15-1
5.9 Summarized maximum palaeo-temperatures reached for each sample in well 132/15-1
5.10 Reconstruction of initial thermal history using the stratigraphy of well 27/13-1
5.11 Summarized maximum palaeo-temperatures reached for each sample in well 27/13-1
5.12 Cenozoic denudation for each well
5.13 Spatilly-averaged denudation rates for the northwestern Irish margin
5.14 Volumes of sediment deposited in the northeastern Irish Rockall Basin
5.15 Comparison between denudation and depostion rates
5.16 Maximum subsidence rates due to sediment loading
5.17 Maximum uplift rates due to sediment unloading

Chapter 1 Introduction

1.1 Aim of this thesis

The aim of this project is to investigate the tectonic, erosional and depositional history of the northwestern Irish continental margin during the Cenozoic, and evaluate the flexural response to onshore denudation and offshore deposition. This work uses techniques such as tectonic geomorphology, seismic reflection interpretation, apatite fission track analysis and flexural modelling.

1.2 Rationale

Oil exploration data allow investigation and a better understanding of the evolution of the North Atlantic passive margin. However, how passive margins evolve during and after rifting is today a subject in debate. The sedimentary record preserved in basins allows a relatively good understanding of the geological history in basinal areas. In basin margins and topographically high areas, preservation of sediments is usually poor and geological methods, in addition to outcrop mapping are needed to understand the tectonic and denudational evolution of passive margins. Alternative methods such as tectonic geomorphology and apatite fission track analysis are required to better understand the evolution of these margins.

The Cenozoic landscape in a passive margin such as northwestern Ireland, was under the effect of processes such as: tectonic activity due to continental rifting, oceanic ridge push, isostatic rebound, variable climate conditions, differential erosion in fractures and lithologies, etc. All of them together contribute to the formation of the landscape.

Denudation of passive margins is very important in geomorphological studies because flexural isostasy in response to denudational unloading can give rise to significant topographic effects along older margins (Gilchrist and Summerfield 1990). Denudational

histories of a number of other passive margins have been quantified using apatite fission track analysis (e.g., Cockburn *et al.* 2000; Gleadow and Brown 2000). Denudation maps for onshore Ireland using apatite fission track modelling have been published recently by different authors (Green *et al.* 2000; Allen *et al.* in press).

Geomorphic studies when combined with thermochronology data, analysis of basin sediments, and flexural modelling, can be a valuable tool in tectonic investigations. The combination of evidence from different geological disciplines allows a more reliable interpretation of the Cenozoic history of the northwestern Irish margin.

1.3 Methods

Onshore northwestern Ireland was investigated in this thesis using fluvial geomorphology and topographical analysis (Fig. 1.1). Geomorphic anomalies such as river knickpoints and high relief suggest recent tectonic activity has occurred. This method has been used in other passive margins to prove tectonic activity and has been applied locally in western Ireland (Dewey 2000) but has not been applied extensively in northwestern Ireland.

The northwestern Irish offshore basins have been investigated using seismic reflection data interpretation in order to compile isopach maps for the Cenozoic (Fig. 1.1). Basin margin denudation is quantified using apatite fission track analysis. This study brings together for the first time in northwestern Ireland the onshore and offshore evolution of a passive margin during North Atlantic rifting and tries to contribute to a better understanding of the relationship between onshore and basin margin denudation, and basin deposition using a flexural model.

1.4 Why northwestern Ireland?

Northwestern Ireland is underlain by Precambrian and Devonian to Carboniferous bedrock, and no Mesozoic or Cenozoic rocks are preserved in the sedimentary record. Seismic reflection and well data in the Rockall Basin reveal an almost complete Cenozoic

sedimentary succession approximately 3 km thick. The Rockall Basin to the west and the Ulster Basin to the east both contain Mesozoic and Tertiary sediments that were deformed by tectonic activity during the Palaeogene (Fig. 1.1). Thus, Cenozoic tectonic activity in northwestern Ireland, which lies between two areas that were tectonically active in the Cenozoic, is highly likely but has not been previously described in detail.

Northwestern Ireland is interesting firstly because of its relatively high topography compared to both the lowlands of central Ireland and the gently west-dipping slope of the Irish Mainland Shelf. This raises the first set of questions: how did the present topography form and why is it located there?

The Rockall Basin lies under a bathymetric trough bordered by a steep scarp, partially formed by Cenozoic normal faulting. This raises the second question: is the topography of onshore northwestern Ireland also fault controlled?

The abundance of Cenozoic sediments in the Rockall Basin and the lack of Cenozoic sediments in northwestern Ireland raises a third question: where did those sediments come from?

And lastly, what flexural effects have been imposed on the lithosphere by the onshore denudation and offshore deposition and can one explain the present day topography by lithospheric flexure?

1.5 Regional setting of the study area

The northeastern Atlantic continental passive margin extends for approximately 3000 km from offshore Norway in the north, to the Rockall and Porcupine Basins in the south (Fig. 1.2). It is bounded to the west by Cenozoic oceanic crust and to the southwest by Cretaceous oceanic crust. The North American and North European plates separated during the Cenozoic along the Reykjanes Ridge and continue to spread to the present day.

The northwestern European continental margin consists of Precambrian to Lower Palaeozoic basement and a series of Devonian to Cenozoic extensional basins (Doré *et al.* 1999). Devonian and Carboniferous basins are today preserved on onshore Ireland. Permo-Triassic rift basins lie offshore northern Scotland and northeastern Ireland. Jurassic and Cretaceous rift basins, such as the north-trending Porcupine Basin, lie to the west of Ireland. Cretaceous to Cenozoic rifting episodes gave rise to further extension in a series of basins further to the west, where approximately 4 km of Cretaceous to Cenozoic successions are preserved (e.g., Rockall Basin). During the Cretaceous to Cenozoic the northeastern Atlantic was affected by a number of large scale, regional events, which included:

- Late Mesozoic to Early Tertiary extension and Cenozoic post-rift thermal subsidence (Doré *et al.* 1999),
- Early Tertiary North Atlantic magmatism (Ritchie *et al.* 1999) and associated uplift and denudation (White and Lovell 1997),
- early Eocene onset of the oceanic spreading centre in the North Atlantic and associated ridge push (Doré and Lundin 1996),
- late Eocene onset of deep water ocean circulation in the north Atlantic following a phase of basin subsidence (Stoker 1998),
- late Eocene to early Oligocene Pyrenean compression (Roberts 1989) and,
- early Miocene Alpine compression (Müller *et al.* 1992).

Ireland has very little onshore Tertiary outcrop, with the exception of the Palaeogene volcanic rocks and Oligocene sediments of the Ulster Basin in northeastern Ireland. Most of the surviving Cenozoic successions lie below sea level and their study is only possible through interpretation of well and seismic reflection data from the offshore basins.

1.6 Structure of the thesis

A geological history of the region is presented in **Chapter 2** with a discussion of previous work and outstanding problems.

In **Chapter 3**, geomorphological observations are used to deduce information about possible tectonic activity in northwestern Ireland. Lithology and topography are quantitatively compared in order to determine whether the landscape is the product of simple differential erosion, or whether other factors like tectonism might have contributed to the present day topography. Analyses of longitudinal river profiles and terraces are used to constrain the location of recent faulting. The word 'recent' is used in this study to mean any time in the Cenozoic.

Chapter 4 presents interpretations of two-dimensional seismic reflection lines that image the Cenozoic section in the northeastern Irish Rockall Basin. Five different Tertiary sedimentary packages are distinguished across the basin. These packages are depth converted and decompacted using all present available well data, yielding spatial estimates of the magnitude of Cenozoic deposition across the Rockall Basin. A short Cenozoic depositional and structural history is also described.

In **Chapter 5**, thermal histories and associated Cenozoic denudation chronologies of four offshore wells are estimated using apatite fission track modelling. Basin margin denudation is then compared with sedimentary deposition in the Rockall Basin throughout the Cenozoic to calculate sedimentary mass balance. The effects of denudational unloading on the Irish Shelf and mainland, coupled with depositional loading of sediments in the Rockall Basin offshore, are used to generate estimates of the

total Cenozoic loads applied to the continental margin. This load induces a flexural response, which is calculated using a one-dimensional flexural model. The flexural uplift may partially explain the present day topography in northwestern Ireland.

Chapter 6 summarizes and discusses the conclusions of this thesis.

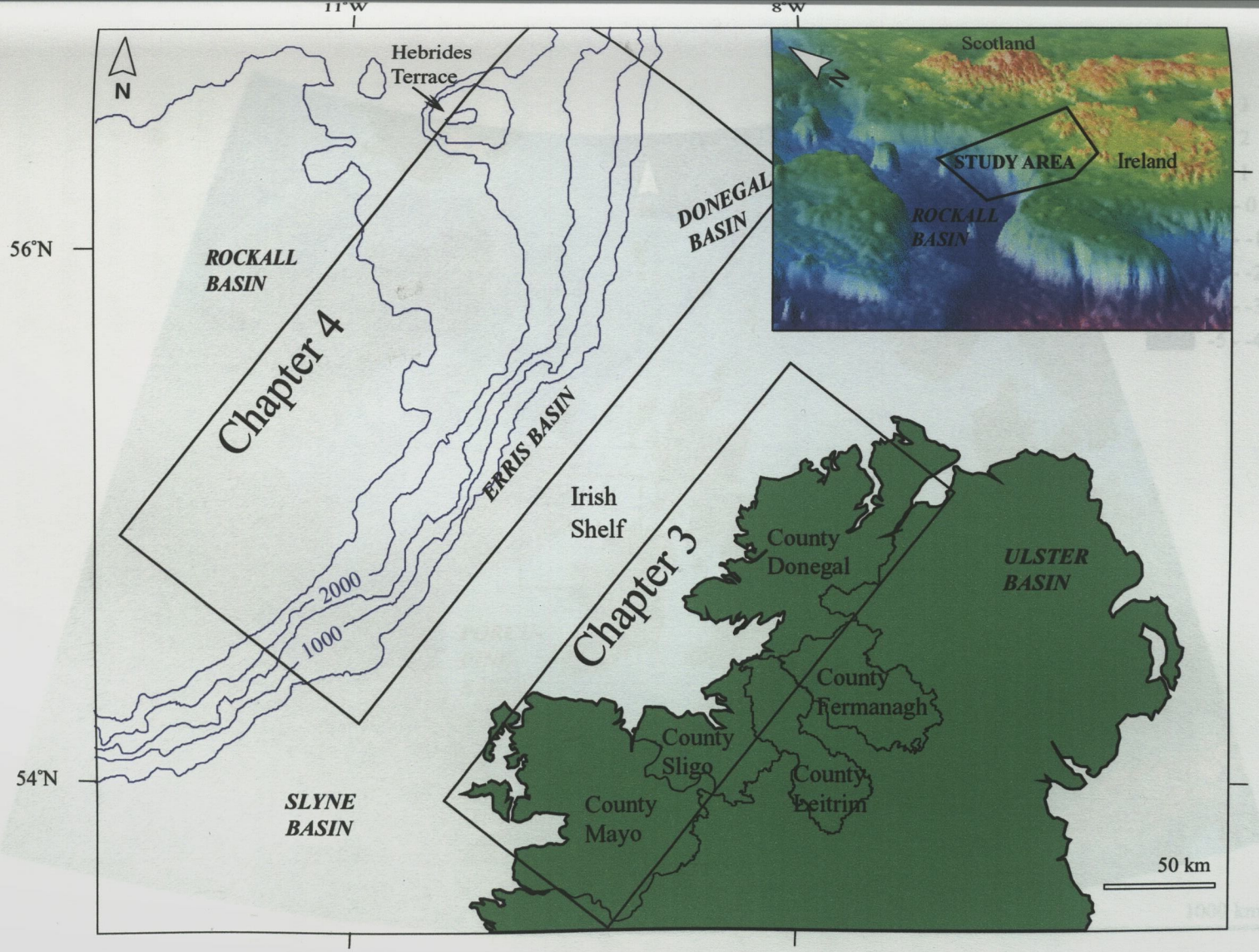


Figure 1.1. Study area: northwestern Ireland with counties marked and offshore basins. Geomorphic tectonics of northwestern Ireland are presented in Chapter 3. Cenozoic seismic interpretation is presented in Chapter 4.

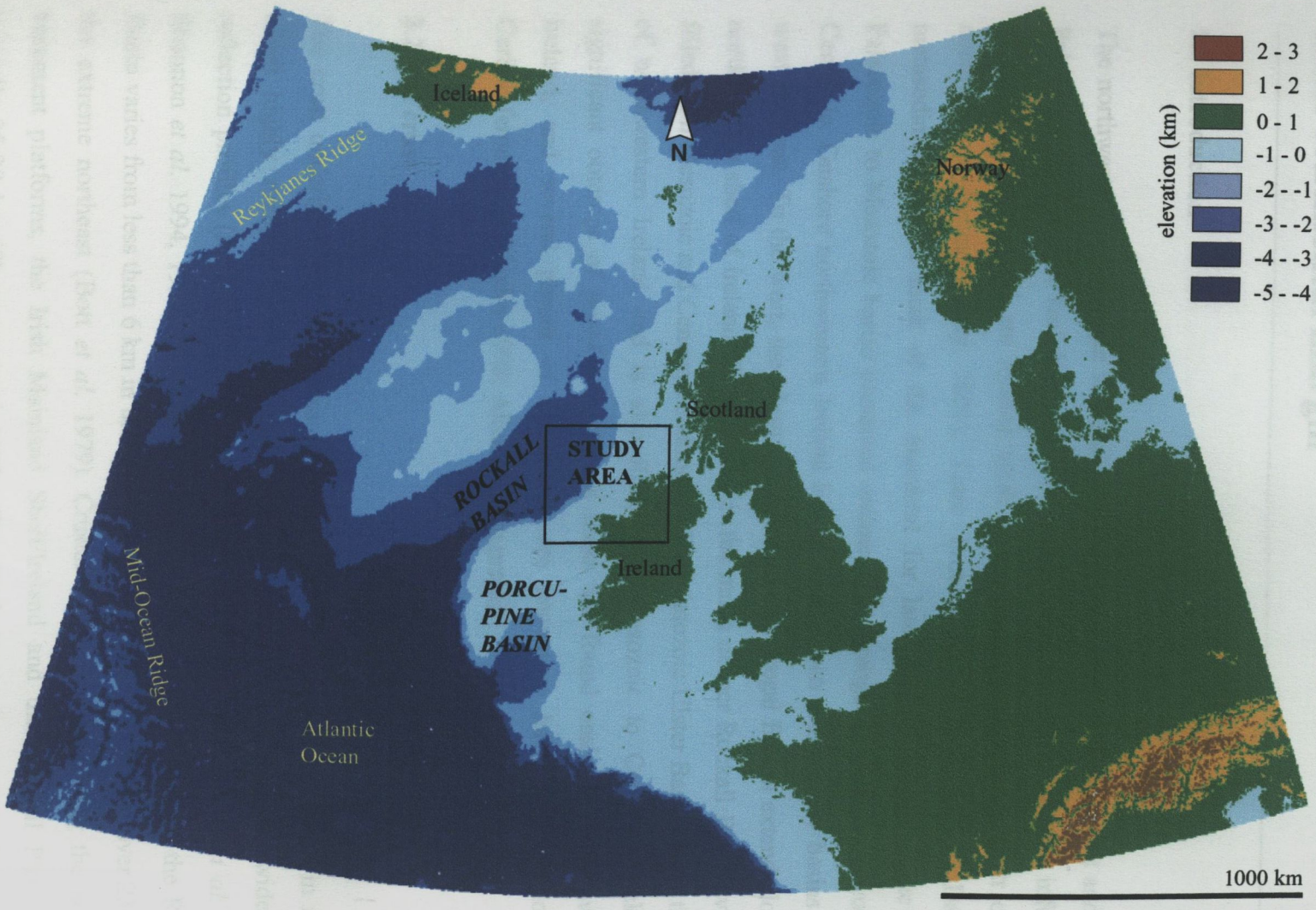


Figure 1.2. Bathymetry and topography of the northeastern Atlantic Ocean and the northwestern european continental passive margin. Study area is shown in a rectangle.

Chapter 2 A review of the geology of the northwestern Irish continental margin

2.1 Introduction

The northwestern Irish margin is underlain by Archean to Silurian basement and Upper Palaeozoic to Mesozoic fault-bounded basins (Fig. 2.1). The oldest rocks are inferred to be Archean in age, and are located north of the trace of Great Glen fault offshore northwestern Ireland (Daly 2001). Later Proterozoic rocks, such as Dalradian metasediments, form most of the basement for later basin formation. The Upper Palaeozoic to Mesozoic basins preserved sediments that range in age from Devonian to Cenozoic. Onshore northwestern Ireland lies today between sedimentary basins to the west and east. To the west, the Mesozoic Slyne-Erris-Donegal Basins extend along the northwestern shelf of Ireland. Further west is the much deeper Rockall Basin, which is filled with Mesozoic and Cenozoic sediments. The Mesozoic Ulster Basin lies to the east of northwestern Ireland and is also filled with Mesozoic to Cenozoic rocks. No significant outcrops of post-Carboniferous rocks are found onshore in northwestern Ireland, and several phases of denudation are known to have occurred in post-Carboniferous time (Naylor 1998; Allen *et al.* in press).

2.2 The crust

The crust underlying the study area is generally accepted to be continental in nature, albeit highly stretched in places, by analysis of seismic refraction and wide-angle reflection profiles (Roberts *et al.* 1988; Joppen and White 1990; Makris *et al.* 1991; Shannon *et al.* 1994, 1995; O'Reilly 1995). The crustal thickness beneath the Rockall Basin varies from less than 6 km in the southwest (O'Reilly *et al.* 1995) to over 23 km in the extreme northeast (Bott *et al.* 1979). Crustal thicknesses underlying the adjacent basement platforms, the Irish Mainland Shelf/Ireland and the Rockall Plateau, are typically 25-30 km (Shannon *et al.* 1995). The similarity in crustal velocity structure

suggests that there is no major compositional difference between the stretched lower crust under the Rockall Basin and the lower crust beneath onshore Ireland (O'Reilly *et al.* 1995). The seismic structure of the continental crust on both sides of the Rockall Basin is three-layered (upper, middle and lower crust), but it is two-layered (upper and lower crust) in the Rockall Basin (Shannon *et al.* 1995).

2.3 Archean and Proterozoic

Crystalline basement to the northwest of the northwestern Irish continental margin comprises two major terranes: the Hebridean Terrane of Archean age and the Colonsay-Islay-Inistrahull Terrane of Early Proterozoic age (Pharaoh *et al.* 1996; Daly 2001). The two terranes are separated by the northeast-trending Great Glen fault (Fig. 2.1).

Onshore northwestern Ireland, Proterozoic rocks are found in the Annagh Gneiss Complex in northwestern County Mayo, the Ox Mountains Complex in counties Mayo and Sligo and the Inishtrahull Gneiss Complex off northeastern County Donegal (Fig. 2.1). The Annagh Gneiss Complex was affected by the Grenvillian Orogeny 1000 My ago (Daly 1995). The presence of Proterozoic Grenvillian granulites on the Rockall Plateau near 56° N (Miller *et al.* 1973) indicates a common shared geological history between the Rockall Bank and Irish Mainland Shelf at least from Grenvillian time (Daly *et al.* 1995).

Dalradian metasediments were deposited in the Neoproterozoic during break-up of the super continent of Rodinia which led to the formation of the Iapetus Ocean. Dalradian rocks are preserved in the north and south of County Donegal, the Ox Mountains and northwestern County Mayo (Fig. 2.1). Precambrian basic igneous intrusives within Dalradian metasediments are also common.

2.4 The Palaeozoic

In the Cambrian the Iapetus Ocean continued to open forming oceanic crust between the Gondwanan and Laurentian continents. Dalradian rocks were then deformed in the Grampian Orogeny during the Early Ordovician time (Phillips 2001). In the Early Ordovician, the closure and subduction of the Iapetus Ocean generated an extensive arc-marginal basin complex. Volcanic rocks within Ordovician sediments are preserved in southern County Mayo (Fig. 2.1).

During the Silurian, deposition continued in the Iapetus Ocean. Sediments deposited on the northwestern shelf of the Iapetus Ocean are currently exposed south of Clew Bay and on Clare Island in County Mayo (Fig. 2.1). During final closure in Late Silurian times, three continental blocks assembled from opposite sides of the Iapetus Ocean: Laurentia, which included northwestern Ireland and Avalonia, including southeast Ireland, and Baltica (Fortrey and Cocks 1988). The position of the suture after closing is located south of northwestern Ireland (Phillips 2001). Large granitic intrusions such as the Donegal Batholith intruded in County Donegal and the Ox Mountains Granodiorite (Fig. 2.1) were emplaced during Caledonian deformation in Early Devonian time (Stillman 2001).

Mountain building during the Caledonian Orogeny reached its maximum in the Devonian and resulted in rapid erosion, and deposition of red sandstone preserved in small Lower and Middle Devonian fault-controlled sedimentary basins in County Mayo, between Castlebar and Lough Conn, in the Curlew Mountains of County Leitrim and at Ballimastocker in northern County Donegal (Fig. 2.1). Both the Grampian and Caledonian Orogenies in northwestern Ireland produced major folds and shear zones that follow a general northeast to east trend. The Termon Granite in western County Mayo intruded during the Devonian and the Donegal Granite was intruded along a major sinistral shear zone.

In the Carboniferous a northward marine transgression reached County Donegal (Sevastopulo and Wyse Jackson 2001). Marine deposits of Lower Carboniferous age are

preserved onshore in the shallow synclines of County Mayo, County Donegal, Omagh and Lough Foyle, northeastern Ireland, as well as offshore in the Erris and Donegal Basins (wells 19/5-1 and 13/3-1) (Fig. 2.1). The Variscan Orogeny culminated in the formation of the super continent of Pangea, and imprinted northwestern Irish rocks with gentle folds. Variscan faults are believed to have been controlled by pre-existing Caledonide structures.

No sedimentary rocks younger than Carboniferous age are preserved in onshore northwestern Ireland, except for the Quaternary deposits of glacial and fluvio-glacial origin. During the Permian, and after the formation of Pangea, initial rifting resulted in dyke intrusion and the initiation of basin formation west of Ireland. Upper Permian evaporites rest unconformably on the Carboniferous in the northeast-trending Erris Basin (well 19/5-1 and 12/13-1a) (Chapman *et al.* 1999) and Slyne Basin (well 27/5-1) (Dancer *et al.* 1999).

Well data indicate that Palaeozoic and older rocks form the basement to the Mesozoic basins offshore western Ireland (Croker and Shannon 1987; Robeson *et al.* 1988). Caledonian northeast to east-trending lineaments have long been inferred to control Late Palaeozoic and Mesozoic basin formation (Roberts and Holdsworth 1999).

2.5 The Mesozoic

Permo-Triassic rifting offshore northwestern Ireland produced a series of half grabens such as the Erris and Slyne Basins, controlled by down-to-the-southeast normal faults (Chapman *et al.* 1999). Triassic sediments in these two basins are mainly sandstones and mudstones of continental affinity, and are identified in several offshore wells. In northeastern onshore Ireland a series of basins developed, such as the Rathlin and Larne Basins (Wilson *et al.* 2001) (Fig. 2.1).

In the Jurassic marine flooding of the Permo-Triassic rift basins took place (Doré 1992). Jurassic sediments are well preserved in both the Slyne and Erris Basins. A phase of east-

west directed rifting occurred in the Middle Jurassic in the Slyne Basin synchronous with a change in sedimentation pattern in the Erris Basin (Chapman *et al.* 1999). In the Late Jurassic previously east-dipping faults were reactivated and rotated changing polarity to west dips (Chapman *et al.* 1999).

The base Cretaceous unconformity, observed in the Slyne Basin, is more pronounced in the Erris Basin. This unconformity suggests a period of widespread denudation along the eastern margin of the Rockall Basin. In the Early Cretaceous extension continued but the stretching direction changed to northwest-southeast in the Late Jurassic (Doré *et al.* 1999; Lundin and Doré 1997). Musgrove and Mitchener (1996) described a Lower Cretaceous syn-rift succession in well 132/15-1, in which Lower Cretaceous sediments overlie crystalline Precambrian basement. During the Late Lower Cretaceous (Aptian-Albian unconformity), reactivation of earlier faults in the Erris Basin documents a minor episode of rifting (Chapman *et al.* 1999).

Extension continued through the Late Cretaceous to the Early Tertiary with thermal subsidence in the Rockall Basin and rock uplift along the basin margin. The Iceland Plume, may have initiated during the Late Cretaceous (Hitchen *et al.* 1997).

2.6 The Cenozoic

The igneous activity associated with Early Tertiary continental break-up generated flood basalts in County Antrim, northeastern Ireland, dykes in northwestern Ireland (Preston 2001), and offshore intrusive complexes such as the Hebrides Terrace Seamount and volcanoclastics and sills (Ritchie and Hitchen 1996) that partially obscure the pre-Tertiary sedimentary sequence of the Rockall Basin. However, the Cenozoic sequence in the Rockall Basin is well imaged on seismic reflection data. Palaeocene extensional activity is well documented by major offsets of a base Tertiary reflector along the faults bounding the eastern margin of the Rockall Basin (Fig. 2.1). Extension of the same age has been also recognised in the Faeroe-Shetland Basin (Dean *et al.* 1999; Holmes *et al.* 1999).

Palaeocene surface uplift over a region of c.2000 km in diameter centred in Greenland (White 1989) resulted in uplift of Precambrian source areas in Scotland and northwestern Ireland (Corfield *et al.* 1999). The Slyne, Erris and Donegal Basins and northwestern Ireland became regions of footwall uplift and erosion (Naylor & Shannon 1982; Stoker *et al.* 1993) and an incipient passive margin developed (Corfield *et al.* 1999). The northwest of Ireland has no extensive mapped Tertiary deposits except for some local late Pliocene lignite and silicious sands in Poulnahallia, Co. Galway (Coxon and Flegg 1987).

In the early Eocene, continental break-up along the Reykjanes Ridge initiated production of North Atlantic oceanic crust and southeast-directed ridge push. In the Rockall Basin pre-existing normal faults were inverted as folds and thrusts after the early Eocene (Roberts 1989; Boldreel and Andersen 1993).

In the late Eocene to Oligocene, the Rockall Basin underwent major subsidence. This is recorded as a regional unconformity (Stoker *et al.* 2001). In the basin margin, studies addressing Cenozoic uplift, cooling and erosion have been carried out in Ireland (McCullogh 1993; Green *et al.* 2000; Allen *et al.* in press), the Slyne Basin (Scotchman & Thomas 1995) and Northern Ireland (Parnell 1991). The northwestern Irish basin margin certainly contributed sediments to the offshore basins to the west, such as Rockall and Porcupine Basins, although the magnitude and pathway of this sediment flux have not been fully established.

The northwestern Irish landscape was described by Charlesworth (1924, 1928) who noted that 'the U-shape valleys of the Donegal Hills, owe their origin to a Tertiary uplift and rejuvenation; glacial erosion has somewhat modified their form, having altered the gradients, widened, over-deepened and over-steepened the valleys'. Charlesworth (1924, 1928) Synge (1963, 1979), Colhoun (1968, 1971), Coxon and Browne (1991) and McCabe (1999) studied the Quaternary glacial deposits of northwestern Ireland. Several phases of glaciation covered the margin with ice, leaving behind glacial deposits, both onshore and offshore Ireland, and bare and rounded hills. Valleys are deeply overspread

with glacial deposits with drumlins and eskers indicating ice flow directions (Fig. 2.2). Two main centres of ice dispersion were located in southern County Mayo and western County Sligo, while there is a local centre in central Donegal. The main ice flow directions were to the west and northwest.

Moraines in western County Mayo mark the western limit of the last glaciation. During a more extensive and earlier glaciation only the higher mountains in County Mayo, remained unglaciated (Synge 1963, 1979). This implies that the maximum thickness of ice during the last glaciations in northwestern Ireland was ~800 m.

2.7 Summary of known Variscan and Caledonide faults

Many structural studies have been done on Carboniferous and older rocks in northwestern Ireland. However, the lack of post-Carboniferous sediments in northwestern Ireland makes the Mesozoic and Cenozoic tectonic history difficult to determine. For this reason one needs to extend to areas such as northeastern Ireland and offshore western Ireland where Cenozoic sediments are preserved and therefore tectonic activity can be easily documented.

The Tow Valley and Sixmilewater faults in the Ulster Basin and the main eastern boundary fault in the Rockall Basin are the best examples of large structures offsetting Tertiary rocks (Fig. 2.1). These faults have offsets of the order of hundreds of metres in Tertiary sediments and igneous rocks, and reactivate pre-existing structures (Kerr 1987). The fault on the western side of the Erris Basin was active at least since Permo-Triassic time (Cunningham and Shannon 1997). Further north, near well 132/15-1, west-dipping north-trending faults rotate Cretaceous blocks, and extensional activity continued into the Early Tertiary. The main north- to northeast-trending fault bounding the eastern side of the Rockall Basin is considered to be a reactivation of a much older structure (Cunningham and Shannon 1997). In the Slyne Basin reactivated structures cause shortening within the Cenozoic section (Dancer *et al.* 1999).

The northeast-trending Great Glen fault is mapped onshore Scotland and can be traced on seismic lines across to the west of Ireland (Fig. 2.1). The Great Glen fault is a major Caledonian structure that underwent several phases of strike-slip movements during the Palaeozoic (Stewart *et al.* 1999). It was reactivated as a strike-slip fault in the Mesozoic and may be presently active, as shown by historic earthquakes (Kennedy 1946; Flinn 1992). Apparent Moho offsets north of Counties Donegal and Mayo are probably due to the Great Glen fault and associated splays (Klemperer *et al.* 1991).

The northeast-trending Leannan fault is a composite structure extending across onshore Ireland from Killybegs to Malin Head in County Donegal. The Leannan fault juxtaposes Dalradian rocks with discordant strikes, and is interpreted as a major late-Caledonian strike-slip fault (Alsop *et al.* 1992). Geophysical data shows that the Leannan fault continues offshore to the northeast and joins the Great Glen fault (Dobson *et al.* 1975; Max and Baker 1978). Dip-slip movement on the Leannan fault, down to the southwest, is shown by the downthrow of Devonian deposits, which suggests several episodes of movement may have occurred (Pitcher and Berger 1972).

The Main Donegal granite is situated close to, and parallel with, a major tectonic slide, within the Dalradian in County Donegal. The crust into which the granite intruded underwent repeated shearing shown by the trace of the granite foliation (Hutton 1982; Alsop 1992). The Gweebarra fault displaces dextrally the Main Donegal Granite.

The northeast to southwest-trending late Caledonian Belshade fault shows a 3.5 km sinistral displacement of the Barnesmore Granite. The Belshade fault continues into Carboniferous basement, where the southeastern block is down-thrown by ~600 m. The Boundary fault crosses and displaces sinistrally the Belshade fault, and cuts the Lower Carboniferous (Fig. 2.1).

Near the western end of the Barnes Lough valley, several northwest trending Tertiary dolerite dykes change direction close to the Barneslough fault. This change in trend, combined with crushed granite and other crushed dolerite dykes (which are undated)

suggests at least some Tertiary movement on the Barneslough fault (Leedal and Walker 1954).

The Highland Boundary fault in Scotland continues into Ireland and can be traced to the west coast along the southern shore of Clew Bay (Max and Riddihough 1975). The Leck fault outcrops between Clare Island and Lough Conn in western County Mayo, running eastwards along Clew Bay with dominant strike-slip displacement during the Silurian and Devonian, and post-Carboniferous down-throw to the north (Phillip 2001). Further east the fault curves into a northeast trend in the southwestern Ox Mountains, where it consists of a series of low angle and vertical fractures displacing Middle Devonian rocks. Some strike-slip movements may be older than Devonian, but probably the most important lateral movements occurred between the Devonian and the Carboniferous.

Several northwest-trending faults are mapped in southern County Mayo, with dextral displacements of Silurian, Ordovician and Dalradian rocks (Graham 1985). The northeast-trending Erriff fault in south County Mayo (Fig. 2.1) has been suggested to have some Cenozoic displacements based on its present day topographical relief of 500 m (Badley 2001) and vertical displacements of present day streams crossing the fault (Dewey 2000).

2.8 Summary

Northwestern Ireland is part of a passive margin that underwent extension during the Mesozoic and Early Cenozoic. The northwestern Irish passive margin is located between the highly extended Rockall Basin in the Atlantic Ocean to the northwest and the Ulster Basin in Northern Ireland to the east, both filled with Palaeogene volcanic rocks, Cenozoic and Mesozoic sediments (Fig. 2.1). Oligocene clays are limited to northeastern Ireland (Wilkinson *et al.* 1980), but no Mesozoic or Tertiary sediments are found in northwestern Ireland. The Caledonian and Variscan Orogenies deformed Palaeozoic and Precambrian rocks. In the next chapter a study of the present day topography and river

profiles will be presented to assess the potential evidence for Cenozoic tectonic reactivation in northwestern Ireland.

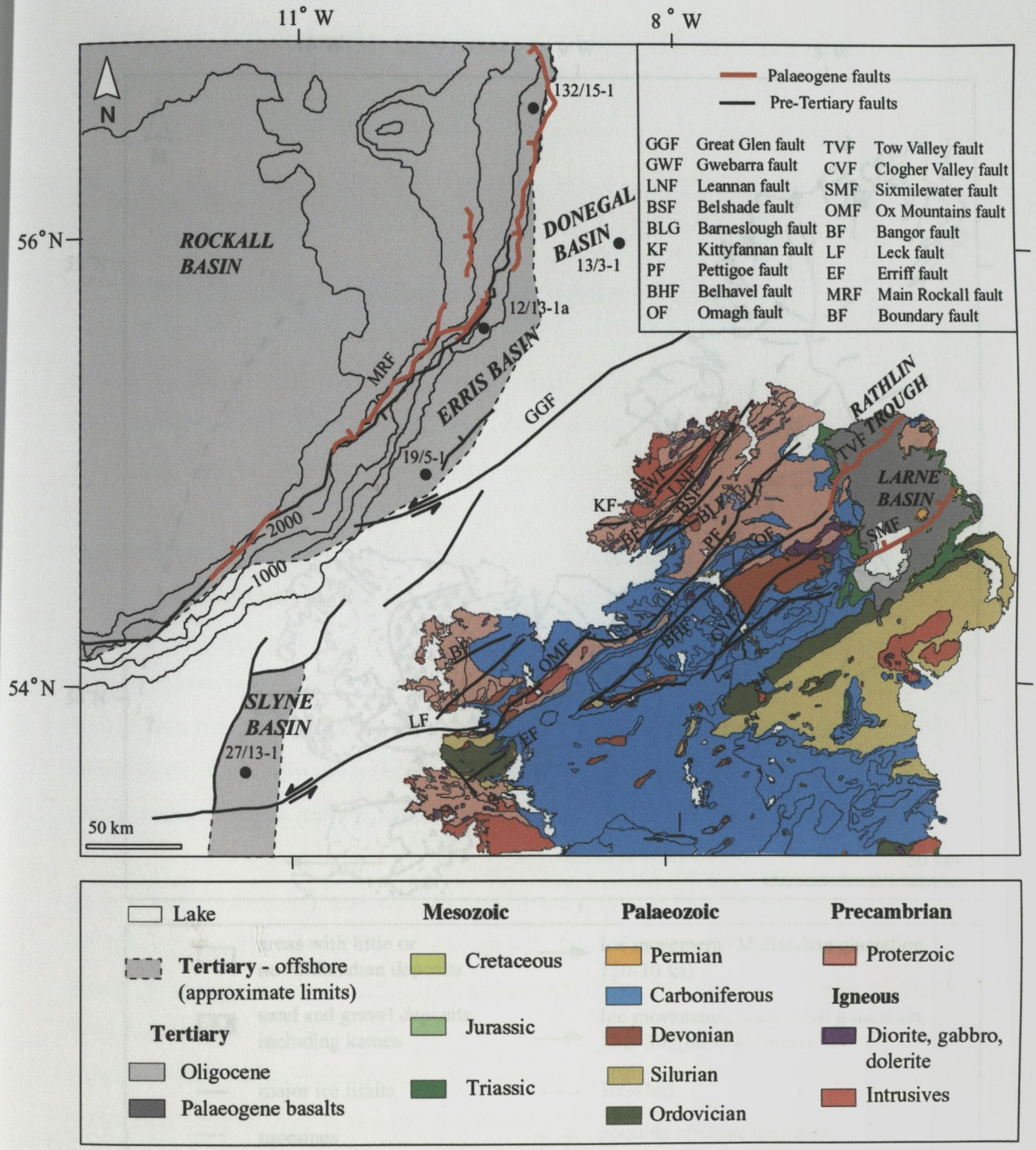


Figure 2.1. The northwestern Irish continental margin and northern Ireland. Onshore geology is simplified from Byrne & O'Dwyer (1994). Offshore wells are shown as black dots and offshore Cenozoic rocks are shown in grey. The limits are taken from interpretation of seismic reflection lines that are, with the wells, the only control for the offshore bedrock geology. Evidence for Tertiary and pre-Tertiary faults come from outcrop studies (Cooper *et al.* 1997). Offshore Tertiary faults come from this work (Chapter 4) and Chapman *et al.* (1999).

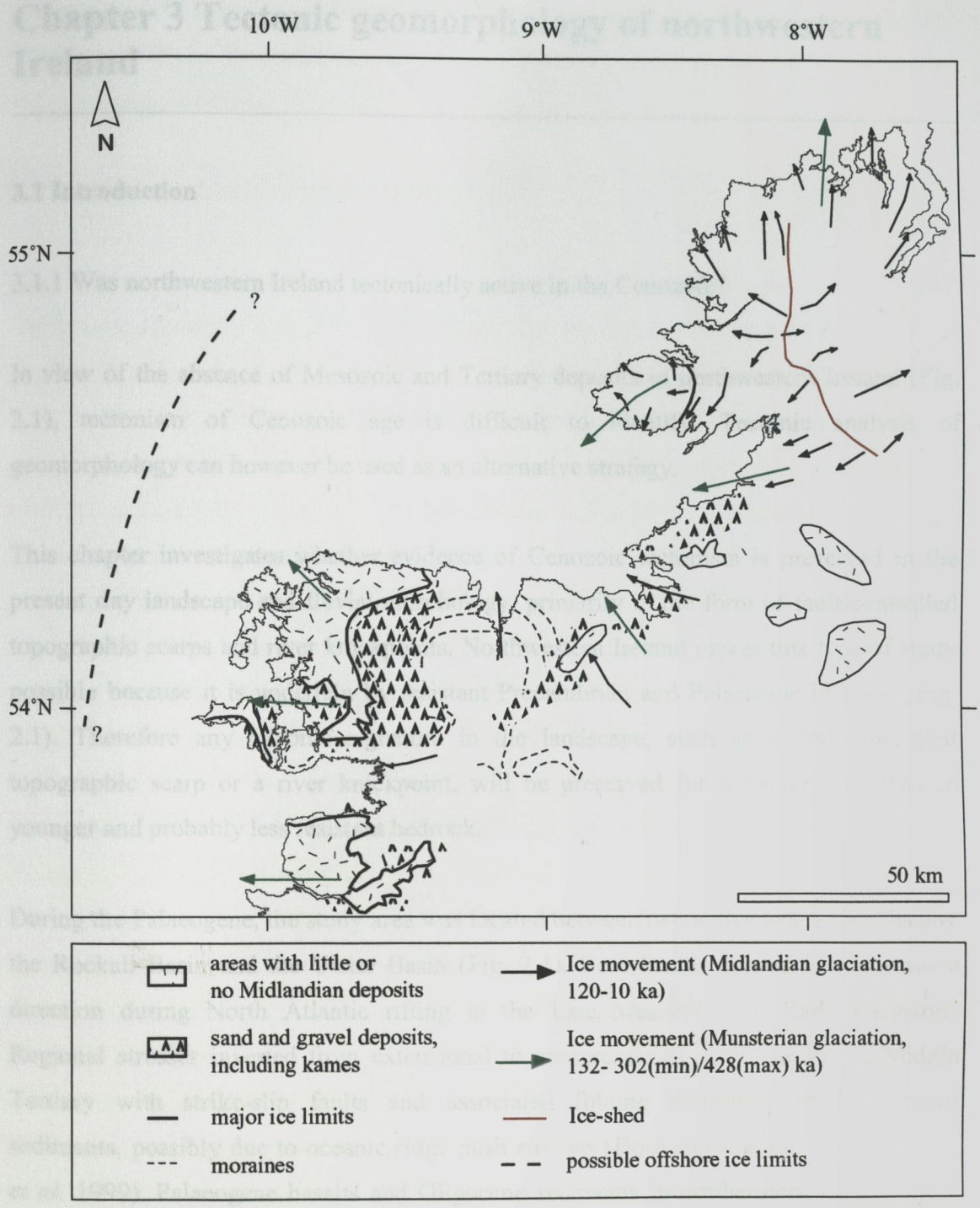


Figure 2.2. Quaternary glaciations. Modified from McCabe *et al.* 1999; Coxon & Browne 1991; Coxon 1993; McCabe 1999; Synge 1968; Charlesworth 1924.

Chapter 3 Tectonic geomorphology of northwestern Ireland

3.1 Introduction

3.1.1 Was northwestern Ireland tectonically active in the Cenozoic?

In view of the absence of Mesozoic and Tertiary deposits in northwestern Ireland (Fig. 2.1), tectonism of Cenozoic age is difficult to identify. Tectonic analysis of geomorphology can however be used as an alternative strategy.

This chapter investigates whether evidence of Cenozoic tectonism is preserved in the present day landscape and fluvial morphology, primarily in the form of fault-controlled topographic scarps and river knickpoints. Northwestern Ireland makes this type of study possible because it is underlain by resistant Precambrian and Palaeozoic bedrock (Fig. 2.1). Therefore any tectonic signature in the landscape, such as a fault-controlled topographic scarp or a river knickpoint, will be preserved for a longer time than in younger and probably less resistant bedrock.

During the Palaeogene, the study area was located between two active extensional basins, the Rockall Basin and the Ulster Basin (Fig. 2.1). Both basins opened in a northwest direction during North Atlantic rifting in the Late Mesozoic and Early Cenozoic. Regional stresses inverted from extensional to compressional sometime in the Middle Tertiary with strike-slip faults and associated folding deforming offshore basin sediments, possibly due to oceanic ridge push stresses (Doré and Lundin 1996; Corfield *et al.* 1999). Palaeogene basalts and Oligocene sediments in northeastern Ireland show considerable faulting (Kerr 1987). Northwestern Ireland, although lacking Tertiary sediments, does contain Palaeocene igneous intrusions (Emeleus and Preston 1969; Mohr 1987; Preston 2001) that are sometimes faulted (Leedal and Walker 1954; Bennett *pers. comm.* 2001; Bennett and Phillips *in press*). It is therefore likely that northwestern Ireland

was tectonically active during at least the Early Cenozoic, as this is the time of maximum tectonic activity in the Rockall Basin, and the effects of this activity might be recorded by the topography of onshore Ireland.

3.1.2 Why is northwestern Ireland high?

The northwestern Irish topography is relatively high compared with the rest of Ireland, with mountains up to 800 m high (Fig. 3.2). The topography of passive margins is not simply the reflection of tectonic processes since the rocks are subjected to some degree of modification by denudational processes. Topography is the result of the complex interaction between crustal processes, including tectonic, igneous and isostatic of flexural activity, and surficial processes, including erosion and sedimentation, which in turn are driven by climate and base level changes. These processes are usually poorly constrained and vary simultaneously making the topographic response difficult to explain (Lifton and Chase 1992). Chapter 3 investigates whether the northwestern Irish topography can be attributed to Cenozoic fault displacements or to other factors such as differential erosion between different lithologies.

The goal of tectonic geomorphology is to deduce information about tectonic processes based on landscape observations (e.g. Burbank and Anderson 2001). Relationships between topography, uplift and denudation were given by Ahnert (1970), for mid-latitude basins in different tectonic settings including passive margins. Relationships between geomorphology and tectonics on passive margins, such as South Africa and Australia, have also been studied (Summerfield 1991; Brown *et al.* 2000; Bishop and Goldrick 2000; Kerr *et al.* 2000; Pazzaglia *et al.* 2000). Pazzaglia *et al.* (1998) compared bedrock fluvial incision and longitudinal profile development in tectonically active and inactive areas.

Ahnert (1996) derived from a global compilation an approximate time scale for landform preservation, with mountain ranges being denuded to 1% of the total in approximately 37 My accounting for isostatic compensation. For denudation rates in valleys as low as 100

m/My (Small and Anderson 1998) so any trace of topography 6 km in amplitude and 10 km wave-length would be erased in 60 My.

The northwestern Irish bedrock is composed mainly of Dalradian quartzites, schists, psammites, and pelites and Carboniferous sandstones, mudstones and limestones (Fig 3.3). The resistance of the northwest Irish bedrock types is probably higher than the mean resistance of Mesozoic and Tertiary sediments (Clayton and Shamoon 1998), because of the higher grade of compaction and metamorphism. Therefore landscape preservation might be higher in northwestern Ireland. However, surface processes in Ireland during the last 250 My are likely to have removed any inherited Variscan and Caledonian landscape, because even low, constant upland denudation rates of 30 m/My would remove an 8 km high mountain range in 250 My. The fact that no Mesozoic and Tertiary sediments are preserved in northwestern Ireland and the fact that Precambrian bedrock is presently exposed at the surface makes low time-averaged denudation rates of 30 m/My even more unlikely.

One possible way of preserving old Variscan or Caledonian topographic remnants is by Late Palaeozoic or Mesozoic sedimentary burial of the landscape followed by exhumation. The preservation of a considerable thickness of Mesozoic and Cenozoic sediments in the offshore basins around Ireland and the lack of extensive Mesozoic and Tertiary sediments onshore Ireland (Fig. 2.1) suggest that most of the country underwent denudation in post-Variscan times (Naylor 1992). Thermochronology data from onshore Ireland also suggest denudation throughout the Mesozoic and Cenozoic (Allen *et al.* in press; Green *et al.* 2000) and with time-variable rates much higher than 30 m/My. Therefore it seems very unlikely that the present day landscape is simply the result of exhumation of a Variscan orogenic belt only. The fact that the present-day topography and drainage is controlled by northeast-trending and east-trending structures might be related to post-Variscan fault reactivation and displacement. This study looks for evidence of recent fault activity in northwestern Ireland.

Several rifting phases recorded in the Irish offshore basins during the Permo-Triassic, Jurassic and Cretaceous are likely to have a profound tectonic effect on the study area. The present day landscape might therefore be explained by reactivation of Variscan and Caledonian structures in post-Carboniferous times.

3.1.3 Structure of Chapter 3

Chapter 3 describes topographical and lithological relationships and longitudinal river profiles along the northwestern Irish passive margin.

First, previous work is summarised and a brief discussion on topography is given. Secondly, methods and data are described. A morphometric analysis introduces the main topographic features in northwestern Ireland and describes general relationships between elevation, slope and relief. Then a comparison between morphometric features and lithology raises the question whether the topography is influenced by tectonic activity.

Then, longitudinal river profiles in relation to bedrock geology and faults are described for separate areas, along with the finding that some of the northwestern Irish rivers are out of equilibrium. The cause of those knickpoints and why the same rock resistance occurs at different topographic levels is discussed, with Cenozoic tectonism suggested as a possible explanation.

The presence of several river knickpoints, topographic scarps or topographic asymmetries within a consistent lithology are used to infer Cenozoic fault activity on some faults previously thought to be inactive. A final structural map derived from this type of evidence is presented at the end of this chapter and compared with previous work on Cenozoic faults, strain orientations, and stress systems. The hypothesis of Cenozoic tectonic activity will be tested against the offshore sedimentary from the Rockall Basin in Chapter 4. Conclusions and a brief discussion of Chapter 3 are also included.

3.2 Previous work

Previous work on Cenozoic tectonics and geomorphology in northwestern Ireland is scarce. Some of the previous landscape studies in Ireland, have suggested relatively late tectonic activity (Farrington 1929; Davies 1970; Mitchell 1980, 1981). Evidence usually comes from topographic, lithological and drainage studies, and scattered Tertiary deposits. However, the subject still remains controversial because of the difficulty of proving Tertiary tectonism in a region of Precambrian to Carboniferous bedrock. Mesozoic basins around Ireland and in Northern Ireland are filled with Tertiary sediments and show clear evidence of Tertiary tectonism thus, onshore Tertiary tectonic activity is also likely.

Dewey (2000) used topography, river knickpoints and Tertiary dyke offsets in southern County Mayo and County Galway to infer Late Cenozoic tectonic activity. Dewey and McKerrow (1963) suggested mid-Tertiary uplift of the pre-Carboniferous land surface in southern Mayo; they believed that this surface uplift was responsible for the superposition of drainage from a deformed Carboniferous cover. Badley (2001) used forward modelling to explain the present-day 500 m- high scarp of the Erriff fault, south Mayo, and inferred a Late Tertiary fault movement. Mohr (1986, 2000) associated morphological offsets observable in the topography of western Ireland with recent tectonic movements. In southeastern Ireland, Cunningham (2001) analysed the relationships between geological structures and landscape morphology and found evidence of Cenozoic tectonic activity.

In Northern Ireland, Tertiary tectonic activity is somewhat easier to determine because fault offsets can be measured in Palaeogene rocks. George (1967) suggested from outcrop studies that a Neogene landform was established after mid-Tertiary tectonic activity ceased.

The Tertiary structural history onshore and offshore Ireland as deduced by several authors is summarised in Figure 3.1. Kerr's (1987) structural analysis in the Rathlin

Trough, Northern Ireland yielded reliable evidence of Palaeogene stratigraphic offsets. He concluded that Northern Ireland was affected by four discrete deformation episodes in the Cenozoic: (1) Palaeocene northeast-directed extension with normal faulting; (2) mid-Eocene to mid-Miocene north-northeast compression and east-southeast-directed extension shown by strike-slip reactivation of Palaeocene normal faults; (3) late Miocene east-northeast-directed extension; and (4) post-Miocene extension. Miller's (1990) structural analysis of Carboniferous basins in northwestern Ireland found similar stress orientations for the Tertiary, although proving the timing of these post-Carboniferous events was a difficult task. Geoffroy *et al.* (1996) found: (1) syn-magmatic northeast to north-northeast-directed extension in Northern Ireland during the Palaeocene; (2) a probably Eocene strike-slip to compressional northeast to north-northeast-directed stress regime associated with the partial reactivation of normal faults formed during the first phase; and (3) an Oligocene north-northeast-directed extension (Fig. 3.1). All of these authors assumed an Andersonian-type fault mechanics and stress-strain relationships, in which northwest-directed extension would produce simple northeast trending normal faults. Heterogeneities in a crust that has been affected by several orogenies, like in northwestern Ireland, can produce strains that are very different from those implied by Andersonian-type stress systems.

This chapter presents a study of the relationships between lithology and topography in northwestern Ireland. Longitudinal river profiles were also studied and the presence of river knickpoints is explained by lithological changes, glacial erosion or deformation of the river bed.

3.3 Data and methods

The geomorphology of northwestern Ireland has been studied in the past using field descriptions and topographic maps. Topography is easier to quantify when digital elevation models (DEMs) are used (e.g., Willgoose 1994; Mayer 2000). Simple geometric properties of the landscape such as asymmetric mountain ranges, linear topographic scarps, and windgaps can be easily identified on DEMs and quantification of

spatial variables such as elevation and relief can be made much more rapidly. The elevation distribution of an area can also be quantified for a uniform lithology to compare topography with rock resistance. If topography is strongly lithologically controlled, similar statistical elevation distributions should be found for regions underlain by the same formation. If the distributions are different, topography may be explained by other causes. Anomalies in the regional drainage pattern or in the morphology of individual catchments, such as river knickpoints found along faults, might suggest recent activity on these structures. In this way recent fault activity or the intensity of erosional processes can be explored from the topography (Ahnert 1970; Summerfield 1991b; Hurtrez *et al.* 1999). If a fault in a Precambrian or Palaeozoic basement was active during the last 65 My, the fault scarp might be preserved in the present day landscape. The preservation depends mainly on the magnitude of the fault offset and on bedrock resistance to erosion.

Digital elevation models for southern County Donegal and Counties Fermanagh, Sligo and Mayo were compiled from 10 m digital contour vector data, produced by the Ordnance Survey of Ireland. The compiled DEMs have a pixel size of 10 x 10 metres. The Arc/INFO and ArcView geographical information system (GIS) software packages were used to compile and manipulate the DEMs. For the rest of the study area, a grid of 200 x 200 m was used. This regional DEM for Ireland (200 x 200 m pixel size) from the Ordnance Survey of Ireland was resampled to 1 x 1 km resolution for regional analysis of northwestern Ireland. The resampled DEM was then used to construct elevation, slope, relief and denudation maps in order to compare these morphometric parameters across the northwest. Slope and relief maps were computed in each cell using their eight surrounding neighbours. A window size of 1 x 1 km guarantees analysis of major valley bottoms and interfluves but ignores any landform smaller than 1 km^2. This resolution was chosen for simplicity of computations and to allow easier comparison between mountain ranges in northwestern Ireland. Digital bedrock geology maps at a scale of 1:100,000 were provided by the Geological Survey of Ireland (GSI). The area covered by this digital data includes sheets 1, 3, 7, 6 and 10 in Counties Donegal (McConnell & Long 1997; Long *et al.* 1999) Sligo and Leitrim (Harney *et al.* 1996) and Mayo (Max *et al.* 1992; Graham *et al.* 1985).

3.4 Morphometric analysis

An *elevation* map shows altitude above sea level (Fig. 3.2). The elevation in the north of the study area in County Donegal (Derryveagh, Blue Stack and Slieve League Mountains) forms a more contiguous area of high topography than the south. However, the topography in County Donegal is highly incised by the Gweebarra and Barnesmore valleys. The southern part of the study area contains the highest peaks, but these are separated by wide plains or valleys such as Swinford, the Mayo lowlands and Glen Nephin (Fig. 3.2). The highest elevation in the area is Mweelrea at 811 m, followed by Nephin at 800 m in County Mayo.

A *hillshade* map enhances linear topographic features at particular orientations, depending on the azimuth of artificial illumination (Fig. 3.3). The structural grain in northwestern Ireland is mainly northeast-striking, and a hillshade from the northwest will best highlight northeast-oriented topographic features. The Derryveagh, Blue Stack, Ox and Partry Mountains show a strong northeast trend. Slieve League, Benbulbin and the Sheeffry Hills trend generally east while the Nephin Begs and Mweelrea show a combination of northeast and east trends. Both the Grampian and later Caledonian orogenies in northwestern Ireland produced major folds and shear zones that vary from northeast to east trend. Variscan structures are of lesser intensity, consisting mainly of brittle faults reactivating earlier structures. Fault movement during these orogenies was considerable but finished about 250 My ago. Reactivation of these faults in later, mainly extensional settings during the Mesozoic and Cenozoic times might be partly responsible for the present day topography.

Slope identifies the maximum rate of change of elevation between a cell and its neighbours in a DEM. The slope values in Figure 3.4 show the maximum slope, measured in degrees, within 1 x 1 km windows. Slope maps, when compared with digital geology allow quick comparison of high slope values with lithological and structural features. High slopes at geological contacts can be explained by differential erosion, due

either to varying rock types or to a highly fractured zone less resistant to erosion. Some of the faults in northwestern Ireland have the same lithology at either side of the fault plane, and present a high slope and relief. Particular attention will be paid to topography that is not lithologically controlled, but structurally controlled. Identification of river knickpoints along these structurally controlled topographic scarps is important to demonstrate recent activity in northwestern Irish faults.

Local relief refers to the difference between the maximum and minimum elevation over a given horizontal scale, in this case a 3 x 3 km window (Fig. 3.5). Greater relief generally implies higher local elevation variations and thus more powerful fluvial and gravitational processes, and higher denudation rates. Surface uplift increases relief and triggers erosion. Relief is a fundamental attribute widely recognised as reflecting the interplay between rock uplift and erosion. Numerical simulations of landscape evolution indicate that climate and tectonic deformation rate are the primary controls on relief (Chase 1992; Rinaldo *et al.* 1995) although rock type and geologic structures are also important factors (Schmidt and Montgomery, 1995). Recent studies by Hurtrez and Lucazeau (1999) in three French drainage basins showed that lithological effect on relief amplitude is minor at various spatial scales. Notice that relief refers to the change in elevation within a particular window size.

Ahnert (1973) and Summerfield (1991) calculated denudation rates out of relief maps. These simple estimations are useful when compared with denudation maps derived from Apatite Fission Track modelling. Summerfield (1991) also showed the correlations between elevation, relief and slope in southern Africa finding a much poorer correlation between elevation and both relief and slope than that one found in northwestern Ireland.

Using the 1 x 1 km DEM I have cross-plotted elevation, slope and relief across northwestern Ireland (Fig. 3.6). Slope and relief are well correlated, but relief and slope are moderately correlated with elevation. It is common to assume that high slopes occur where the elevation is also high, but in northwestern Ireland high relief does not occur only at high elevations when analysis is done on a 1 x 1 km grid size, but also at low

elevations (Fig. 3.6B). Some of the northwestern Irish topography such as Benbulbin and the Partry Mountains form plateaux 500 m high with low slopes and low relief summits.

At a much larger scale, Summerfield (1991), working on the passive margin of southern Africa, showed a poor correlation between elevation and relief but a strong correlation between slope and relief using a 25 x 27 km grid. Anhert (1970) using a 20 x 20 km grid, also showed a linear relationship between slope and relief when relief is less than 1100 m. The correlation obtained between elevation and relief for northwestern Ireland is much better than that obtained by Summerfield (1991). However, the differences in grid size might not make these correlations comparable, because increasing the grid size one loses the detail on the different morphological features on the elevation model.

The northwestern Irish topography shows a mean elevation of 113 m, mean relief of 74 m and mean slope of 1.5°. Maximum relief is 615 m. A linear relationship between slope and relief is obtained with a correlation coefficient of 0.95 (Fig. 3.6A). The trend shows a strong correspondence between low relief and low slope in northwestern Ireland with relief between 0 and 300 m associated with slopes lower than 6°. Examples of high relief with low slope are common but no areas are observed to have low relief and high slope. Relief is a sensitive function of window size and this result is a consequence of the 1 x 1 km grid spacing.

Comparison of the elevation, slope and relief maps shows that the Derryveagh, Slieve League and Nephin Beg Mountains have high elevations (>400 m), high relief (>400 m) and high slope (>8°) (Figs. 3.2, 3.4 and 3.5). In contrast, the Ox and Bluestack Mountains also have high elevations (>400 m) but with lower relief of less than 400 m and slopes less than 8°.

The correlation coefficient between elevation and slope is 0.71 and between elevation with relief is 0.72 (Fig. 3.6C). A strong correlation would have correlation coefficients of 1. At elevations under 200 m, slope is generally below 5°. Elevations between 200 and 300 m show slopes between 1° and 7° and relief between 75 and 300 m. At elevations of

300 m slopes between 0° and 6° and relief between 10 and 300 m values are common. These complicated relationship between elevation, relief and slope are better correlated than that found by Summerfield (1991) on the southern African passive margin. This result might be a consequence of Quaternary glaciation, as glaciers erode leaving behind steep mountain walls at either side of a valley and that would increase the correlation between relief, slope and elevation.

It is well established that denudation rate increases with basin relief (Schumm 1963). Ahnert (1970) suggested a simple equation to estimate denudation rates using a 20 x 20 km window in mid-latitude drainage basins ranging in size from several hundred km^2 to over 100,000 km^2:

$$d = 0.1535\ r \qquad \text{(eq. 1)}$$

where d is denudation rate in mm/ky and r is relief in metres. Summerfield (1991) used the same equation to calculate denudation rates on the southern African passive margin. Summerfield and Hulton (1994) established a significant correlation between denudation rate and relief for basins exceeding 500,000 km^2. Thus, using Eq. 1 on the not much smaller drainage basins of in northwestern Ireland might be justified. It will be shown that the denudation map obtained from Eq. 1 share some similarities with independent denudation estimates from apatite fission track analysis (AFTA) (method described in Section 5.3).

The relief grid shown in Figure 3.5, with pixel size of 1 x 1 km was used to generate estimates of denudation rate in each pixel using Eq. 1 (Fig. 3.7). The relief-derived denudation rates are highest in southern Mayo, the Nephin Begs, Sligo, Slieve League and northern Donegal, with maximum values of approximately 60 to 100 m/My (Fig. 3.7). The Ox and the Barnesmore Mountains show lower denudation rates of between 20 and 60 m/My. Extrapolation of rates of denudation from relief maps over geological time requires assumptions about the magnitude and distribution of local relief associated with the palaeotopography. In other words, these rates are valid estimates based on the

present-day topography, but palaeo-relief values may have been very different. How far back these denudation rates can be applied is hard to know, but it is instructive to compare them with denudation rates derived from apatite fission track thermochronology, which allows estimation of denudation over geologically long periods of time (10s to 100s).

Figure 3.8 is taken from Allen *et al.* (in press) and shows denudation rates from 66 to 10 My, from two different fission track annealing models (Laslett *et al.* 1987; Gallagher *in prep.*). These models are discussed in more detail in Section 5.2.3; for the moment, it is sufficient to note that the two models yield slightly different palaeotemperature values during cooling. Palaeotemperature values were converted to denudation estimates by Allen *et al.* (in press) using a palaeo-geothermal gradient of 22 $°Ckm^{-1}$. These estimates, in turn, were converted to denudation rates by dividing the time interval for which the sample thermal histories are well constrained (66 to 10 My; Allen *et al.* in press). The spatial patterns are generally similar to that generated by the present-day relief (Fig. 3.7), although the magnitudes differ considerably. The Laslett *et al.* (1987) annealing model yields Cenozoic denudation rates of up to 19 m/My for the Ox and Blue Stack Mountains, and up to 62 m/My in southern Mayo, Sligo and northern Donegal. The Gallagher (in prep.) model shows denudation rates of up to 24 m/My for the Ox and Blue Stack Mountains and maximum denudation values of 28 m/My for southern Mayo, Sligo and northern Donegal.

In summary, denudation rates derived from both relief relationships and fission track thermochronology show low denudation rates (~20 m/My) for the Ox and Blue Stack Mountains and higher values (up to ~60 m/My) for southern Mayo, Sligo and northern Donegal. Relief-derived denudation maps show in general higher denudation rates with a maximum of 100 m/My, whereas fission-track-derived maps show maximum denudation rates of approximately 60 m/My. Further subdivision of the fission-track-derived denudation maps into shorter time slices (e.g., Miocene to present, Fig. 5.17) do not correlate with the relief-derived denudation map, suggesting limitations of one of these methods.

3.5 Lithology and topography

Precambrian rocks in northwestern Ireland, mainly Dalradian quartzites, schists, psammites, pelites, gneisses, marbles and metadolerites, surround Ordovician, Silurian, Devonian and Carboniferous basins filled mainly with shales, sandstones and limestones. Silurian to Devonian granites are common and usually intrude along northeast trending structures with a wide variety of compositions and crystal sizes. Tertiary dolerite dykes are generally northwest-trending in the north of the study area, but strike east and northeast in the south (Fig. 3.9).

Topographical data may be combined with geological maps to qualitatively and quantitatively compare elevation with relative resistance of different rock formations. Rock strength is a physical property that is difficult to measure because it depends on many variables (Lifton and Chase 1992). These include composition and age of the rock (Clayton and Shamoon 1999), grain or crystal size, bedding orientation, intensity of joints or fractures (Weissel and Seidl 1997), foliation, climate and degree of weathering (Hack 1960), spacing, orientation and width of partings within the rocks (Selby 1980), time of exposure, and scale at which the measure of rock strength is made (Schmidt and Montgomery 1995). Rock resistance is here defined at the landscape scale. All these variables should be considered for a detailed study of lithological control on topography. Clayton and Shamoon (1998) produced a scale of rock resistance for British lithologies based on relief attributes. By analogy with their work, rock resistance in northwestern Ireland can be organised in decreasing order as: Precambrian quartzite, Devonian granite, Precambrian metasediments, Precambrian schists, Silurian granite, Ordovician shales and sandstones, Precambrian gneiss and Lower Carboniferous lithologies.

The following qualitative description mainly compares relief within the same rock formation, therefore no relative rock resistance scale is necessary. This work ignores the possibility of a spatially heterogeneous distribution of planes or zones of weakness within

the same formation in order to simplify the analysis, although considerable errors might be introduced by this omission.

An area within the same rock type under similar climate conditions, comparable base level, surrounded by similar formations and acted upon by the same erosional processes, should show similar elevation distributions unless tectonic activity modifies the topography. In this section and Section 3.7, I demonstrate qualitatively and quantitatively that topography in northwest Ireland is not always controlled by simple differential erosion of the various rock types and that other processes such as tectonic rock uplift or erosion of weak, fractured or jointed rock might be responsible for local values of high relief.

The Main Donegal granite was intruded along a major northeast-oriented Caledonian shear zone during the Early Devonian (Hutton 1982) and forms peaks between 400 and 700 m in the Derryveagh Mountains (Figs. 3.9, 3.10). The Derryveagh Mountains form relief of 400 and 500 m along the Gweebarra Valley and this high relief is not lithologically controlled as it occurs in the same formation. Instead, the relief appears to be structurally controlled by the Gweebarra fault. Similarly, the Slieve League peninsula in southern County Donegal contains areas of both high and low elevation spanning up to 500 m of relief within the same lithological formations (the Termon Pelite and Slieve Tooey Quartzite) which also suggests that the topography is structurally controlled rather than lithologically.

Carboniferous basins in Ireland typically form areas of low elevation and low relief. An exception to this general rule is the Benbulbin Mountains in County Sligo, where Carboniferous limestones, shales and sandstones form a 400 to 500 m high plateau. The plateau is adjacent to the topographically lower Moinan/Dalradian metamorphic inlier of psammitic paragneisses at the northern tip of the Ox Mountains Complex. This observation suggests that harder rocks are not necessarily higher in elevation, and less resistant formations such as the Carboniferous lithologies can form high topography when structurally controlled. The Mweelrea Hills and Partry Mountains, with a relief of

up to 500 m within the conglomerates and sandstones of the Mweelrea Formation, also appear difficult to explain by lithological differences and a structural control appears likely. These examples suggest that other mechanisms of mountain formation, beyond simple differential erosion, have to be taken into account in northwestern Ireland.

Another possible explanation for high relief within the same rock formation is by erosion of Quaternary ice sheets. Ice sheets are capable of incising deeply into the landscape creating high local relief. Glaciers may have used pre-existing Tertiary valleys to flow and incise into the weakest lithologies, fractures or fault scarps. The effect of glacial erosion is therefore important, but sometimes difficult to discriminate from other processes when studying the northwestern Irish landscape. However, some of the present day topographic features, such as wind gaps in the Ox Mountains, do not appear to be highly incised by ice as no glacial deposits are found (Fig. 2.2). Other valleys, with a U-shaped cross-sectional profiles and with till deposits on their floors, are considered to have formed at least partially by differential erosion due to ice sheet incision.

The Nephin Beg and Ox Mountains are underlain by resistant Precambrian quartzites and schists and are surrounded by low topography developed on less resistant Carboniferous limestones, sandstones and mudstones. The Blue Stack Mountains are underlain by the Devonian Barnesmore granodiorite and are surrounded by lowlands cut on Dalradian psammites and pelites. In these cases lithology has a larger influence on the topography.

In section 3.7, each mountain range in the study area will be examined separately in terms of lithology, topography, morphology and structurally-controlled river knickpoints. These analyses will be used to test the hypothesis that tectonism played a part in generating the landscape of northwestern Ireland.

3.6 River longitudinal profiles

The longitudinal profile of a river is the gradient line of its bed surface from the source to the mouth. Pazzaglia *et al.* (1998) stated that the longitudinal profile "is arguably the

most outstanding expression of the dynamic feedback between rock uplift processes, which construct topography and rock erosion processes, which destroy topography".

An important function of the graphic representation of the longitudinal profile is the identification of locations in the profile where there is a pronounced local change in the stream gradient, called knickpoints. Knickpoints can be concave-up or convex-up depending on the processes by which they form (Ahnert 1996). Here I consider only convex-up knickpoints (Fig. 3.11), which can form by a number of mechanisms:

- Relative drop in base level, due for example to marine regression or regional surface uplift.
- A change from more resistant to less resistant lithology (Miller 1991).
- Tributary junctions with incised trunk channels.
- An active fault crossing a river with the downthrown block downstream.

During equilibrium transport conditions the bedload transport equals the bedload removal at a particular point in the river profile. When uplift on the upper part of the profile occurs, the rate of bedload removal increases where the gradient is higher and a knickpoint is formed (Ahnert 1996) (Fig. 3.11). Once formed, knickpoints migrate upstream by headward erosion. Their position is dictated by the time elapsed since knickpoint formation and the knickpoint propagation rate. The propagation rate in turn depends on climate, tectonics and bedrock type. Pazzaglia *et al.* (1998) documented survival of knickpoints in the Susquehanna River on the eastern North America passive margin, over million-year time spans using fluvial terraces. Similar conclusions were reached for passive margin streams in eastern Australia (Young and McDougall 1993).

River knickpoints on active margins have been used to infer Cenozoic faulting in the New Madrid seismic zone (Merritts and Hesterburg 1995) and other tectonically active areas (Merritts and Vincent 1994; Rosenbloom and Anderson 1994). Zaprowski *et al.* (2001) showed a relation between Late Cenozoic exhumation of the Laramide Rocky Mountains and knickpoint propagation. Pazzaglia *et al.* (1998) compared long profile

development on both active and inactive settings. Whipple and Tucker (1999) derived a relationship for the system response time to tectonic perturbations in bedrock river channels.

Weissel and Seidl (1998) working on the Australian passive margin, located a major knickpoint zone 200 km from the river mouth associated with escarpment retreat, despite differences in bedrock lithology. Wheeler (1979) described the shape of longitudinal profiles in Great Britain (e.g., Greta River, Canberra, southwest England) and explained some of the stream convexities by recent faulting (Jennings 1972) or changes in lithology.

The following analysis of river profiles in northwestern Ireland aims to improve understanding of the origin of knickpoint formation in this area and to find out if river knickpoints are consistently present along faults. Hack (1973) found that the equilibrium longitudinal profiles of bedrock streams on the eastern Atlantic margin closely approximated exponential functions. Northwestern Irish rivers present a wide diversity of profile shapes, commonly far from the exponential shape that characterises rivers in equilibrium between rock uplift and vertical channel incision. The headwater tributaries of many rivers draining the northwest of Ireland are bedrock-floored and these are more resistant to erosion and more likely to record longer-term tectonic deformation than alluvial channels. Bedrock rivers in northwestern Ireland flow primarily across Carboniferous and Dalradian basement. Profiles with convex-up reaches are common and those that cannot be attributed to changes in hydrology or lithology may represent deformation of the longitudinal profile by tectonic displacements. Profile construction was done in those areas where glacial erosion is less pronounced and, when possible, where lithology does not change across a mapped fault. Several stream profiles were analysed where rivers crossed the same fault.

3.6.1 Data and methods

River profiles were compiled in Counties Mayo, Sligo, Leitrim, Fermanagh and Donegal. The method consisted of digitising rivers from scanned Ordnance Survey of Ireland (OSI) topographic maps at a scale of 1:50,000. Horizontal distance downstream from the river source was measured every 10 m of vertical elevation using the river trace marked on the topographic map. Topographic and geologic maps were scanned as individual sheets and geo-referenced using Arc/Info. ArcView was used to view the scanned maps, digitise the rivers, and compile tables of elevation versus horizontal distance from source to mouth. Geological boundaries can easily be located when the digitised rivers are overlain on the scanned geological map. Horizontal errors on the order of ±10 m were introduced during geo-referencing and this must be considered when interpreting the position of knickpoints against geological boundaries.

Rivers studied in northwestern Ireland range from 3 to 30 km in length, with catchment areas of approximately 100,000 km^2. Longitudinal profiles were first constructed across those faults that have some topographic expression in the present day landscape, such as a topographic scarp, high relief, or asymmetric mountain cross-section. Faults running along wind gaps were also considered for river profile construction, because of the potential of being tectonically controlled. Special attention was given to sites where rivers flow across faults within the same formation. When possible, several longitudinal profiles were analysed across a single fault, in order to discriminate between local knickpoint control and larger scale controls such as fault activity, which should express itself at different locations along strike.

3.7 Relationships within individual mountain ranges

A landscape and fluvial study of each range is presented in this section. The ranges examined include the following: in northeastern County Donegal the Urris Hills, Knockalla Hills and Lough Salt Mountains; in northwestern County Donegal the Derryveagh Mountains; in southern County Donegal the Blue Stack Mountains and

Slieve League; in County Sligo, Benbulbin and the Ox Mountains; in northern County Mayo, the Nephin Beg Mountains; and in southern County Mayo, the Mweelrea, Sheeffry and Partry Mountains (Fig. 3.10).

3.7.1 Northeastern Donegal

The Urris Hills, Knockalla Hills and Lough Salt Mountains trend northeast and are about 23 km long, 3 km wide and up to 0.5 km high (Fig. 3.12). They are bounded by the Leannan fault and the Swilly Slide. The ranges are underlain by the Slieve Tooey Quartzite Formation, a whitish quartzite with pebble beds. The Slieve Tooey Quartzite Formation also underlies lowlands to the northwest of the Urris Hills (Fig. 3.13, cross section B). This suggests that the topography of the northwest flank of the Urris Hills is not due solely to resistance of the underlying lithology. To the southeast the contact between the quartzite and the less resistant psammitic and semipelitic schists of the Termon Formation is coincident with a change in elevation (Fig 3.13), suggesting that this lithology change might be responsible for some of the observed relief. A pocket of Devonian conglomerates and sandstones is faulted against Dalradian quartzite by the Leannan fault (Fig. 3.14) and this vertically dipping fault in places controls the topography of the Knockalla Hills.

Six river profiles across the Leannan fault show a convexity upstream of the fault zone (Fig. 3.14 and 3.15). The Bunlin River contains two knickpoints. The upper one at 190 m above sea level (asl) is underlain by the Termon Formation and is located upstream of a set of north-northwest trending faults (splays of the Leannan fault) that control the topography southeast of Lough Salt Mountain (Fig. 3.14). Glacial erosion has intensified the valley wall and possibly the knickpoint. The lower knickpoint is 30 m high and 80 m asl. The narrow valley of the Bunlin River is also occupied by the Leannan fault, although lithology within this valley changes from the Termon Formation to metadolerite and that can intensify knickpoint development.

The Crockanaffrin stream is underlain by a uniform lithology (Termon Formation) and contains a knickpoint at 60 m asl upstream of the Leannan fault (Fig. 3.15). The valley of the Crockanaffrin stream is V-shaped and not intensively glaciated and knickpoint preservation is probably more likely in here than other more glaciated valleys. The Leannan River contains two knickpoints at 60 and 30 m asl. The higher knickpoint might be partially due to lithological change, as at that point the river flows from the Termon Formation across a metadolerite intrusion to the Upper Crana Quartzite Formation (3.16). The lower knickpoint occurs in a fairly uniform lithology, marking a change from the Upper Crana Quartzite to the Lower Crana Quartzite Formation. This lower knickpoint is more likely to be associated with activity on splays of the Leannan fault.

Although lithological changes might play a large local role on knickpoint formation, the presence of consistent knickpoints upstream of the Leannan fault on six rivers (Fig. 3.15), and the non-lithologically controlled topography of the Urris Hills (Fig. 3.13B) suggest recent movement on the northeast-trending Leannan fault with a down throw to the northwest. Present day seismic activity in Ireland show historic seismic centres (Jacob 1993) possibly related to the Leannan fault.

3.7.2. Northwestern Donegal

A deep northeast-trending valley along the Gweebarra fault (Fig. 3.16) separates the highest peaks of the Derryveagh Mountains (Slieve Snagh, 678 m and Dooish, 652 m) from the Glendowan Mountains (Crockskallabagh, 494 m). A northwest-trending valley divides Errigal (751 m) from Crocknafarragh (517 m). The Main Donegal Granite underlies most of the Derryveagh and Glendowan Mountains (Fig. 3.17). The Gweebarra fault trends northeast and runs along a long, narrow valley for ~20 km along Glen Lough in the northeast, through the incised valley of Lough Beagh, through a wind gap at 240 m asl and southwest to Lough Barra and Gweebarra Bay (Fig. 3.16). The wind gap is located between peaks of 676 m and 539 m elevation where a dense array of Palaeogene dykes occurs (Fig. 3.17). Drainage at this point diverts in 4 directions into the catchments of the Gweebarra, the Owencarrow, the Clady and the Leannan rivers.

The Gweebarra River runs parallel to the Gweebarra fault in the Main Donegal Granite, a coarse biotite granite and granodiorite. Two knickpoints are located upstream of the Gweebarra fault (Fig. 3.18). One at 170 m asl is likely to be structurally controlled as it occurs in an area of uniform lithology. Tertiary dolerite, basalt and gabbro dykes are common in this area, but are mainly located upstream of the knickpoint and are unlikely to be controlling it (Fig. 3.17). A second, 5 km broad knickpoint at 75 m asl is also located upstream of the Gweebarra fault. Its origin is not clear. As will be shown, other longitudinal profiles also show knickpoints at this elevation, raising the possibility that they may be due to regional changes in base level.

Two northwest-trending valleys run perpendicular to the underlying geological structure and thus do not appear to be lithologically controlled. One valley, which controls the Clady River, runs along Lough Nacung and separates Errigal (751 m) and Tievealehid (429 m) from Crocknafarragh (517 m) (Fig. 3.16). The drainage has been suggested to be pre-glacial in age based on superimposition of the river on an older basement (Pitcher & Berger 1972). The Clady River runs perpendicular to a contact of metadolerite and quartzite and differential erosion has given rise to a pronounced knickpoint (Fig. 3.18). The second valley runs along the Altan Lough and separates Errigal (751 m) from Aghla More (584 m) (Fig 3.16). Both valleys have been scoured by glacial erosion as shown by their steep-side walls and flat valley bottoms.

East-trending faults separate the high ground around Tievealehid (429 m) and Errigal (751 m) from the lowlands south of Ballyness Bay (Fig. 3.16). The Aspick River flows across the Lower Falcarragh Pelite Formation (carbonaceous pelite schist) and east-trending microgranites (Fig. 3.17). A river knickpoint that occurs between 50 and 100 m asl might be the result of movement on any of the five east-trending faults with down throw to the north (Fig 3.18).

3.7.3 Southern Donegal

Slievetooey (472 m) and Slieve League (595 m) Mountains are oriented roughly east-west while Common Mountain (500 m), Crocknapeast (497 m) Mulnanaff (475 m) and Crownarad (493 m) Mountains define a northeast trend (Fig. 3.19). These peaks surround the 10 km wide, rounded, south-flowing drainage basin of the Glen River (Dury 1964; Reffay 1966).

The Slieve Tooey Formation, a whitish quartzite with pebble beds, underlies Slievetooey Mountain (Fig. 3.20). This formation outcrops at the northern side of the southern Donegal peninsula. This resistant quartzite formation has a varied topographic signature, being low in the south and high in the north. It can be divided into three blocks separated by the east-trending Kittyfannan fault (Fig. 3.21). The northern block shows higher elevations than the two blocks in the south, which have similar but lower elevation distributions (Fig. 3.21). This implies that the topography is not lithologically controlled but structurally by possibly down to the south movement on the Kittyfannan fault.

The Owenwee River (north) runs from Crockuna (400 m) to Loughros Beg Bay across the Slieve Tooey Quartzite Formation (Fig. 3.20 and 3.22). A deeply incised U-shaped valley suggests considerable glacial erosion, which accentuated the 100 m high knickpoint at 160 m asl. The valley is aligned with the Kittyfannan fault for at least 5 km. The glaciated valley shows a marked contrast in slope on either side, with the southern wall steeper than the northern wall. If the slopes are structurally controlled, this would suggest down throw movement of the Kittyfannan fault to the north, which is opposite to the kinematics inferred from the elevation distributions across the fault. The Glen River crosses the same fault and shows a steep slope at its head. A knickpoint at 160 m, downstream of the mapped fault, is possibly related to a dyke intrusion (Cooper *et al.* 1997) (Fig 3.22).

The Ballaghdoo fault trends northeast and separates generally lower topography to the west from higher topography to the east (Fig. 3.20). The fault follows the Ballaghdoo and Glengesh valleys. The Crow Stream, a tributary of the Glen River, flows across this fault and does not show any knickpoints associated with this structure (Fig. 3.22).

The contact between the Slieve League Formation and the Termon Pelite Formation forms a knickpoint in both the Glen River and the Crow Stream (Figs. 3.20 and 3.22). The Owenwee (south) and the Murlin rivers also show knickpoints upstream of the Slieve League Formation contact (Figs. 3.20 and 3.22). All of these knickpoints are almost certainly due to changes in lithology.

3.7.4. Croaghgorm or Blue Stack Mountains

The Blue Stack Mountains contain 16 peaks over 400 m and are highly dissected by northeast to east trending valleys. The highest peaks in the Blue Stack Mountains (561, 674, 626, and 641 m) occur in an area bounded by the Barnesmore Gap to the southeast and the Lough Finne Valley to the northwest. The drainage divide between north and south-flowing catchments cuts across the deeply incised Barnesmore Valley, forming a prominent windgap (Fig. 3.23).

Most of the high topography in the Blue Stack Mountains is underlain by the Barnesmore Granite (monzogranite, leucogranite, aplogranite and granodiorite), the Lough Mourne Formation and the Lough Eske Psammite Formation (Fig. 3.24).

The Silurian-Devonian Barnesmore Granite is sinistrally displaced by the Belshade fault, dextrally displaced by the Barneslough fault and fractured but not laterally displaced by the Barnesmore fault (Long *et al.* 1999). The granite northwest of the Belshade fault forms generally higher topography than that to the south (Fig. 3.21). Likewise parts of the Lough Mourne Formation northwest of the Belshade fault show higher elevations than areas to the southeast. This consistent difference across the Belshade fault suggests that

the topography in this area may be affected by fault activity in northeast trending fault with down throw to the southeast or differential erosion due to fracturing.

The Laghy River shows a knickpoint at 170 m asl upstream of the Laghy fault and the Finmore Slide (Fig. 3.25). The Finmore Slide juxtaposes very different rocks, with the Dalradian Croaghgarrow Formation (schists and aluminuous schists) on the southern side of the fault and the Mullyfa and Deele Formations (psammite, pebble beds, marble and schists) on the northern side (Fig. 3.24). The Laghy fault juxtaposes the Mullyfa and Deele Formations to the south with the less resistant Ballyshannon Limestone Formation to the north.

The Oily River profile shows a knickpoint at 80 m asl, which is probably due to the presence of a microgranite intrusion. However splays of the northeast trending Killybegs fault are situated downstream of this knickpoint (Fig. 3.25).

The Clogher River contains a small knickpoint upstream of the Barnesmore fault, although the resistant basal clastics of the Ballina Limestone Formation could also be responsible for the knickpoint (Fig 3.24 and 3.25).

The Corabber River shows a large knickpoint immediately upstream of the Boundary fault (Fig. 3.25). Here the Boundary fault separates the Dalradian Lough Mourne Formation from the Carboniferous Banagher Sandstone Formation. Thus, there is a large contrast in rock erodibility across the fault, making it difficult to eliminate lithological origin for this knickpoint. Also notice that the heads of the two tributaries of the Eany River are very steep, and this might also be associated with lithological changes across the Boundary fault.

Two tributaries of the Eany River show knickpoints at 145 m asl (Fig. 3.25). Knickpoint consistency upstream of the Eglish fault suggests movement on this structure or preferential erosion of the faulted zone.

The Owenea River shows a knickpoint in the banded semi-pelitic and psammitic schists of the Termon Pelite Formation upstream of the north-northeast trending Aghla fault (Fig. 3.25). This fault also controls the topography of the western side of Crockmore Hill and the Owengarve River catchment, which trends perpendicular to the Owenea stream (Fig. 3.24).

The Clady, the Barnes and the Eddrim Rivers all contain a knickpoint upstream of the Barneslough fault (Fig. 3.25). The Barnes shows a knickpoint at 200 m asl within the Barnesmore granite and Lough Mourne Grit formations, and the river follows the trend of the Barneslough fault for about 3 km. The Clady shows a pronounced knickpoint at 250 m asl at the contact between the sandstones of the Banagher Formation and the Ballyshannon Limestone formation. The Eddrim shows a small knickpoint as it flows through the Bundoran Shale Formation and crosses the Barneslough fault. Long *et al.* (1997) showed an unfaulted Palaeogene dyke across the Barneslough fault (Fig. 3.24), making it difficult to suggest Cenozoic tectonic activity on the fault, even though the Eddrim, Clady and Barnes Rivers show consistent knickpoints. Interestingly, the three rivers all show consistent sinistral step in their courses when they cross the fault. The sinistral offset ranges from a couple of hundred metres in the Eddrim River, to ~1km in the Clady and Barnes Rivers.

The Ballintra River profile has a convex-up shape, unlike any of the other catchments draining the Blue Stack Mountains (Fig 3.25). Near the headwaters, a small change in gradient is associated with the contact between Dalradian psammitic paragneisses and the Ballyshannon Limestone Formation. However, most of the convex-up profile is developed within the Ballyshannon Limestone Formation and is immediately upstream of the Laghy fault. Thus it is possible that down throw movement to the northwest on the Laghy fault is responsible for this unusual profile.

In summary, most of the rivers in the Blue Stack Mountains show knickpoints with a lithological control. However, the Eglish, Aghla, Barneslough and Laghy faults appear to

give rise to a series of knickpoints in adjacent catchments. Movement on these faults is suggested as a possible origin for knickpoints.

3.7.5. Sligo Mountains

The Sligo Mountains are dissected by three valleys that converge in Manorhamilton Town (Fig. 3.26). The east-trending Glencar Lough valley separates Benbulbin (526 m) and Truskmore (647 m) from Crockauns (463 m). The northwest-trending Glenade Lough valley and a northeast-trending valley also separate areas of higher topography up to 450 m high. These valleys all contain prominent wind gaps, with two rivers presently flowing in opposite directions suggesting drainage reversal after valley formation. Thus, the topography of the Sligo Mountains developed under a markedly different drainage system than the present set of catchments, and excavation of the three large valleys must predate the establishment of the present rivers. Glacial erosion was clearly involved in valley excavation, because of the steep walls on either sides of these valleys, but only partially involved in valley formation, because valleys are not the result of simple glacial erosion. The northern side of the Sligo Mountains was more deeply scoured by glacial erosion than the south, as shown by the corries and steeper northern walls of Benbulben and Truskmore (Fig. 3.26).

The Sligo Mountains are composed of approximately flat-lying Lower Carboniferous sediments, including limestones, sandstones and shales (Fig. 3.27). They are topographically higher than the northern tip of the Ox Mountains to the south, even though the latter are underlain by more resistant Pre-Cambrian paragneisses (relative resistance estimated from Clayton and Shamoon 1998). The Sligo Mountains contain dramatic relief of up to 200 m in only 250 m of horizontal distance within the same Lower Carboniferous succession. It is hard to explain the topography by differential erosion due to lithological differences, as for example the Dartry Limestone Formation and the underlying formations, occur at very different elevations north and south of the Glencar fault (Fig. 3.21). The high relief, a wind gap, one river knickpoint and elevation

differences within the same formation all suggest possible tectonic activity along the east-trending Glencar fault, south of Benbulbin, with a down throw to the south.

The Drumcliff River flows across the calcareous Benbulbin Shale Formation along the Glencar fault, and shows a knickpoint at 20 m asl (Fig. 3.28). The westernmost tributary of the Bonet River shows a knickpoint at 65 m asl at the head of the river above a north-northwest fault. Another knickpoint at 25 m appears to be lithologically controlled by the contrast between the Oakport Limestone Formation and psammitic paragneisses, because none of the other three crossings of the fault by the river further upstream result in a knickpoint.

The Duff River shows a knickpoint at 130 m asl, upstream of the northwest-trending Glenade fault (Fig. 3.28). The bedrock lithology changes across the fault from the Benbulbin Shale Formation to the Mullaghmore Sandstone Formation. Southeast of the Duff River, the Glenade fault controls the orientation of the Glenade Valley, and the valley is incised up to 500 m. The valley contains a wind gap near its northwestern end (Fig. 3.26).

The Belhavel fault or lithological changes probably controls the steep channel gradient at the head of the Bonet River (Fig. 3.28). A convex-up knickpoint 15 m high at 120 m asl occurs upstream of an east-trending fault (Fig. 3.26). The Dartry Limestone Formation, a massive cherty calcarenite wackstone, outcrops on either sides of the fault and therefore the knickpoint is not lithologically controlled. Lower elevation distributions in two patches of the Dartry Limestone Formation that outcrop south of the fault suggest that the southern block of the Belhavel fault may have been downfaulted (Fig. 3.21).

To summarise, the east trending Glencar fault controls the high relief, windgap, river knickpoint of the Drumcliff River and the different elevation distributions north and south of the fault, suggesting down throw to the south. Other northwest and east trending faults with similar kinematics, including the Belhavel fault might also control knickpoint formation.

3.7.6. The Ox Mountains

The Ox Mountains rise from the Carboniferous plain a few kilometres south of Sligo Town and trend southwest for about 40 km to near Foxford (Fig. 3.29). They form a linear range with a linear drainage divide that is asymmetric in cross section, with a steep slope (up to 30°) on the northwest side and a gentle slope (up to 10°) on the southeast side (Fig. 3.30). The distribution of surface slopes and lithological dips reflects an asymmetric tilt block with a linear drainage divide close to the northwestern flank of the range (Fig. 3.29). The height and width of the topography near Knockalongy (544 m, 512 m) gently diminishes towards the southwest. The highest relief in the Ox Mountains is found along the northwestern side where the Ox Mountains fault and associated faults were mapped (Harney *et al.* 1996) (Fig. 3.32).

The range is underlain by Dalradian metasediments of the Ox Mountains Inlier as well as by a Cambro-Ordovician succession, Late Silurian granodiorite and Early Devonian monzogranite (Fig. 3.32). The surrounding lowlands are underlain by Carboniferous formations. The range is bounded by the northeast-trending Ox Mountains fault to the northwest and by a Carboniferous unconformity to the southeast, where onlap shows that there was already some topography in pre-Variscan time.

Two prominent valleys cut across the Ox Mountains, the northeast-trending Easky Lough Valley and the northwest-trending Lough Talt Valley (Fig. 3.29). Both valleys contain wind gaps at about 200 m below the surrounding peaks, at the northwestern flank of the range, suggesting 200 m of topographic incision prior to the development of the wind gaps. The presence of these wind gaps at the northwestern side of the Ox Mountains, the tilted nature of the block and the displaced drainage divide may indicate tectonic activity on the Ox Mountains fault with a down throw to the northwest.

The linearity of the Ox Mountains might be explained by differential erosion of the underlying bedrock coupled with the strong regional structural grain, or by tectonic

displacements on the Ox Mountains fault. Because lithological changes are considerable within this area, from Dalradian to Carboniferous sediments, a more detailed study was done to understand the role of rock resistance on topography. If differential erosion were the main process of mountain formation in the Ox Mountains, an equivalent topographic scarp should be present on the southeastern flank of the range, but it is not.

In several areas, the same formation underlies a wide range of elevations. Semi-pelitic schists of the Carrick O'Hara Formation form the highest topography of the Ox Mountains at Knockalongy (544 m) and north of Lough Talt (413 m). However this formation also underlies low elevations, for example in the Owenboy River valley. Several faults cut the Carrick O'Hara Formation in the Owenboy River valley and higher erodibility or tectonic activity might be responsible for these low elevations. In the southeastern Ox Mountains this same formation outcrops at elevations less than 100 m (Figs. 3.29 and 3.32).

The Leckee Quartzite Formation, with presumably a higher erosive resistance than the semi-pelitic schists (Clayton and Shamoon 1998), underlies relatively low topography. Aluminous schists of the Ummoon Formation outcrop at Knockachree (535 m) over a wide range of elevations. The Easky Adamellite Formation (monzogranite) forms high relief varying in elevation from 512 m at Farbreagabeg to 190 m at Easky Lough. This lithology forms a topographic scarp dipping up to 28° on the northwestern side, compared to 5° slope on the southeastern side (Fig. 3.30); therefore lithology is not controlling topography in this case and a structural control is suggested for the formation of the northwestern Ox Mountains topographic scarp.

The Ox Mountain Granodiorite is elongated northeastwards and is cut by a northwest-trending fault. Elevation distributions on either side of the fault are very different (Fig. 3.31). The northern block contains higher elevations and slopes of up to 36°, compared with slopes of about 5° in the southeastern side (Fig. 3.30). The granodiorite is bounded to the northwest by less resistant schists the Carrick O'Hara and Ummoon formations and Carboniferous sediments; to the southeast by the Ummoon Formation against the Leckee

Quartzite Formation, and also by Lower Carboniferous rocks. It is therefore unlikely that differential erosion was the main process of scarp formation and movement on the Ox Mountains fault is once again suggested.

Three longitudinal profiles were constructed for rivers crossing the Ox Mountains fault (Fig. 3.33). The Crowagh River shows a concave-up knickpoint at 300 m asl in the Carrick O'Hara Formation, upstream of a north-northeast trending fault that is parallel to the Ox Mountains fault. The Easky River shows a convex-up knickpoint at 160 m asl, possibly controlled by a northwest-trending fault, the Ox Mountains Fault, or by differential erosion between amphibolites of the Attymass Group and the Carboniferous Ballina Limestone Formation. The Owenmore River shows a convex-up, 10 m high knickpoint at 135 m asl, again between the Attymass Formation and the Ballina Limestone Formation.

Although morphological and lithological evidence (e.g., mountain asymmetry, wind gaps, non-lithologically controlled topography) suggests a structural control and possible recent movement (?Cenozoic) on the Ox Mountains fault, it is difficult to corroborate this using river knickpoints because of the strong lithological differences.

Three longitudinal profiles were also constructed for rivers flowing off the southeastern flank of the Ox Mountains. The Owenboy River contains a convex-up knickpoint at 180 m asl that may be due to differential erosion between amphibolite basic metavolcanics in the New Antrim Member and schists of the Meelick Member of the Ummoon Formation. However, a north-northwest trending fault is located downstream of the knickpoint, and controls the location of the Glenmore Valley, suggesting a structural control.

The Owenaher River shows a convex-up knickpoint at 125 m asl. The river flows from semipelitic and aluminious schists of the Ummoon Formation across a northeast-trending fault into the schists, marbles and metavolcanics of the Corradrishy Formation. The Lough Talt River contains a convex knickpoint at 127 m asl along the same northeast-trending fault and flows from quartzites to schists.

River knickpoints are found consistently in streams flowing across the Ox Mountains fault, a northeast-trending fault and a north-northwest trending fault. Although lithological differences are also plausible causes of knickpoint generation, other morphological anomalies, such as the asymmetry and linearity of the range, the presence of wind gaps and high relief within the same formations, points towards activity on at least the northeast-trending Ox Mountains fault with a down throw to the northwest.

3.7.7 Nephin Beg Mountains

The Nephin Beg Mountains have a semicircular morphology diminishing in altitude in a clockwise direction from Nephin (800 m) to Corslieve (541 m) across the Owenmore valley to Maumakeogh (379 m) (Fig. 3.34). Farther west lie Corraun Hill (541 m), Slievemore (671 m) and Croaghaun (688 m) on Achill Island. To the southeast, the 3 km wide valley of Glen Nephin and Glen Hest divides Nephin (800 m) from Croaghmoyle (430 m).

The highlands of the Nephin Beg Mountains, Corraun Hill, and Achill Island are largely underlain by Dalradian quartzites and schists from the Nephin and Bangor/Corslieve Formations (Fig. 3.35 and 3.36). However, these rocks also form areas of low topography such as near Carrowmore Lake and west of Glenamong Mountain (Fig. 3.36 and 3.37). A strip of Devonian and Carboniferous sandstones runs from southern Corraun Hill eastward along the northern shores of Clew Bay and into the valleys of Glen Hest, Glen Nephin and Croaghmoyle Hill. The adjacent lowlands are generally underlain by Lower Carboniferous sandstones, shales and limestones. However, Carboniferous sandstone also underlies the relatively high topography of Slieve Fyagh (331 m) and Maumakeogh (379 m) north of the Owenmore Valley (Fig. 3.35).

Because the topography of the Nephin Beg Mountains appears at first view to be lithologically controlled, I have plotted elevation versus lithology (Fig 3.38), showing that this is not the case. Assuming that rock resistance to erosion depends on its degree of

metamorphism, mineralogy and grain size, a rough relative resistance scale was made from shales and sandstones to psammites, schists and quartzites (Fig. 3.38). This is consistent with the scale of rock resistance given in Great Britain by Clayton and Shamoon (1998). If topography were simply controlled by lithology a linear trend between elevation and rock resistance would be expected. However, mountains in County Mayo do not give rise to a linear trend (Fig. 3.38). Surprisingly, quartzitic formations do not form much higher mountains than sandstones do, while schists underlie a wide variety of elevations. Again, it seems clear that the topography is not a direct product of simple differential erosion, and a tectonic origin is possible.

The Nephin Beg Mountains consist largely of a series of faulted blocks, with the faults approximately oriented radially outwards from the lowlands at the centre of the range (Fig. 3.35). In some cases faults are associated with steep-walled topography. However, other faults cross the Nephin Begs without any topographic expression. The elevation distribution of faulted blocks within the Nephin Formation (schists and quartzites) are generally very similar, with the exception of blocks on Nephin and Birreencorragh Mountains (Fig. 3.37). Two Devonian formations, the Croaghmoyle and Birreen sandstones, also show consistently different elevation distributions on either side of a north-northwest-trending fault, with lower elevation distributions on the southwestern side of the fault (Fig. 3.37). This fault runs perpendicularly to Glen Nephin, a wide, incised glaciated valley. The presence of Cenozoic sediments offshore in the Irish Mainland Shelf, Porcupine Basin and Rockall Basin, and the size of the valley with up to 500 m relief suggest that this valley was one of the sedimentary conduits possibly active during the Cenozoic. This inferred drainage no longer exists and a wind gap is left with two catchments flowing in opposite directions (Fig 3.35). Combined evidence from consistently higher elevation distributions at the eastern side of a north-northwest trending fault, the presence of the windgap, and river knickpoint evidence described below is suggestive of differential vertical movement on the fault with the southwestern side down thrown (Fig. 3.35).

River profiles were constructed along several streams in the Nephin Beg Mountains (Figs. 3.35 and 3.39). The Heathfield River flows across sandstones, shales and limestones of the Downpatrick Formation (Fig. 3.35) and shows a knickpoint at 100 m asl upstream of a northwest-trending fault (Fig. 3.39). However, intra-formational changes in lithology may also control the formation of this knickpoint.

The Ballinglen River shows a knickpoint at 110 m asl within the Downpatrick Formation, although it is coincident with a change from sand and shales to limestone. A stream close to Downpatrick's Head flows across the same intra-formational contact, away from the Bangor Fault, and also forms a knickpoint, so lithological control cannot be ruled out. The Ballinglen River and a north-trending fault run along a linear and incised valley with valley side slopes of up to 30° (northern part of Fig. 3.40).

The Owenmore River is the only catchment that flows directly across the Nephin Begs. Interestingly, this antecedent valley occurs where the northeast-trending Bangor fault cuts across the axis of the Nephin Begs (Fig. 3.35). Four rivers show a gradient increase upstream of the Bangor fault (Fig. 3.39). The Oweniny River shows a knickpoint at 130 m asl, coincident with a contact between the Minnaun Sandstone Formation and the Downpatrick Formation. However, two smaller streams including the Bellananaminnaun River flow across the same formational contact without forming any knickpoints. Therefore the knickpoint in the Oweniny River is unlikely to be formed by differential erosion due to lithology. The Glencullin River shows a knickpoint at 125 m asl, upstream of the Bangor fault. Rock type changes from the Downpatrick Formation to the Minnaun Sandstone Formation and as demonstrated before the contact between these two formations does not form knickpoints elsewhere, except where bounded by the Bangor fault. The Owenmore River profile is interesting because of its broad convex-up shape. The underlying lithology changes downstream from Carboniferous sediments to Dalradian quartzites and other metamorphic rocks and to the Pre-Dalradian Annagh Division gneiss. The broad gradient increase located in the Owenmore Valley might be a result of the complicated hydrology (Fig. 3.39). River profiles in arid climates, because of the lack of drainage in the headwaters, generally show convex profiles similar to the

Owenmore River profile. Ireland and the Owenmore River far from an arid climate, is drained by several tributaries born ~20 km away from the Owenmore Valley. The complicated drainage caused by peat-land between the headwaters and the mouth of the Owenmore River might cause this convexity in the river profile.

The Owenduff River and a tributary of the Owenmore with its headwaters in the Nephin Begs both show knickpoints upstream of a northeast-trending fault. This fault runs along the wide wind gap between Nephin Beg and Corslieve Mountains with topographic slopes as high as 45° (Fig. 3.40).

The Glennamong River shows two knickpoints at 135 and 60 m asl within the quartzites and schists of the Annafrin Formation, upstream of a northeast-trending fault (Fig. 3.39). The Altaconey River also contains a knickpoint upstream of the same structure and this consistency suggests a structural control. The Srahmore River has a different profile shape and a broader knickpoint (Fig. 3.39). This knickpoint may be related to some of the splays on the same northeast-trending fault.

The Glasheens River shows a knickpoint at 127 m asl (Fig. 3.39), directly upstream of an east-trending fault that separates the Dalradian Birreencoragh Schist from the Carboniferous Minnaum Sandstone formations (Fig. 3.36). The Deel River also shows a broad knickpoint at 237 m asl across the same fault but the shape of the knickpoint is different. A structural control for knickpoint formation is also suggested.

A tributary of the Newport River (*Newport (1)* in Fig. 3.36), with its headwaters north of Croaghmoyle, shows two knickpoints at 265 and 130 m asl (Fig. 3.39). The first knickpoint is located in Devonian conglomerates of the Croaghmoyle Formation. This appears to rule out a lithological control and the knickpoint may be instead be controlled by a north-northwest-trending fault with possibly down throw to the west (Fig. 3.37). Elevation distributions within the Croaghmoyle Formation are different on either side of the fault, and possibly control a wind gap previously discussed (Fig. 3.37). A second knickpoint on this river is located at the contact between the Croaghmoyle Formation and

sandstones and siltstones of the Carboniferous Capnagower Formation; therefore, knickpoint formation due to lithology is difficult to rule out (Fig. 3.39). One kilometre to the north, a second tributary of the Newport River (*Newport (2)*) shows a knickpoint within the Capnagower Formation possibly controlled by a north-trending fault with down throw to the west.

A third tributary of the Newport River (*Newport (3)*), with its headwaters south of Croaghmoyle, shows two knickpoints. One occurs at 190 m asl within the sandstone of the Birreen Formation and is possibly controlled by a north-northwest fault (Fig. 3.39). The second knickpoint is at 100 m asl at a contact between Devonian sandstones and Carboniferous limestones.

A northeast-trending structure, an extension of the Ox Mountains Fault, runs southeast of Beltra Lough along the steep slopes (up to 45°) of the northwest flank of Croaghmoyle (Fig. 3.40). Croaghmoyle Mountain is underlain by sandstone of the Birreen Formation. The asymmetry of this mountain is shown by high topographic slopes on its northwestern side and much gentle slopes on the southeastern side, suggesting a tilted block similar to the Ox Mountains.

In summary, relatively good evidence suggesting Cenozoic dip-slip movement on the Bangor fault, a north-northwest trending fault in Glen Nephin, two northeast trending faults and the southeastern extension of the Ox Mountains fault was found from consistent river knickpoints, antecedence, wind gaps and variations in elevation distributions. As the Owenmore River is the only large catchment that is clearly antecedent to the topography that surrounds it, the Owenmore catchment is an ideal area for studying river incision into the present day topography. Section 3.9 presents analysis of the gravel and bedrock terraces within this catchment.

3.7.8. Southern County Mayo

Much of the high topography of southern County Mayo, including Croagh Patrick (764 m), the Sheeffry Hills (762 m), Ben Gorm (700 m) and the Mweelrea Mountains (814 m) has an east-west trend. The main exception to this are the Partry Mountains, which trend northeast and form a 600 m high plateau whose margins were scoured by glacial erosion leaving steep walls up to 500 m high (Fig. 3.41). The dominant east-west trend appears at first view to be controlled by the strike of the underlying bedrock (Fig. 3.42). However, the northwest-trending Doolough Valley that dissects the Mweelrea Mountains and the Sheeffry Hills trends oblique to the formational strike, parallel to several northwest-trending faults. The northeast-trending Erriff Valley also cuts obliquely across the Ordovician Mweelrea Formation, separating the Partry Mountains from the Mweelrea Mountains and the Sheeffry Hills. The Erriff fault bounds the southeastern edge of the Erriff Valley for much of its length (Dewey 2000; Badley 2001). Three fault-bounded blocks of Mweelrea Formation show similar elevation distributions, although areas northwest of the Erriff fault have slightly lower overall elevations (Fig. 3.43).

The Bunanakee River (Fig. 3.42) shows knickpoints within the Mweelrea Formation (Fig. 3.44). They cannot be lithologically controlled as the river twice crosses the contact between sandstones and shales of the Mweelrea Formation upstream without showing any convexities. These knickpoints might be controlled by northwest-trending faults.

The Glencullin River shows a knickpoint at 240 m asl at a northwest-trending fault in sandstones of the Derrylea Formation (Fig. 3.44). A second knickpoint at 210 m asl, with a height of 150 m, is very likely controlled by a vertically dipping basic intrusive body and has been accentuated by glacial erosion.

Three profiles across the Erriff fault show knickpoints upstream of this northeast-trending structure (Fig. 3.44). The Aille River shows a knickpoint at 110 m asl upstream of the Erriff fault. Lithological changes are considerable from the Glenumera Formation to the Derrylea Formation and from the Bohanun Volcanic Formation to Lower Carboniferous

limestone, making it difficult to rule out lithology as the cause of the knickpoint. However, it is worth noting that the contact between the Glenumera and Derrylea formations does not form knickpoints elsewhere, for example on the Derrycraff and Glencullin Rivers.

The Derrycraff River shows a knickpoint at 85 m asl directly upstream of the Erriff fault at a contact between sandstone and limestone. The Owenduff River has a knickpoint at 50 m asl, also upstream of the Erriff fault. Lithological changes are also considerable in this stream from the Glenumera Formation to the Mweelrea Formation and it is difficult to rule out lithology as the cause of knickpoint formation.

However, combined evidence from three knickpoints on three streams, along with the topographic signature of the 500 m relief on the northern flank of the Partry Mountains, argues in favour of tectonic activity on the Erriff fault, as previously suggested by Badley (2001) and Dewey (2000).

The Owenduff River shows a second knickpoint at 200 m asl within the Mweelrea Formation. This formation, although having slate and sandstone members, does not usually form knickpoints unless bounded by a fault as shown in the Bunanakee River. A third knickpoint at 120 m asl might be caused by a contact between the Mweelrea Formation and Glenummera Formation, or by a northwest-trending fault (Fig. 3.44).

To summarise, tectonic movement on the Erriff fault with a down throw to the northwest, and movement in northwest-trending faults is suggested as the origin of some of the river knickpoints in southern County Mayo.

3.8 Summary of suggested Cenozoic active faults

Section 3.7 presented evidence of knickpoints in a number of catchments in northwestern Ireland. Lithologic control of knickpoints was discriminated by locating knickpoints along stream reaches in the same geological formation. Those knickpoints located

upstream of faults, and not likely to have been formed by differential erosion due to different lithologies, are suggested to have a structural component. Some aspects of the morphology of the northwestern Irish landscape such as high relief, linearity and asymmetry of topography across structural grain, and wind gaps, are difficult to explain in terms of simple differential erosion due to lithological resistance or glaciation, and fault displacements can be invoked to explain some of these fluvial and topographic features.

Results indicate that fault reactivation of northeast, east, and northwest-trending structures during the Cenozoic might have been partially responsible for some of the present day topography in northwestern Ireland (Fig. 3.45). Possible Cenozoic displacements are suggested for the following faults: the northeast-trending Leannan, Gweebarra, Eglish, Aghla, Barneslough, Ox Mountains, Bangor, the Erriff fault, and two northeast-trending faults in the Nephin Beg Mountains; the east-trending Kittyfannan and Glencar faults; the northwest-trending Glenade fault, a northwest-trending fault in Glen Nephin and several northwest-trending faults in southern County Mayo (Fig. 3.45).

In northern County Donegal, northeast-trending faults down throw to the northwest. The northeast-trending Eglish-Belshade faults down throw to the southeast while the northeast-trending Laghy fault down throws to the northwest. Recent movement on these two faults might replicate the present day Donegal Bay. Most of the northeast-trending faults in County Mayo down throw to the northwest. If these sense of movements are correct, several stress systems are need to explain the kinematics.

To infer the age of the knickpoints, and thus place constraint on the timing of fault movement is a more difficult task. Knickpoint retreat depends on several variables. River terraces if datable, allow us to extrapolate the past history of a particular river including its response to tectonic activity. Various authors have shown in other parts of the world that rates of tectonic rock uplift or river incision may be inferred using the age and geometry of fluvial terraces (Rockwell *et al.* 1984; Bull and Kneufer 1987; Merritts *et al.* 1994). In general, there are few datable markers in the landscape of northwestern Ireland

that would allow determination of the timing of fault activity. Examples of offset across Palaeocene dykes have been recognised (Bennett *pers. comm.* 2001; Bennett and Phillips *in press*). Thus, I simply summarise the locations and inferred kinematics of possible tectonic displacements, in order to compare them for consistency with the tectonic history derived from offshore basin deposits and from elsewhere along the northwestern European continental margin. However, in the Owenmore River catchment in northern County Mayo, which is antecedent to the Nephin Beg Mountains, a sequence of strath and gravel fill terraces are preserved. In the next section these terraces will be described in order to understand the evolution of the Owenmore River.

3.9 Fluvio-glacial terraces on the Owenmore River, Bangor, County Mayo

3.9.1 Introduction

Not many rivers in northwestern Ireland seem to have left any evidence of their former beds or courses, in the form of strath or fill terraces. However, a sequence of terraces preserved along the Owenmore River, northwestern County Mayo, has the potential to reveal details of the incision history of the river. The Owenmore River, already discussed in Section 3.7.7, cuts across the axis of the Nephin Beg Mountains and has a broad convex-up longitudinal profile, which I argued is controlled by the Bangor fault. A series of fill and strath terraces are preserved along the Owenmore River (Plate 3.1 and 3.2) (Fig. 3.46). The aim of this section is to describe these terraces and discuss how and when they formed. This allows possibly estimation of river incision rates and discussion of the incision history of the river.

Fieldwork was done from Bellacorick Power Station to Bangor, County Mayo, along the river course. The lower part of the catchment, where the terraces are exposed, lies between Irish National Grid coordinates, 87000, 320000, and 95000, 324000. Bedrock exposures are most common along the Owenmore River or its tributaries. The position and altitude of bedrock, sand and gravel deposits were measured using a hand-held GPS receiver with a ±10m vertical accuracy.

3.9.2 Strath terraces

Strath terraces are sub-horizontal bedrock surfaces which mark the incised former river bed. If the river subsequently incises into its bed, strath terraces can be locally preserved along the valley walls. Sub-horizontal bedrock surfaces and exposures of the steep former channel walls were found intermittently along the Owenmore Valley cut into Carboniferous and Dalradian bedrock and overlain by variable thicknesses of sands and gravels (maximum 12 m) (Plate 3.3). These bedrock steps are located in at least five tributaries of the Owenmore River (Fig. 3.46) (Plate 3.4). They occur approximately 500 m away from the present course of the Owenmore River, in the outer part of meanders where lateral fluvial erosion is highest. Best exposure occurs within present-day tributary channels, where the streams flow over Carboniferous and Dalradian bedrock. The terrace risers, which mark the palaeo-channel walls, form steps that range in height from 2 to 6 m (Plate 3.5). The terrace treads are at least a few metres wide but hard to measure as they are covered on vegetation, till, sand and gravel deposits (Plate 3.3).

The Carboniferous bedrock consists of a sequence of alternating shales and sandstones; the shale is quite soft and easily erodible, possibly leaving the sandstone beds standing out as resistant ledges. Beds are horizontal or nearly horizontal, resulting in a stepped topography. This might lead to belief that the terrace treads are a consequence of differential erosion. However, the terraces form at similar elevations in both Carboniferous and Dalradian bedrock. Independent of the bedrock, and dip of the beds, they consistently lie about 50 m above the present bed of the Owenmore River, suggesting that they are remnants of a strath terrace. The steep walls of the bedrock terrace trends approximately parallel to the present Owenmore River, which also suggests that these terraces have a fluvial origin rather than being formed by simple differential erosion. From the evidence above, the bedrock surfaces are interpreted as a strath terrace, with ~50 m of river incision since strath formation (Fig. 3.47).

3.9.3 Sand and gravel deposits

Sands and gravels are deposited on top of the bedrock strath surfaces (Plate 3.3). At least two sets of sand and gravel deposits were identified of varying thickness (1-6 m) above bedrock (Plate 3.6 and 3.7). These are shown in Figure 3.45 as T-1 and T-2, T-2 being the oldest. When only one deposit was observed it was classified as T-2. T-2 was often present at both sides along the Owenmore River Valley (Plate 3.1 and 3.2).

Both T-1 and T-2 are composed of sand and gravels with sedimentary structures suggestive of fluvial deposition. The sand grains are medium to coarse and are often well sorted, well washed, and sometimes have sedimentary structures such as parallel lamination, cross bedding and graded bedding (Plate 3.8 and 3.9). They are found in beds with variable thickness, ranging from 5 cm to more than 1 m. Sands are often channelised between coarser clastic material (Plate 3.10) or lie parallel to the gravel beds.

Fill terrace deposits are composed of clastic material up to 12 m thick in places and extend up to 1 km along the valley (Plate 3.1 and 3.7). Clasts are of variable sizes, are often imbricated and sometimes graded. The gravels contain both well-rounded and subangular clasts. Some of the clasts were broken down in situ by frost shattering, indicating that cold climate conditions existed both before and after deposition (Plate 3.11 and 3.12). A mixture of rounded and very angular clasts suggests a relatively short transport distance. The clast imbrication indicates transport from east to west. Gravel composition is variable but the common presence of decalcified fossils (Plate 3.13 and 3.14) suggests transport from the Carboniferous basin deposits of northern County Mayo to the east. This east to west direction is consistent with the main direction of local Pleistocene ice flow (e.g., Coxon & Browne 1991). The gravels and sand in the fill terraces and overlying the straths may have been deposited during an interstadial period during ice melt, but the strath terrace may well be older than Quaternary.

The sand and gravel deposits are sometimes overlain by one or two levels of diamictions, which are unsorted deposits of unknown origin. These deposits are of variable thickness,

often poorly sorted, sub-angular, clast-supported conglomerates with a clay matrix. Approximately 1-2 m of organic peat material lie on top of the diamictions.

3.9.4 Palynological analyses

The ages of the strath terrace remnants would prove whether they are Quaternary or Tertiary. Determining an age is useful to estimate a rate of fluvial incision in the Owenmore River.

Eight organic-rich clay samples were taken immediately above the straths or within bedrock joints (Fig. 3.46) and analysed for their pollen content. Palynology provides a useful means of estimating the age of a sedimentary deposit based on the presence or absence of various marker species (Clayton and Coxon 1999). Palynology has been used in Ireland to date unconsolidated deposits as old as pre-Pliocene (Coxon and Coxon 1997). Analyses were carried out in the Palynology Laboratory in the Department of Geography, Trinity College by Dr. Peter Coxon. The procedure is explained in Appendix 2.

3.9.5 Palynological results

Pollen grains are abundant in most of the samples but no specific pre-Quaternary species were found (Table 3.1). Distinctive pollen was recognized in only four of the eight samples analysed including grains of *Corylus* (hazel), *Ericaceae* (heather), *Pinus* (pine), *Ulmus* (elm), *Alnus* (alder), *Betula* (birch), *Calluna* and *Polipodium*.

Ulmus disappeared due to disease 4000 years ago and *Alnus* first appeared 7500 years ago (Bradshaw 2001). Sample 2 contained abundant *Ulmus* and some *Alnus* pollen grains indicating an age between 7500 and 4000 years. Sample 2 also contained four pollen grains of *Corylus* and twenty pollen grains of *Ericaeae.* Sample 3, which contains grains of *Ericaceae*, *Pinus,* grass and *Betula*, may be pre-Holocene in age. Sample 5 contained a *Betula* pollen grain with an odd shape (betuloides) and is not likely to be pre-Quaternary.

Although the overall abundance of pollen in the samples was promising the study concluded a Holocene age for the sand and gravel deposits and a minimum age of Holocene for the strath terraces.

3.10 Conclusions

(1) Many of the river profiles in northwestern Ireland are out of equilibrium and contain knickpoints. Some of the knickpoints in northwestern Ireland have a strong lithological control. In particular, metadolerite intrusions control a number of knickpoints, with examples on the Leannan and Bunlin Rivers in northeastern County Donegal; the Clady River in northwestern County Donegal; the Owenboy River in the Ox Mountains; and the Glencullin River in southern County Mayo. Formational contact knickpoints are also commonly found where lithology changes from a Dalradian quartzite to a pelite (e.g. Slieve Tooey Quartzite Formation to Termon Pelite Formation), Ordovician sandstones to slates (e.g. Mweelrea Formation to Glenumera Formation) or at intraformational contacts like the limestone member in the Downpatrick Sandstone Formation.

(2) Knickpoints are sometimes located upstream of faults within the same geological formation. In these particular cases knickpoint formation must have a structural control. The presence of knickpoints in several catchments flowing across the same fault might suggest recent tectonic activity on that particular fault. However, preferential erosion along a fault zone is also a possibility.

(3) A regional morphometric and lithological analysis concludes that the topography of northwestern Ireland cannot be explained solely by differential erosion due to lithology only and a partial structural control is suggested particularly for the Partry Mountains, Mweelrea Mountains, Sligo Mountains, Ox Mountains and Derryveagh Mountains. Some fault-bounded topography has a present-day relief of up to 500 m. Topographic scarps

within the same lithological formation also suggest a structural control on the topography.

(4) Movement on a number of faults is inferred from a combination of evidence, including river knickpoints, morphological anomalies, non-lithologically controlled high relief and wind gaps. Cenozoic displacements are suggested for the Leannan, Gweebarra, Barneslough, Aghla, Kittyfannan, Eglish-Belshade, Laghy, Glenade, Glencar, Ox Mountains, Bangor and Errif faults. These faults trend northeast, east and northwest. From the topography and river knickpoint formation, one can infer a down throw direction. Most of the faults seem to have been down thrown to the northwest, a conclusion consistent with that of Dewey (2000), and one that is compatible with fault movement along offshore northwest Ireland in the eastern Irish Rockall Basin. The depositional and structural history of the Rockall Basin is the subject of Chapter 4.

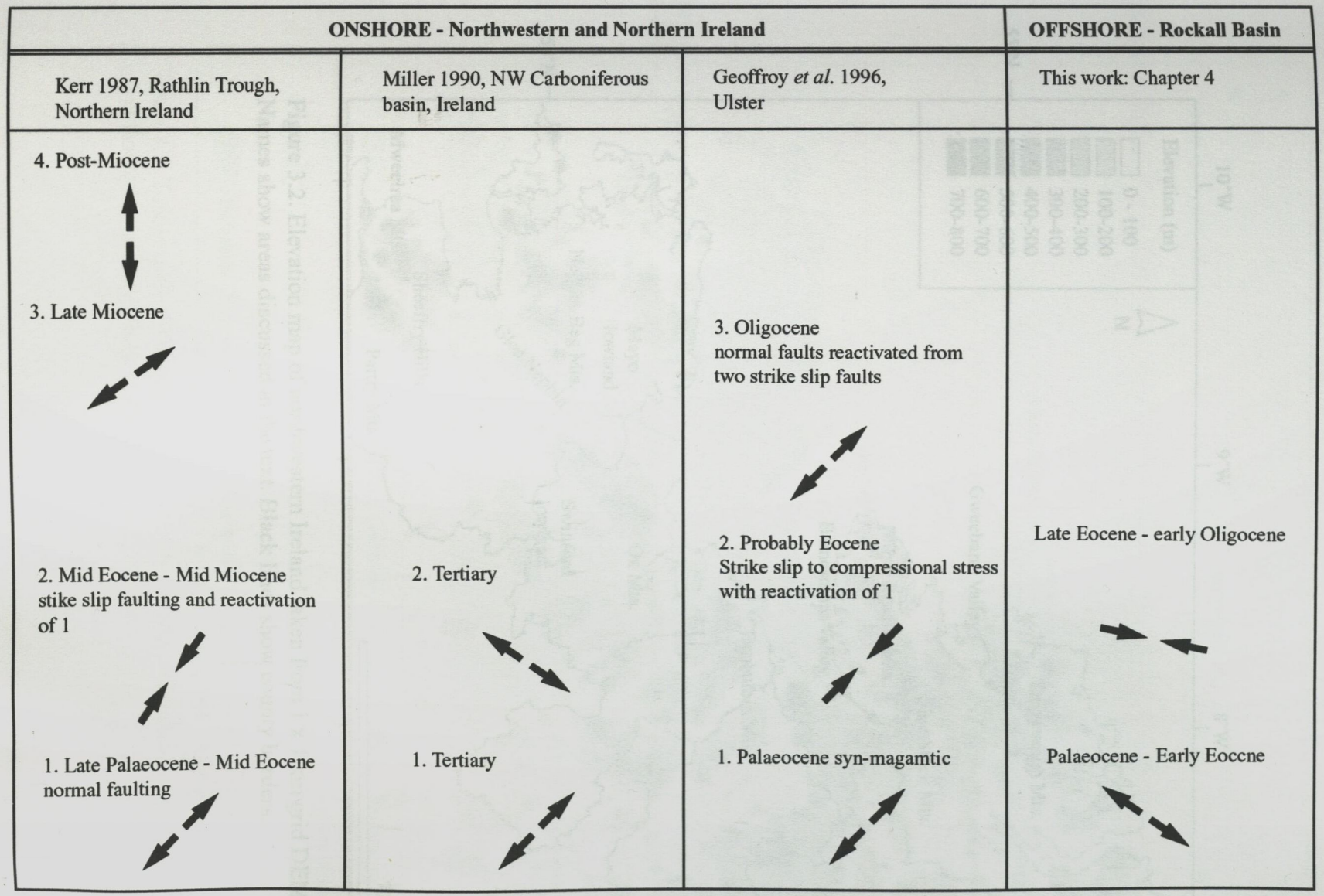


Figure 3.1. A comparison of Tertiary extension directions inferred from fault analysis in the northwestern Irish margin from various sources. Fault analysis was done measuring fractures, fault displacement and shortening from outcrop bedrock onshore and seismic data offshore. Stress directions are only approximations, given the heterogeneities of the upper crust.

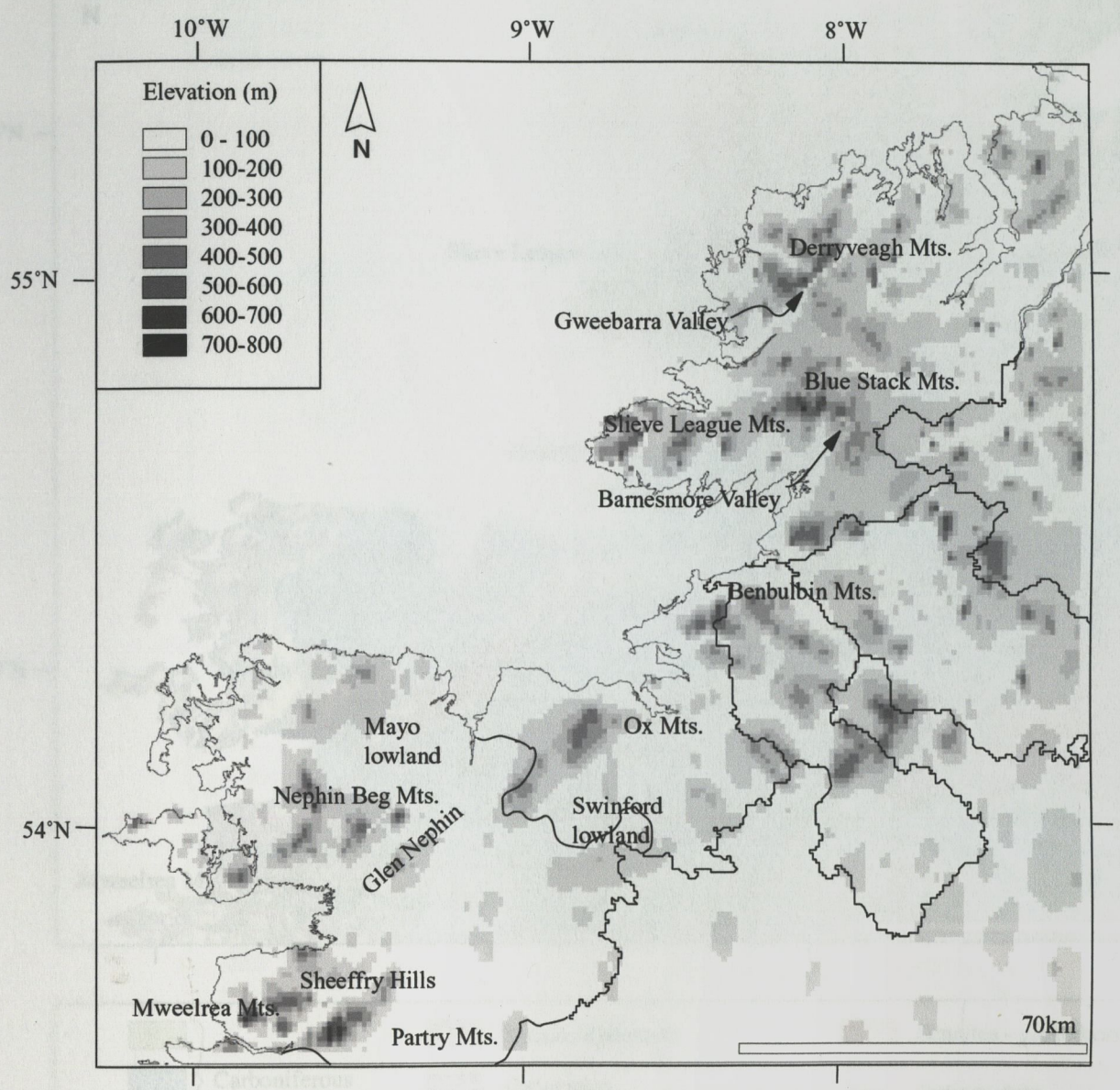


Figure 3.2. Elevation map of northwestern Ireland taken from 1 x 1 km grid DEM. Names show areas discussed in the text. Black lines show county borders.

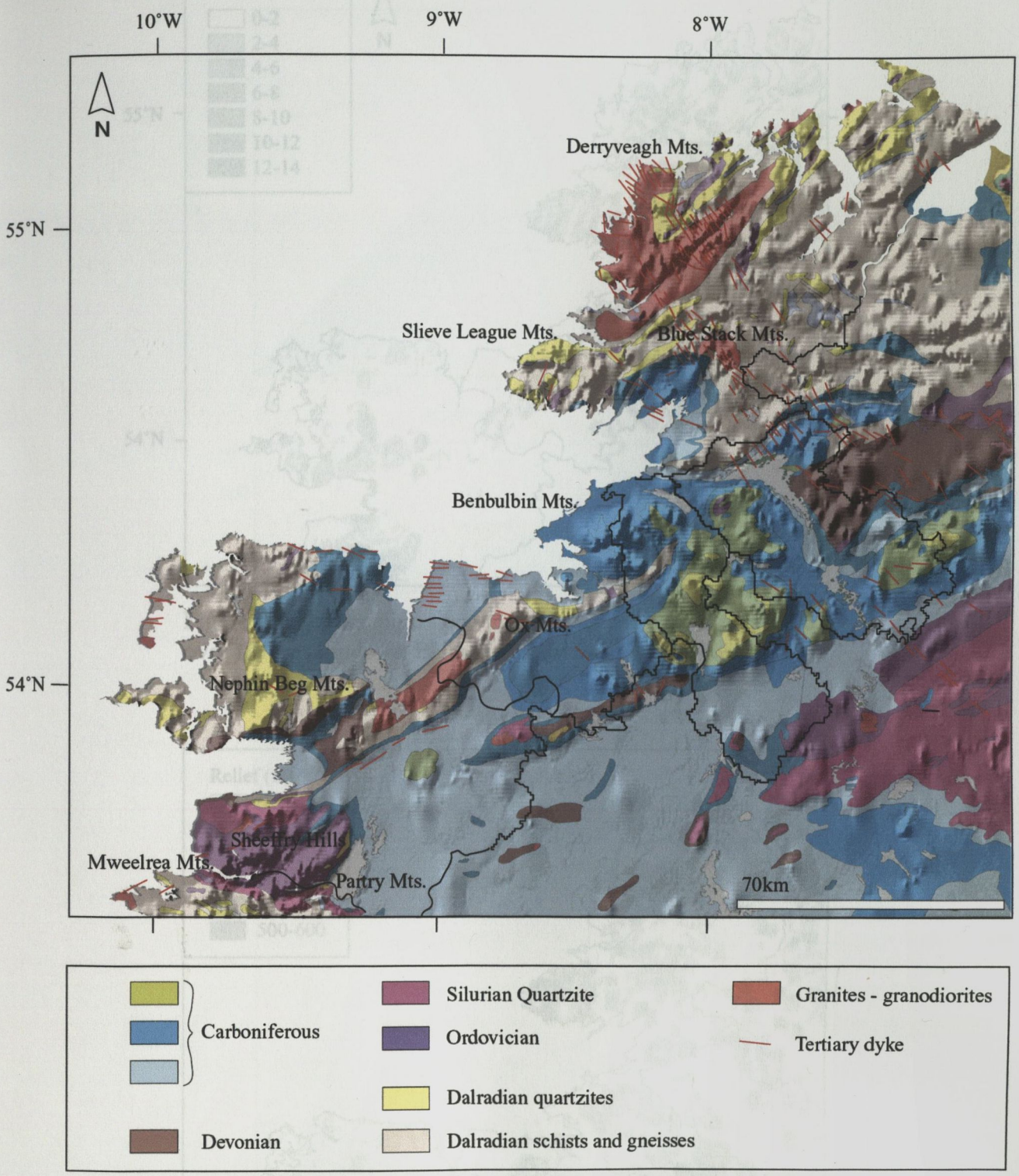


Figure 3.3. Topographic hillshade at 45° from the northwest and generalised bedrock geology in northwestern Ireland. Black line shows county oultine.

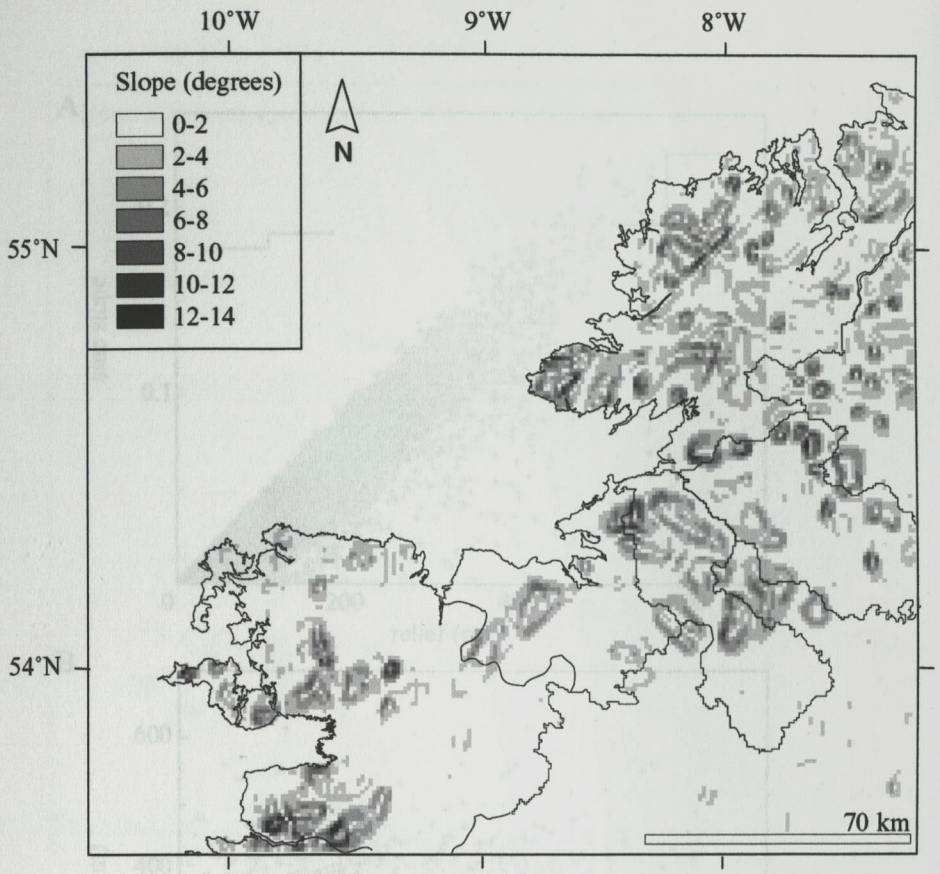


Figure 3.4. Topographic slope in northwestern Ireland measured over 1x1 km windows. Black line shows county outline.

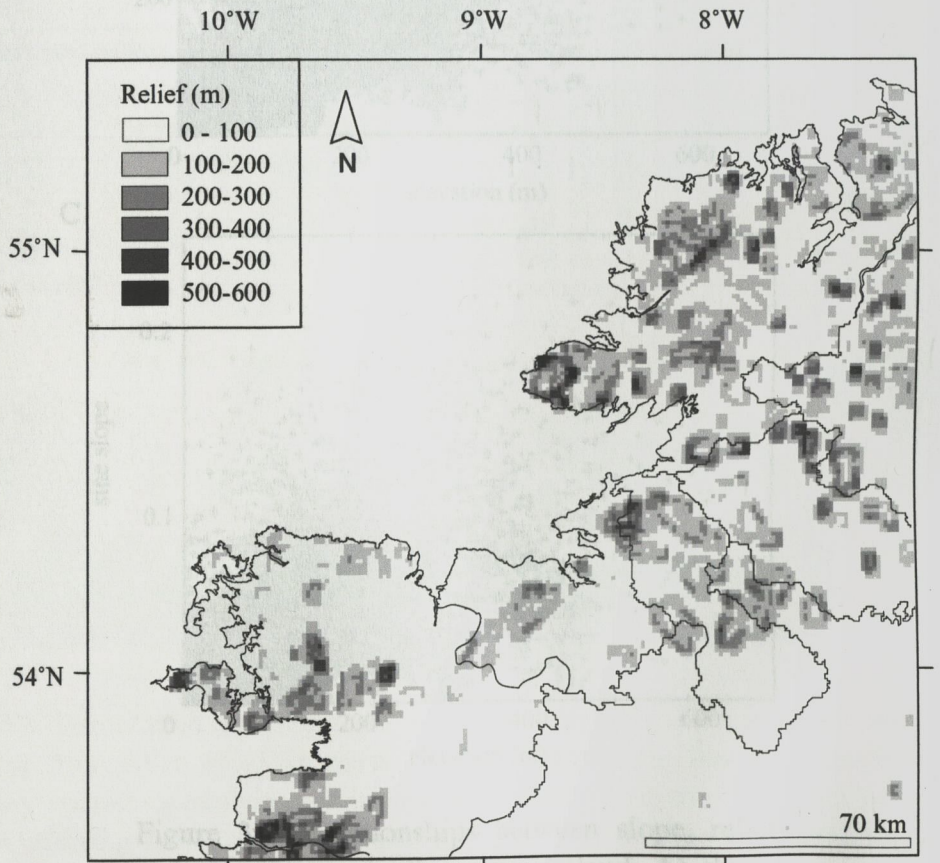


Figure 3.5. Relief in northwestern Ireland measured over 1x1 km windows. Black line shows county outline.

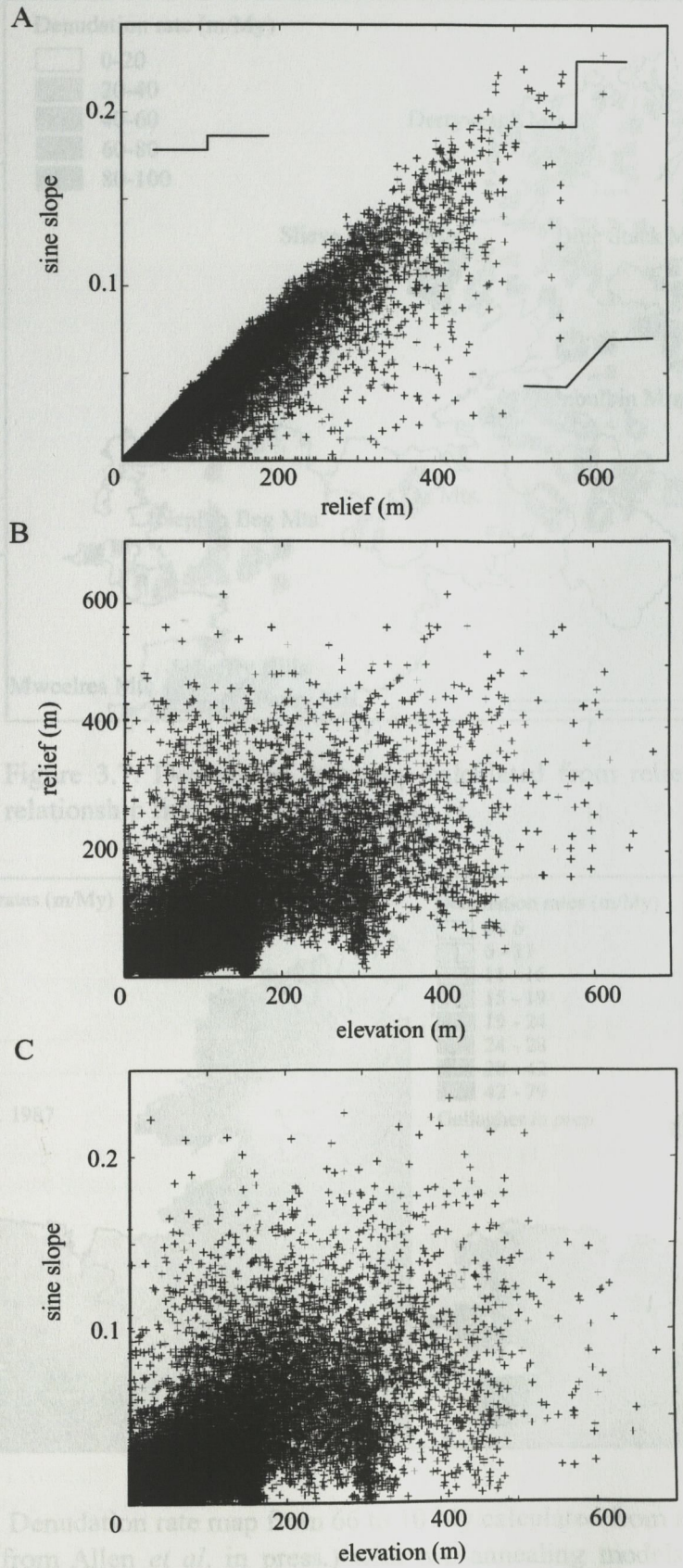


Figure 3.6. Relationships between slope, relief and elevation in northwestern Ireland. A) shows sketches of hypothetical slope-relief relationships.

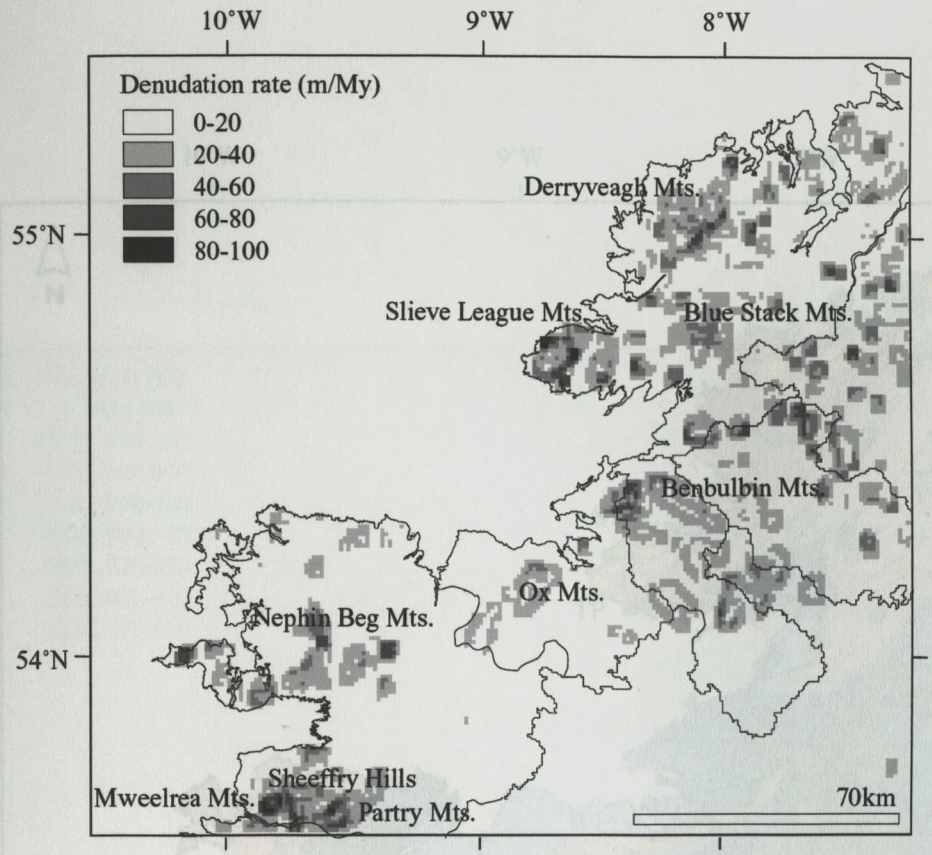


Figure 3.7. Denudation rate map calculated from relief using relationship from Ahnert (1970) (eq. 1).

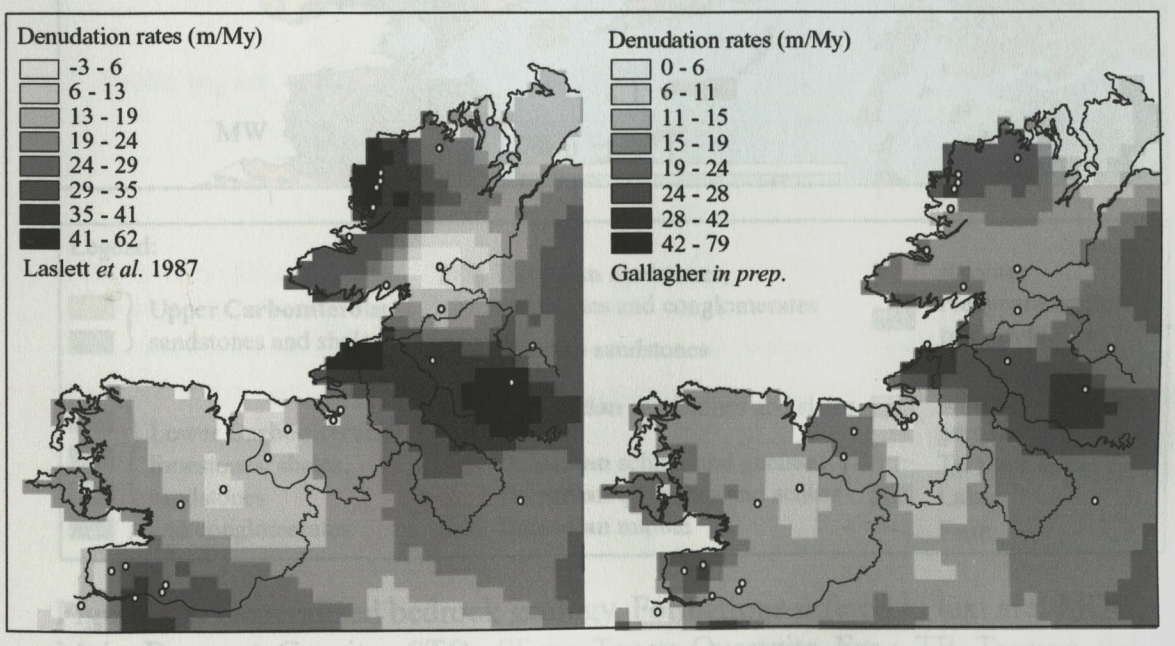


Figure 3.8. Denudation rate map from 66 to 10 My calculated from apatite fission track data (modified from Allen *et al.* in press.) with two annealing models. Models are based on laboratory annealing experiments in Durango apatite. Laslett *et al.* (1987) model is biased towards inferring rapid, recent cooling from 60°C to surface temperatures, and therefore overestimates denudation in the most recent time interval. Gallagher (*in prep.*) is a preliminary new annealing model that accounts for the low temperature limitations in the Laslett *et al.* (1987) model.

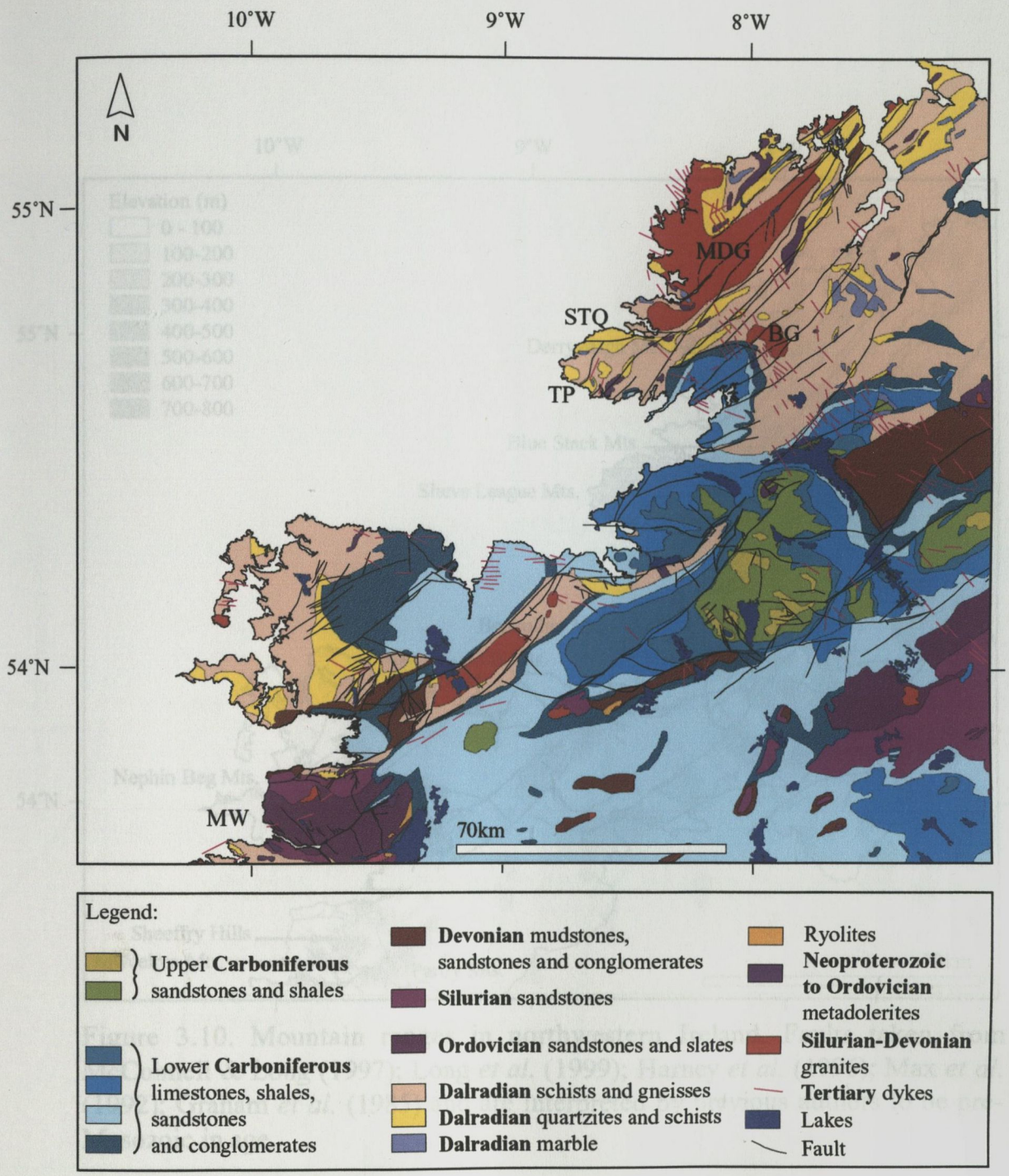


Figure 3.9. Generalised bedrock geology. Formations refered in text are: MDG, Main Donegal Granite; STQ, Slieve Tooey Quartzite Fm.; TP, Termon Pelite Fm.; BG, Barnesmore Granite; MW, Mweelrea Formation.

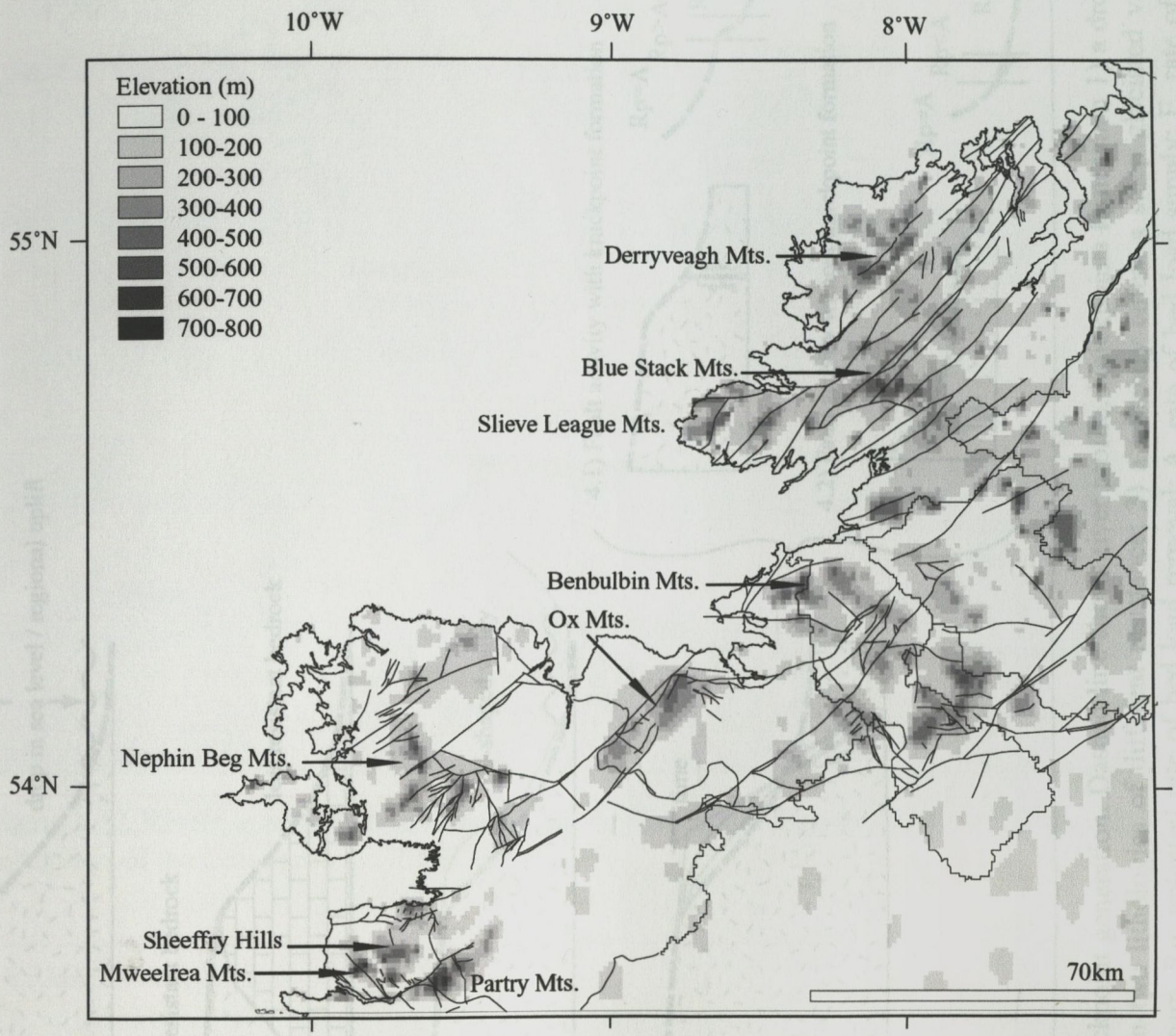


Figure 3.10. Mountain ranges in northwestern Ireland. Faults taken from McConnell & Long (1997); Long *et al.* (1999); Harney *et al.* (1996); Max *et al.* (1992); Graham *et al.* (1985) and are interpreted by previous authors to be pre-Mesozoic in age.

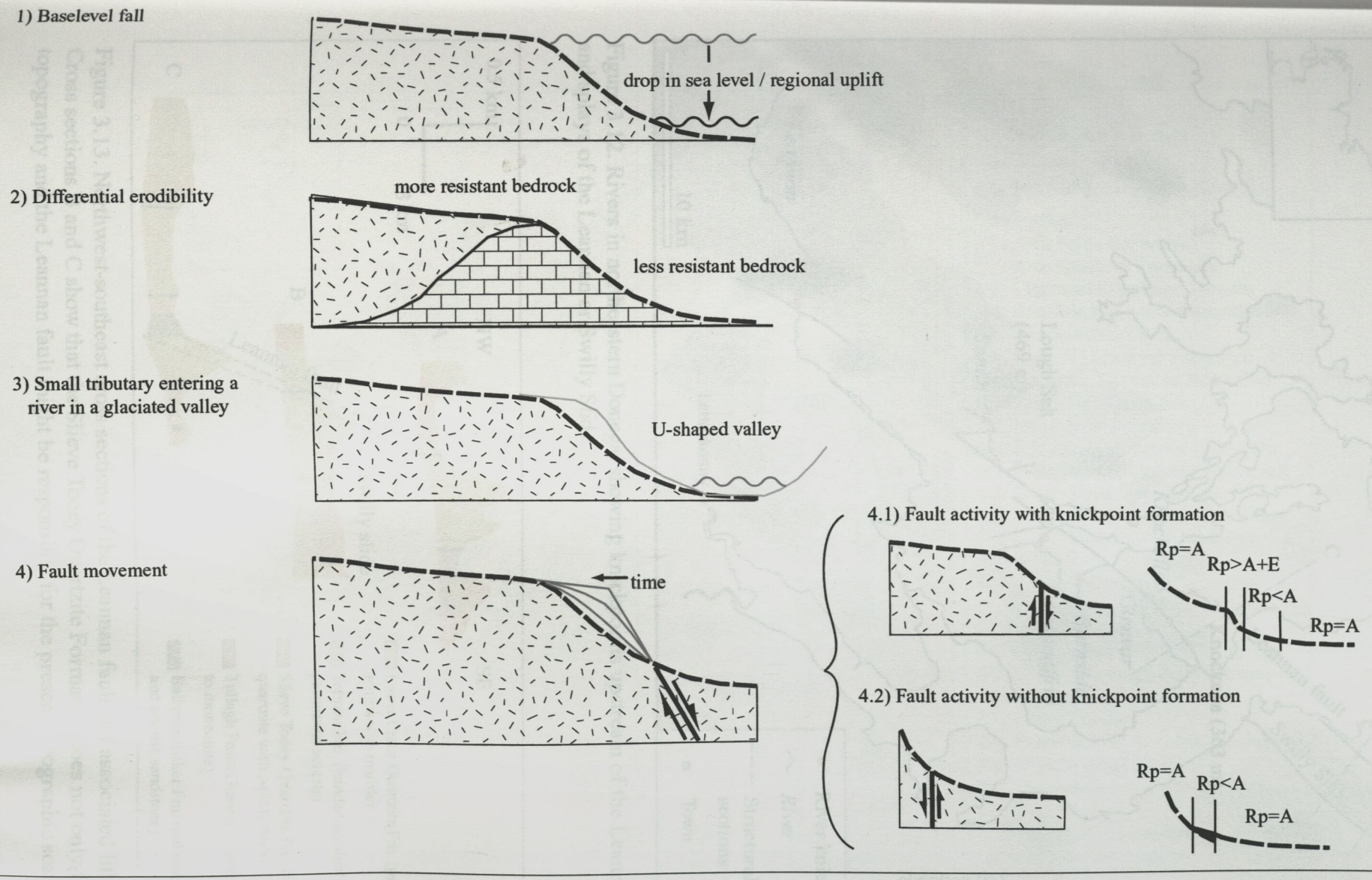


Figure 3.11. Four different mechanisms of knickpoint generation. Dashed line shows river profile. Knickpoints form when 1) a drop in sea level or regional uplift occurs; 2) the river flows in two lithologies of different resistance; 3) a tributary enters a steep glaciated valley; 4) fault movement with the downthrow block downstream. Rp, potential rate of bed load removal; A, rate of bed load supply; E, rate of local vertical incision.

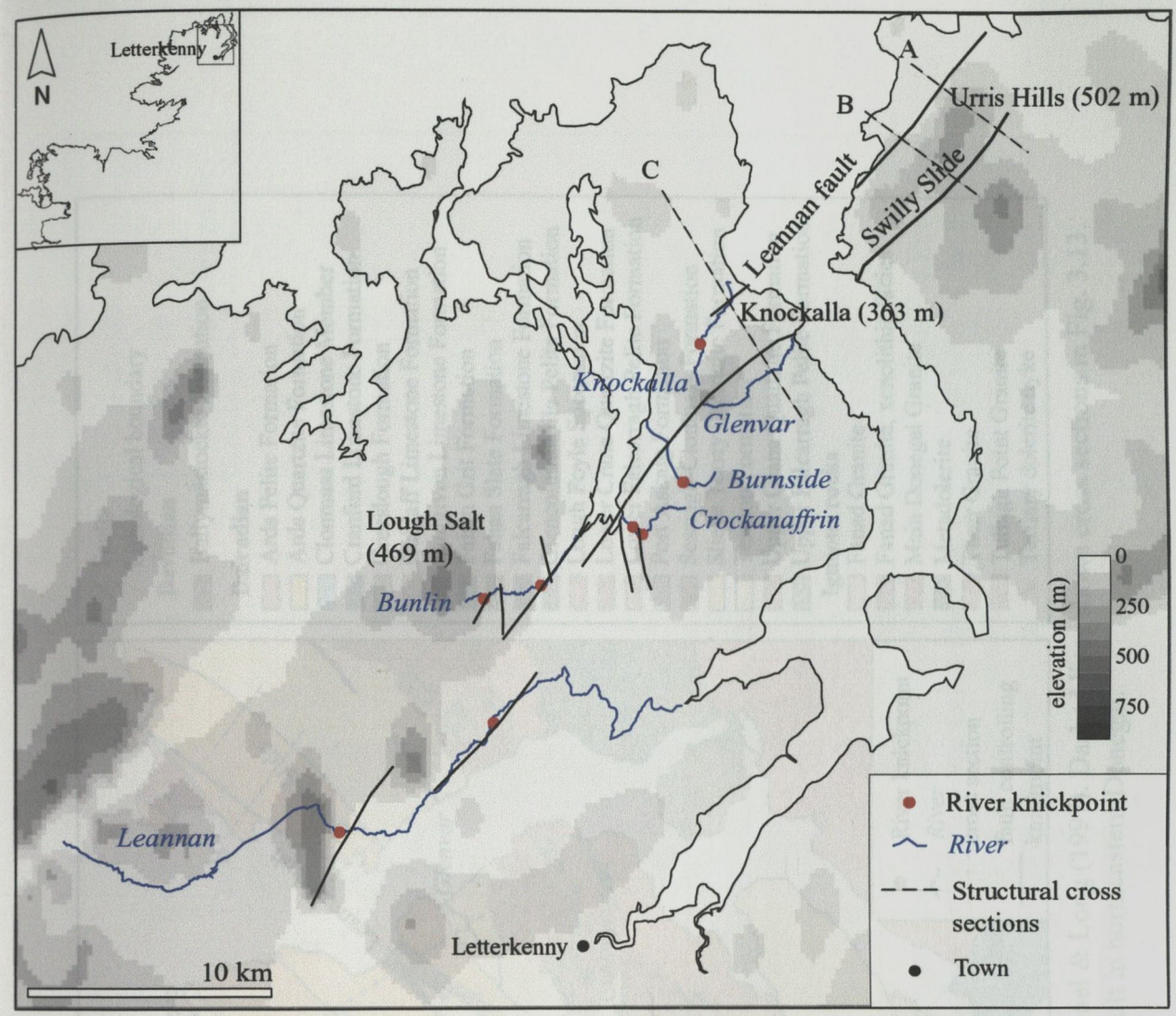


Figure 3.12. Rivers in northeastern Donegal showing knickpoints upstream of the Leannan fault and splays of the Leannan or Swilly Slide.

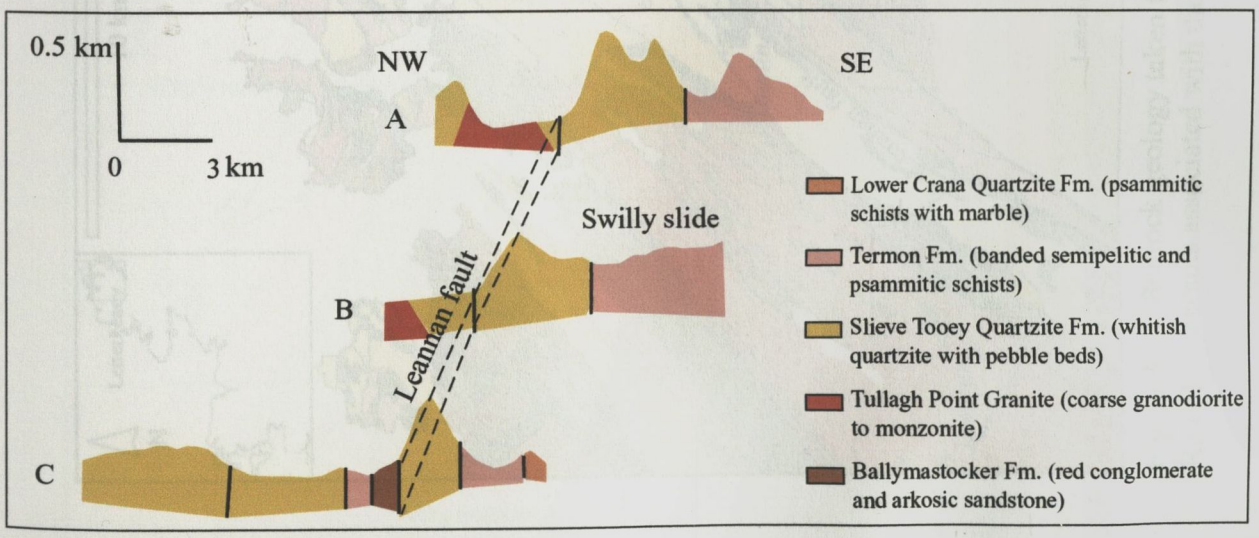


Figure 3.13. Northwest-southeast cross sections of the Leannan fault and associated lithology. Cross sections B and C show that the Slieve Tooey Quartzite Formation does not only form high topography and the Leannan fault might be responsible for the present topographic scarp.

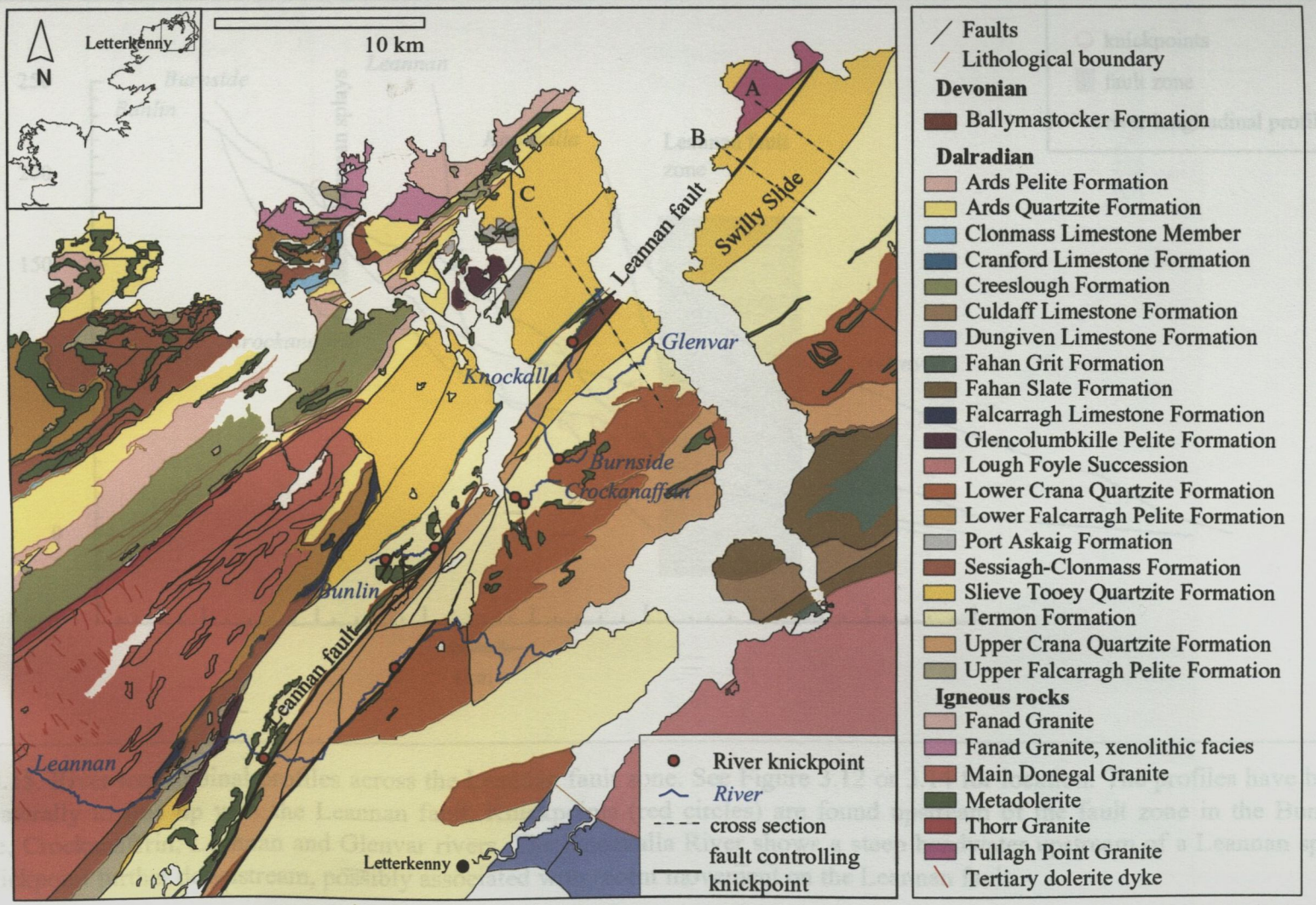


Figure 3.14. Bedrock geology taken from McConnel & Long (1997). Dashed lines shows cross sections in Fig. 3.13. River knickpoints associated with the Leannan fault in northeastern Donegal.

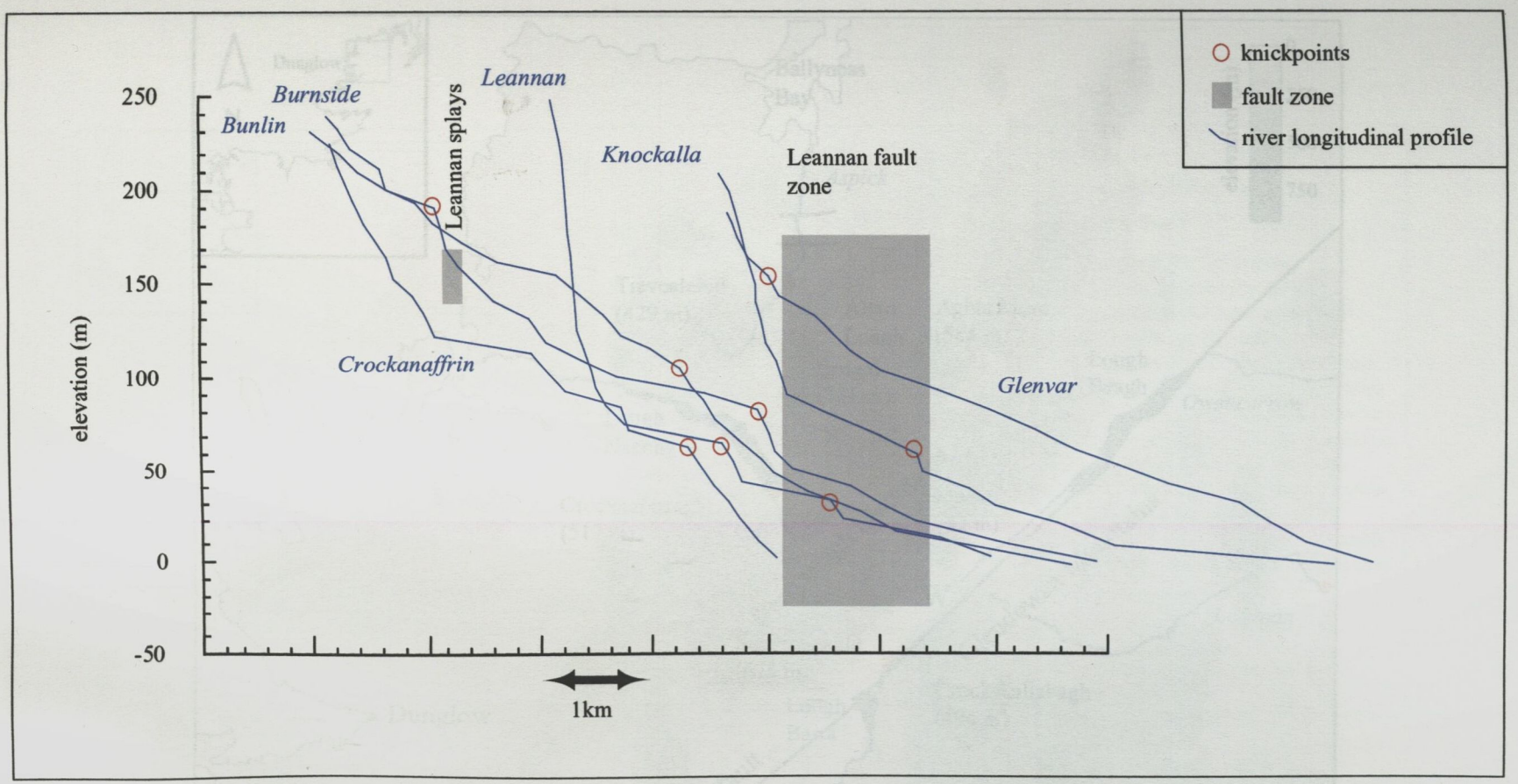


Figure 3.15. River longitudinal profiles across the Leannan fault zone. See Figure 3.12 or 3.14 for location. The profiles have been shifted laterally to line up with the Leannan fault. Knickpoints (red circles) are found upstream of the fault zone in the Bunlin, Burnside, Crockanaffrin, Leannan and Glenvar rivers. The Knockalla River shows a steep headwater upstream of a Leannan splay and a knickpoint further downstream, possibly associated with recent movement on the Leannan fault.

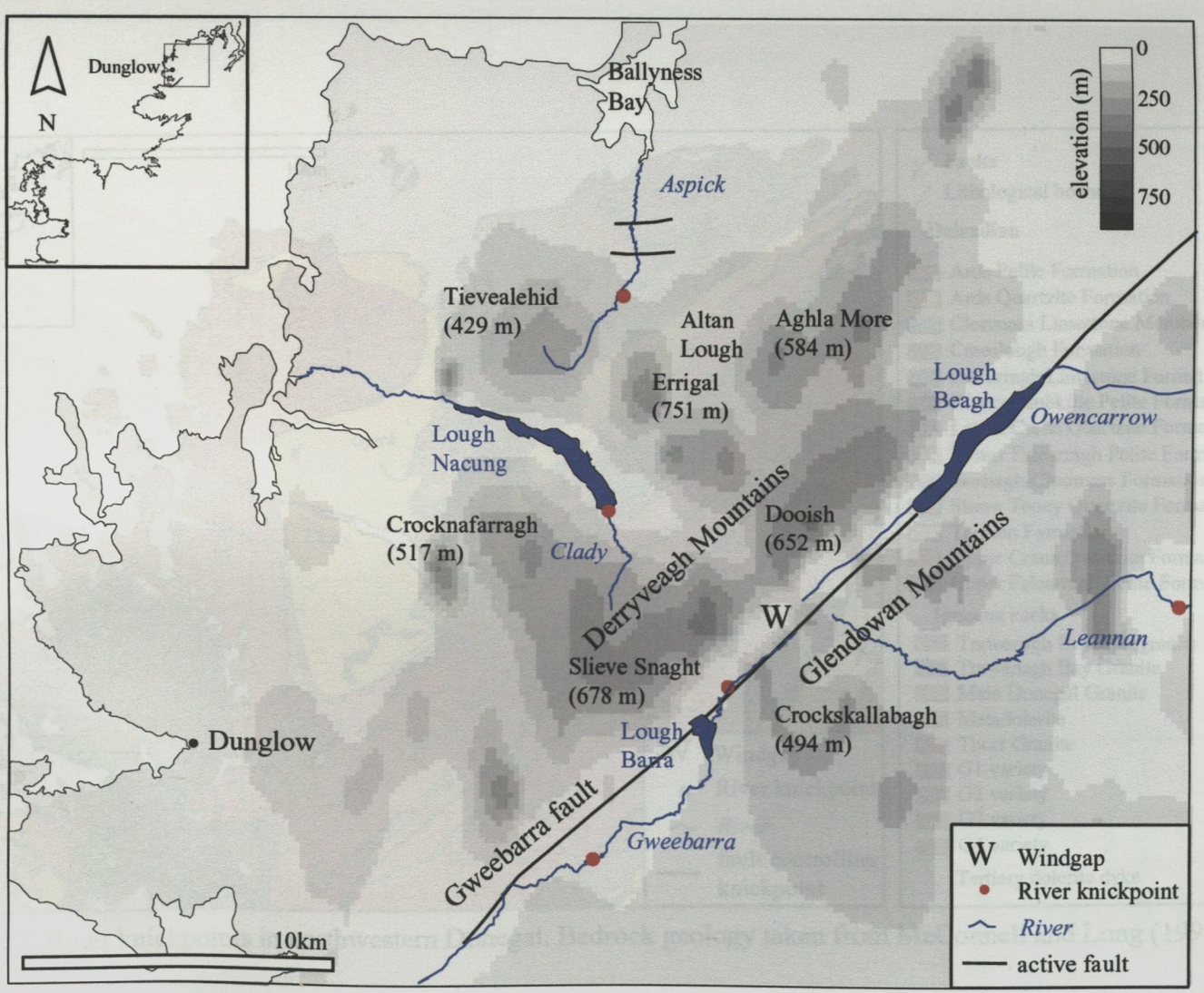


Figure 3.16. Rivers and knickpoints in northwestern Donegal.

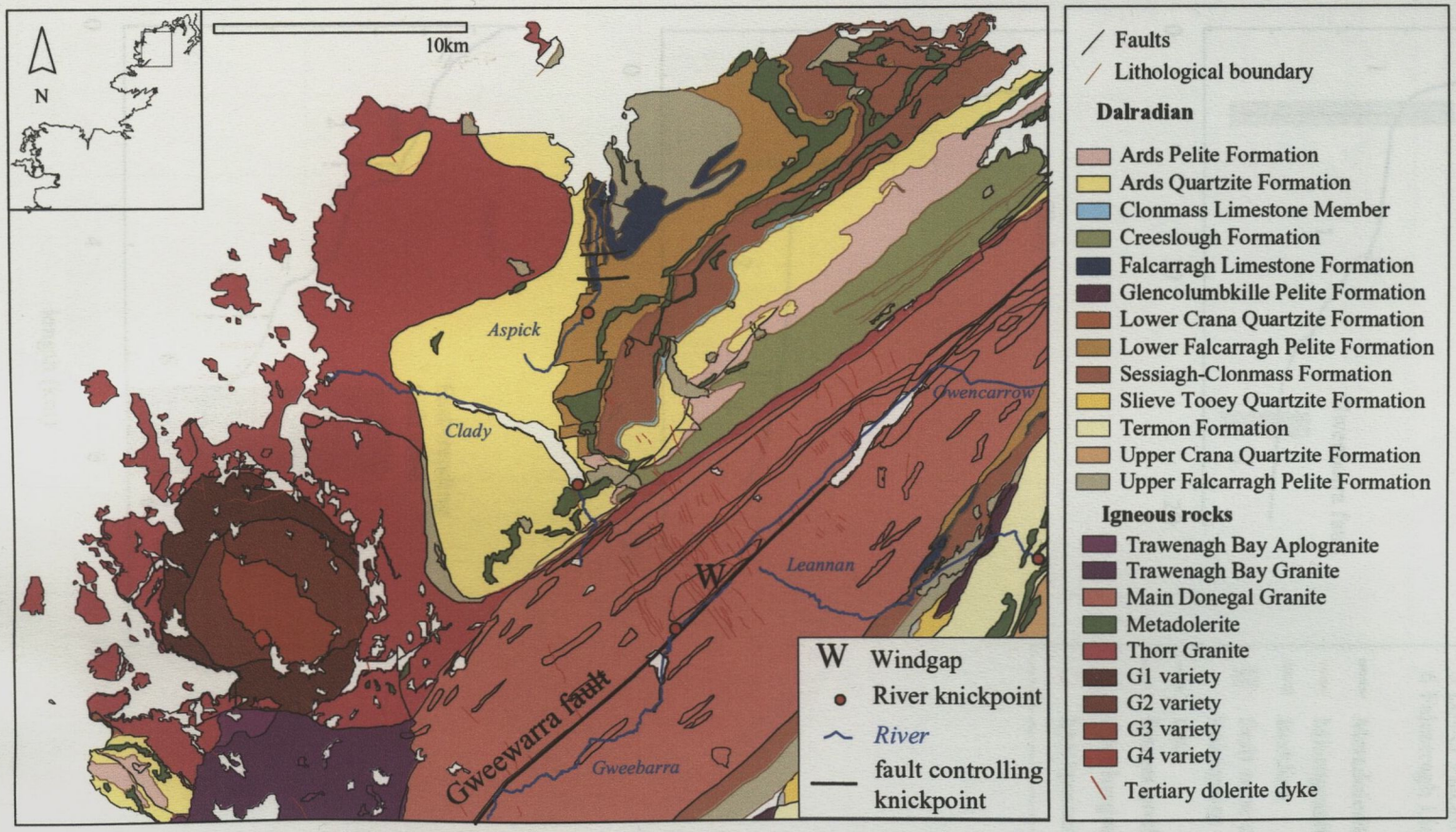


Figure 3.17. River knickpoints in northwestern Donegal. Bedrock geology taken from McConnell and Long (1997).

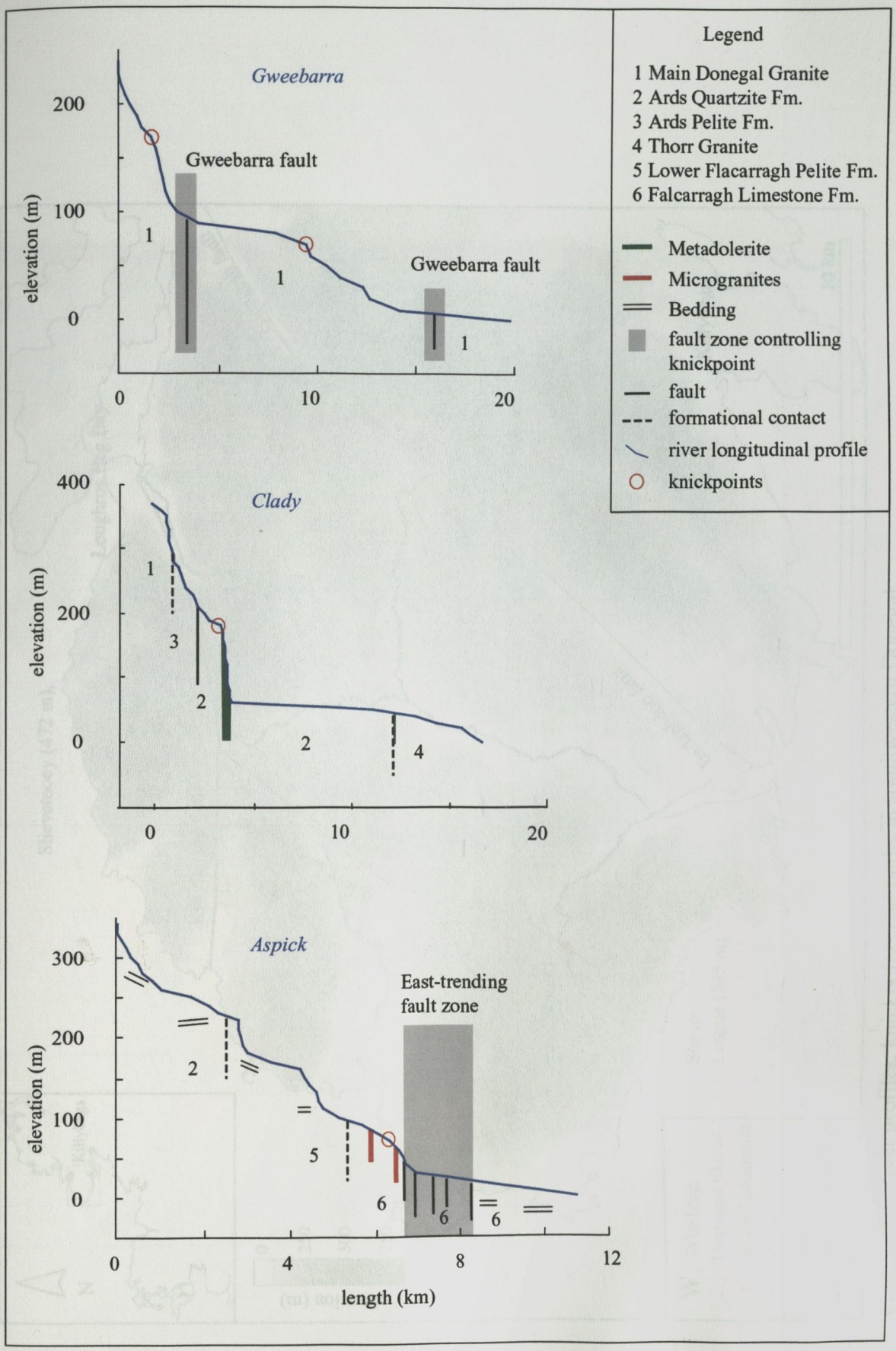


Figure 3.18. River longitudinal profiles and knickpoints from the Derryveagh Mountains.

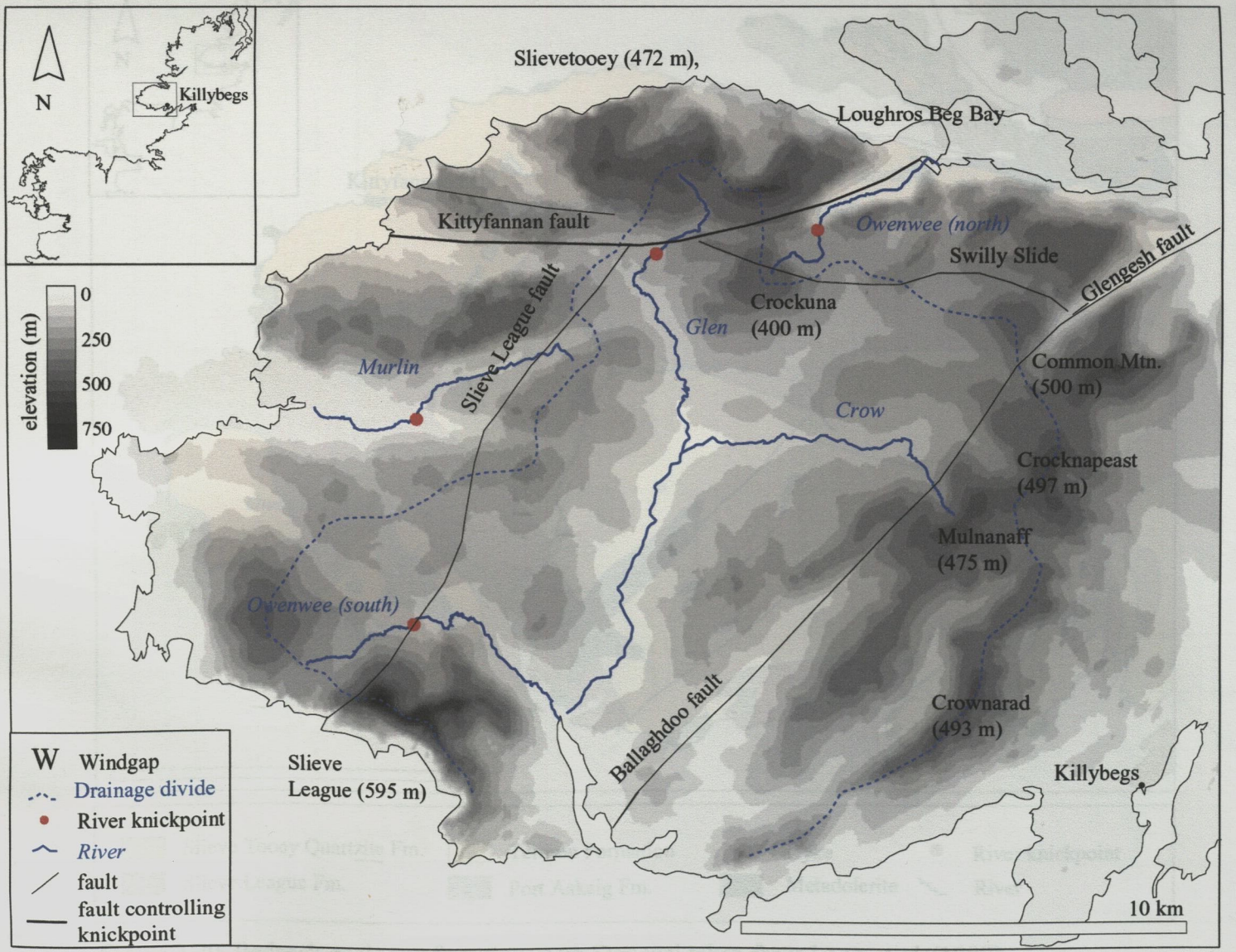


Figure 3.19. River profiles, knickpoints and faults in southwestern Donegal.

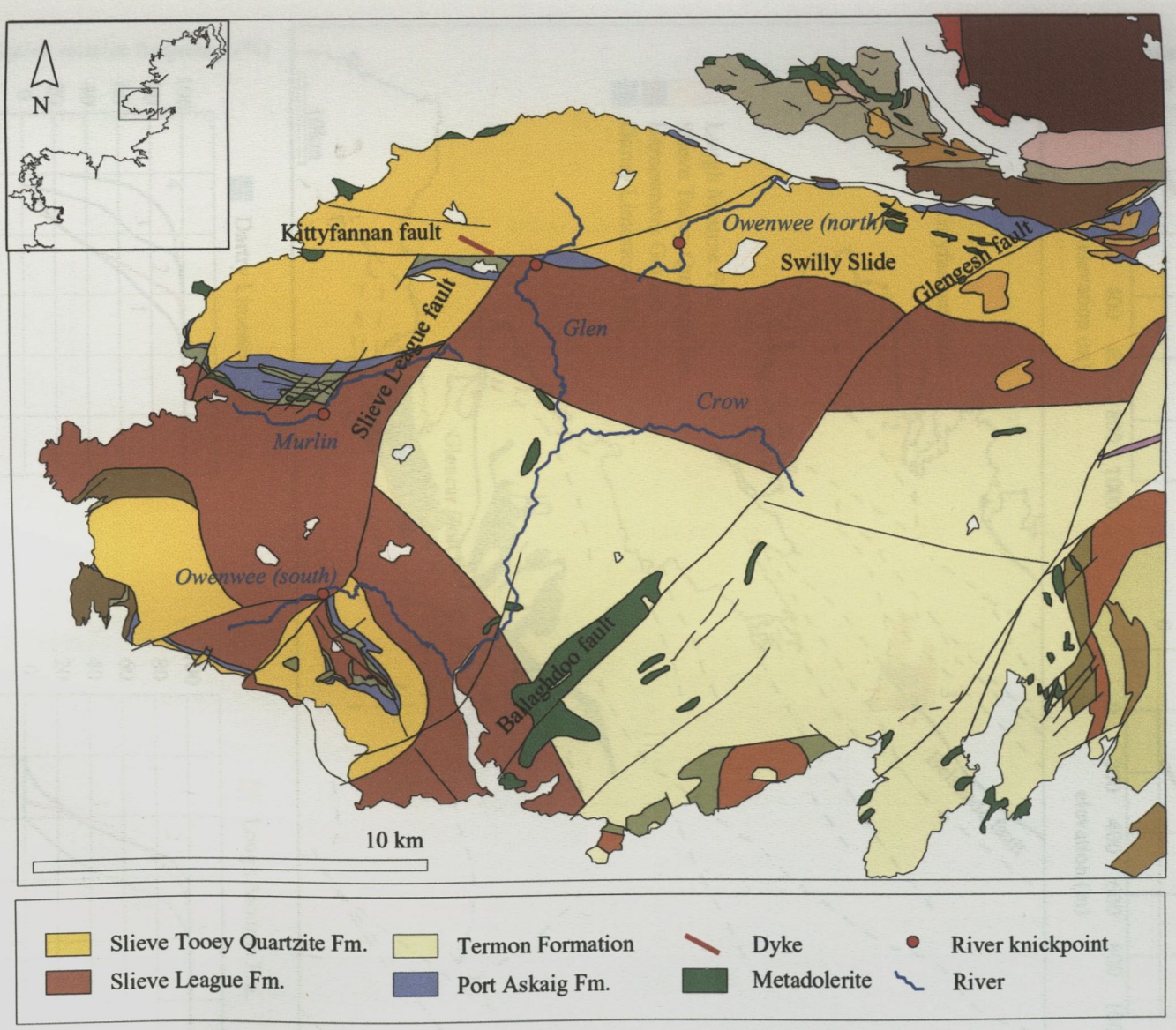


Figure 3.20. Bedrock geology of southwestern Donegal taken from Long *et al.* (1999).

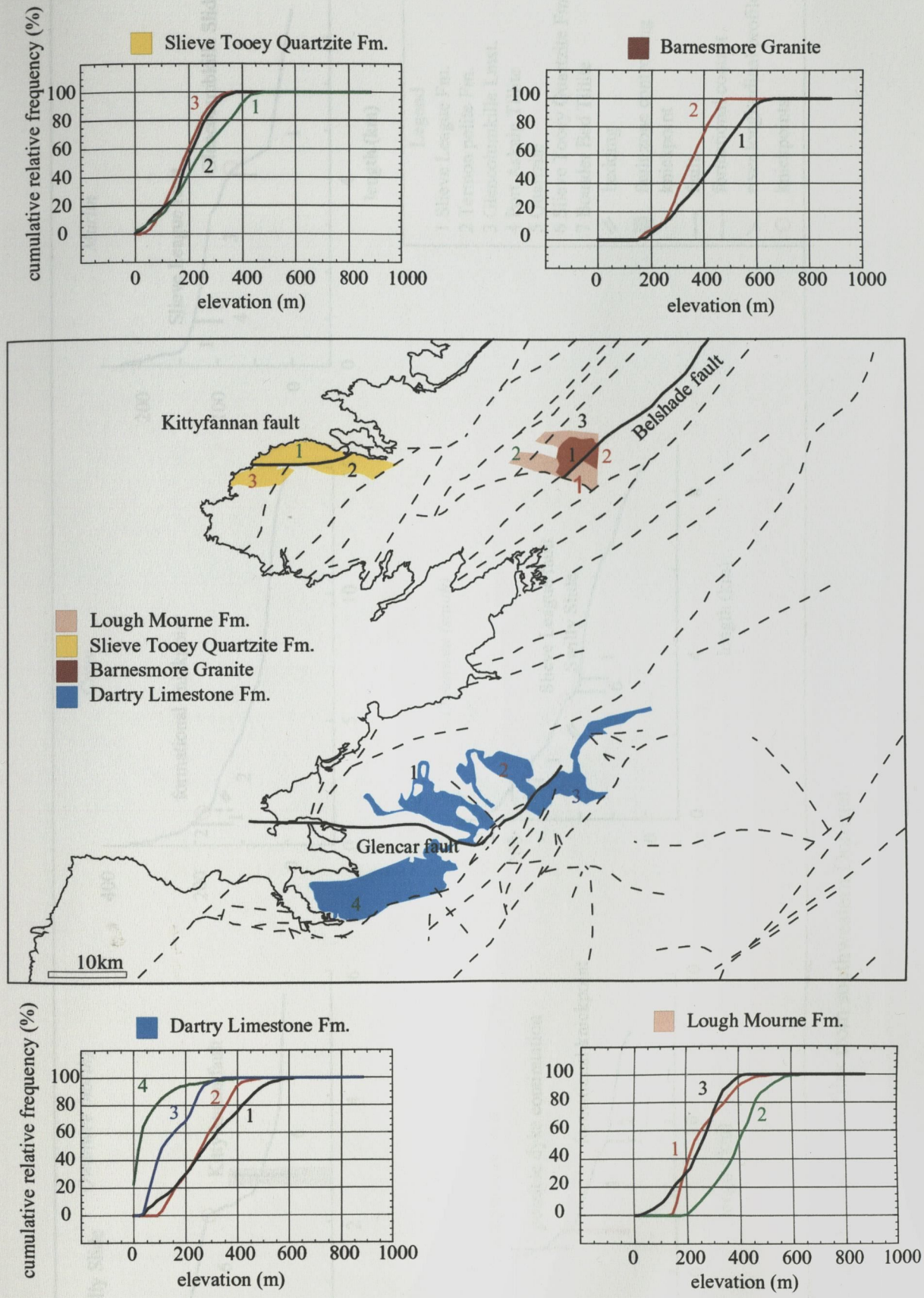


Figure 3.21. Comparison of elevation distributions within the same formation across faults. Solid lines are faults with different elevation distributions in the same formation on either side. Dashed lines are other faults and are modified from Long *et al.* (1999) and Harney *et al.* (1996).

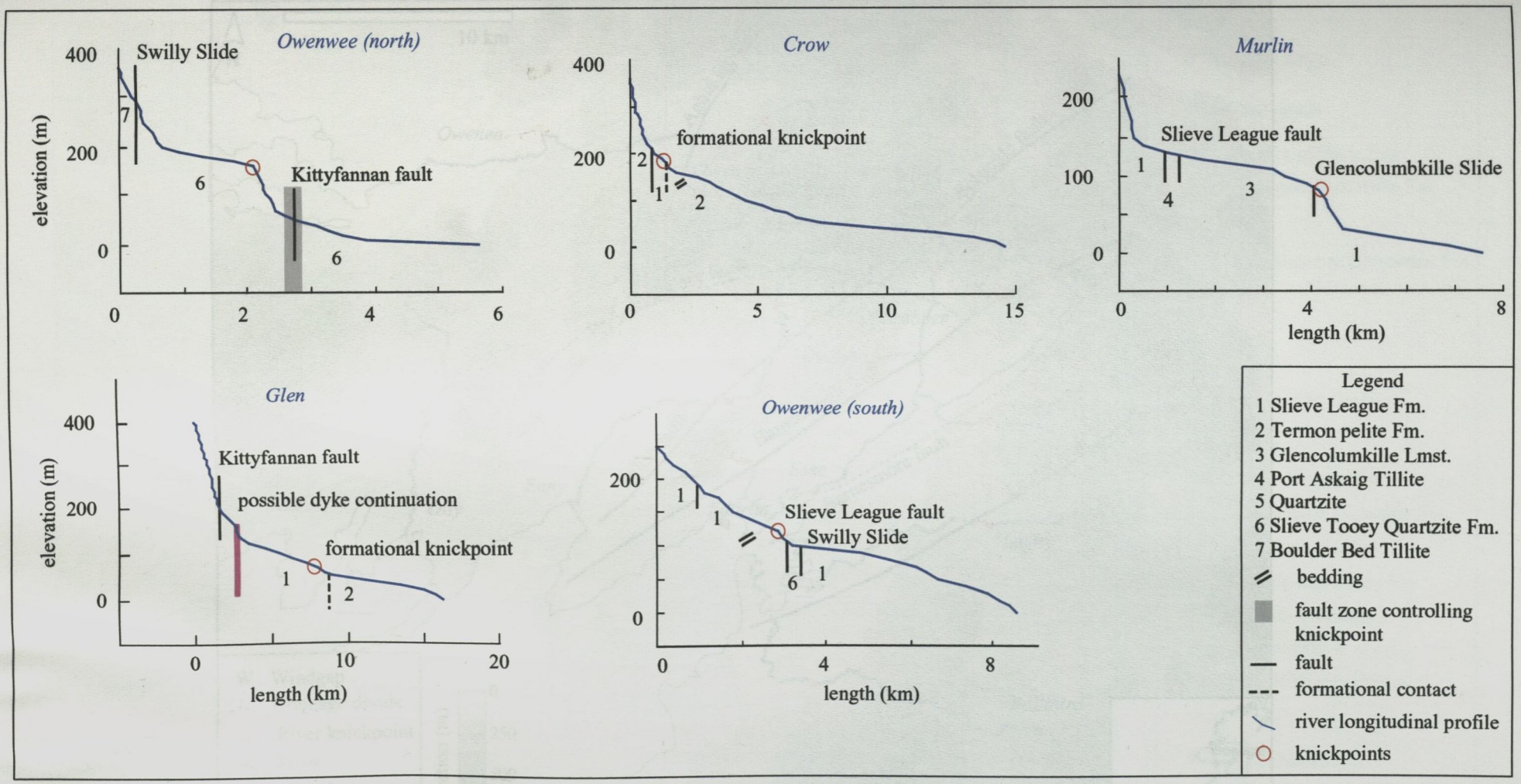


Figure 3.22. Longitudinal river profiles from southwestern Donegal.

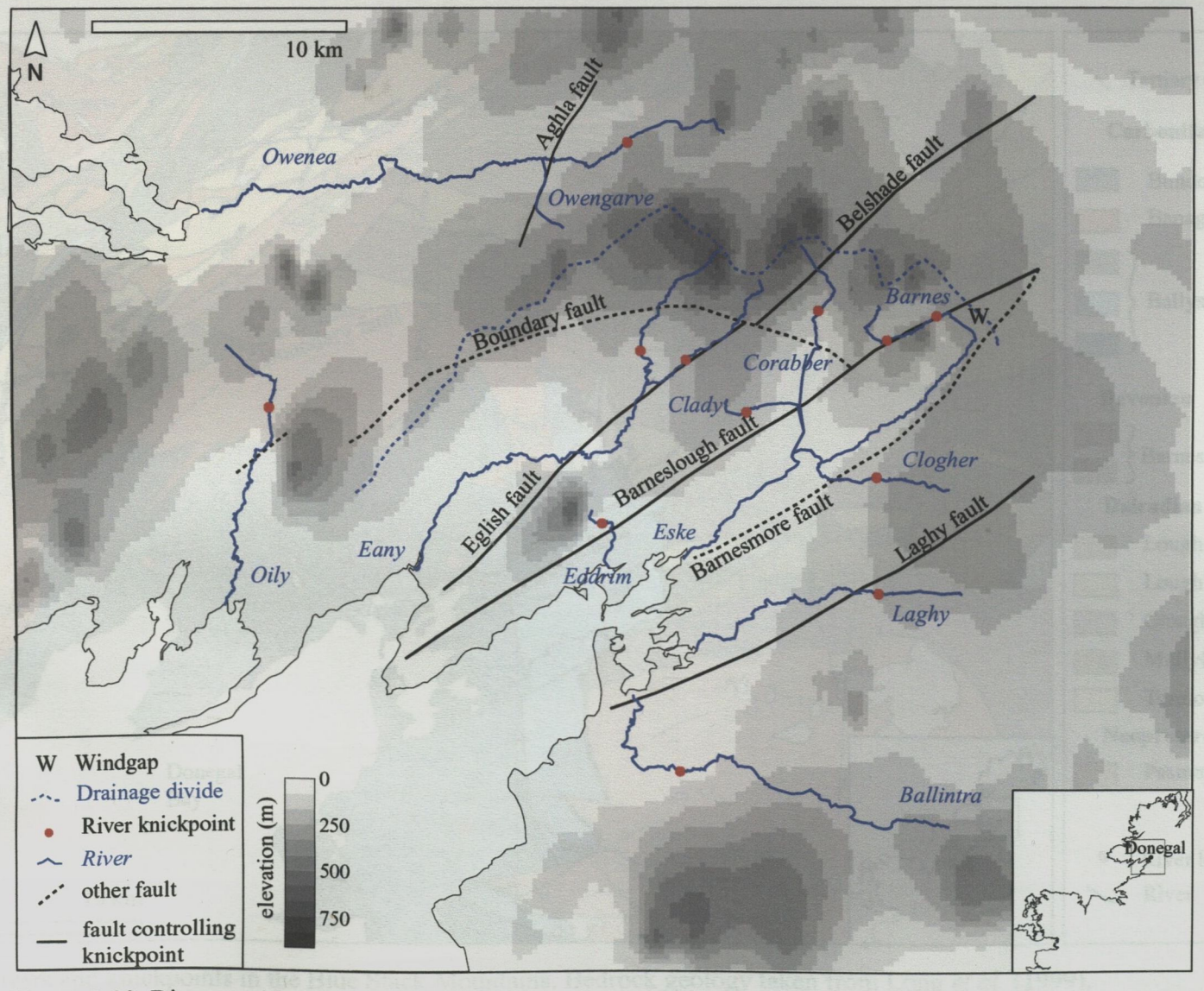


Figure 3.23. Rivers and knickpoints in the Blue Stack Mountains.

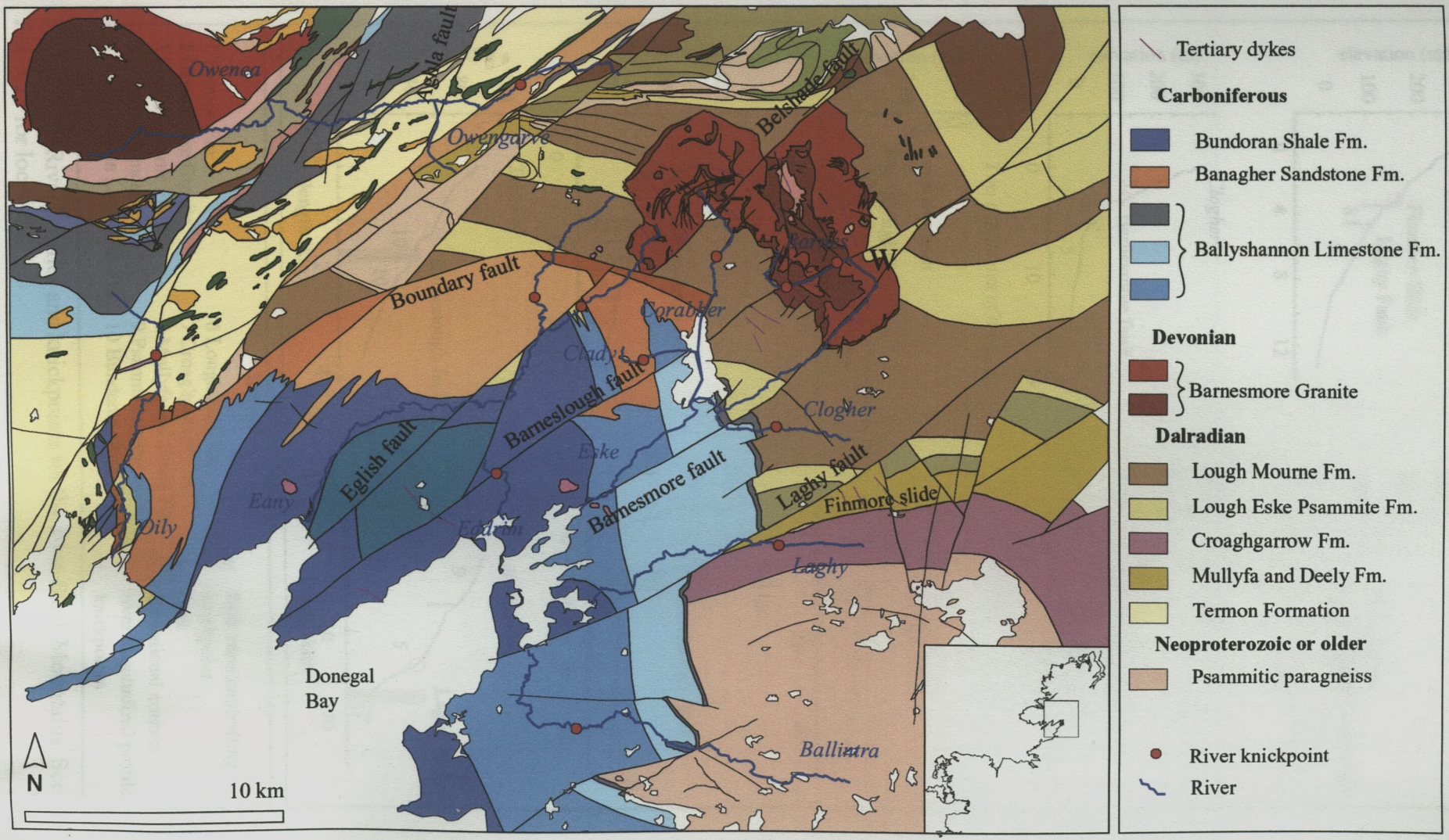
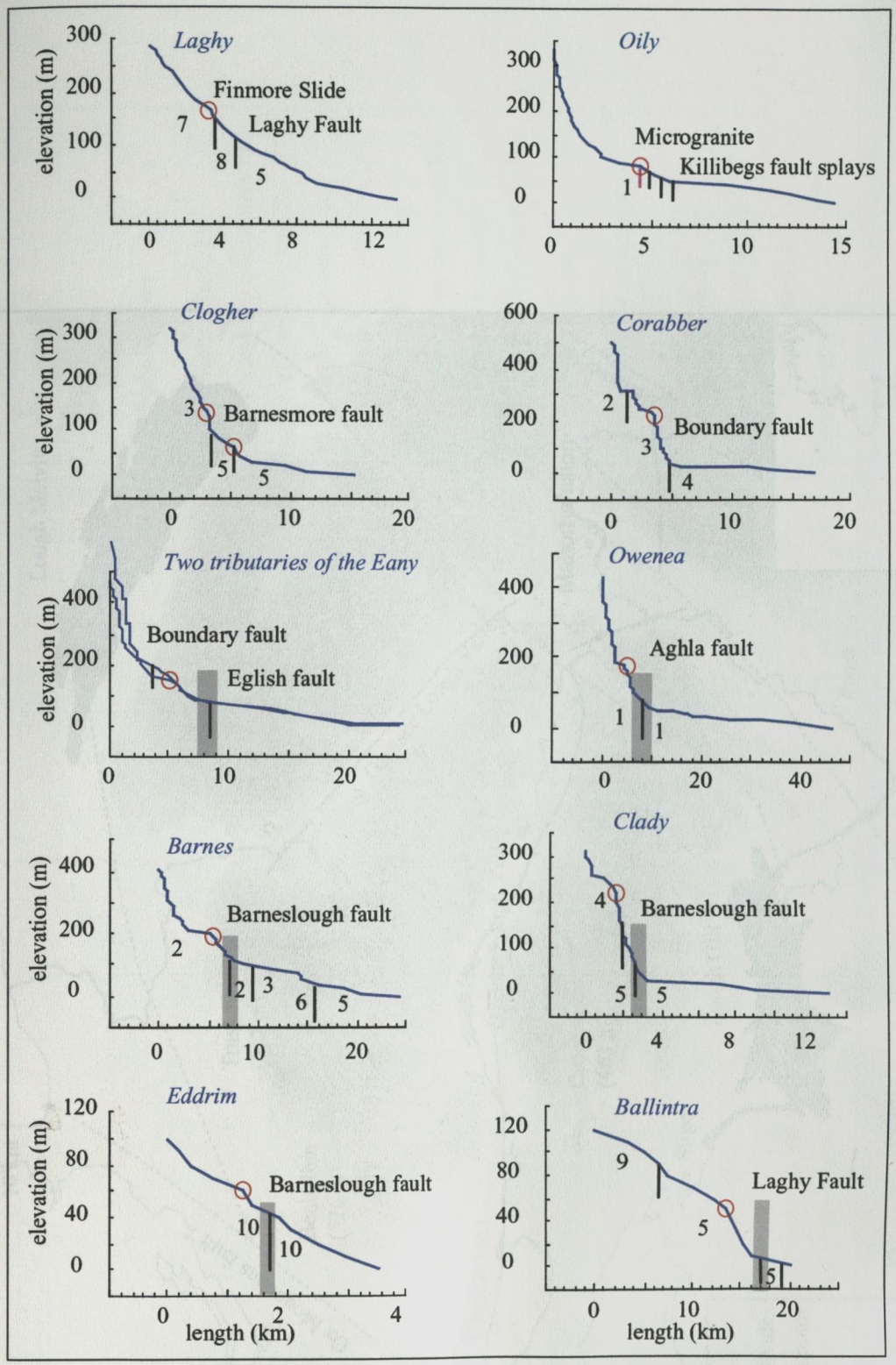


Figure 3.24. Rivers and knickpoints in the Blue Stack Mountains. Bedrock geology taken from Long *et al.* (1999).



Legend

1 Termon Fm.
2 Barnesmore Granite
3 Lough Mourne Fm.
4 Banagher Sandstone Fm.
5 Ballyshannon Limestone Fm.
6 Lough Eske Fm.
7 Croaghgarrow Fm.
8 Mullyfa and Deely Fm.
9 Psammitic paragneiss
10 Bundoran Shale Fm.

fault zone controlling knickpoint
fault
formational contact
river longitudinal profile
knickpoints

Figure 3.25. River profiles and knickpoints for the Blue Stack Mountains. See Fig. 3.23 for locations.

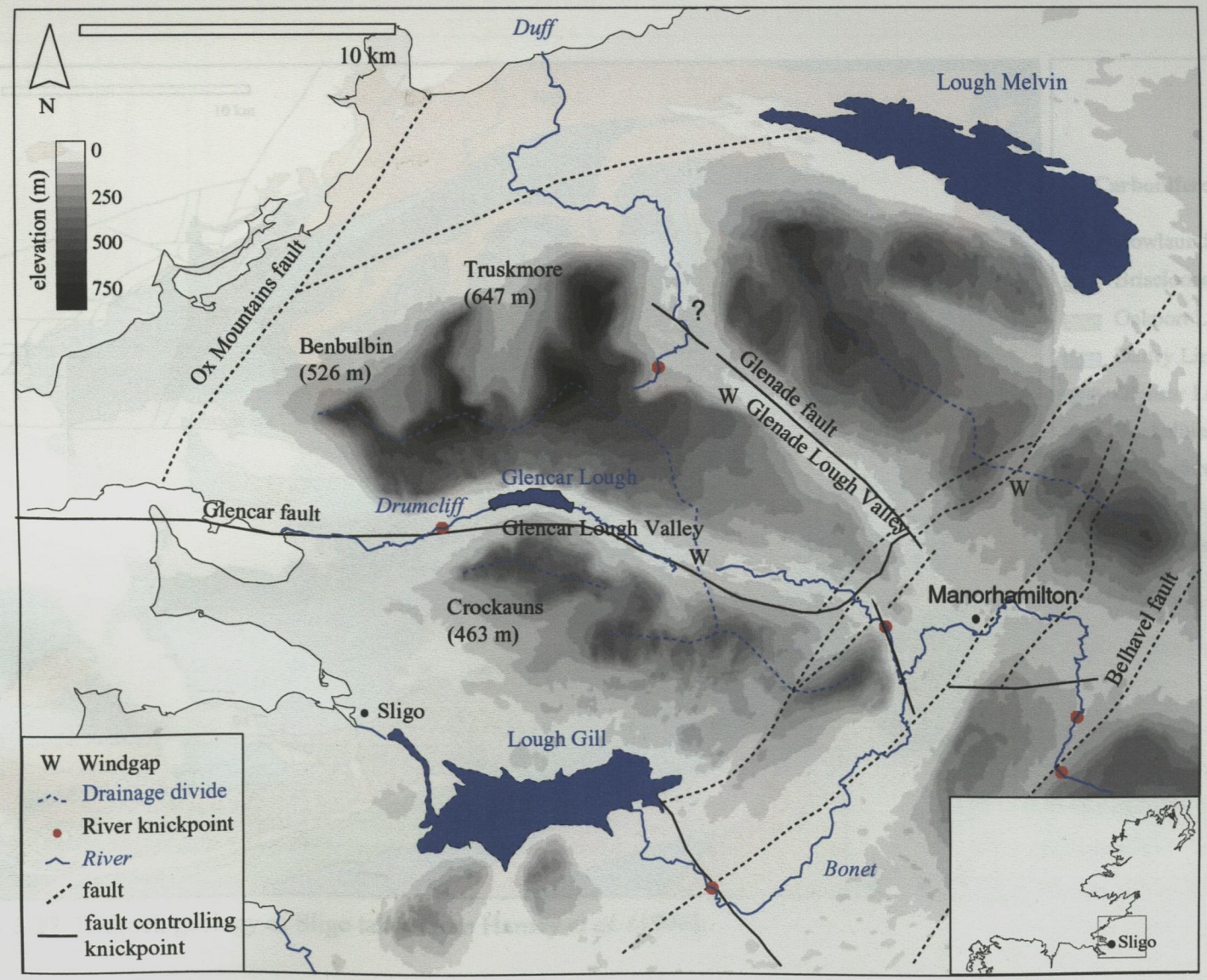


Figure 3.26. Rivers and knickpoints in the Sligo Mountains.

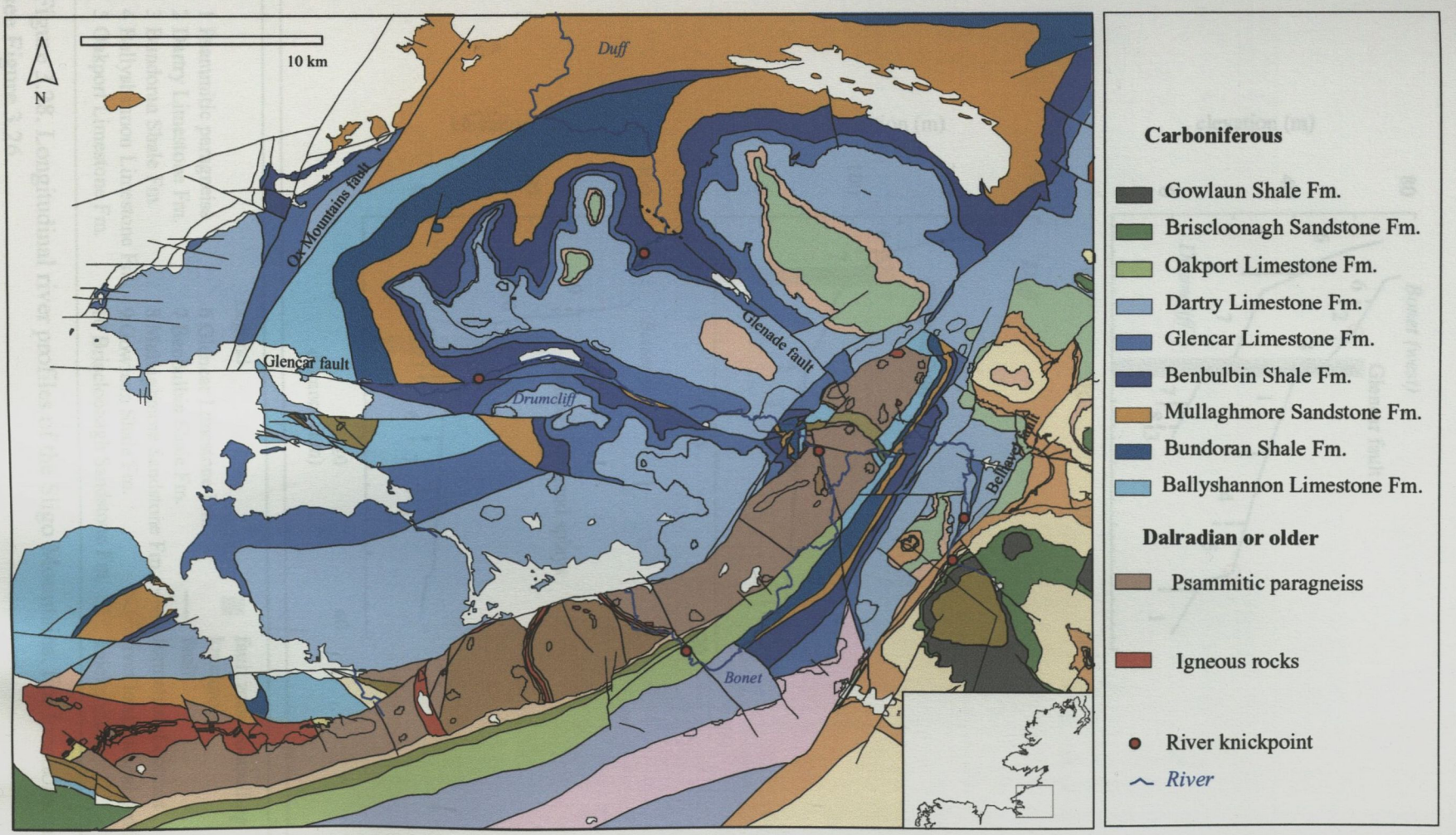


Figure 3.27. Bedrock geology of Sligo taken from Harney *et al.* (1996).

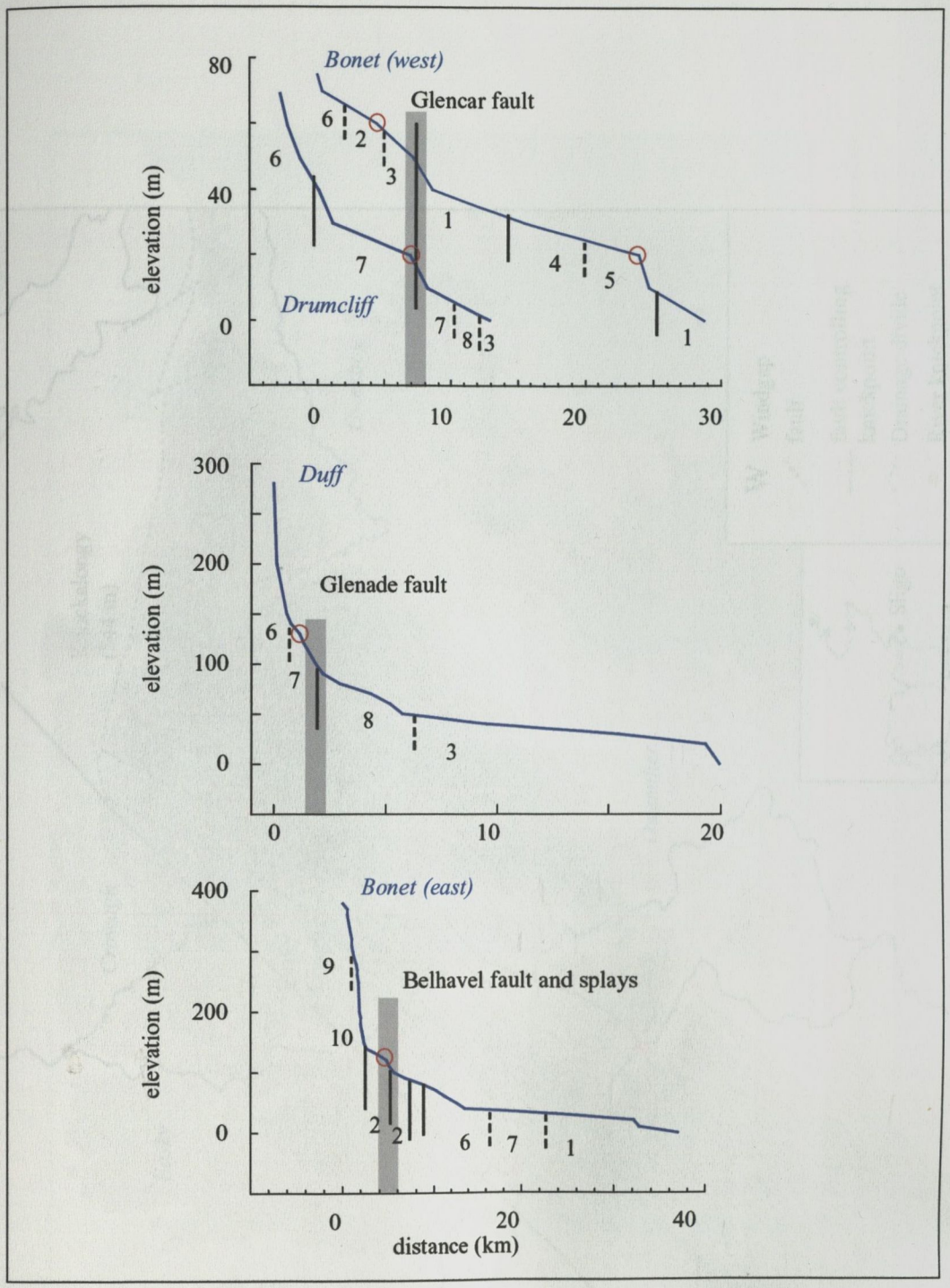


Figure 3.28. Longitudinal river profiles of the Sligo Mountains. For locations map see Figure 3.26.

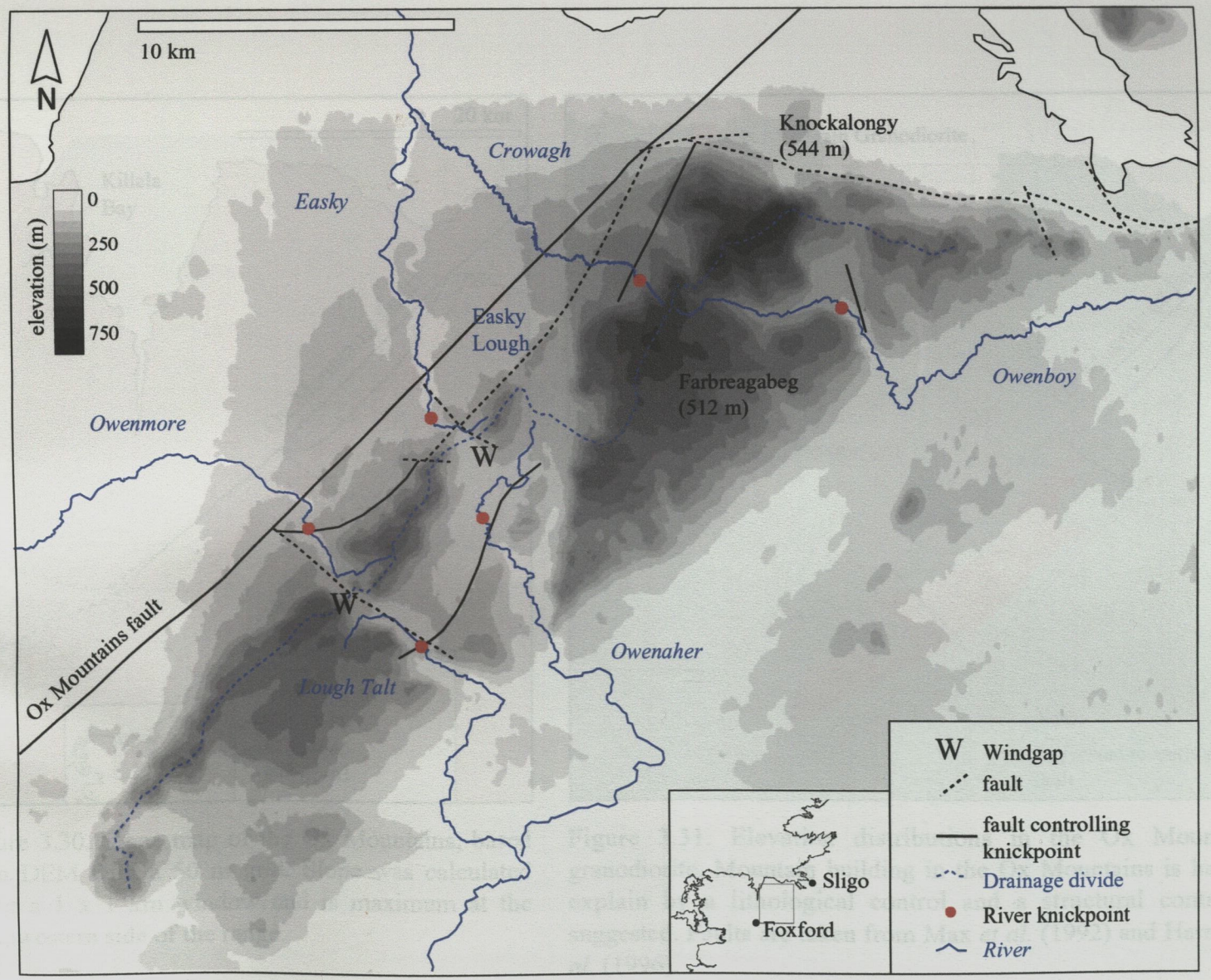


Figure 3.29. Rivers and knickpoints in the Ox Mountains.

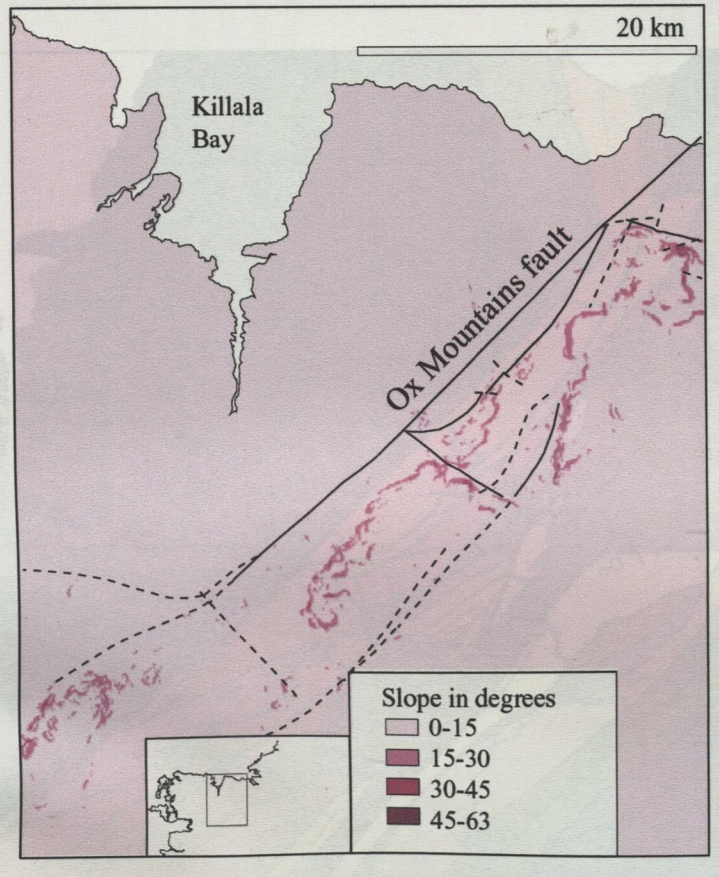


Figure 3.30. Slope map of the Ox Mountains, based on a DEM with a 50 m grid. Slope was calculated using a 1 x 1 km window and is maximum at the northwestern side of the range.

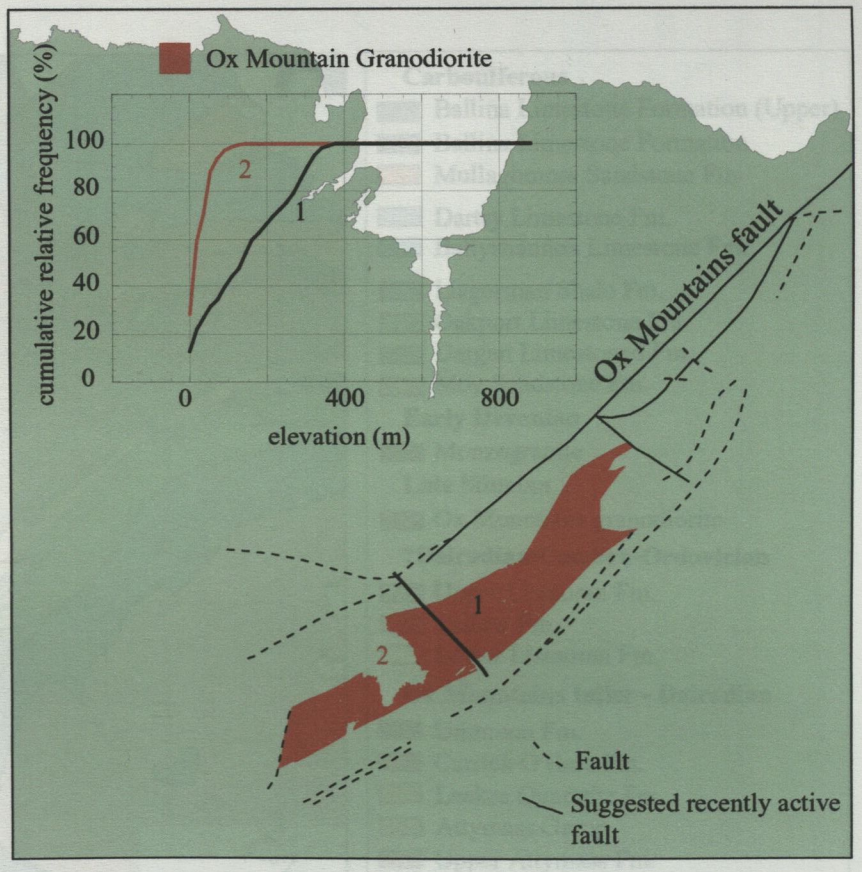


Figure 3.31. Elevation distributions in the Ox Mountains granodiorite. Mountain building in the Ox Mountains is hard to explain by a lithological control and a structural control is suggested. Faults are taken from Max *et al.* (1992) and Harney *et al.* (1996).

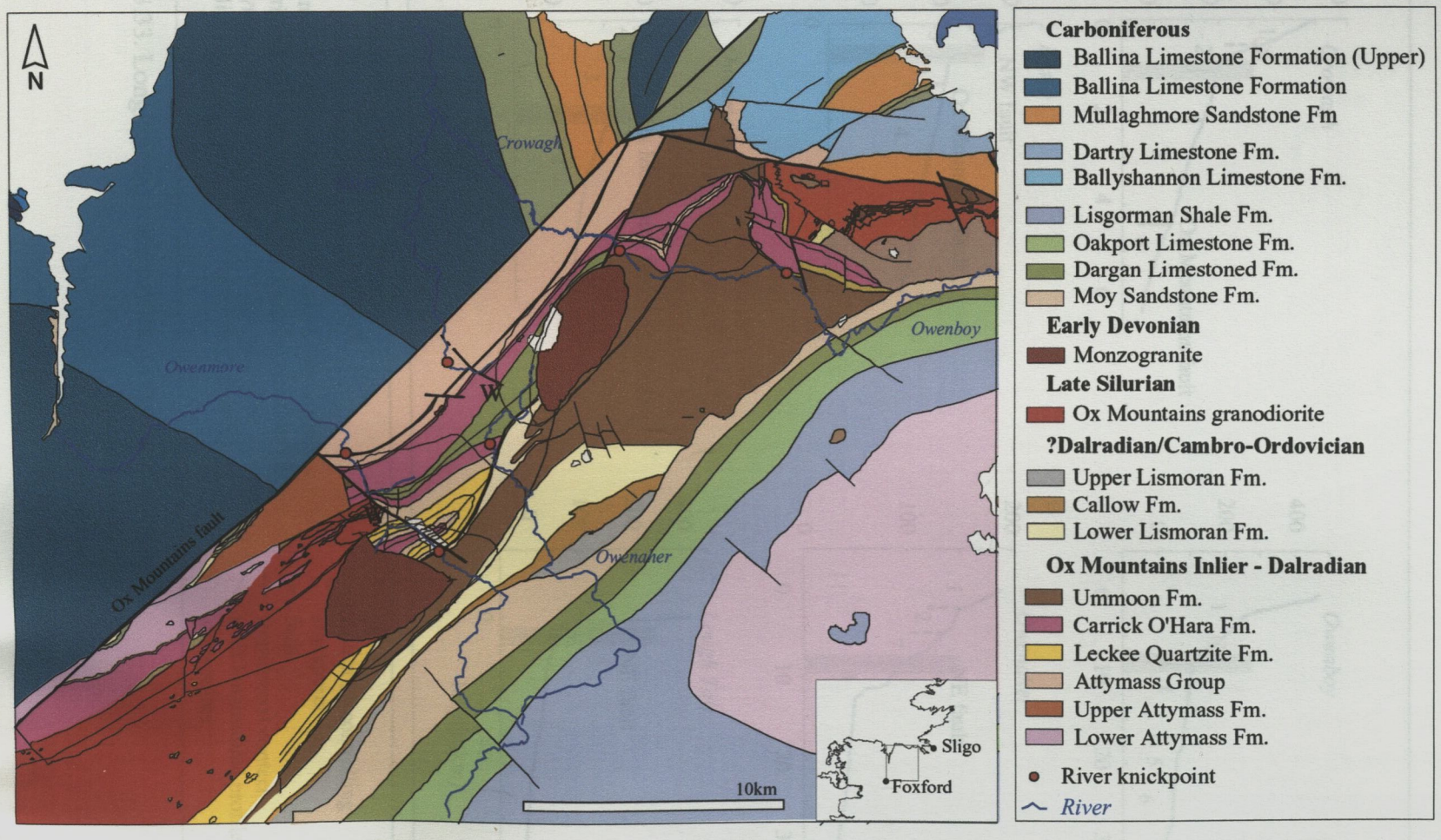
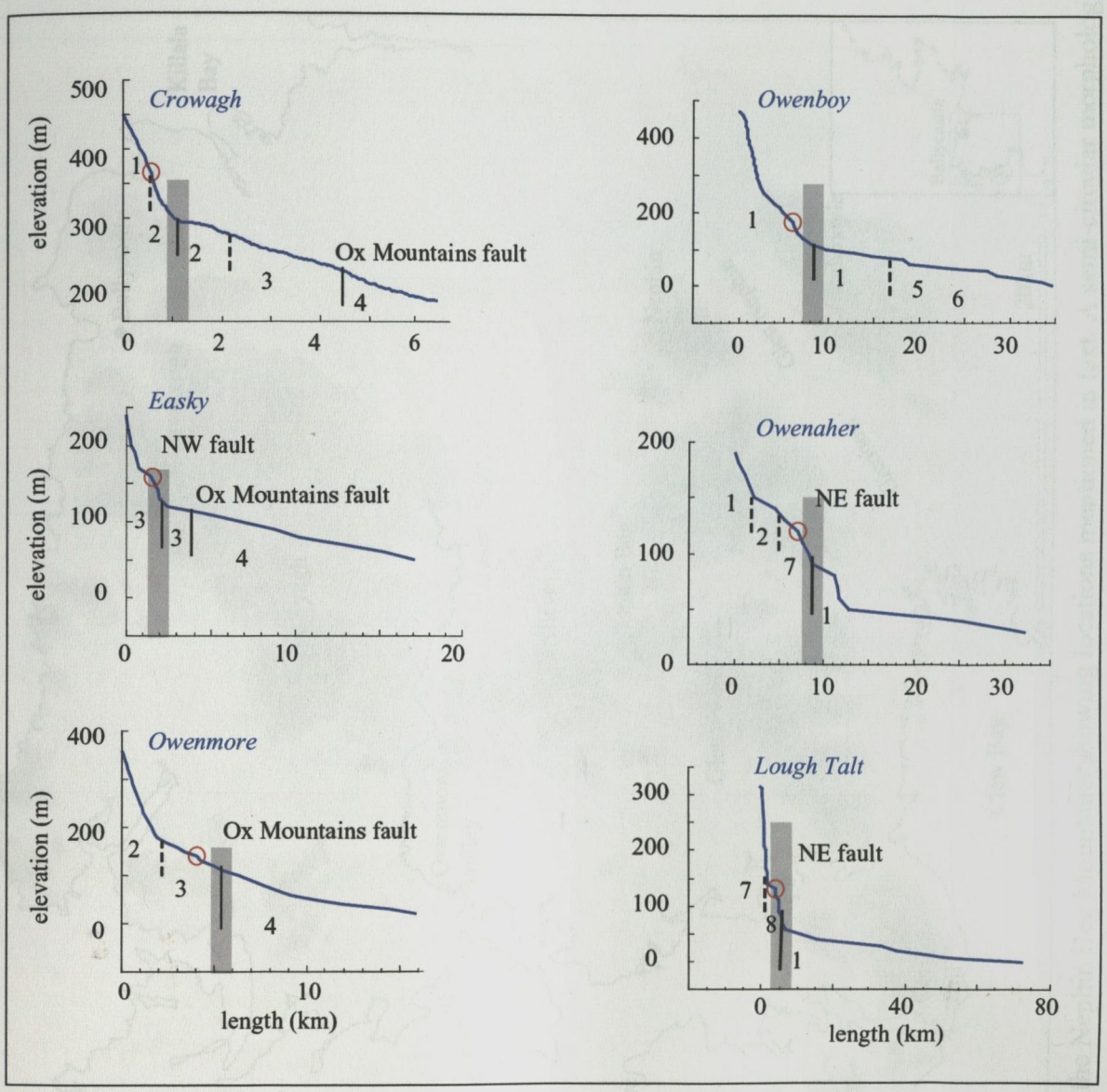


Figure 3.32. River knickpoints in the Ox Mountains. Bedrock geology taken from Max *et al.* (1992) and Harney *et al.* (1996).



Legend

1 Ummon Fm.	5 Moy Sandstone Fm.
2 Carrick O'Hara Fm.	6 Dargan Limestone Fm.
3 Attymass Group	7 Corradrishy Fm.
4 Ballina Limestone Fm.	8 Leckee Quartzitic Fm.

fault zone controlling knickpoint
fault
formational contact
river longitudinal profile
knickpoints

Figure 3.33. Longitudinal river profiles in the Ox Mountains.

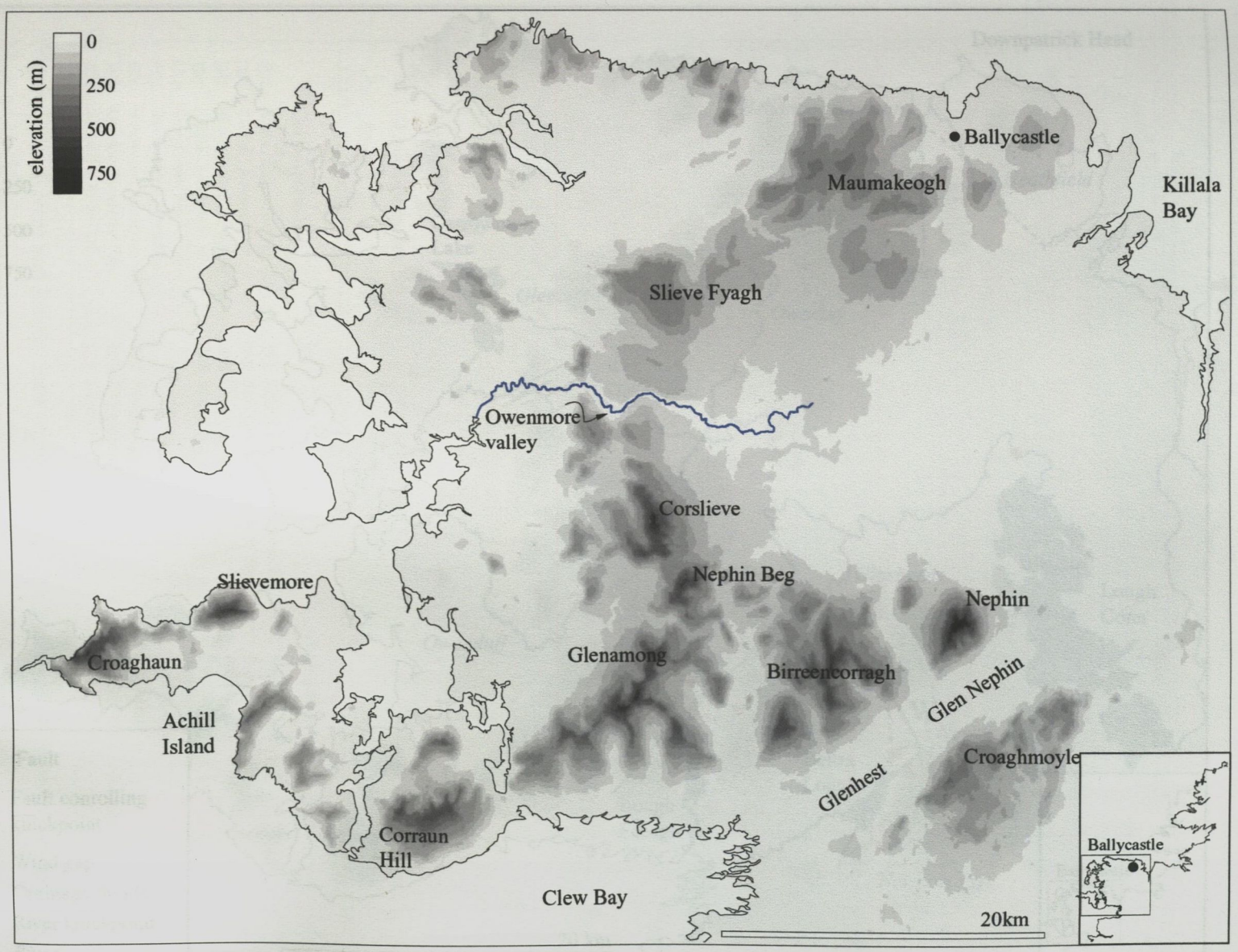


Figure 3.34. Topography of the Nephin Beg Mountains showing locations mentioned in text. A semi-circular morphology defines this range with only one antecedent river, the Owenmore, flowing across the axis of the range.

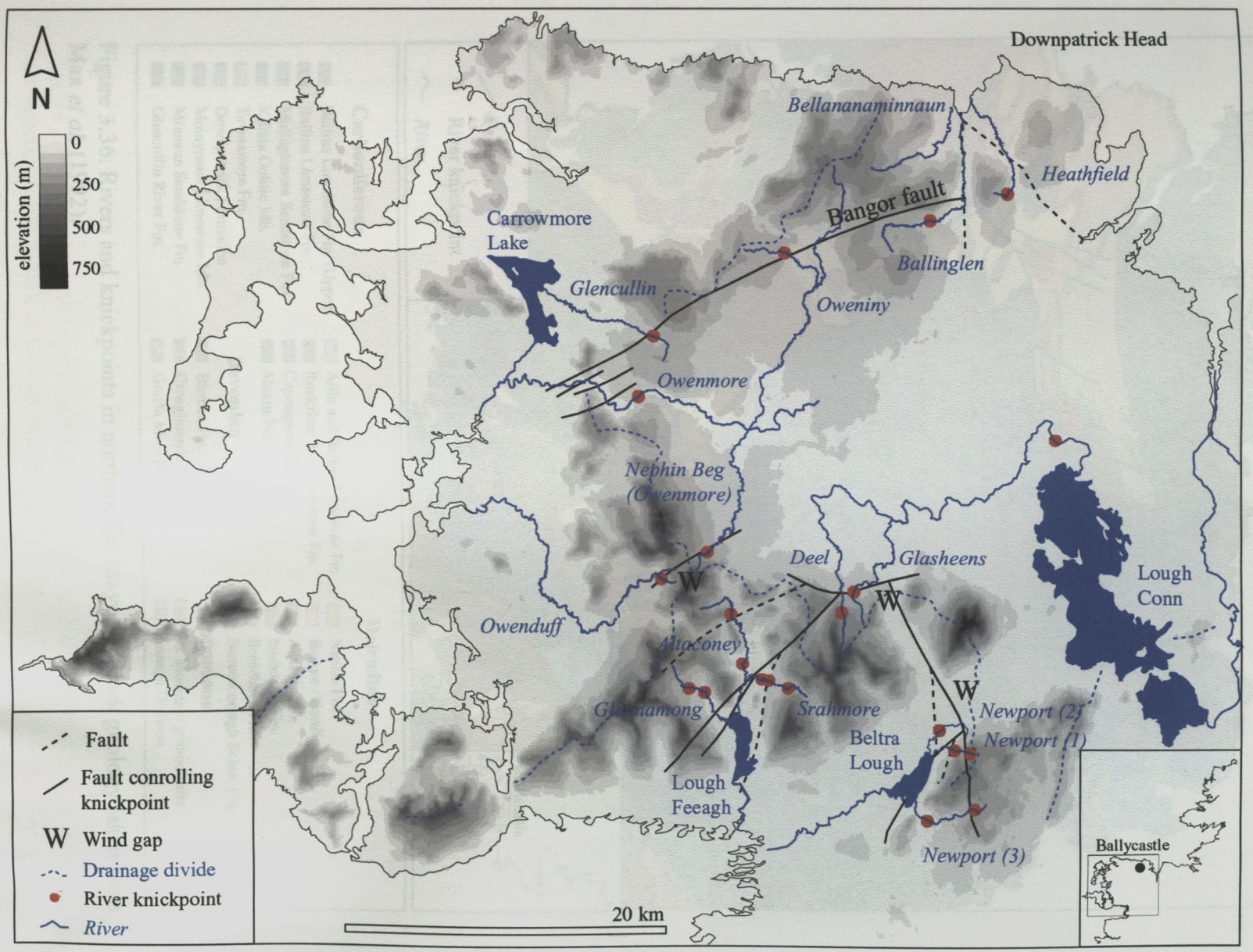


Figure 3.35. Rivers and knickpoints in the Nephin Beg Mountains.

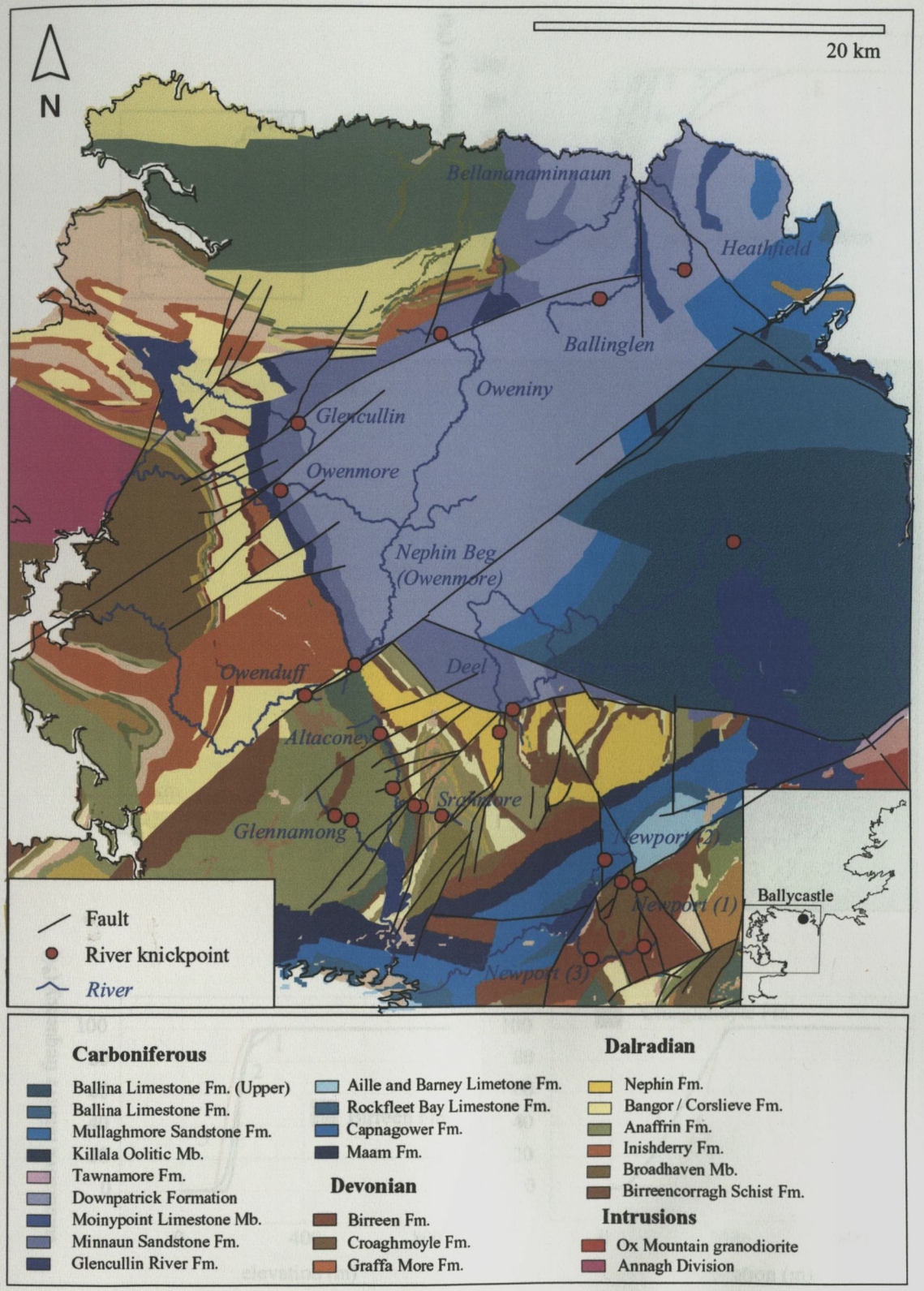


Figure 3.36. Rivers and knickpoints in northern Co. Mayo. Bedrock geology taken from Max *et al.* (1992).

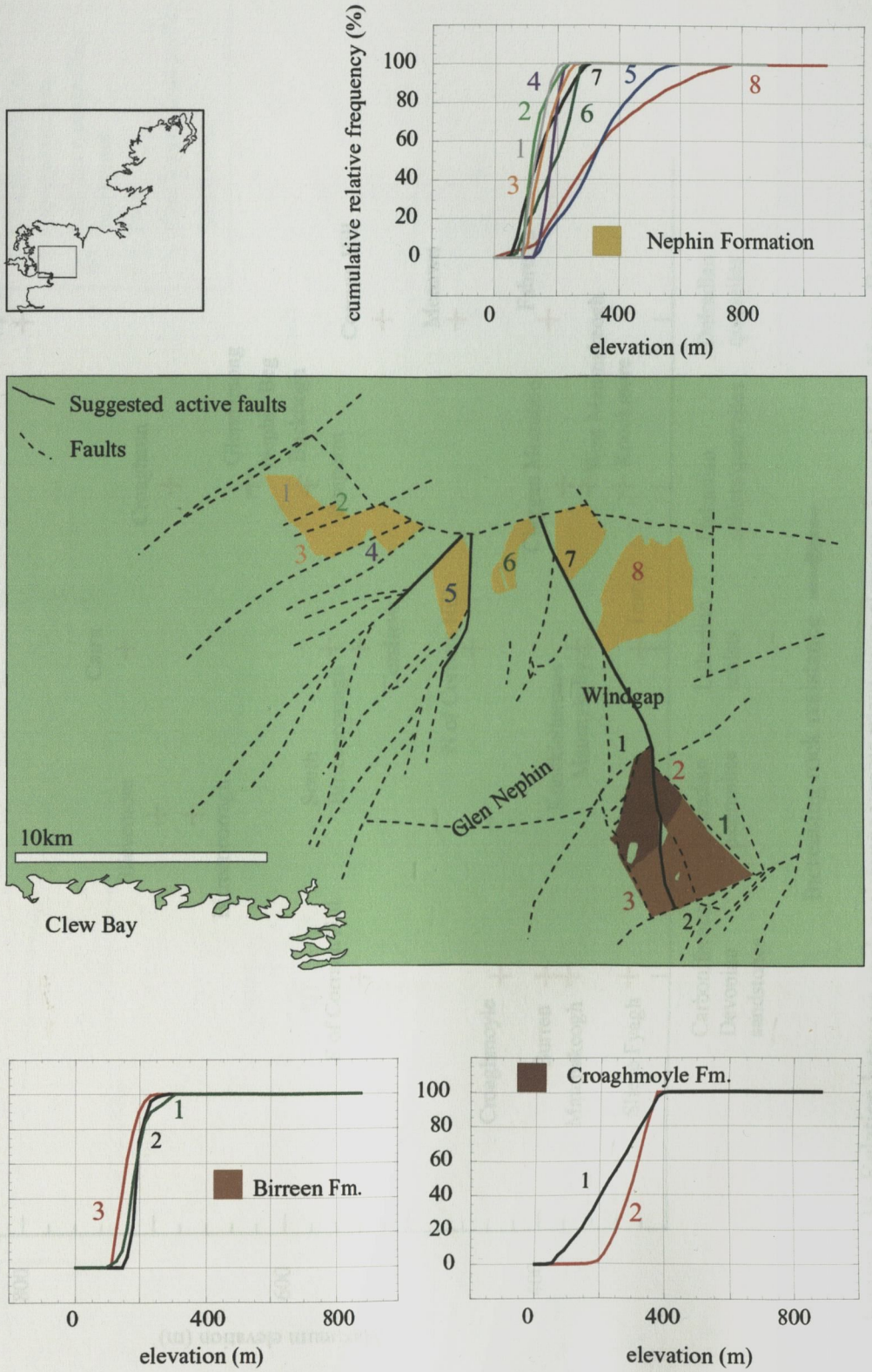


Figure 3.37. Elevation distributions for the Nephin Beg Formation, Birreen Formation and Croaghmoyle Formation in County Mayo. Faults taken from Max *et al.* (1992).

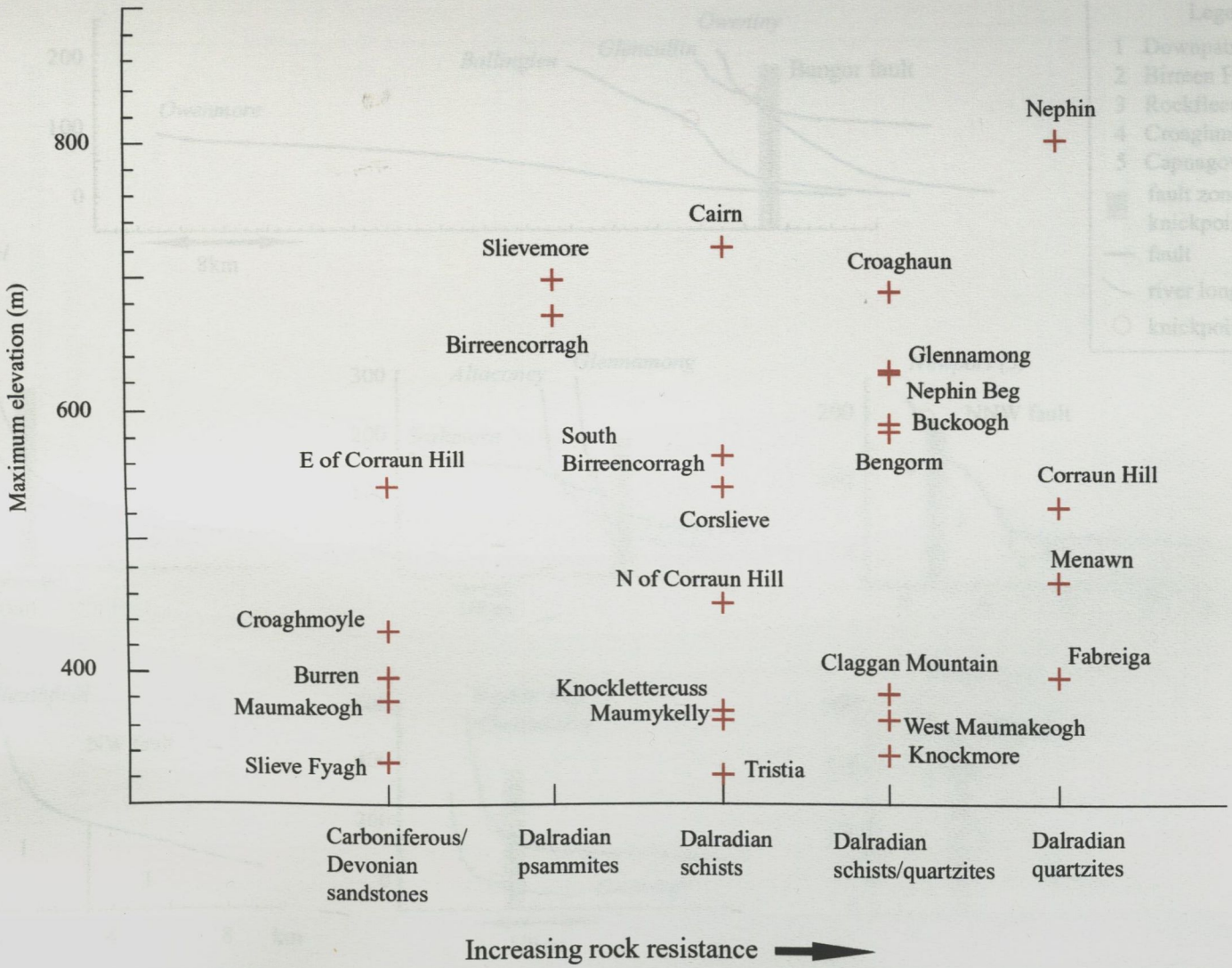


Figure 3.38. Relation between rock resistance versus maximum elevation in north Co. Mayo. Resistancy of rocks is taken from the scale of Clayton and Shamoon (1998) for similar rocks in Great Britain.

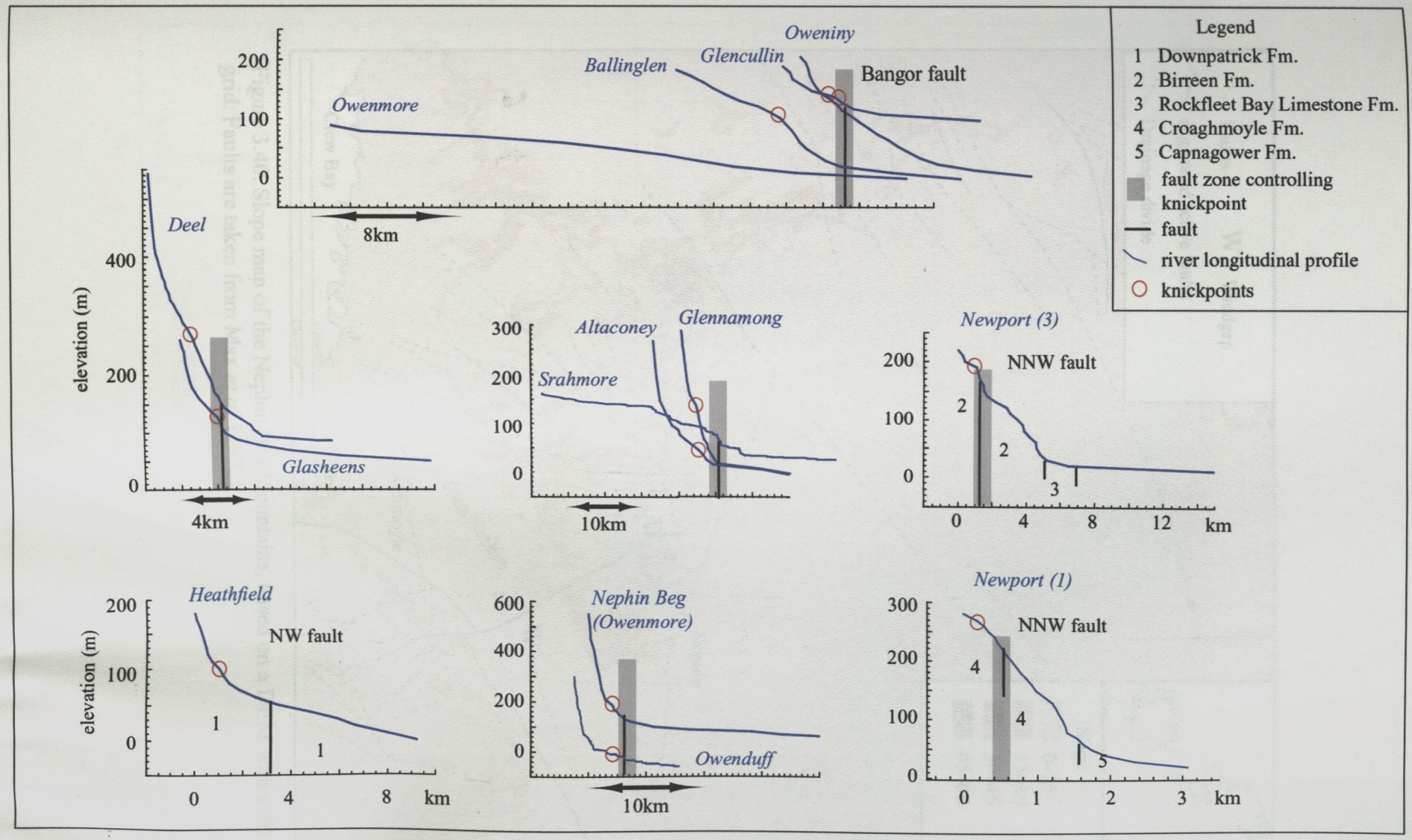


Figure 3.39. Longitudinal river profiles for the Nephin Beg Mountains. See Figure 3.35 for river locations.

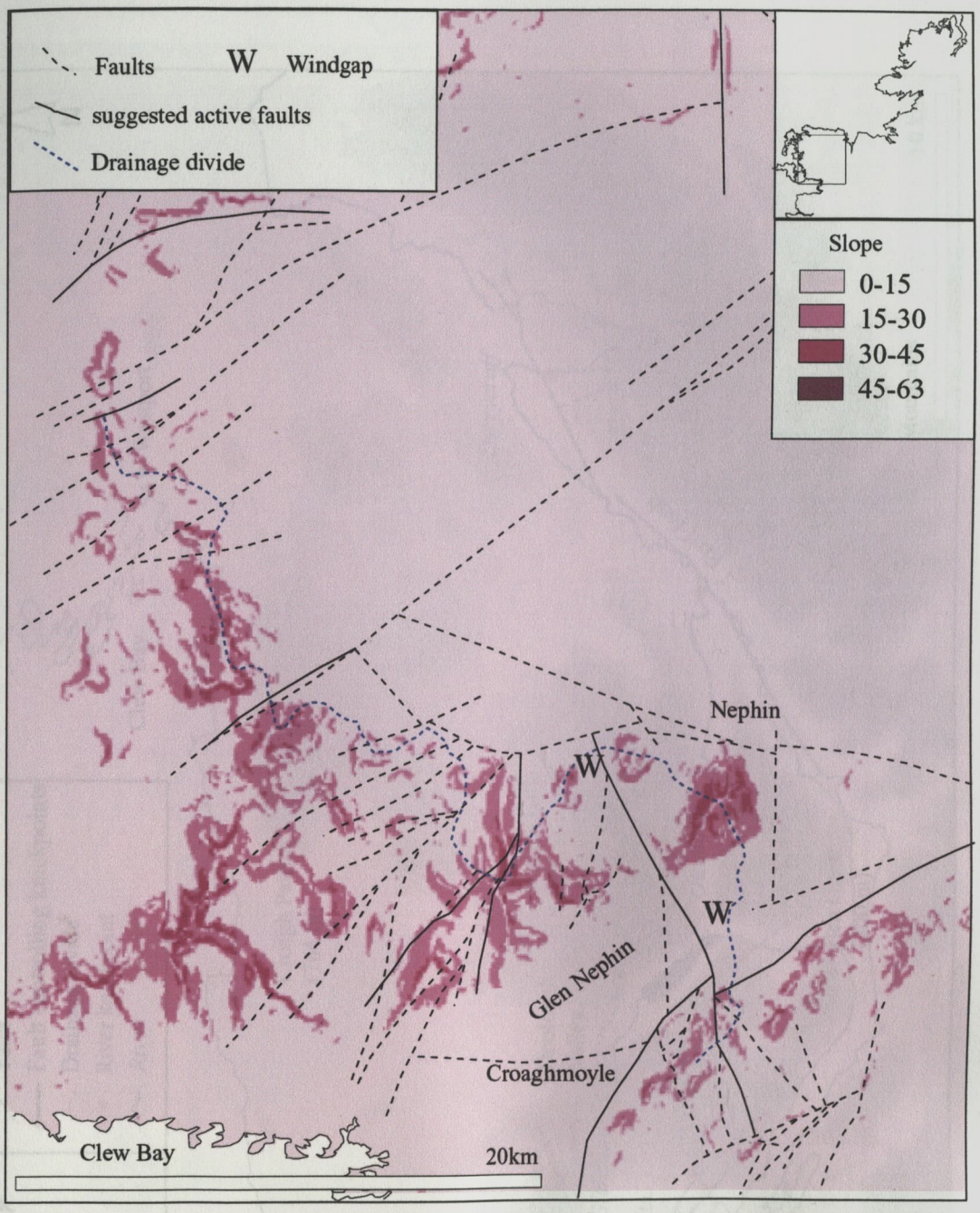


Figure 3.40. Slope map of the Nephin Beg Mountains, based on a DEM with a 50 m grid. Faults are taken from Max *et al.* (1992).

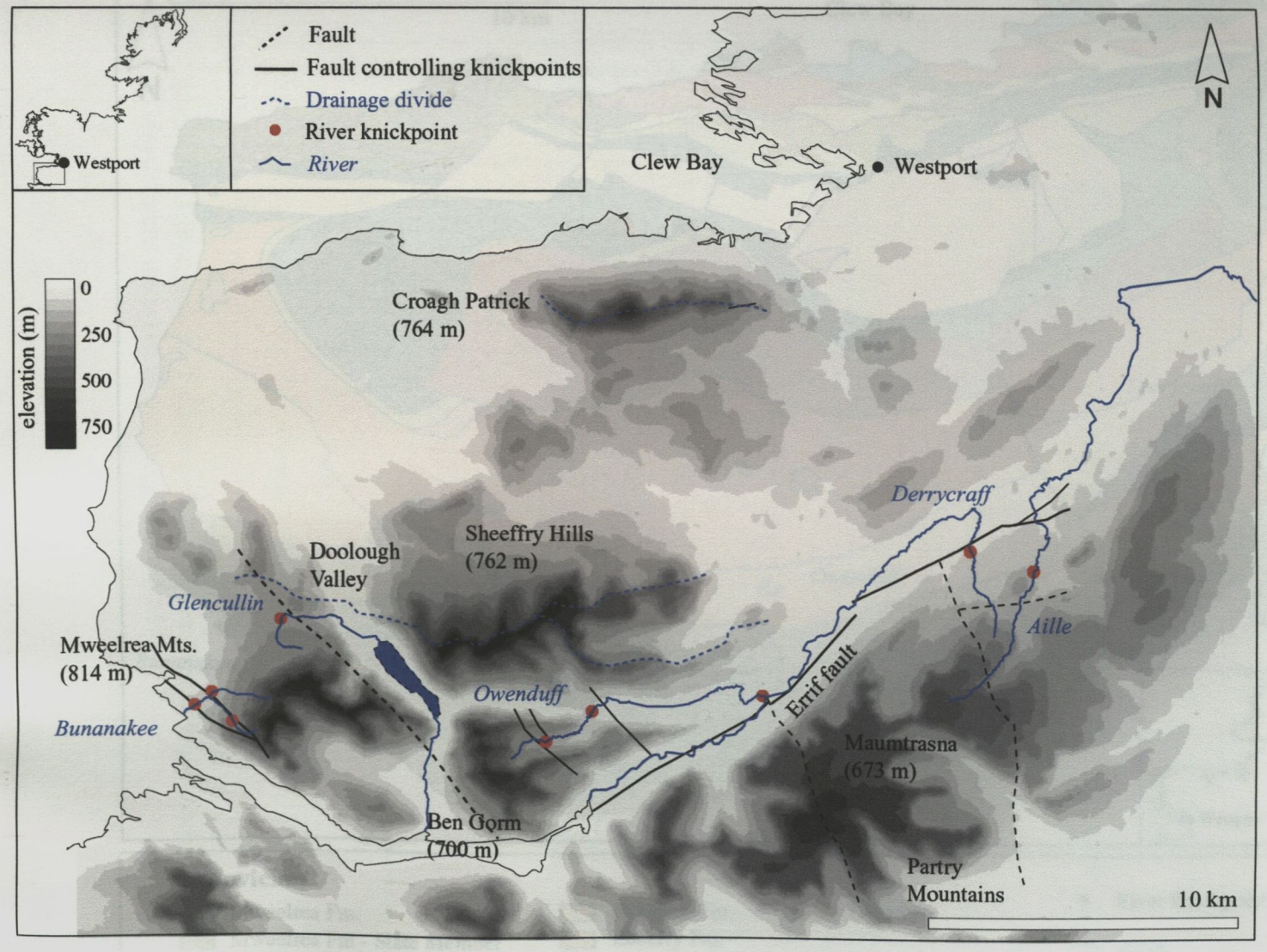


Figure 3.41. Topography, rivers and river knickpoints from southern Co. Mayo.

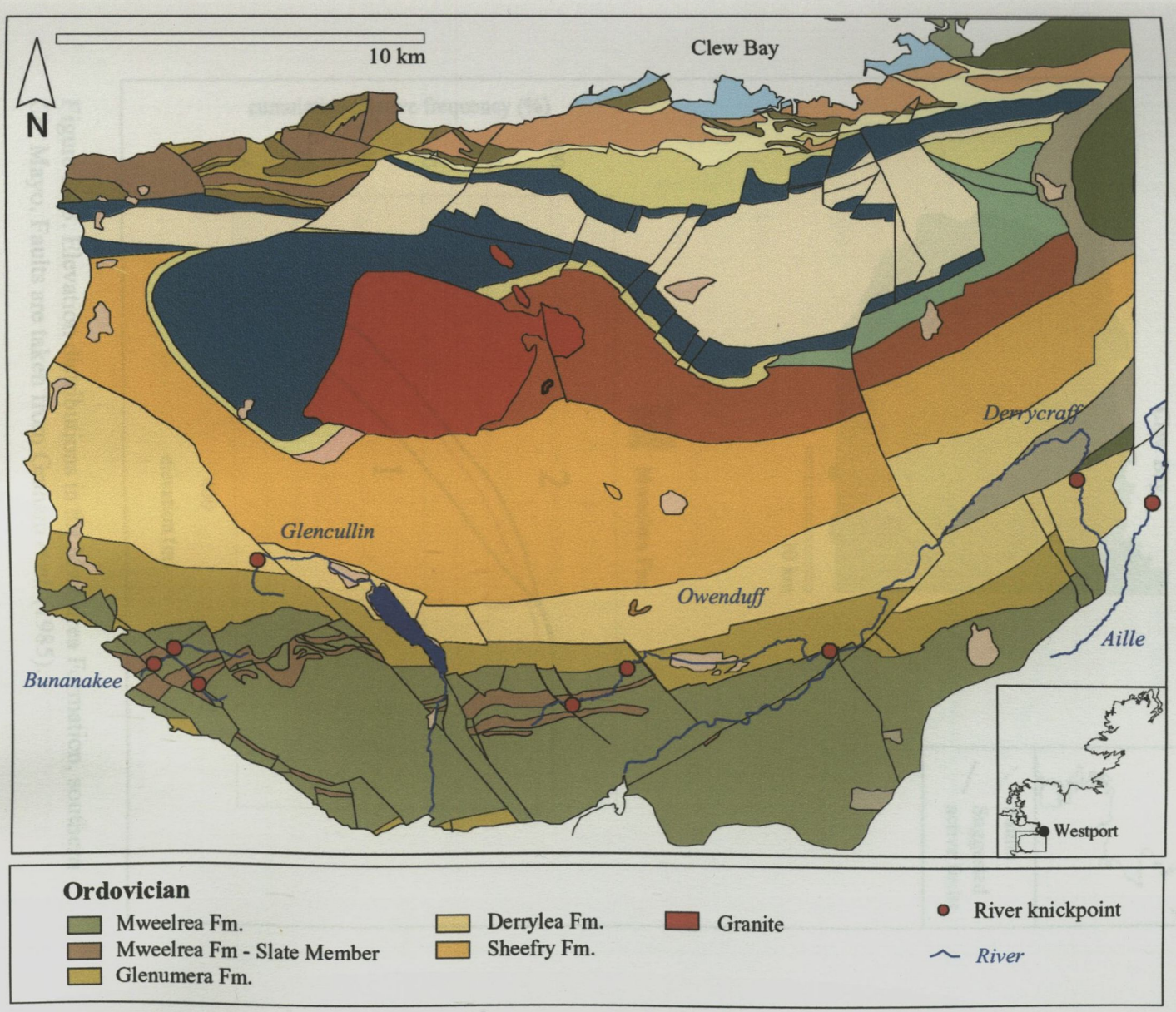


Figure 3.42. River knickpoints in southern Co. Mayo. Bedrock geology taken from Graham *et al.* 1985

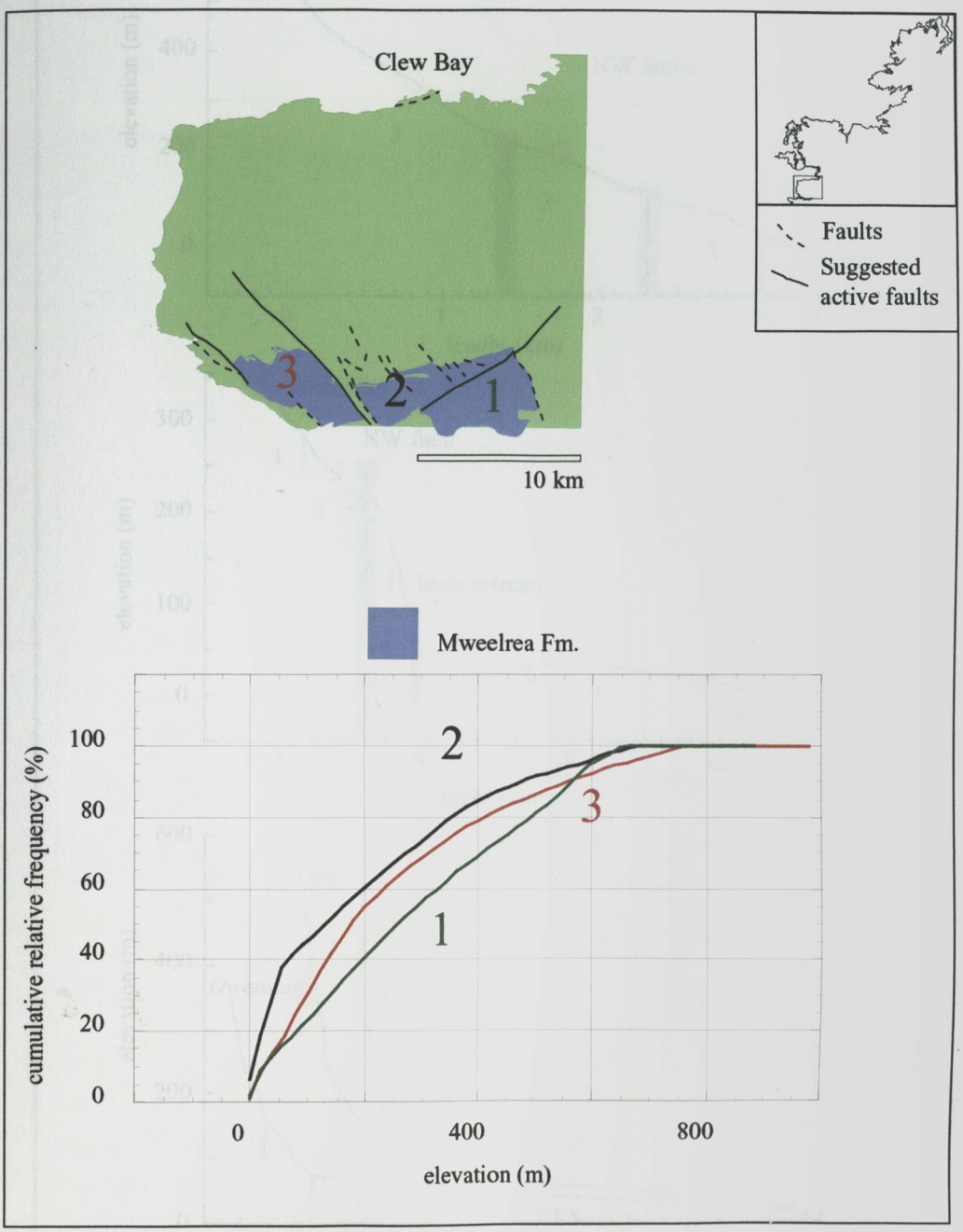
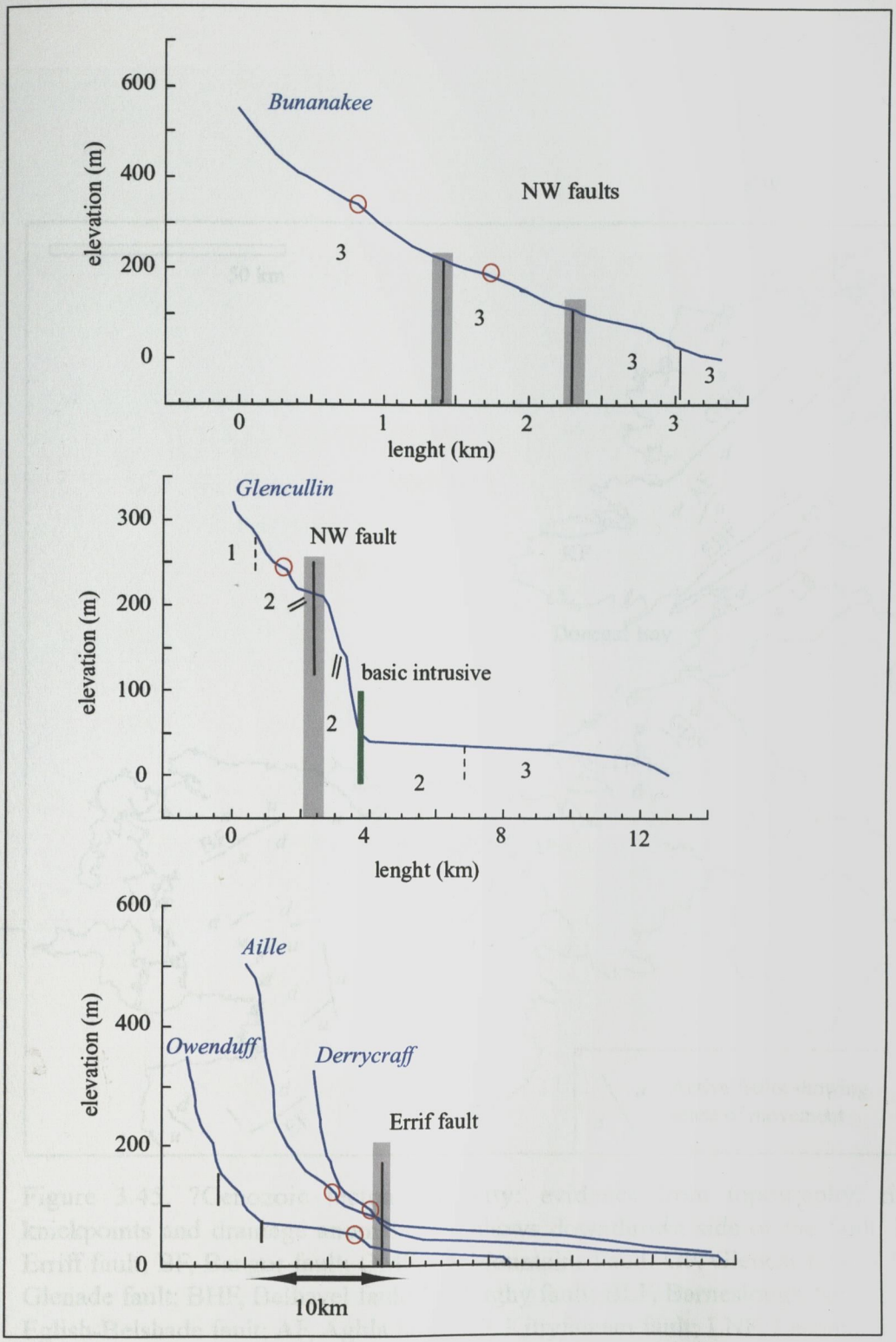


Figure 3.43. Elevation distributions in the Mweelrea Formation, southern Co. Mayo. Faults are taken from Graham *et al.* (1985).



Legend

1 Glenummera Fm.
2 Derrylea Fm.
3 Mweelrea Fm.
4 Lower Carb. Lmst.

fault zone controlling knickpoint
fault
formational contact

river longitudinal profile
knickpoints
bedding

Figure 3.44. Longitudinal river profiles for the Partry Mountains and Mweelrea Mountains.

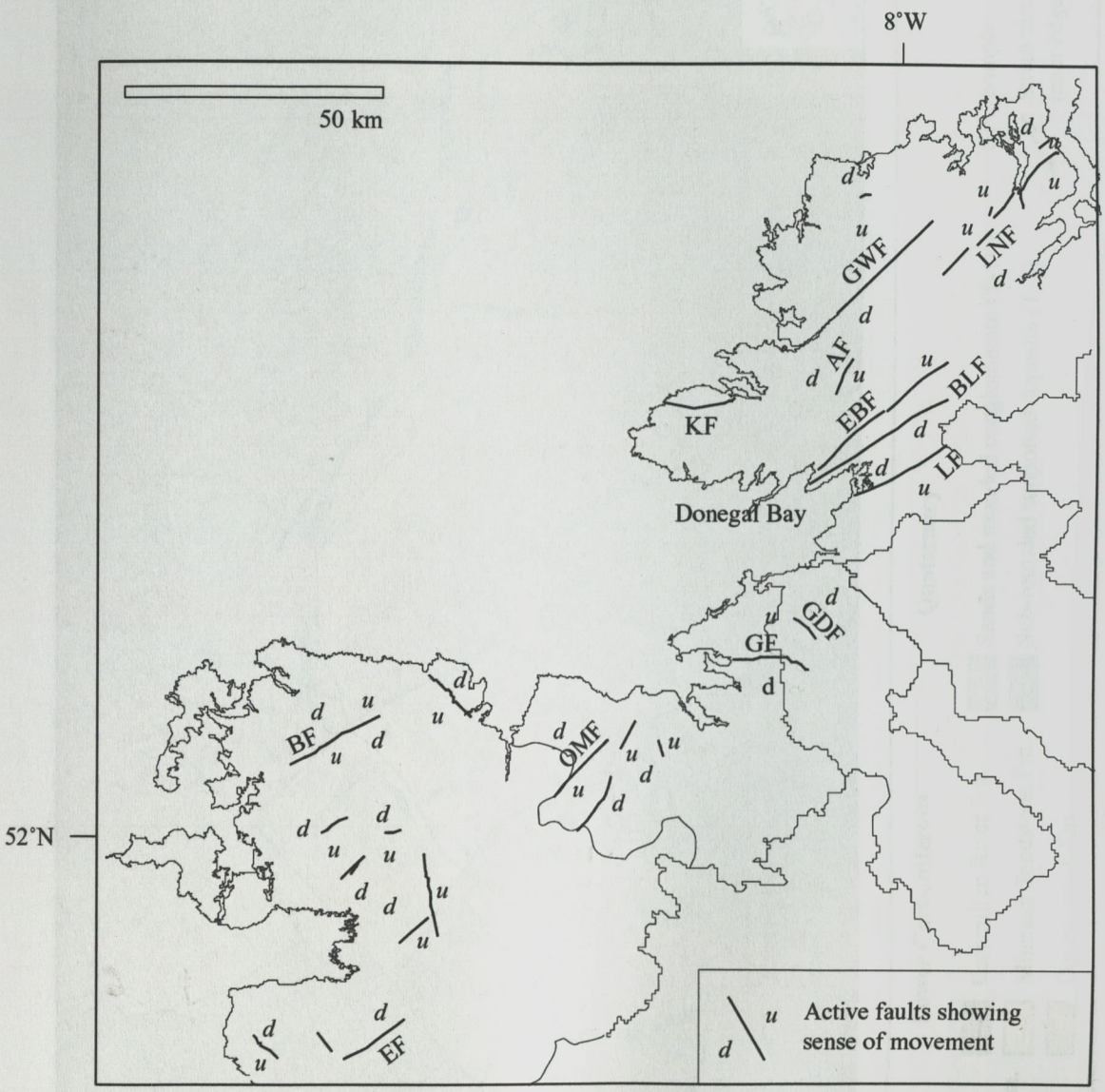


Figure 3.45. ?Cenozoic tectonic activity: evidence from topography, river knickpoints and drainage anomalies. d, shows downthrown side of the fault. EF, Erriff fault; BF, Bangor fault; OMF, Ox Mountains Fault; GF, Glencar fault; GDF, Glenade fault; BHF, Belhavel fault; LF, Laghy fault; BLF, Barneslough fault; EBF, Eglish-Belshade fault; AF, Aghla fault; KF, Kittyfannan fault; LNF, Leannan fault; GWF, Gweebarra fault.

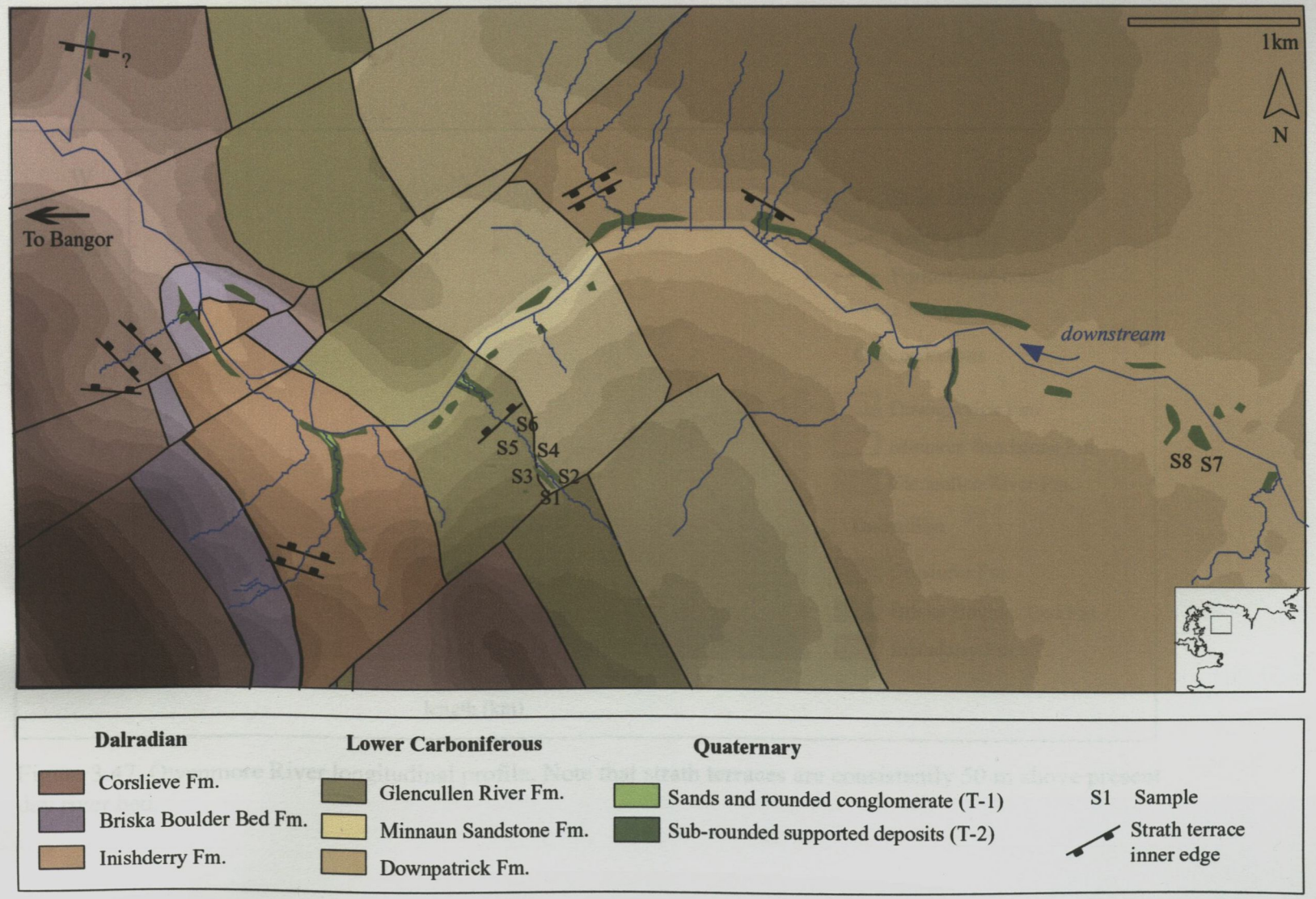


Figure 3.46. Owenmore River over bedrock, showing position of sand and gravels deposits, strath terraces and samples. Bedrock geology taken from Max *et al.* (1992).

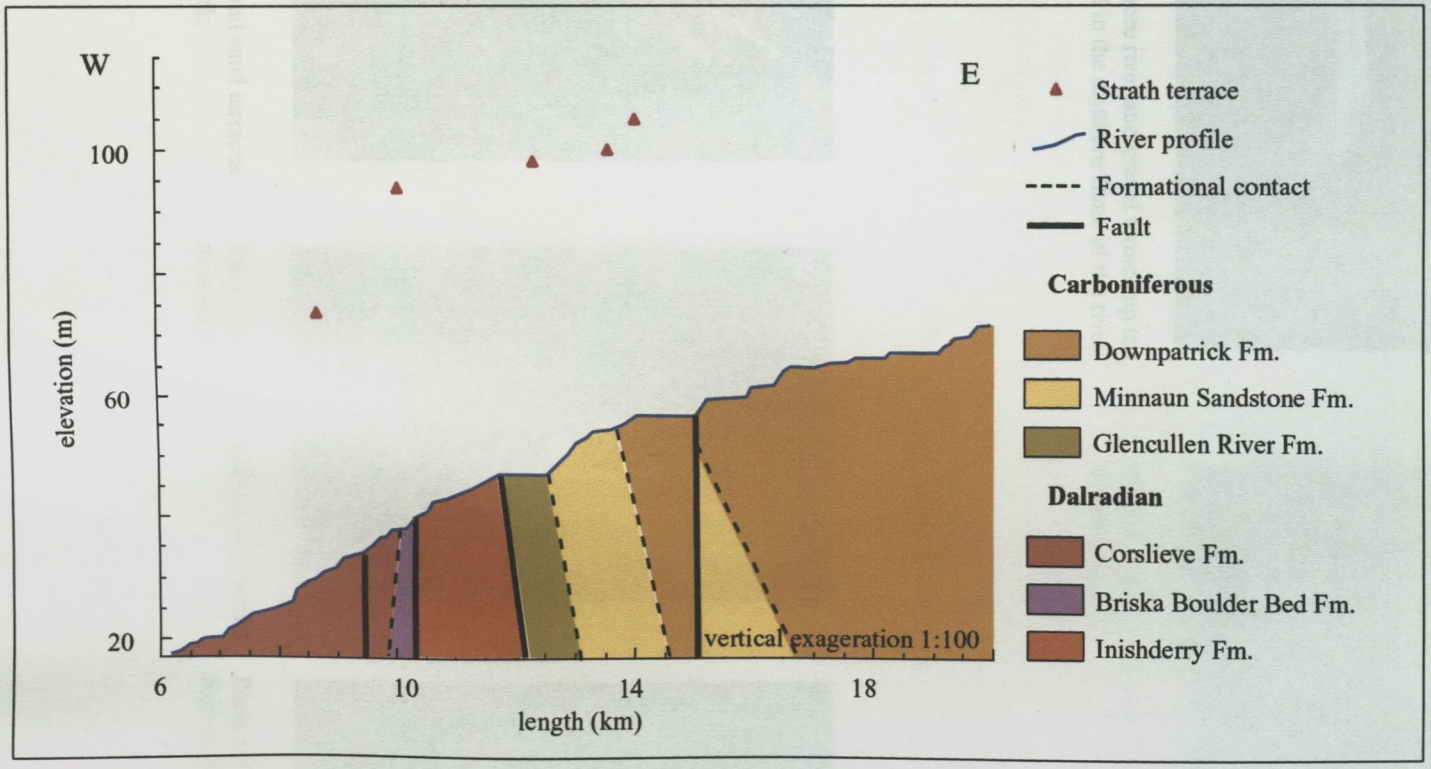


Figure 3.47. Owenmore River longitudinal profile. Note that strath terraces are consistently 50 m above present day river bed.



Plate 3.1. Owenmore river and gravel terrace up to 12 m high located in the southern flank of the river valley.



Plate 3.2. Gravel terrace (T-2) in northern shore of the Owenmore river.

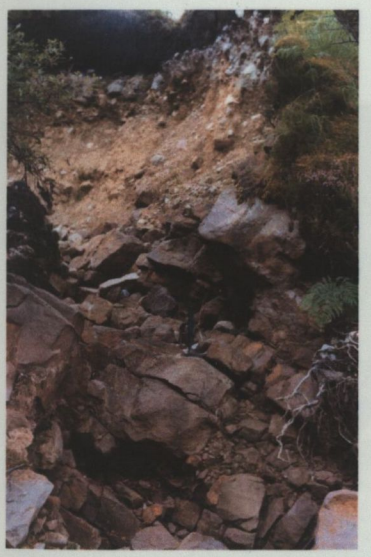


Plate 3.3. Gravel and sand terraces often lie on bedrock.

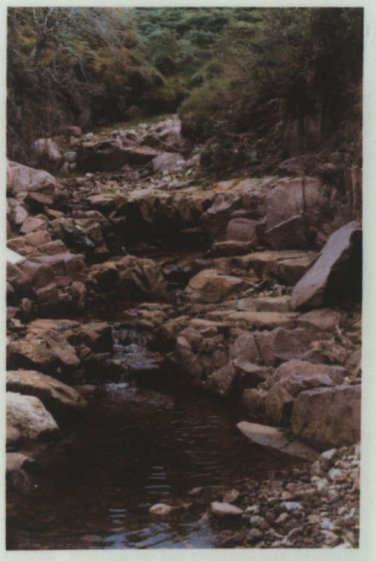


Plate 3.4. Stepped bedrock interpreted as a strath terrace.



Plate 3.5. Strath terrace up to 6 m high forming cascades.



Plate 3.6. Two generations of gravel and sand terraces (T-1 and T-2). T-1 at the bottom is younger than T-2.



Plate 3.7. Two generations of sand and gravel terraces (T-1 and T-2).



Plate 3.8. Internal sedimentary structure of T-2, with coarse graded sands and gravels.



Plate 3.9. Parallel and cross lamination in coarse sands.



Plate 3.10. Erosive surface within sands and gravels.



Plate 3.11. Clasts broken by frost shattering, previous to deposition.



Plate 3.12. Sub-rounded clasts and boulders, broken down by frost shattering after deposition.



Plate 3.13. Decalcified and weathered fossil.



Plate 3.14. Decalcified crinoid within gravel deposit.

Sample	Elevation asl (m)	Grid reference (Irish national grid)	Sediment	Pollen
S1	135	90005 321088	Clay in fractured bedrock	Organic material. No pollen.
S2	125	89937 321197	Red clay	*Corylus* (hazel), *Ericaceae* (heather), *Pinus* (pine), *Ulmus* (elm), *Alnus* (alder) and grass.
S3	148	90044 321009	Turf and clay clast	*Ericaceae*, *Pinus*, grass and *Betula* (birch).
S4	157	90130 320908	Clay on bedrock pocket	Plant fragments. No pollen.
S5	66	93818 321177	Clayish clast	*Betula*
S6	116	89853 321270	Clay in fractured bedrock	*Ericaceae*, *Calluna* and *Polipodium*
S7	66	93817 321177	Clay matrix	Very few plant fragments. No pollen.
S8	108	89853 321270	Clay in fractured bedrock	No pollen.

Table 3.1. Sample types and pollen content.

Chapter 4 The Cenozoic of the northeastern Irish Rockall Basin

4.1 Introduction

A series of sedimentary basins lie off the northwest coast of Ireland, including the Slyne, Erris, Donegal and Rockall Basins (Fig. 4.1). The first three contain Upper Palaeozoic, Mesozoic and thin Cenozoic rocks, based on current well information. The Rockall Basin is the largest of the Irish offshore basins, 250 km wide by 600 km long. Little is known about the history of basin formation and deposition, due to a lack of wells drilled and the masking effect of Cretaceous and Palaeogene igneous sills on seismic data. The pre-Tertiary history of the Rockall Basin has been modelled (Shannon *et al.* 1999; Nadin *et al.* 1999) but remains unclear. However, it does contain a thick sequence of Cenozoic sediments, unlike other offshore basins around northwestern Ireland where the Cenozoic is thin or absent. The Irish Rockall Basin therefore has the potential to reveal information on the Tertiary depositional history of northwestern Ireland.

In the last few decades a number of studies have been made on the Rockall Basin crustal structure (Shannon *et al.* 1999; O'Reilly *et al.* 1995; England 1995; England and Hobbs 1997), general stratigraphy and structure (Corfield *et al.* 1999; Naylor *et al.* 1999; Boldreel and Andersen 1993; Waddams and Cordingley 1999; Walsh *et al.* 1999), basin development and rifting phases (Smythe 1989; Shannon *et al.* 1995; Musgrove and Mitchener 1996; Cole and Peachey 1999; Nadin *et al.* 1999; Shannon *et al.* 1999), volcanism (Morton *et al.* 1988; Wood *et al.* 1988; Hitchen *et al.* 1997; Ritchie *et al.* 1999), heat flow (Green *et al.* 1999; Parnell *et al.* 1999; Clift 1999) and uplift of the basin margin (Hillis 1995; Nadin *et al.* 1999; White and Lovell 1997). Although a wide array of literature exists, the timing of rifting and age of the Rockall Basin sedimentary sequence is poorly known.

The Cenozoic structural and sedimentary evolution has also been studied in the Rockall Basin (Masson and Kidd 1986; Shannon *et al.* 1993; Howe *et al.* 1994; Egerton 1998; Armishaw *et al.* 1998; Holmes *et al.* 1998; Tate *et al.* 1999; Stoker 1997, 1998; Stoker *et al.* 2001; Austin 2001). With new data being released by oil exploration companies (e.g. wells, 2D and 3D seismic surveys), our understanding of the geometry and age of the Cenozoic section has improved considerably. There still is not enough well control to trace the base Tertiary unconformity with complete confidence across the basin.

To better understand the Cenozoic evolution of the northwestern Irish continental margin, I have interpreted the Cenozoic seismic packages of the northeast Irish Rockall Basin using 2D reflection seismic lines and available wells from TotalFinaElf Exploration UK during the year 2000.

Section 4.2 in this chapter introduces the northwestern Irish offshore basins and summarises their geological history. The northeast Irish Rockall Basin and Erris Basin are the most relevant to this study, as they are closest to northwestern Ireland, and therefore are studied in more detail.

Section 4.3 lists the data sets used, including seismic, well data and previous literature.

Section 4.4 describes each Cenozoic seismic package mapped and gives the ages of the intervening unconformities based on previous work. Offshore Cenozoic sedimentary depocentres and phases of progradation will be also described. This section also contains depth-converted and de-compacted isopach maps of these intervals.

Section 4.5 presents the Cenozoic structural history of the northeastern Rockall Basin. Quantification of offshore sedimentation and onshore denudation, along with modelling of the flexural deformation of the northwestern Irish margin, is presented in chapter 5.

4.2 Previous work and geological history of each basin

The northwestern Irish offshore basins have been explored during the last few decades mainly on the basis of their hydrocarbon prospectivity. The earliest detailed description of the seismic stratigraphy of the Rockall Basin were presented by Roberts (1975), Roberts *et al.* (1981), Dingle *et al.* (1982) and Masson and Kidd (1986) and reflectors were dated using deep-sea drilling project (DSDP) boreholes. Naylor and Shannon (1982) also presented a preliminary study of the Rockall Basin. Today, the volume of literature on the Rockall Basin is large, but because not many wells are drilled strictly within the basin many interpretations remain unclear. A recent nomenclature study in the Rockall Basin has been published by Naylor *et al.* (1999), which this work follows. The following sub-sections present a brief geological history of each of the offshore basins off northwestern Ireland.

4.2.1 The Rockall Basin

The Rockall Basin is a broad ?Late Palaeozoic - Mesozoic (Smythe 1989; Shannon 1991a; Shannon *et al.* 1995; Shannon *et al.* 1999) rift basin which lies to the northwest of the UK and Irish continental margins. It extends from the Wyville-Thomson Ridge in the north to the Charlie Gibbs Fracture Zone in the south (Fig. 4.1). To the south near the Charlie Gibbs Fracture Zone, the mouth of the Rockall Basin opens up into Late Cretaceous ocean crust (Londale and Shor 1979). Water depths in the Rockall Basin range from 1000 m in the northeast to 4000 m in the southwest. The Irish continental shelf is about 200 m deep. The basin slope lies between depths of 1000 to 2000 m, where major Cenozoic faults occur. The basin bathymetry is defined by these Cenozoic structures.

In the central and northern parts of the Rockall Basin the continuity of the basin floor is interrupted by the isolated bathymetric highs of the Rosemary Bank, Anton Dohrn and Hebrides Terrace Seamounts (Fig. 4.1). The Hebrides Terrace, located within the study

area, is part of a major Palaeocene to early Eocene intrusive complex (Nolan *et al.* 1999; Omran 1990) and changes seabed depths from 1875 m to 1125 m.

The crust underlying the Rockall Basin appears to be continental in nature, based on seismic refraction and wide-angle reflection profiles (Roberts *et al.* 1988; Makris *et al.* 1991; Hauser *et al.* 1995; Shannon *et al.* 1994, 1995, 1999; O'Reilly *et al.* 1995, 1996, 1998; Jacob *et al.* 1995; England 1995; England and Hobbs 1997). It was earlier argued to be oceanic (Roberts *et al.* 1981; Joppen and White 1990) or mixed continental/oceanic (Megson 1987) in nature. Figure 4.2 shows the location of regional seismic lines used by different authors to interpret the nature and structure of the crust. The thickness of the crust underlying the adjacent basement platforms (e.g. the Irish Mainland Shelf and Rockall Bank)(Fig. 4.1) is typically 25-30 km (Shannon *et al.* 1995; Klemperer *et al.* 1991). Thinly stretched continental crust lies beneath the Rockall Basin. Crustal thickness beneath the Rockall Basin varies from less than 6 km in the southwest (O'Reilly *et al.* 1995) to over 23 km in the extreme northeast (Bott *et al.* 1979). The seismic character of the continental crust is three-layered on both sides of the Rockall Basin (upper, middle and lower crust) and two-layered beneath the Rockall Basin (upper and lower) (Fig. 4.3) (O'Reilly *et al.* 1995).

The basement where the sedimentary basins lie on is made of Pre-Cambrian metamorphic and granite rocks. To the west of the Rockall Basin, dredged samples from the Rockall Bank are geochemically similar with onshore outcrops in western Ireland (Daly *et al.* 1995). Pre-Cambrian basement is also suggested to occur below the Rockall Basin based on seismic refraction properties in the RAPIDS profile (Shannon *et al.* 1994; O'Reilly *et al.* 1995) (Fig. 4.3).

The basement and crust are offset by major faults. The WESTLINE seismic reflection profile proved that the floor of the Rockall Basin is formed by rotated blocks separated by mainly east-dipping faults and filled by wedges of sediment (England and Hobbs 1997). Klemperer *et al.* (1991) interpreted the WIRE 1 and 3 profiles by showing the

Great Glen fault and associated northeast trending strike-slip faults as near vertical structures that cut the whole crust and the upper-most mantle (Fig 4.4).

Within the Rockall Basin and above this Pre-Cambrian basement lies a sedimentary section. The exact age of the sedimentary section is uncertain due to the lack of wells and poor seismic visibility caused by flood basalts erupted in late Palaeocene and early Eocene (Mussett *et al.* 1988; Stoker *et al.* 1993). It was suggested by Shannon *et al.* (1995) that Late Palaeozoic, Mesozoic and Cenozoic rocks occur in the Rockall Basin (Fig. 4.3), based on the considerable thickness of sediments, seismic properties and the occurrence of the same sediments in the adjacent basins such as the Slyne, Erris and Donegal Basins. Shannon *et al.* (1995) and Smythe (1989) suggested a rifting event as early as Late Carboniferous. Later Permo-Triassic, Late Jurassic (Shannon *et al.* 1999) and Late Lower Cretaceous (Musgrove and Mitchener 1996) are the most likely ages for rifting in the Rockall Basin based on seismic interpretation and basin modelling.

Faults on this margin dominantly trend northeast, north, northwest and east (Fig. 4.5):

(1) Northeast-trending elongated fault blocks down-throw to the northwest (e.g. Erris High), occur in the eastern part of the Rockall Basin. In the northeastern Irish Rockall Basin, most of these faults were active during Mesozoic-Cenozoic extension.

(2) North-trending faults are common in the northern Rockall Basin, and Waddams and Cordingley (1999) suggested that these faults were active during Jurassic rifting. Mapping of north trending structures between the Hebrides Seamount and the Donegal Basin section has shown the margin of the Rockall Basin to be structurally elevated in the area (Nolan and Wilson 1999).

(3) Northwest-trending transfer faults or lineaments segment Mesozoic and Cenozoic basins along the northeastern Atlantic margin. These include the Wyville-Thomson Ridge, the Ness Fault Zone and the Anton Dohrn Transfer Lineament (Tate *et al.* 1999, Doré *et al.* 1999). These lineaments are either parallel or continuous with fracture zones in the Atlantic seafloor.

(4) East to northeast-trending lineaments dissect the basin margin and basement highs within the Rockall Basin. The northeast-trend of the main basin boundary fault swings to an east trend towards the south. This swing can also be observed onshore in the Clew Bay fault.

The eastern margin of the Rockall Basin is comprised of numerous discrete sub-basins 40-100 km in length and 10-30 km in width (Fig. 4.5). Carboniferous basin formation was followed by Permo-Triassic rifting in the Erris, Donegal and possibly Rockall Basins. Permo-Triassic asymmetrical half grabens are present in the Slyne, Erris and Donegal Basins (Fig. 4.5).

4.2.2 The Slyne Basin

The Slyne Basin is a north-northeast trending asymmetrical half-graben located on the Irish Shelf, west of County Mayo (Fig. 4.5). The Slyne Basin is bounded to the west and southwest by the Slyne High and passes to the north into the en echelon Erris Basin, partially connected westwards to the Rockall Basin.

The Slyne Basin contains Carboniferous, Permo-Triassic strata (wells 18/20-1 and 27/5-1) (Dancer *et al.* 1999) and a 2.5 km section of Jurassic (well 27/13-1) unconformably overlain by thin Cretaceous to Quaternary sediments. A major rifting episode occurred during the Middle Jurassic (Dancer *et al.* 1999). Inversion after the Middle Jurassic may have removed up to 1.2 km of sediments based on thermal chronological data (Scotchman & Thomas 1995).

The Slyne Basin is controlled by a down to the east fault along its western margin (Fig. 4.5). The Slyne Basin is separated from the Erris Basin to the north by the Great Glen Fault (Trueblood and Morton 1991; Trueblood 1992) (Fig. 2.1).

4.2.3 The Erris Basin

The Erris Basin is a narrow, elongate, Late Palaeozoic-Mesozoic half-graben located in northwestern offshore Ireland, between the Rockall Basin and the Irish Mainland Shelf (Fig. 4.5). The Erris Basin trends northeast and is separated from the Rockall Basin by the fault-bounded Erris High to the west. The Erris High or Ridge is a relatively narrow (5-7 km) elongate, intermittent feature, for approximately 150 km made of Palaeozoic or older rocks and forms a horst bounded by two faults active during Cenozoic times (Cunningham and Shannon 1997). The Erris Basin is situated above a zone of transitional crust, separating a crustal thickness of ~30 km on the Irish Shelf from the thinly stretched continental crust of the Rockall Basin (~8 km) (Shannon *et al.* 1999).

Two wells, 12/13-1a and 19/15-1, were drilled in the Erris Basin and proved Carboniferous, Permo-Triassic, Lower-Middle Jurassic and Cretaceous sediments beneath a thin Tertiary cover. The Erris and Donegal Basins contain approximately 2.5 km of Carboniferous rocks (Robeson *et al.* 1988).

The Erris Basin has been divided by Chapman *et al.* (1999) into sub-basins separated by diffuse transfer faults. Rifting events have been proposed for the Carboniferous, Permo-Triassic, Middle-Late Jurassic and Late Early Cretaceous (Chapman *et al.* 1999).

4.2.4 The Donegal Basin

The east-northeast-trending Donegal Basin lies offshore northwestern Ireland (Fig. 4.5). The basin is surrounded by Pre-Cambrian basement.

Well 13/3-1 penetrated Carboniferous sediments, overlain unconformably by thin Miocene and Plio-Pleistocene sediments. The Carboniferous succession is comparable to exposures in onshore Ireland (Robeson *et al.* 1988). Maturity levels in well 13/3-1 may indicate 2-3 km of post-Westphalian D section removed (Robeson *et al.* 1988), implying

the Donegal Basin underwent major denudation in post-Carboniferous time. Based on seismic interpretation, Mesozoic sediments may also occur in part of the basin.

A northeast-trending south-dipping fault divides the Donegal Basin into the Main Donegal Basin and the South Donegal Basin. Seismic interpretation indicates a dextral strike-slip movement on northeast-trending faults (Dobson and Whittington 1992).

4.3 Data and methods

The study area was defined by available seismic and well data, and is contained within coordinates 56° 40' N to 54° 40' N and 9° 00' W to 12° 00' W (Fig. 4.5). Exploration well data from each of the basins is given in Table 4.1. The stratigraphy of each well has been summarised from the composite well logs (Fig 4.6). Data from four exploration wells in the eastern Rockall Basin and northwestern Ireland indicate a range of sedimentary lithologies and thicknesses along the margin from Archean to Carboniferous to lowermost Jurassic, with locally thick Cretaceous submarine sediments, Tertiary marine strata (Murphy and Croker 1992) and Quaternary sediments. While these four exploration wells represent the primary control on sedimentary facies and age in this study, other shallower wells and boreholes in the Rockall Basin region were also used for age and lithological calibration (Table 4.2). Jakovides (2000) reviewed the biostratigraphy of wells 132/15-1, 12/13-1a and shallow British Geological Survey (BGS) boreholes, using palynology, nannopalaeontology and micropalaeontology.

Well 132/15-1 drilled a total of 2830 m of Cenozoic sediments lying on Cretaceous and granitic basement (Fig. 4.6) (Musgrove and Mitchener 1996). It is the only well available today drilled strictly in the Rockall Basin and is therefore extremely valuable for dating Cenozoic basin-wide seismic reflections. The other wells, 12/13-1a, 13/3-1 and 19/5-1 (Fig. 4.6), were drilled in the Erris and Donegal Basins, and in each the Cenozoic section is thinner, with a maximum of 500 m. Well 12/13-1a, drilled in the Erris Basin, contains Eocene and thin Palaeocene sections lying on Cretaceous sediments. Well 19/5-1, also in the Erris Basin, has a thin Neogene sequence lying unconformably on Jurassic rocks.

Well 13/3-1, drilled in the Donegal Basin, has a thin Tertiary section lying unconformably on Carboniferous sediments.

A network of 2D reflection seismic lines crossing the eastern Rockall, Erris and Donegal basins (Fig. 4.7) allowed the interpretation of five different Cenozoic packages (Fig. 4.8a). The names of the seismic surveys are listed in Table 4.3. The seismic lines were available in digital format and were analysed on a Sun Solaris workstation using the Landmark Seisworks 2D and EarthVision software. Cenozoic unconformities (Fig. 4.9) were digitally mapped over a period of one month at the TotalFinaElf offices in Aberdeen. Five different surfaces were interpreted and transformed into grids as isochron maps in TWT. Each of these surfaces was used for further analysis such as depth conversion, decompaction and flexural modelling.

Exploration wells and boreholes have been used to calibrate the different surfaces on the seismic lines, (e.g., base Tertiary) allowing extrapolation of the given information to the rest of the basin (Fig. 4.7). The seismic interpretation was done both (1) by following a reflection originally taken from the seismogram of the well and, followed along the seismic line based on its reflectivity properties and, (2) by its unconformity nature either by onlap, downlap, truncation or reflection termination (Fig. 4.9).

The Rockall Basin changes trend from north to northeast at 55° 40' N (Fig. 4.7). North of this latitude available seismic lines are spaced from 1 to 3 km apart, and with well 132/15-1 allowing good Tertiary calibration. To the south, the spacing is much larger, ranging from 3 to 9 km, and no wells are drilled strictly in the basin. The seismic interpretation of unconformities in the north is therefore better calibrated in terms of wells and seismic resolution than in the central and southern portions of the study area, and this must be considered during the interpretation of the maps from the seismic. Isopach maps were constructed by subtracting the oldest surface to the youngest.

Velocity information from wells 132/15-1, 12/13-1a and 19/5-1 were used to convert seismic travel times to depth. Published biostratigraphic data were used to constrain the

age of the seismic sequences. Porosity data from well 132/15-1 were used to decompact both the well and the rest of the basin. Accumulation rates were estimated from decompacted isopachs.

4.4 Cenozoic stratigraphy

4.4.1 Introduction

Cenozoic sediments and regional unconformities are widely recognised throughout the western Irish offshore basins including the Porcupine Basin (Tate 1993; Naylor and Anstey 1987), Slyne Basin (Dancer *et al.* 1999), Erris Basin (Chapman *et al.* 1999) and Rockall Basin (Stoker *et al.* 2001; Austin 2001). In onshore northwestern Ireland and the Irish Shelf little or no Tertiary sediment is preserved. Therefore the western offshore basins provide a window into the Cenozoic history of Ireland. A generalised cross section from northwestern Ireland to central Rockall Basin shows (Fig. 4.8b), in succession, Dalradian, Carboniferous, Mesozoic and Cenozoic rocks at or near the surface. Decreasing age from east to west indicates, a long-term denudation of onshore Ireland and accumulation of the eroded sediment into the offshore basins. Decreasing elevation from east to west might also indicate recent surface uplift in Ireland and subsidence in the Rockall Basin.

In this section I present basin unconformities interpreted from the seismic across the offshore basin and up the eastern margin slopes onto the Irish Shelf. I describe the seismic facies of the five seismic Cenozoic packages, which are bounded by unconformities or conformable high amplitude reflections. Isochron maps of the seismic are presented in milliseconds TWT and compacted and decompacted isopach maps are shown in metres. These were calculated to quantify the amount and the rate of sediment accumulation in the offshore basins.

The Rockall Basin has a very thick Cenozoic sedimentary section and regional seismic correlation of intra-Tertiary reflections and unconformities interpreted by previous

authors has established a reliable seismic stratigraphy for the Cenozoic sequence in the Rockall Basin (Table 4.4). Stoker *et al.* (2001) dated three Upper Cenozoic packages and unconformities based on nannoplankton evidence taken from several shallow boreholes from the western and northern Rockall Basin. Shannon *et al.* (1993) described the seismic facies of each Tertiary package and dated basin reflections based on shallow DSDP (deep-sea drilling project) boreholes drilled in the southern Rockall Basin, Hatton Rockall Basin and Rockall Bank (Naylor and Shannon 1982; Masson and Kidd 1986). Corfield *et al.* (1999) based their seismic interpretation on wells 163/6-1A and 132/15-1 drilled in the UK sector of the northeast Rockall Basin. This study uses base Palaeocene, base Eocene and upper Eocene tied by well data and the last three seismic packages have been dated using Stoker *et al.* (2001) interpretations.

4.4.2 Seismic interpretation

Seismic stratigraphic interpretation is based on the identification and correlation of seismic unconformities separating and bounding packages with relatively different seismic signatures (Mitchum and Vail 1977; Vail 1987; Emery and Myers 1996). These seismic unconformities are marked by reflection terminations (onlap, downlap and toplap), by differences in the amplitude and frequency spectra of the adjoining packages, and often by regional continuous reflections.

For this study, the seismic interpretation was done using digital 2D seismic surveys with a line spacing ranging between 1 and 10 km (Fig. 4.7, Table 4.3). Five regional Cenozoic unconformities are recognised in this study: base Palaeocene, base Eocene, and three post-late Eocene surfaces (Fig. 4.9). These surfaces are defined by unconformities or sometimes by a high amplitude reflection. The nature and timing of erosional events after the late Eocene are poorly constrained due to the lack of wells and uncertainties in the seismic interpretations of complex continental slope stratigraphy. This problem has been recognised by Stoker et al (2001), Corfield *et al.* (1999) and Egerton *et al.* (1999). This work combines evidence from previous work (Table 4.4) with well data to suggest ages for the five different packages mapped. Despite a limited dataset, a seismic interpretation

of the Cenozoic section in the Rockall Basin, and a depth conversion and decompaction were done in this study using all available information (Tables 4.1 and 4.3). However it must be stressed that, in the absence of good well control in the Rockall Basin, the ages assigned to the regional unconformities mapped in this study are preliminary.

In this work, despite limited data, it was possible to assign ages to the Rockall Basin Cenozoic unconformities that were both internally consistent with the limited well data and seismic lines, and within the schemes of other workers.

Well 132/15-1, the only well in the Rockall Basin *sensu stricto*, penetrated 2830 m of Cenozoic sediments and provides the best control for the base Palaeocene and base Eocene unconformities (Fig. 4.6). Well 132/15-1 began recovering samples in middle to upper Eocene sediments very close to a regional unconformity seen on seismic reflection lines tied to the well, and which is inferred to be upper Eocene in age. Well 12/13-1a, on the basin margin drilled a thin Palaeocene section and 167 m of Eocene mudstones (Fig. 4.6). The basin margin Eocene from well 12/13-1a cannot be easily correlated to the Rockall Basin due to its margin location, but the low amplitude seismic facies of this package can arguably be correlated with similar low amplitude facies down into the basin.

Shallow boreholes drilled by the British Geological Survey in the western and eastern margins of the Rockall Basin penetrated an upper Cenozoic sequence described by Stoker *et al.* (2001). Correlation across regional lines in the basin (e.g. lines NA-15 and WRM96-103) is important in order to assign ages to the mapped unconformities in the eastern Rockall Basin. By seismic stratigraphic correlation, Stoker *et al.* (2001) inferred ages for the three youngest unconformities in the Rockall Basin as upper Eocene, early-middle Miocene and early Pliocene, which they named C30, C20 and C10 respectively (Table 4.4). These ages are also used in this study.

Regional seismic lines such as WRM96-103 (see Fig. 4.10 for location) cross the Rockall Basin and were used to correlate western unconformities dated by borehole sediments

from other studies with the northeast Irish Rockall Basin reflections picked in this study. Line WRM96-103 shows the best possible picks for top upper Cretaceous, top Balder Formation (base Eocene), Reflection C (upper Eocene) and a reflection B (upper Eocene-middle Miocene) (BGS-Geoteam 1996). These interpretations were combined with the Cenozoic reflections of Stoker *et al.* (2001) and together form the best available control for dating Cenozoic unconformities. Regional lines NA-15 and NA-25 (see Fig. 4.10 for location) were also used for correlation of regional reflections across the basin.

Once five different surface reflections were mapped and preliminary ages assigned, isochron maps were built for the Palaeocene, Eocene, Oligocene, Miocene and Plio-Pleistocene packages. This was done importing the line picks from Seisworks into EarthVision and interpolating the scattered point data from the seismic lines into 2D minimum tension grids. The calculation did not extrapolate outside data areas. Distance between seismic lines vary from less than 1 km in the north to up to 10 km in the south of the study area (Fig. 4.7). Grid spacing was chosen to be 1 km in order not to lose resolution in areas where the seismic network is dense although errors might be introduced where the seismic network is coarse. These errors must be considered when interpreting the isochron and isopach maps, in particular for the southern part of the study area.

The study area is divided in Quads. with numbers that vary from UK to Irish waters (Fig. 4.10). During description of different sedimentary packages and structures mention will be given to these Quads. as a coarse geographical reference.

4.4.3 The Cenozoic section

The Cenozoic isochron map (Fig. 4.11) was constructed subtracting base Tertiary to seabed. The Cenozoic isochron shows maximum thickness of sediments in the north of the study area (<2506 ms), minimum in the south (<1400 ms) and an eroded Cenozoic section at the basin margin (<600 ms). The Cenozoic succession in the Rockall Basin is conformable in the basin centre and thins unconformably (through both onlap and

downlap) onto the basin margins over about 30 km of horizontal distance (Fig. 4.11). The basin margin contains a thin Tertiary section that pinches out towards Ireland, and a continuous Quaternary layer is present across the basin and shelf. Cenozoic sediments thins towards the east, suggesting surface uplift of the eastern margin of the Rockall Basin (Fig. 4.8b).

Tertiary relative uplift in Britain and Ireland (Roberts 1989; Brodie and White 1995; Rowley and White 1998) and a period of Tertiary exhumation in Ireland (Allen *et al.* in press; Green *et al.* 2000) provide provenance sources for this Cenozoic section. Thermal subsidence following the Aptian-Albian rift phase was active during the Cenozoic and, along with loading of Tertiary sediments and Palaeogene intrusives, may have enhanced the generation of accommodation space in the basin.

4.4.4 Base Palaeocene and Palaeocene section

4.4.4.1 Characteristics of the unconformity and geology

The base Palaeocene is directly observed in well 132/15-1 (Fig. 4.6) and from there it is possible to trace it using seismic stratigraphic techniques further south into Quad. 5 and north of Quad. 12, where the seismic coverage is good. Towards the basin margin the base Palaeocene becomes unconformable and is seen onlapping onto Pre-Cambrian, Carboniferous or Mesozoic basement. The presence of Palaeocene and Eocene intrusives in the overlying section makes the base Palaeocene sometimes difficult to pick.

The base Palaeocene is characterised by an upwards increase in seismic velocity, from low velocity Upper Cretaceous rocks to the high amplitude Palaeocene section. Correlation with well 132/15-1 shows that the Upper Cretaceous rocks are mostly mudstones, whereas the lower Palaeocene includes basalts, turbiditic sandstones, deep marine mudstones and thin limestones with higher velocities. A local intra-Palaeocene unconformity is recognised on some of the lines south of Quad. 5 (Fig. 4.9). The intra-Palaeocene unconformity was ignored in this work, because it is not regional and,

because of the lack of time to do the interpretation. The upper Palaeocene section contains thin sand units within a shaly succession. Thus the Palaeocene coarsens upwards, suggesting a shallowing event. Well 12/13-1a has 71 m of Palaeocene mudstones with some siltstones, showing that at the margin the Palaeocene is generally thin or missing as shown in some marginal seismic lines. Shallow BGS drilling on the Erris Ridge shows Palaeogene volcaniclastics and shell fragments (Stoker *et al.* 1999; Haughton 2000).

4.4.4.2 Seismic facies

The high amplitude seismic response seen in the Palaeocene sequence is caused mainly by Palaeocene to Eocene igneous sills and dykes, recognised on the seismic lines by characteristic discontinuous plate-shaped reflections. Intervals of thin limestones in the lower Palaeocene and some local sandstones in the upper Palaeocene are also responsible for the increased reflectivity (e.g., Fig. 4.35).

4.4.4.3 Isochron map description

The Palaeocene sequence is thickest in the north, with a maximum thickness of 1450 ms, and thins to the south and east (Fig. 4.12). A major depocentre surrounds the Hebrides Seamount, which was being constructed at this time as an active volcanic centre (Nolan *et al.* 1999; Omran 1990) and probably provided a local source of volcaniclastic material. A smaller depocentre is also seen in the south, possibly with a sedimentary source in Ireland. Palaeocene normal faults are common throughout the northwestern Irish margin. However, no normal faults have been found on the seismic lines adjacent to the southern depocentre, suggesting that deposition is not fault controlled (Fig. 4.12). Where the eastern basin margin fault was active, the isochron thickness is less than it is along the segment of the margin that shows no evidence of Palaeocene fault activity.

4.4.4.4 Seismic characteristics in different parts of the study area

In Quad. 5, particularly on line 0597-68b (see Fig. 4.10 for location) the Palaeocene is conformable with, or onlaps onto, Upper Cretaceous sediments. The Palaeocene lies on Lower Cretaceous or older faulted blocks tilted 45° to the west. The Palaeocene sequence generally onlaps onto faulted blocks Mesozoic or Pre-Cambrian in age. Some of these Mesozoic and older structures were reactivated in the Palaeocene as normal faults.

Line NWI93-110, to the south of the study area in Quad. 19, shows Palaeocene beds onlapping onto the base Tertiary unconformity without being displaced by a single normal fault. Underlying faulted blocks of pre-Tertiary rocks show strata tilted 45° to the southeast; pre-Tertiary strata are truncated by the base Tertiary unconformity, indicating significant erosion of the fault-block topography.

In Quad. 18, the Palaeocene again onlaps onto faulted blocks where the base Palaeocene is normally offset. At the margin (e.g. line NWI91-102) Palaeocene beds are parallel to basement and are tilted 30° to the northwest, towards the basin. East of the margin, Palaeocene sediments are eroded and toplap against the seabed, suggesting tilt after deposition. Younger sediments, perhaps Plio-Pleistocene (by correlation with well 19/5-1), lie above an Eocene progradation sequence and dip northwest at 10°. This implies a post-Palaeocene, pre-Pliocene tilting of the margin to the northwest by approximately 20°.

4.4.4.5 Interpretation

Evidence from seismic interpretation suggests that Palaeocene sedimentation in the eastern Rockall Basin occurred as onlapping infill, rather than in the form of progradational wedges. This suggests rapid and ongoing basin subsidence in order to create sufficient accommodation. Unlike the northeastern Rockall Basin, where late Palaeocene progradation is widely recognised in offshore basins east of Britain (Clarke 1999; Underhill 1991) and in the Porcupine Basin (Naylor and Anstey 1987). This

difference might be explained by differences of sizes in drainage basins. A small drainage basin west of Scotland and northwest of Ireland, perhaps not too different to the present day, provided less sediment during late Palaeocene. A bigger drainage basin east of Britain and southern Ireland would explain extensive sedimentation and progradation in the North Sea and the Porcupine Basin during the Palaeocene.

4.4.4.6 Summary

- A base Palaeocene unconformity is recognised in the northeastern margin of the Irish Rockall Basin.
- Palaeocene mudstones, sandstones and limestones onlap onto the basin margin.
- Two major sedimentary depocentres have been recognised in the south and north of the study area (Fig. 4.12).
- The eastern basin margin of the Rockall Basin is faulted intermittently (in space) with maximum normal offset at base Palaeocene and diminishing throughout the Palaeogene.
- Palaeocene normal faulting and Palaeocene sedimentary depocentres do not correlate well. This suggests mechanisms such as flexural uplift, rather than local fault uplift, to create a sedimentary source.

4.4.5 Base Eocene unconformity and Eocene section

4.4.5.1 Characteristics of the unconformity and geology

The base Eocene unconformity is visible in wells 132/15-1 and 12/13-1a. lower Eocene reflections are observed to downlap onto the base Eocene unconformity in Quads. 5 and 19 (e.g. lines TRHP016, INROCK96-12, Fig. 4.10) and they become conformable towards the basin centre (e.g., lines GER96-50, GER96-37). North of the study area, in the UK sector of the Rockall Basin, wells 164/25-1 and 164/25-2 show a similar depositional hiatus in the early Eocene (Egerton 1998). This unconformity is of regional

character and appears to be synchronous with the opening of the North Atlantic and onset of a ridge push dominated stress regime (Doré *et al.* 1999).

Well 132/15-1 drilled a sequence of Eocene sandstones, siltstones, shales and intrusives in the basin, while well 12/13-1a drilled siltstones and shales in the Erris Basin.

4.4.5.2 Seismic facies

The Eocene has a general low amplitude facies, with the exception of local high amplitude intrusives and high velocity sand units downlapping towards the basin suggesting a progradation of unknown environment (Fig. 4.14). Low amplitude reflections sometimes lose reflectivity and the internal structure of the Eocene is hard to pick. In the basin slope the structure is commonly chaotic.

4.4.5.3 Isochron map description

The Eocene sequence is widely present in the Rockall Basin, with maximum thickness of 1101 ms in the northeast, a minimum of 389 ms in the south and, a discontinuous cover of <300 ms on the Erris Basin (Fig. 4.13). Maximum deposition occurs in the northern part of the study area, particularly where the basin changes trend from northeast to north. Along the basin margin, seismic lines trending northeast, parallel to the basin margin, show highly variable thicknesses of Eocene sediments above the Palaeocene section (Fig. 4.13). The Eocene thins rapidly to the east on the present day continental shelf, where basement is now mantled only by thin Plio-Pleistocene sediments.

4.4.5.4 Seismic characteristics in different parts of the study area

In Quad. 5, where well control is given by 132/15-1, a local top-lower Eocene unconformity separates lower Eocene sand-rich section from middle to upper Eocene mudstones. The lower Eocene section contains high amplitude reflections, probably sands and volcanics. The middle and upper Eocene is dominated by low amplitude reflections,

consisting mainly of thick mudstones. These mudstones commonly contain undulating subhorizontal structures that are interpreted as post-depositional gravitational detachment surfaces created in wet and muddy sediment. On the basin slopes the internal structure of the Eocene section is not visible or is chaotic, possibly due to gravitational processes.

Within the basin, Eocene beds are downlapping or conformable. In Quad. 5 high amplitude reflections are observed to downlap to the southwest (Fig. 4.14) (e.g., lines INROCK96-12, SRT-96-228, GER96-52) or to the northwest (e.g., lines NWI93-124, NWI93-226), implying both northeast and southeast sedimentary sources (Fig. 4.15). These reflections are interpreted as prograding sand-dominated fans based on their geometry in the seismic sections. The interpretation is supported by the composite log in well 132/15-1, which shows sand bodies in the lower Eocene and an upward increase in sandstone content (Fig. 4.6). These data suggest a relative basin shallowing event starting at the end of the Palaeocene and finishing in the early Eocene. The middle and upper Eocene is dominated by mudstones, implying that the basin began deepening after early Eocene time and sand input decreased.

In Quad. 12, the Eocene is more chaotic and lacks internal structure, possibly due to gravitational processes. Around well 12/13-1a, a progradation of unknown environment is seen in the basin margin. Down in the basin the Eocene seismic facies lacks structure but presents the same low amplitude signature observed in the seismic facies of the marginal Eocene sediments. Therefore, the Eocene section in this area is only tentatively correlated from margin to basin. However, correlation of base Eocene unconformity from well 132/15-1 in Quad. 132 to Quad. 12 indicates a similar position for the base Eocene unconformity.

The lower Eocene downlap or progradation of unkown enviroment along the margin is also seen in Quads. 18 and 19 (Fig. 4.15). The Eocene was more intensively eroded in Quad. 19 (e.g., lines NWI91-104, GER96-37 and NWI91-106), although the line NWI91-108 again shows local marginal progradation (Fig. 4.15). The best examples of this progradation are found in Quad. 18 (e.g., lines NWI91-101 and NWI91-102). High-

amplitude reflections downlap onto the base Eocene unconformity. Younger lower amplitude reflections dip at a steeper angle. This suggests that basin slope may have steepened during late Palaeocene to early Eocene times, possibly suggesting marginal surface uplift. This progradation is situated above a major base Palaeocene and base Eocene normal fault that offsets both base Palaeocene and base Eocene unconformities (Fig. 4.13, 4.15).

4.4.5.5 Interpretation

Sand progradation of unknown environment was interpreted from the seismic and located near the basin slope, suggesting a sedimentary source coming from the southeast and east of the basin, possibly from Ireland.

Like in the Palaeocene, early Eocene normal faulting does not have a big effect on changes in sedimentary thickness, with the exception of a northeast-trending fault in Quad. 19. Here again other mechanisms, rather than fault uplift, such as flexural uplift might explain sedimentary thickness changes.

Before the middle-late Eocene there is no evidence for deep-water circulation within the UK sector of the Rockall Basin (Egerton 1998), consistent with the relatively shallow setting inferred in this study. In the Porcupine Seabight basin, offshore western Ireland, Tate (1993) concluded that regressive-transgressive cyclicity occurred throughout the early Palaeogene with a major transgressive episode induced by renewed extension in the late middle-Eocene. This event promoted a change in the style and depth of sedimentation in the basin, which has continued until the present (Tate, 1993).

4.4.5.6 Summary

- Early Eocene sand progradation of unknown environment was common in the northeastern Irish Rockall Basin and the sedimentary source was coming from the east and probably from Ireland, as well as Scotland (Fig. 4.15).

- Maximum Eocene deposition occurs where the margin changes trend from northeast to north.
- There is no clear relationship between mapped early Eocene normal faults and progradational packages, which indicates that sedimentary source is not related to fault activity.

4.4.6 Post-late Eocene unconformity and ?Oligocene section

4.4.6.1 Characteristics of the unconformity and geology

The post-late Eocene unconformity is a markedly angular boundary and is commonly onlapped by middle to Upper Cenozoic drift deposits along both eastern and western margins of the Rockall Basin. The unconformity erodes upper Eocene sediments, and post-upper Eocene sediments onlap onto it (yellow unconformity in Fig. 4.9). Well 132/15-1 only began recovering samples in upper Eocene sediments, just below the unconformity, which is seen on seismic lines tied to the well. Stoker *et al.* (2001) mapped this unconformity and denoted it as C30; he assigned it an age of late Eocene, based on calcareous nannoplankton in BGS borehole 94/1 drilled in the western margin of the Rockall Basin (Stoker 1997). This borehole penetrated the unconformity and recovered shallow marine mudstones and sandstones of late Eocene age, with upper Eocene deep marine limestones resting on top of the unconformity. This suggests a rapid subsidence event. Rapid subsidence is also apparent from the change in geometry of the pre- and post-unconformity sequences, corresponding to a change from shelf-margin to basin infill to a predominantly ponded-basin infill (e.g., Fig. 4.32). Other evidence for substantial late Eocene subsidence is provided by BGS short core 57-12/18, which proved middle to upper Eocene near-shore conglomerate from the top of Anton Dohrn Seamount at a present water depth of 705 m (Stoker *et al.* 2001). Rocks of similar age have also been proven by BGS boreholes 94/2 and 94/3 on the Rockall Bank, and 94/7 on the George Bligh Bank, where the unconformity surface occurs at or near the sea bed (Stoker 2001), and in well 164/25-2 on the northeast flank of the basin (Egerton 1998).

In this study, regional mapping and correlation of this late Eocene unconformity was done following line GER96-50 (Fig. 4.10) from Quad. 5 to the southwest (basin centre) along lines NA-15, NA-25 and WRM96-103. Well 132/15-1 was linked to well 12/13-1A using lines INROCK96-12, WM-90-394A, GER96-09 and NWI93-183 (Fig. 4.10).

Stoker (1998) described an upper Eocene to lower Miocene package (megasequence RTc) as predominantly deep marine contourites preserved as mounded, elongate, and broad, sheeted, sediment drifts with associated sediment waves. The package is seen in the form of slope apron bodies, with internal deformation possibly caused by slide/debris flow (Stoker *et al.* 2001).

4.4.6.2 Seismic facies

The late Eocene unconformity is marked by a high amplitude reflection, sometimes offset by small faults (Fig. 4.32). The upper unconformity is marked also by a high amplitude reflection but of less intensity than the late Eocene unconformity. Low amplitude reflections are characteristic of the ?Oligocene section, although the reflections are sometimes continuous and easier to follow across than in the upper Eocene section.

4.4.6.3 Isochron map description

The upper Eocene to lower Miocene succession from Stoker *et al.* (2001) is here presented as ?Oligocene. The ?Oligocene isochron map (Fig. 4.16) shows small local sediment depocentres adjacent to and downslope of the basin margin in Quad. 11 and south of Quad. 5, suggesting local sediment input from the Irish Shelf and Mainland during post-late Eocene time.

4.4.6.4 Seismic characteristics in different parts of the study area

A Post-late Eocene progradation of unknown environment in Quads. 18, 19 and 11 appears to have been sourced from the southeast (Fig. 4.15). Two sets of prograding

sigmoidal clinoforms are locally identified, one on top of the other (e.g., line GER96-24). Progradation extends up to 6 km away from the basin slope, at which point the reflections are parallel to the late Eocene unconformity and are locally eroded by a later (?early Miocene) unconformity (e.g., line GER96-36). In the northern parts of the study area, this post-late Eocene progradation is not visible. Some beds downlaping onto the late Eocene unconformity are seen in INROCK96-12 (Quad. 5), but low amplitude reflections are mainly observed to onlap onto the late Eocene unconformity.

4.4.6.5 Interpretation

Sea level was rising at this time (Haq *et al.* 1987). Basin deepening began in middle to late Eocene time possibly accentuated by basin thermal subsidence after Cretaceous and Early Tertiary extension. Progradation suggests an increase in sediment input from the east, possibly from Ireland, during post-late Eocene (possibly Oligocene) time.

A widespread post-late Eocene unconformity was followed by a marked change in sedimentation style. These events have been attributed to submarine erosion by deep-water bottom currents (Miller 1982) following a major phase of subsidence (Stoker 1998) and mark the onset of bottom current activity in the Rockall Basin. Simultaneously, there was significant lateral migration of sediment by upslope accretion onto the flanks of the basin, including the construction of the Feni Ridge on the western side of the Rockall Basin (Stoker 1998).

The origin of this unconformity may be a combination of the following events: (1) basin subsidence that led to the deposition of deep marine sediments (Stoker *et al.* 2001), (2) regional uplift and Oligocene-Miocene compression (O'Driscoll *et al.* 1995), (3) changes in the intra-plate stress regime across the margin, possibly triggered by regional tectonic events postdating the early Eocene (Doré *et al.* 1999). In addition, a major reorganization of spreading rate and direction occurred in the North Atlantic during this time, possibly caused by the cessation of sea-floor spreading in the Labrador Sea (Nunns 1983; Hinz *et*

al. 1993). The timing of the post-late Eocene subsidence was broadly coeval with the culmination of the Pyrenean Orogeny to the southeast (Knott *et al.* 1993).

4.4.6.6 Summary

- The low reflectivity of Post-late Eocene sediments indicate a lithology rich in mudstones.
- Reflections generally onlap onto the basin margin, following the already recognised rise on sea-level or/and basin subsidence.
- A small progradation event of unknown environment is seen off west of Ireland.

4.4.7 ?Lower Miocene unconformity and ?Miocene section

4.4.7.1 Characteristics of the unconformity and geology

A second post-late Eocene unconformity is located on top of the ?Oligocene section described above (section 4.4.6). Overlying beds onlap onto this unconformity on the basin slope, but become conformable towards the basin centre. In Quad. 5, the lower Miocene unconformity is visible south of well 132/15-1 (Fig. 4.9). It lies above sediments of presumed Oligocene age, although there are no wells to directly constrain the age in the overlying sequence. The reflection can be traced in line WRM96-103 across the basin from east to west. This unconformity is correlated with reflection C20 of Stoker *et al.* (2001), who dated it as lower Miocene in age based on BGS borehole 94/1 at the western margin of the Rockall Basin (Table 4.4). A seismic sequence was mapped between this presumed ?lower Miocene unconformity and a lower Pliocene unconformity. The age of the latter is based on available wells and boreholes on the Irish margin and corresponds to C10 of Stoker *et al.* (2001).

Reflections in the sediments above the ?lower Miocene unconformity have low amplitude suggesting a lithology rich in mudstones and poor in sandstones. In the south of the study area, the ?lower Miocene unconformity and ?Oligocene slope sediments downlap onto

the late Eocene unconformity. Basinal reflections of presumed Miocene age onlap onto the ?lower Miocene unconformity (e.g., lines NA-15 and GER96-50). In some lines (e.g., WRM96-103A) no downlap or onlap is seen and reflections are uninterrupted so the ?Oligocene and ?Miocene sequences cannot be distinguished.

4.4.7.2 Isochron map description

The thickness of this possibly ?Miocene package is shown in Figure 4.17. Thickness in the north of the study area range between 0 to 200 ms and increase to generally 400 ms towards the southwest. Reflections onlap onto the ?lower Miocene surface and this package can be visualised as a sedimentary wedge pinching out northeastwards (Fig. 4.17).

4.4.7.3 Seismic facies

The internal reflection of the ?Miocene section are of lower amplitude and less continuity than the ?Oligocene section (Fig. 4.9). The ?lower Miocene reflection itself results from a rapid increase downward in seismic velocity, apparently related to an increase in hardness caused by compaction and silica diagenesis (Dolan 1986). Balddauf (1986) speculated that the increase in hardness and diagenesis was due to an oceanographic event, but the precise mechanism remains unclear. The increase in seismic velocity is not always obvious (Fig. 4.32) and in some cases it is hard distinguishing between the ?Oligocene and ?Miocene sequences.

4.4.7.4 Interpretation

The basin continued to subside during Miocene time. The early Miocene unconformity might be explained by a change in the intraplate stress regime during this time possibly explained by the late early Miocene culmination of the Alpine orogeny, together with further changes in the Atlantic sea-floor spreading geometry which caused compressional deformation in the Faeroe region (Boldreel & Andersen 1993). Along the northwestern

UK margin, north of the study area, the two main effects of this stress change were the subsidence of the Greenland-Scotland and Wyville-Thomson Ridges (Wright & Miller 1989) and the possible uplift of the Hebridean margin (Anderton *et al.* 1979; Stoker 1997). The former led to the onset of deep-water exchange between the North Atlantic and Arctic water masses (Stow & Holbrook 1984; Tate, 1993; Jansen *et al.* 1995) during middle or even late Miocene time (Eldholm 1990; Boldreel & Andersen 1993). The latter initiated the growth of a shelf-margin clastic wedge along the eastern flank of the Rockall Basin during the Plio-Pleistocene.

4.4.7.5 Summary

Reflections of ?Miocene age onlap onto the ?lower Miocene unconformity and have low amplitude suggesting a lithology rich in mudstones and poor in sandstones. The sedimentary package can be visualized as a sedimentary wedge pinching out northeastwards (Fig. 4.17).

4.4.8 ?Lower Pliocene and Plio-Pleistocene section

4.4.8.1 Characteristics of the unconformity and geology

Seismic lines that tie well 132/15-1 (e.g., lines INROCK96-12 and SRT96-228) show two of the youngest unconformities in the basin, both inferred to be Plio-Pleistocene in age by correlation with BGS borehole 11/20-sb01 (Stoker 1999). This borehole was drilled in the upper basin slope in Quad. 11 and recovered upper Pliocene and younger sediments. Correlation between the borehole and well 132/15-1 was done using seismic lines NWI-91-116, NWI93-183 and WHR93-203 (Fig. 4.10). This unconformity is at least late Pliocene in age, if not older (Stoker 1999). Stoker (2001) dated this regional Rockall unconformity (C10) as early Pliocene based on nannoplankton data on western and northern cores in the Rockall Basin. This is the best existing age constraint on Neogene reflections, and in this study I have treated the uppermost regional reflection mapped in the northeastern Irish Rockall Basin as early Pliocene. An intra Plio-

Pleistocene unconformity is also locally recognised in the north of the study area (Fig. 4.14) but is not visible to the south and was not mapped in this study.

The Plio-Pleistocene package shows excellent examples of downlaps and eroded topsets (e.g., line NWI93-226) (Fig. 4.14), suggestin a progradation deltaic in origin. Sedimentary beds increase in dip as they prograde in a westward direction (e.g., line NWI91-130). Progradational sediments have been mapped in Quad. 5 and north of Quad. 12 with general sediment transport directions to the northwest and southwest (e.g., line NWI93-121) (Fig. 4.15). To the north of the study area the Plio-Pleistocene package can be traced from the margin into the basin (e.g., lines NWI93-123, NWI93-124 and GER96-09). I have used these lines to date the youngest seismic package in the Rockall Basin. In most of the seismic lines, the marginal slope is steep, so it is not easy to correlate prograding packages between margin and basin. Evidence for gravitational sliding is common. To the south, reflections in the Plio-Pleistocene package are parallel to each other, and commonly show evidence for sliding and slumping on steep slopes (e.g., lines NWI-91-102 and GER96-17). Two separate progradational events may be separated by an intra Plio-Pleistocene unconformity (e.g., line NWI93-124).

4.4.8.2 Isochron map description

Two sedimentary depocentres were mapped, south and east of the Hebrides Seamount (Fig. 4.18). Their positions coincide with the Donegal and Barra Fans, in the north and south respectively, described by Armishaw *et al.* (1998), Holmes *et al.* (1998) and Stoker *et al.* (2001). The Donegal Fan is elongate along the basin margin. North of the study area significant volumes of sediment accumulated on the Hebridean Shelf margin.

4.4.8.3 Seismic facies

Internal reflections in the Pliocene to Quaternary sections are of high amplitude and good lateral continuity, sometimes defining local unconformity surfaces (Fig. 4.9). Progradational beds are well imaged and topsets and downlaps are therefore easy to map

(Fig. 4.14). The high reflectivity might be due to sand rich units. The early Pliocene unconformity surface is characterised, not by its high reflectivity but by its unconformity nature.

4.4.8.4 Interpretation

Further north of the study area, in middle Miocene to early middle Pleistocene time, sediment pathways were focused on the Barra and Sula Sgeir Fans, probably fed by fluvial systems draining the Scottish landmass (Holmes *et al.* 1998; Armishaw *et al.* 1998). Climate deterioration after late Pliocene time culminated in widespread glaciation on the Hebridean Shelf in the middle Pleistocene, and grounded ice sheets reached the shelf edge on at least two occasions during the last 500 ky, depositing vast amounts of glacially reworked sediment directly onto the Hebridean Slope (Stoker 1998). This event is also likely to have happened in the Irish Shelf, possibly with Ireland partially feeding the Donegal Fan (Fig. 4.15, 4.18).

4.4.8.5 Summary

Plio-Pleistocene deltaic progradational sediments have been mapped in Quad. 5 and north of Quad. 12 with well-defined clinoforms and with general sediment transport directions to the northwest and southwest (Fig. 4.15). The high reflectivity might reflect sand rich units. Two separate progradational events may be separated by an intra Plio-Pleistocene unconformity.

4.4.9 Depth conversion

4.4.9.1 Introduction

Mapping of regional reflections and the determination of isochron thickneses was done on reflection seismic sections in which the vertical scale was in two way travel time (TWT). In order to construct isopach maps the depth to each reflection must be converted

from milliseconds into metres. Isopach maps are essential in this work for calculation of the flexural effect of the Cenozoic section along the northwestern Irish margin (Chapter 5).

Because several of the seismic lines intersect wells that have been logged, 132/15-1 and 12/13-1a, the thickness of the sediment packages between the mapped unconformities can be determined in both vertical distance in metres from the well (T) and in time from the seismic data (t). From these measurements, an interval velocity (V) [m/s] for each package can be calculated:

$$V = \frac{Thickness(m)}{thickness(s)} \times 2 \qquad \text{(eq. 4.1)}$$

where the time thickness is in TWT and therefore must be multiplied by two in equation 4.1. V represents the best available velocity estimate for each package. Where interval velocities from two wells are available for the same package, a linear combination of interval velocities is used to determine velocity (V) [m/s] as a function of interval thickness (t) [s]:

$$V = a \times t + b \qquad \text{(eq. 4.2)}$$

where a and b are constants. Once interval velocity is known, ideally as a function of package thickness (t), then the thickness in metres (T) of each package, at each location, can be calculated:

$$T = V \times \frac{t}{2} \qquad \text{(eq. 4.3)}$$

where t is in TWT [s] and is converted to one way time dividing it by 2. In this way the isopach map is constructed.

The Cenozoic interval is almost complete in well 132/15-1 and thin in the rest of the wells (e.g. 12/13-1a). The lack of Cenozoic well control in the south affects the quality and reliability of the isopach results and limits their interpretation because of the uncertainties on the interval velocity. Therefore caution must be taken when interpreting the Cenozoic depth-converted maps, especially for the southern part of the study area.

4.4.9.2 Cenozoic

Interval velocities for the entire Cenozoic section above the base Palaeocene unconformity were obtained from wells 132/15-1 and 12/13-1a (Table 4.6). These velocities are combined to yield an expression for interval velocity (V) [m/s] as a function of thickness (t) [s]:

$$V = 339t + 1650 \qquad \text{(eq. 4.4)}$$

This function is obtained from a linear relation between time and velocities given by wells 132/15-1, 12/13-1A (Fig. 4.19). We depth convert using:

$$T = V \times \frac{t}{2} = (339t + 1650)\frac{t}{2} \qquad \text{(eq. 4.5)}$$

where T is depth [m]. This conversion can be done with confidence for isochron thickness up to 2.528 s, but thickness greater than 2.528 s results in velocities higher than 2408 m/s, which might be too high for Cenozoic sediments. Maximum Cenozoic isochron thickness is 2.506 s, equivalent to 3009 m after depth conversion (eq. 4.5).

4.4.9.3 Palaeocene

The same comments and caveats given above apply for the Palaeocene and overlying sections. The Palaeocene isochron was obtained by substracting the base Eocene from the base Tertiary isochrone. Depth conversion was done using wells 132/15-1, with a

Palaeocene thickness of 0.618 s, and 12/13-1a, with a thickness of only 0.035 s (Table 4.7). The following function was obtained (Fig. 4.20):

$$V = -1700t + 4117 \qquad \text{(eq. 4.6)}$$

This negative relationship implies decreasing velocity with thickness, whereas normally velocity increases with depth. This anomalous relationship might be explained by the abundance of limestone or intrusive horizons, as shown by well 132/15-1 that considerably increases the interval velocities. The use of this negative function (eq. 4.6) might introduce some errors in the final Palaeocene isopach map, overestimating the highest values and underestimating the lowest. The maximum velocity of 4115 m/s and minimum of 1538 m/s appear to be unrealistic. A constant Palaeocene interval velocity of 3055 m/s, based only on well 132/15-1, might be a more reasonable alternative, but in this work, despite the possible errors, equation 4.6 was used to decompact the Palaeocene section, because of the abundance of igneous intrusives in the study area. More well control is needed to constrain a general Palaeocene velocity function.

4.4.9.4 Eocene

The Eocene isochron was obtained by substracting upper Eocene from the base Eocene isochrones (Fig. 4.13). Depth conversion for the Eocene section was done using wells 132/15-1, 12/13-1a and boreholes 83/24-sb02, 16/28-sb01 (Table 4.8). The thickness in metres from the well logs and the thickness in time from the seismic sections tied to the wells were used to derive the following function (Fig. 4.21):

$$V = 600t + 1684 \qquad \text{(eq. 4.7)}$$

Velocities ranging between 1685 and 2344 m/s were used to depth convert depending on the isochron thickness (Table 4.8).

4.4.9.5 Late Eocene to seabed

The final depth conversion calculation involves the package between the late Eocene unconformity and the seabed. Wells 132/15-1, 12/13-1a and 83/24-sb02 were used to calculate the depth conversion function (Fig. 4.22):

$$V = 200t + 1911 \qquad \text{(eq. 4.8)}$$

The depths in metres and seconds are given in Table 4.9. Velocities obtained from this relationship range between 1911 m/s for the thinnest sections to 2135 m/s for the thickest sections. The maximum thickness in this package are 1.123 s and 1199 m (Table 4.9).

The three uppermost sedimentary packages mapped in this study - ?late Eocene to ?early Miocene, ?early Miocene to early Pliocene and early Pliocene to seabed - were not depth converted in the same way as above due to the lack of well control on the depths to the bounding reflections. Instead, constant velocities were applied to each of the three packages. Velocities of 2000, 1900 and 1800 m/s, respectively were used to depth convert the upper three sections - ?late Eocene-?early Miocene, ?early Miocene-early Pliocene and early Pliocene-seabed (equivalent to RT-c, RT-b and RT-a of Stoker *et al.* 2001). The values for these velocities are based on the results obtained for the depth conversion of the late Eocene to seabed package. This package resulted in a velocity function ranging between 1911 m/s for the thinnest sections to 2135 m/s. For this reason, the average of 2000 m/s was taken as the velocity for the ?late Eocene-?early Miocene package, 1900 m/s for the ?early Miocene-early Pliocene package and 1800 m/s for the early Pliocene-seabed package. A summary of the velocity functions and assumed constant velocities is shown in Table 4.10.

4.4.9.6 Isopach maps

Figure 4.23 shows isopach maps for the different sedimentary packages. The Palaeocene interval is the thickest, with a maximum thickness of 1232 m and a mean value of 800 m.

There are major depocentres north of the Hebrides Terrace Seamount and in the south of the study area reflecting denudation from Scotland and northwestern Ireland respectively (Fig. 4.23).

The Eocene isopach map has a maximum value of 1340 m and a mean value of 476 m. The thickest Eocene deposits occur in the north of the study area (Fig. 4.23) and around the Hebrides Terrace Seamount. Some local depocentres with Eocene progradational beds appear to have been sourced from northwestern Ireland to the southeast (Fig. 4.15).

The ?Oligocene isopach map shows maximum value of 601 m and a mean of 206 m (Fig. 4.23). Local depocentres are located downslope of the main basin bathymetric boundary defined by earlier major normal fault activity. These depocentres are shown in seismic sections as prograding wedges with a sedimentary source from the east.

The ?Miocene isopach map shows a maximum value of 483 m and a mean value of 215 m. The deposits are relatively thin and evenly distributed (Fig. 4.23). Local thickness, appear to tie to areas of progradation (Fig. 4.15).

The early Plio-Pleistocene isopach shows an increase in sediment thicknesses relative to the previous interval. Maximum thickness in the uppermost interval is 816 m, with a mean value of 254 m. Two depocentres are located in the north of the study area, the southern being up to 570 m thick and the northern one up to 800 m thick (Fig. 4.18). They are part of the Donegal Fan (Stoker *et al.* 2001).

4.4.10. Decompaction

Decompaction removes the progressive effects of rock volume changes with time and burial. Any compaction history is likely to be complex, being affected by lithology, overpressuring, diagenesis and other factors. The measure of the degree of compaction of sediments is the porosity, ϕ, defined as the ratio of the pore volume to the total volume. To calculate the original thickness of a sedimentary layer (before being compacted by

any overlying sediments) at a time in the past, it is necessary to know the variation of porosity with depth, a quantity usually measured in wells. For normally compacted sediments, the variation of porosity with depth may follow a linear trend (Falvey and Middleton 1981) or exponential paths (Sclater and Christie 1980). In this study, compaction is assumed to obey the following exponential relationship:

$$\phi = \phi_o e^{-cz} \qquad \text{(eq. 4.9)}$$

where ϕ is porosity, ϕ_o is surface porosity (e.g., of uncompacted sediment), z is depth, and c is a depth scale that depends on lithology and describes the rate at which porosity decreases with depth (Sclater and Christie 1980). Decompaction is useful to calculate the amount of subsidence caused by sedimentary compaction and to calculate accumulation rates.

4.4.10.1 Decompaction of well 132/15-1

The only well where porosity measures were taken was well 132/15-1. Therefore, this represents the only data that can be used to constrain a decompaction function. Using well 132/15-1, the best-fit porosity-depth relationship is (Fig. 4.24):

$$\phi = 0.662e^{-0.00044z} \qquad \text{(eq. 4.10)}$$

Extrapolation of this relationship at depth to the present surface yields both the inferred surface porosity ϕ_o and the depth scale c (Fig. 4.24). Considerable errors are introduced decompacting a basin with just one well, but in this study this is the only available data set to use for decompaction.

Equation 4.10 was embedded in a decompaction code written in Matlab, following Allen and Allen (1990) (Appendix 3). Well 132/15-1 was decompacted first, and then the individual isopach maps were made using their decompaction function. The present-day stratigraphic depth below the seabed of Cenozoic layers in the well is shown in Table

4.11. The age of each package is given by limited well data or based on the stratigraphic dating of Stoker *et al.* (2001). The water column is assumed to have a small effect on compaction of Cenozoic sediments because the basin is assumed to have been deep since the Palaeocene (perhaps excluding the early Eocene) based on the facies observations in wells (Section 4.4). Subtraction of the present day water depth at well 132/15-1 from the present stratigraphic thickness is necessary before carrying out the decompaction.

To calculate the thickness of a sedimentary layer at any time in the past, it is necessary to move the layer up the porosity-depth curve (Fig. 4.24). The decompaction program yields decompacted depths at different times in the decompaction history (Table 4.12). Values are given in metres and represent depths below seabed. The decompacted subsidence history of the well can be plotted on a diagram of depth versus age (Fig. 4.25). It is important to point out that this plot ignores any palaeobathymetric or eustatic corrections.

The total subsidence is made of two components: any tectonically driven subsidence plus subsidence due to sediment load. The effects of the sediment load can be subtracted using an isostatic/flexural model. Thus, the tectonically-driven subsidence can then be obtained. Ideally correction based on palaeobathymetic and eustatic data should also be applied, but again the lack of well coverage in the Rockall Basin allowed only a preliminary estimation of the tectonically-driven subsidence (Fig. 4.26).

Backstripped porosities have been calculated using a single porosity-depth curve for the different sedimentary packages (Fig. 4.24). From this curve a different value can be given to each package depending on the depth of the layer and the age (Table 4.13). For example, the porosity in the Palaeocene at the present day is different than the one at early Eocene times just after deposition.

The bulk density of the sedimentary column ($\overline{\rho_s}$) is then given by:

$$\overline{\rho_s} = \sum_i \left[\frac{\overline{\phi}_i \rho_w + (1 - \overline{\phi}_i \rho_{sgi})}{S} \right] y_i \qquad \text{(eq. 4.11)}$$

where $\overline{\phi_i}$ is the mean porosity of the sedimentary layer, ρ_w is water density, ρ_{sgi} is the sediment grain density of the layer, y_i is the thickness of the layer, and S is the total decompacted thickness of the column (Allen and Allen 1990). Bulk density for each time period is presented in Table 4.14.

The loading effect of the overlying sediment can be treated as a problem of local (Airy) isostatic balance. Where sediment is replacing a column of water,

$$Y = S\left(\frac{\rho_m - \overline{\rho}_s}{\rho_m - \rho_w}\right) \qquad \text{(eq. 4.12)}$$

where Y is the depth to the basement corrected for sediment load and ρ_m is mantle density (Allen and Allen 1990) (Table 4.15, Fig. 4.26). Using all this equations, a maximum tectonic subsidence of 1550 m, not corrected for palaeobathymetry or eustacy, is obtained. This preliminary result for the tectonically driven subsidence will be compared with flexurally driven subsidence in Chapter 5.

4.4.10.2 Decompaction of the northeastern Irish Rockall Basin

Next, this calculated decompaction was applied in two dimensions to the five seismic unconformities mapped in the eastern Irish Rockall Basin using the same porosity-depth curve from well 132/15-1 (Fig. 4.24). Three-dimensional matrices were constructed for the base and top of each sedimentary package. Each *x*, *y* position contains the horizontal coordinates of the surface grid. The *z* position contains the vertical height of the surface grid (e.g., base Palaeocene, base Eocene, etc.). Decompaction of these matrices (Appendix 4) creates four-dimensional matrices (e.g., *Nzb*, *Nzt*) where *x* and *y* are horizontal coordinates of each surface, *z* is the vertical height of each surface, and *t* is time. In this way the *x*, *y* and *z* coordinates for each unconformity are calculated at 0, 5, 20, 35 and 50 My. The results are shown as a decompacted isopach map for each of the five mapped time intervals in the Cenozoic (Fig. 4.27).

The decompacted Palaeocene isopach has a maximum thickness of 1666 m and a mean thickness of 1205 m. A major depocentre is located around the Hebrides Terrace Seamount and another one in the south of the study area (Fig. 4.27). The decompacted Eocene isopach has a maximum thickness of 1470 m and a mean of 648 m with major deposition in the north (Fig. 4.27). The decompacted ?Oligocene isopach has maximum thickness of 645 m and a mean of 282 m with small depocentres along the basin margin (Fig. 4.27). The decompacted ?Miocene section has a maximum thickness of 553 m and a mean of 248 m with possibly a depocentre in the south (Fig. 4.27). The decompacted Plio-Pleistocene isopach has a maximum value of 816 m and a mean of 254 m with a depocentre in the north corresponding with the Donegal Fan (Fig 4.28).

4.4.11 Accumulation rates and summary

Sediment accumulation rates can be calculated from the decompacted isopach values. The following expression was used:

$$AR = \frac{\bar{T}}{t} \qquad \text{(eq. 4.13)}$$

where AR is the accumulation rate [m/My], $\bar{T}$ is the thickness of each package [m], and t is the duration of each package [My].

During the Palaeocene (Fig. 4.27), a major depocentre developed in the northwest, both north and south of the Hebrides Terrace Seamount. There was also a local depocentre in the southwest of the study area west of Donegal Bay. Total accumulation rates, averaged over the study area, were 93 m/My (Table 4.16). The Palaeocene facies onlap onto a base Tertiary unconformity in both the northeastern Irish Rockall Basin and the Irish Shelf. No progradation has been recognised in the Palaeocene, although the lack of well data poorly constrains the position of the base Tertiary in the basin. The Palaeocene has the highest accumulation rates in the Cenozoic. This high accumulation rate might be related to a major phase of igneous activity in the North Atlantic during the Palaeocene caused by the formation of a hot spot centred over East Greenland (White 1989). The consequence was a significant amount of coarse clastic material shed into the surrounding basins as a result of rock uplift and denudation of the Scottish and Irish basement. In the North Atlantic Igneous Province, an initial phase of magmatism happened at 62 My and a later phase at 55 My (Ritchie *et al.* 1999).

The Eocene saw a considerable decrease in accumulation rates to 38 m/My (Table 4.16). This might be related to the collapse of the Palaeocene thermally supported hot spot topography and the onset of the sea-floor spreading in the North Atlantic in the early Eocene (Srivastava and Tapscott 1986). A depocentre is located in the northeast of the study area (Fig. 4.27) with thickness up to 1470 m. Progradational fans are located in both the north and the south of the study area (Fig. 4.15), suggesting that Ireland as well Scotland was providing sediments to the northeastern Rockall Basin at that time. According to the decompacted Eocene isopach map (Fig. 4.27) accumulation rates were higher in the Scottish margin than off Ireland during the Eocene.

During late Eocene/early Oligocene tectonic inversion occurred (see section 4.5) (Roberts 1989; Bodreel and Andersen 1993; Doré *et al.* 1999), and major subsidence took place in the Rockall Basin (Stoker *et al.* 2001). The ?Oligocene and ?Miocene isopach maps (Fig. 4.27) show a decrease in accumulation rates from 38 m/My in the Eocene to 24 and 14 m/My in the ?Oligocene and ?Miocene, respectively (Table 4.16). Prograding sediments from northwestern Ireland were deposited in ?Oligocene times (Fig. 4.15). The margin appears to be quieter and more uniform in terms of deposition during the ?Miocene, in contrast to earlier periods.

Plio-Pleistocene accumulation rates are relatively high, at up to 51 m/My (Table 4.16). During this time another progradation phase took place in the north of the study area, with sediment input from Scotland and to a lesser extent, from Ireland (Fig. 4.15). The location of this progradation coincides with the present Donegal Fan.

4.5 Structure of the Rockall Basin

4.5.1 Introduction

Regional plate reconstruction in the northeastern Atlantic (Ziegler 1978; Knott *et al.* 1993; Doré 1999) reflect mainly Mesozoic-Cenozoic extensional faulting, reactivating major Precambrian, Caledonian and Variscan structural trends. The Rockall Basin underwent major extension during the Early Cenozoic, Mesozoic and possibly the Upper Palaeozoic (Shannon *et al.* 1995).

The study area includes the northeastern Irish Rockall and Erris Basins. The Slyne Basin was not studied because of its complexity and lack of time for the seismic interpretation. The Donegal Basin consists mainly of Carboniferous sediments and is not much use for Tertiary tectonic reconstruction. The main structural elements are shown in Figure 4.5 and were taken from Naylor *et al.* (1999). The Rockall Basin bathymetry changes trend from north in the north of the basin, to northeast in the centre of the basin, and back to north in the south of the basin (Fig. 4.1). The Rockall Basin is bounded to the north by

the northwest trending Wyville Thomson Ridge, and to the south by the west-northwest trending Charles Gibbs Fracture Zone. The east and west sides of the basin are bounded by north, northeast and east trending extensional faults that dip towards the basin (Corfield *et al.* 1999) (Fig. 4.1).

4.5.2 Structural history of the Rockall Basin

During the Late Palaeozoic and Early Mesozoic, rifting may have commenced in the Rockall Basin as in the bordering perched basins such as the Slyne, Erris and Donegal Basins (Shannon *et al.* 1995). The timing of rift initiation is, however, controversial. Thermal subsidence followed into the Early Jurassic. Deposition in the basins was probably limited, and in any case preservation is poor.

During the Late Jurassic (Lundin and Doré 1997) and Early Cretaceous (Musgrove and Mitchener 1996) another rift phase occurred, with extension localised on north-trending structures. Lundin and Doré (1997) observed that Late Jurassic rifts have a predominant north trend (North Sea, Halten Terrace, East Greenland, Porcupine Basin and southern and northern Rockall Basin) implying an east-west stretching direction.

In the Aptian-Albian northwest-directed stretching (Knott *et al.* 1993; Cole and Peachey 1999) resulted in major block rotation along pre-existing faults. Seismic interpretation indicates that block rotation diminished in the Upper Cretaceous.

Early Cenozoic extension affected the base Tertiary horizon, producing discontinuous normal offsets of up to 1000 ms on the main basin boundary fault. Extensional faults active during this phase trend north or northeast. Normal displacement appears to have ceased by early Eocene. The general north to northeast trend of the Rockall Basin and the Erris and Donegal Basins is normal to the stretching directions in the Mesozoic and Early Cenozoic.

Late Eocene-early Oligocene compression, due to north Atlantic ridge push, is recognised in the Rockall Basin (Boldreel and Andersen 1993; Doré and Lundin 1996; Doré 1997) and in this study, as inversion occurs along previous extensional faults.

4.5.3 Pre-Tertiary structural elements of the study area

North of the study area (Quad. 5) a structural high runs north-south and was probably formed during Late Jurassic-Early Cretaceous rifting. To the south, the Erris High or Ridge trends northeast (Fig. 4.5) and is onlapped by Permo-Triassic, Lower Jurassic, Cretaceous and Lower Tertiary sediments (Cunningham and Shannon 1997). Permo-Triassic rifting in the Erris Basin produced a series of half-grabens bounded by down to the southeast faults (Chapman *et al.* 1999). Caledonian faults were reactivated at the beginning of the Triassic as strike-slip faults (Roberts *et al.* 1990) with probable right lateral displacement (Gómez Ballesteros 1999). Cretaceous normal faults striking northwest, and an angular unconformity at the base Cretaceous (well 12/13-1A) provide evidence of Late Jurassic to Early Cretaceous extension (Chapman *et al.* 1999). During the Aptian-Albian a minor episode of rifting reactivated earlier faults (Chapman *et al.* 1999).

A number of lineaments, generally trending northwest, are visible in magnetic and gravity maps onshore and offshore Ireland (Readman *et al.* 1995). These include the Anton Dohrn lineament and the Wyville Thomson Ridge (Fig. 4.1) and both appear as extensions of oceanic transfer zones (Rumph *et al.* 1993; Doré and Lundin 1996, 1997; Tate *et al.* 1999). In the study area, these have been interpreted by Naylor *et al.* (1999) as transfer zones (Fig. 4.5).

4.5.4 Cenozoic tectonics in the northeast Rockall Basin

4.5.4.1 Introduction

A structural interpretation of the Cenozoic section on the seismic lines indicated on Figure 4.7 has provided a new Tertiary structural framework for the northeastern Irish Rockall Basin. A Tertiary tectonic map of Britain, Ireland and adjacent areas has already been published by Pharaoh *et al.* (1996) (Fig. 4.28), and the structural elements described therein can be compared with the Tertiary structural map obtained from this study (Fig. 4.29, 4.30). This section will describe Cenozoic structures from this study in the northeastern Irish Rockall Basin. The importance and intensity of Tertiary tectonics in offshore sediments will then be compared with onshore tectonic geomorphology from Chapter 3.

Early Cenozoic extension and intra-Cenozoic inversion is recognised along other northeast Atlantic marginal basins such as the Faraeo-Shetland Basin and Vøring Basin (Doré *et al.* 1999). After a major Aptian-Albian rift phase, extension continued from the Late Cretaceous to the early Eocene (Cole and Peachey 1999), resulting in reactivation of previous Mesozoic faults. Palaeocene extension coincided with the intrusion and extrusion of igneous rocks in the British Tertiary Igneous Province (Bott and Watts 1971; Dewey and Windley 1988). Intra-Cenozoic inversion is also recognised in the Rockall Basin (Boldreel and Andersen 1993; Corfield *et al.* 1999). Boldreel and Andersen (1993) dated this inversion as late Palaeocene to Miocene and it broadly coincides with the onset of sea-floor spreading in the North Atlantic between the Rockall-Hatton Bank and Greenland at 53 My (Srivastava and Tapscott 1986).

Normal, reverse and possibly transform faults are recognised in the Irish sector of the northeastern Rockall Basin. Evidence comes from structural interpretation of two-dimensional seismic lines (Fig. 4.7). Dating of the structures mapped is based on the ages attributed to each unconformity and sedimentary package within the Cenozoic (Table 4.4).

4.5.4.2 Palaeocene to early Eocene

After a Cretaceous rift phase, extension continued into the Palaeocene and early Eocene. Most of the extension was accommodated along the main boundary fault zone defining the eastern margin of the northern Rockall Basin (Fig. 4.5).

The main boundary fault zone can be traced from north to the south in pre-Tertiary strata (Fig. 4.5 or 4.28). Faults in the zone usually down-throw to the northwest and west on most of the seismic lines (Fig. 4.14), with discontinuous offsets in sediments of Palaeocene and early Eocene age.

The interpretation of the Palaeocene to early Eocene faults is shown in Figure 4.29. East of well 132/15-1 a west-dipping and north-northeast trending normal fault offsets the base Tertiary unconformity by 450 ms and the base Eocene unconformity by 150 ms (Fig. 4.29). Major activity on this structure had apparently ended by middle to late Eocene time, as post Eocene sediments are not seen offset on seismic lines. This fault was active in the Cretaceous as a north-northeast trending normal fault. Normal offset at the base Tertiary increases from 450 ms (Fig. 4.29, line SRT-96-226) to up to 650 ms in the south (Quad. 132) (GWH-92-103; see Fig. 4.10 for line location). In Quad. 5, the main north-trending basin boundary fault can be traced further south but does not deform Tertiary sediments. Extension in Quad. 5 and northern Quad. 12, appears to be accommodated by smaller-scale, north-trending normal faults. These structures sit on top of Cretaceous ridges with offsets of less than 400 ms for the base Tertiary and 100 ms for the base Eocene.

In Quad. 12, the base Tertiary is offset normally by 700 ms at the western side of the Erris Ridge, west of well 12/13-1a (Fig. 4.29). The eastern side of the Ridge is also normally offset, but by less than 100 ms. Offset on the west of the Erris Ridge decreases to about 300 ms in the south, where extension is accommodated by two normal fault strands (Quad. 12, Fig. 4.29).

The main boundary fault can be traced into Quad. 11, where maximum observed offsets range from 1000 ms in line NWI91-116 to 700 ms in line NWI93-113. The fault is interrupted in southern Quad. 11 and in northern Quad. 19. Also, Cretaceous structures change orientation from northeast trending in Quad. 11 to north-trending to the south (Fig. 4.29) (NWI93-108). Therefore it appears that during the Palaeocene to early Eocene the north-trending Cretaceous faults bounding the eastern Rockall Basin were not reactivated, but the northwest trending faults were, at least in the southern part of the study area. The main basinal fault reappears in western Quad. 18 but is discontinuous along strike with a normal offset of 1000 ms or more.

East or northwest-trending normal faults are located in Quad. 132 (Fig. 4.29). The exact trend is hard to tell on 2D seismic lines and their interpretation is open to discussion. They dextrally offset the main boundary fault. Two examples are found east of well 132/15-1 where the margin changes trend from north-northwest to north-northeast, and south of well 132/15-1 where the margin is interrupted by an approximately east-trending north dipping structure with some normal component (Fig. 4.29). The first example west of well 132/15-1 is best shown in line SRT-96-230, where the margin is normally offset by the main boundary fault and below it, a compressional structure, appears to be related to a deeper strike-slip fault. Although the strike-slip fault is not visible on the seismic, the dextral offset of the main boundary fault suggests the presence of this strike-slip fault. South of well 132/15-1 in the border between the Irish and UK waters, another dextral offset of the main boundary fault is seen, on line OH-48 volcanic rocks seem to have intruded facilitated by a possible strike-slip structure. Line OH-13 shows an east dipping structure with possibly an associated anticline disrupting the Eocene sediments. Two more seismic lines cut oblique to this structure, and all of them show some broken reflections. Thus, the Palaeogene extensional stress might have been accompanied by a transtensional component, reflected on strike-slip faults with normal component, that were inverted in the Eocene.

4.5.4.3 Middle to late Eocene to present

The North Atlantic Mid-Ocean Ridge started spreading 53 My ago (Srivastava and Tapscott 1986). Accompanying this spreading, the current work shows that a change in stress direction from extension to compression took place in the middle to late Eocene. Compressional structures first appear in late Eocene in the eastern Irish Rockall Basin and shortening appears to have ceased after early ?Oligocene times (Fig. 4.30).

In the very north of the study area, in Quad. 132, a west-northwest to east-northeast trending anticline is oriented perpendicular to the margin and sits above an older Mesozoic north dipping, east trending normal fault (Fig. 4.30). The anticline folds the base Palaeocene and base Eocene unconformities and may also deform the upper Eocene unconformity (Fig. 4.31).

In Quad. 5, five anticlinal structures have been mapped trending parallel to the basin margin (Fig. 4.30). One of them, located between Quads. 5 and 132, trends north-northeast with a maximum amplitude at 5° 22' N, 9° 24' W; fold amplitude decreases north and south of this point. Line 4 runs perpendicularly to the anticline axis (Fig. 4.32). In this line, the base Palaeocene is normally offset by 250 ms, while the base Eocene unconformity, along with the overlying middle Eocene sediments, are offset by the same fault with a reverse sense of slip, forming an anticline. The anticline is not well imaged on other seismic lines that are not perpendicular to the fold axis. However, a second north-northeast trending anticline, possibly a continuation of the last structure, is visible in line GWH-92-104B and folds the late Eocene unconformity, suggesting that shortening continued until late Eocene or early Oligocene time. This anticline is located above a rotated faulted block comprised of easterly dipping Mesozoic and Palaeocene sediments (Fig. 4.30 and Fig. 4.32). The anticline has a maximum relief of 100 ms.

Other north trending anticline structures are located on Quad. 5 (Fig. 4.30) and they usually sit above pre-Tertiary normally faulted rotated blocks. The base Palaeocene unconformity is normally faulted and the base Eocene unconformity and lower Eocene

sediments are folded as an anticline (e.g., line OH-58). Line 0597-62 shows evidence that this structure has a tectonic origin (A1 in Fig. 4.30), as it is underlain by a Palaeocene and Pre-Tertiary east dipping normal fault trending north-northeast and a Pre-Tertiary rotated faulted block. Again, the anticline is larger in relief where the fault trends north-northeast (A1 in Fig. 4.30). Three kilometres west of this structure, there is another north-trending anticline with a wavelength of 4 km and relief of 100 ms but with no visible underlying structure (A2 in Fig. 4.30).

An east trending anticline is located in southern Quad. 5 (A3 in Fig. 4.30). It overlies a west-northwest trending Mesozoic structure and folds middle to upper Eocene sediments and the upper Eocene unconformity (e.g., line GER96-51). The base Palaeocene and base Eocene unconformities are folded with a relief of 200 ms (e.g., line TRH005).

In southern Quad. 5, the middle to upper Eocene package contains a big scale concave-up surface, that suggest post-depositional detachment created by slumping and compaction of wet muddy sediments (Fig. 4.33). It is best observed in seismic sections parallel to the basin margin. This detachment surface is 18 km long and 3 km wide (e.g., Line 5, NWI91-180, see Fig. 4.10 for location). To the south of the structure reflections downlap onto the basal surface and at its base broken high amplitude reflections stack thrusting one on top of the other indicative of slumping in a south to north direction (Fig. 4.33). It might be interpreted as a gigantic slump delimited by two east-notheast trending detachment surfaces (Fig. 4.30). Late Eocene to early Oligocene compression, indicated by anticline structures in this section might have played a role in slump formation.

In Quads. 12 and 11 the margin changes trend from north to northeast. In northern Quad. 12 two anticlines trending northeast and parallel to the margin, were mapped (A4 and A5 in Fig. 4.30). A 2.5 km wide anticline is seen in two seismic lines folding lower to middle Eocene sediments (A4 in Fig. 4.30). It sits above an east-northeast trending northwest dipping normal fault that in turn displaces probable Mesozoic sediments. West of this structure a small flower structure reverses Palaeocene sediments and the base Eocene

unconformity by reactivation of an older structure (A5 in Fig. 4.30, e.g., line E95IE07-21).

In western Quad. 12, three west-northwest trending anticlines perpendicular to the basin margin, were mapped (Fig. 4.30). Line 6 (see Fig. 4.10 for location) shows that, in at least three places, pop-up structures with possibly strike-slip faults reversing lower and middle to upper Eocene sediments. Although, it should be noted that lack of well control makes sequence ages in this area uncertain and volcanics make the pre-Tertiary hard to interpret. The southernmost west-northwest trending anticline is the most obvious compressional structure in the study area (Fig. 4.34, and A6 in 4.30). It has a relief of 300 ms and a wavelength of 3 km. It folds the upper Eocene unconformity, suggesting a late Eocene to lower Oligocene age for the shortening. A parallel line to Line 6 is NWI91-180 and shows the continuation of this anticline, making it possible to measure an exact trend. Line NWI91-180 shows two reverse faults offsetting the base Palaeocene and Eocene unconformities and folding upper Eocene unconformity, possibly reactivated along a deeper non-visible structure (Fig. 4.34). No pre-Tertiary section is visible underneath this structure because of poor seismic resolution, probably due to overlying Palaeogene intrusives, which are very common in the study area.

South of the anticline structure described above, the main marginal fault is inverted with an associated anticline trending northeast and parallel to the basin margin (A7 in Fig. 4.30 and Fig. 4.35). The main marginal fault offsets normally the base Eocene unconformity by 500 ms measured vertically (Fig. 4.35). Middle to upper Eocene sediments form an anticline with reflections onlapping against the main Rockall Basin boundary fault. It is interpreted in this work that the anticline is formed by transpressional reactivation on splays of the main basin boundary fault.

North of the west-northwest trending anticline previously described (A6 in Fig. 4.30), the main basin boundary fault appears extensional and no evidence of shortening is seen. To the south of the west-northwest trending anticline, shortening has taken place while to the north extension has taken place (Fig. 4.30). If the anticline was formed by transpressional

stress on a west-northwest fault, then a sinistral movement is suggested to have occurred in the late Eocene. Some of the late Eocene compressional structures appear to have a transpressional origin in deeper structures, forming flower structures in Palaeocene and Eocene sediments. However, the coarse grid of the 2D seismic data does not give a clear picture on the exact structural style

4.5.4.4 Summary of tectonic structures

After an Aptian-Albian rift phase, extension continued into the Palaeocene and early Eocene. Discontinuous normal faults are mapped along the main basin boundary fault in the northeast Irish Rockall Basin (Fig. 4.29). Within the study area, normal offset seems to increase to the south. East trending normal faults offset dextrally the main basin boundary fault, suggesting a transtensional regime.

Compressional structures occur in the late Eocene in the eastern Irish Rockall Basin. East, north and east-northeast trending anticlines were mapped in the Eocene (Fig. 4.30) and appear to end after the early Oligocene. Some of these anticlines are formed by reactivation of older north-northeast trending normal faults, while others appear to have been caused by reactivation of older west trending strike-slip faults.

4.6 Conclusions

(1) The Cenozoic succession in the Rockall Basin is conformable in the basin centre and thins unconformably (through both onlap and downlap) onto the basin margins over about 30 km of horizontal distance. Palaeocene and ?Miocene packages are seen onlapping onto their respective basal surfaces. Eocene, ?Oligocene and Plio-Pleistocene locally downlap onto their basal unconformities. Cenozoic faulting and folding is also recognized discontinuously along the northeastern boundary of the Rockall Basin.

(2) During the Palaeocene a major depocentre developed in the northwest of the study area, both north and south of the Hebrides Terrace Seamount. There was also a local

depocentre in the southwest of the study area. Mean Palaeocene accumulation rates, averaged over the study area, were 93 m/My.

(3) Early Eocene sand progradation of an unknown environment was common in the northeastern Irish Rockall Basin in both the north and the south of the study area, suggesting that Ireland as well as Scotland was providing sediments to the northeastern Irish Rockall Basin. A depocentre is located in the northwest of the study area where the margin changes trend from north to northeast, with thickness of up to 1470 m.

(4) Discontinuous normal faults are mapped along the main basin boundary fault in the northeastern Irish Rockall Basin offsetting base Tertiary to base Eocene. Base Tertiary offsets are on the order of hundreds of metres while base Eocene offsets decrease to approximately tens of metres. Within the study area, normal offsets seem to increase in magnitude to the south.

(5) During the late Eocene/early Oligocene, tectonic inversion and major subsidence took place in the Rockall Basin. Late Eocene to early Oligocene compression and transpression gave rise to east, north and east-northeast trending anticlines and a transpressional regime. Some of these anticlines are formed by reactivation of older north-northeast trending normal faults. This event is coeval and compatible with southeast-directed North Atlantic ridge push.

(6) The post-late Eocene unconformity is a markedly angular boundary that erodes upper Eocene sediments, and post-upper Eocene sediments onlap onto it. The ?Oligocene isochron map shows small local sediment depocentres adjacent to and downslope of the basin margin with progradation of unknown environment, suggesting local sediment input from the Irish continental margin during post-late Eocene time. The post-late Eocene and pre-Pliocene isopach maps show a decrease in mean accumulation rates from 38 m/My in the Eocene to 24 and 14 m/My in the ?Oligocene and ?Miocene, respectively

(7) Basinal reflections of presumed Miocene age onlap onto the ?lower Miocene unconformity. Reflections in the sediments above the ?lower Miocene unconformity have low amplitude suggesting a lithology rich in mudstones and poor in sandstones. This package can be visualised as a sedimentary wedge pinching out northeastwards.

(8) Plio-Pleistocene mean accumulation rates are relatively high, at up to 51 m/My. During this time a deltaic progradation phase took place in the north of the study area, with sediment input from Scotland and, to a lesser extent, from Ireland. The location of this progradation coincides with the present Donegal fan. Two separate progradational events are separated by a local intra Plio-Pleistocene unconformity.

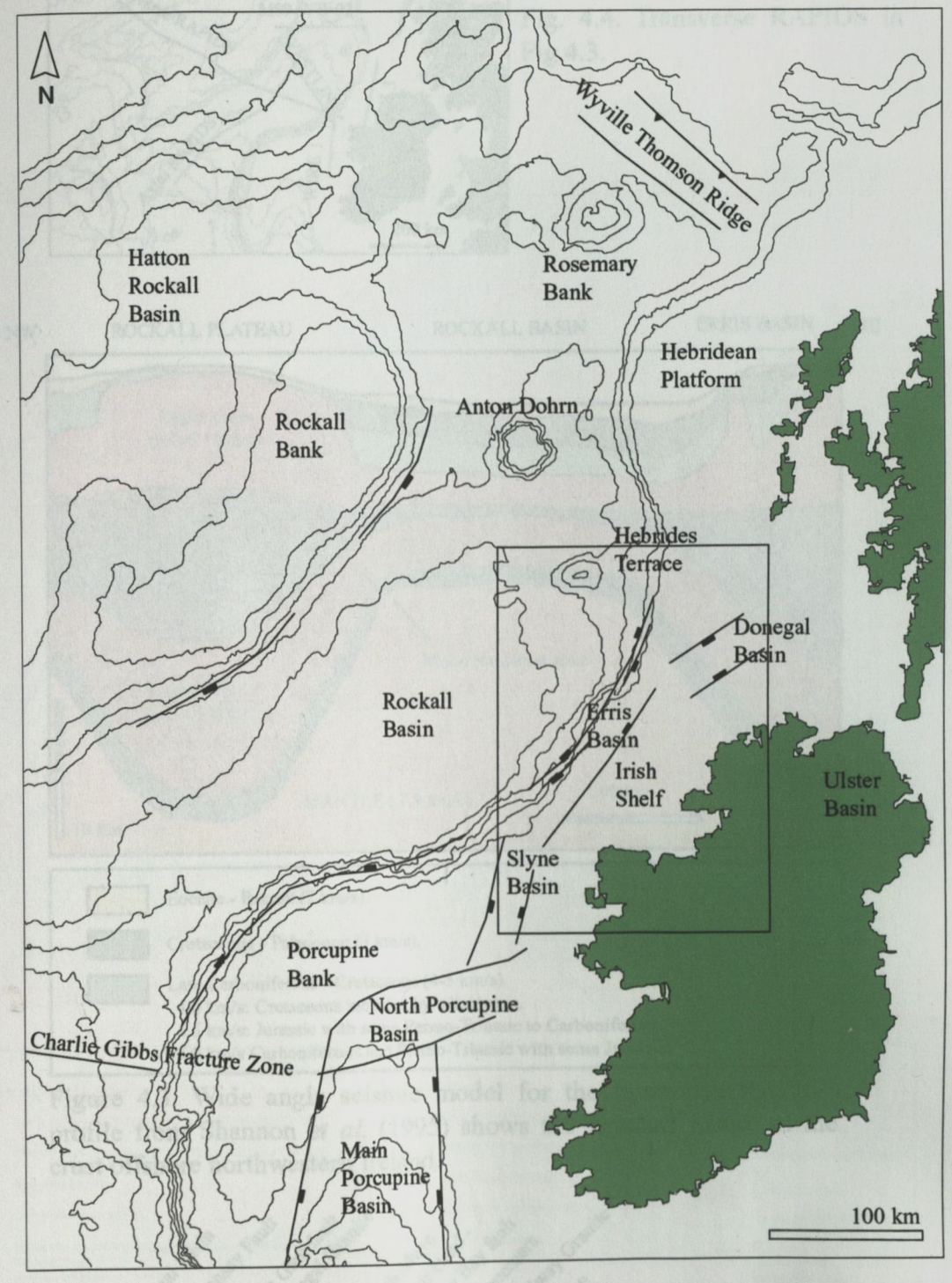


Figure 4.1. Bathymetry of northwestern Ireland and location of main structural boundaries of the Rockall Basin and adjacent late Palaeozoic to Cenozoic basins in pre-Tertiary time (adapted from Corfield *et al.* 1999). Barbs indicate thrust faults, blocks indicate normal faults. Study area is shown by the rectangle. Contour interval is 500 m.

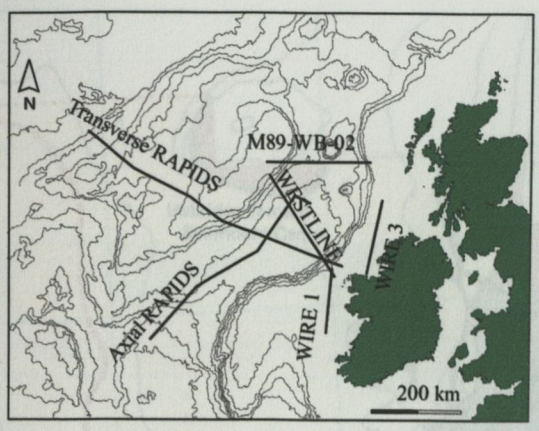


Figure 4.2. Location of regional seismic lines across the Rockall Basin. WIRE 1and 3 are shown in Fig. 4.4. Transverse RAPIDS in Fig.4.3.

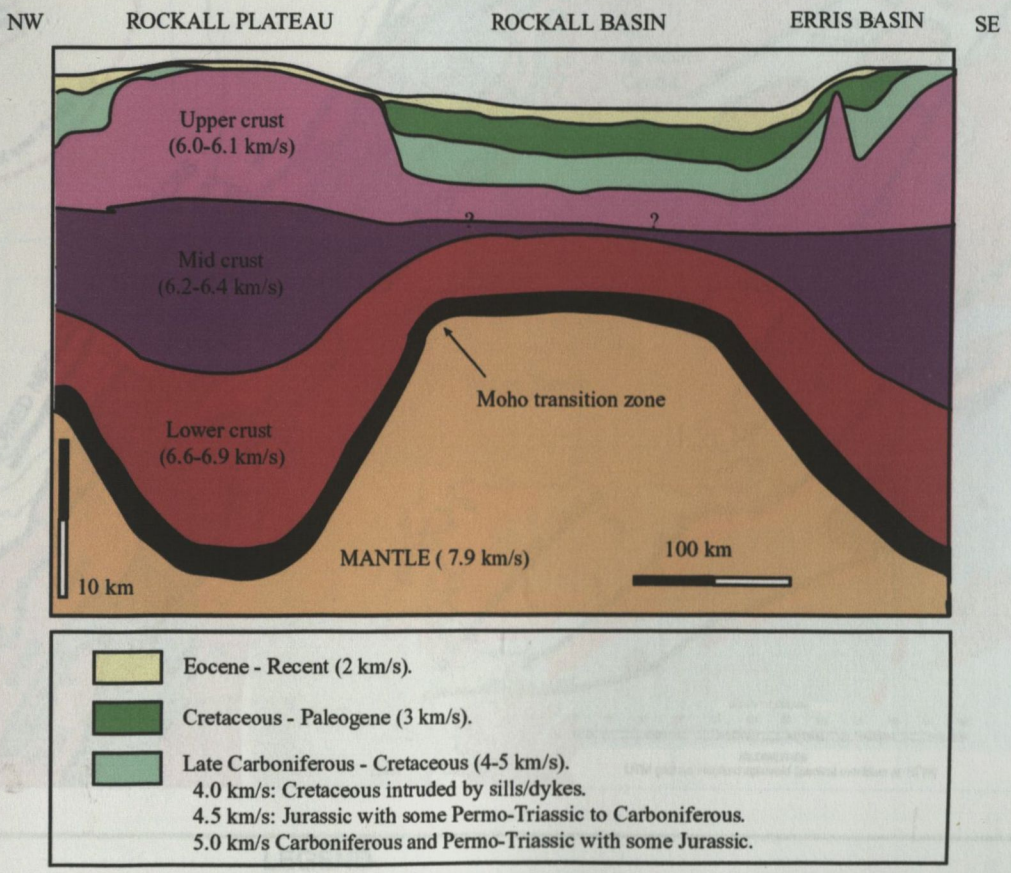


Figure 4.3. Wide angle seismic model for the transverse RAPIDS profile from Shannon *et al.* (1995) shows the streched nature of the crust offshore northwestern Ireland.

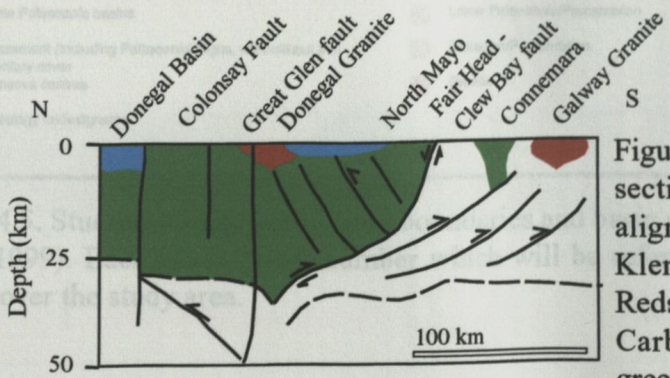
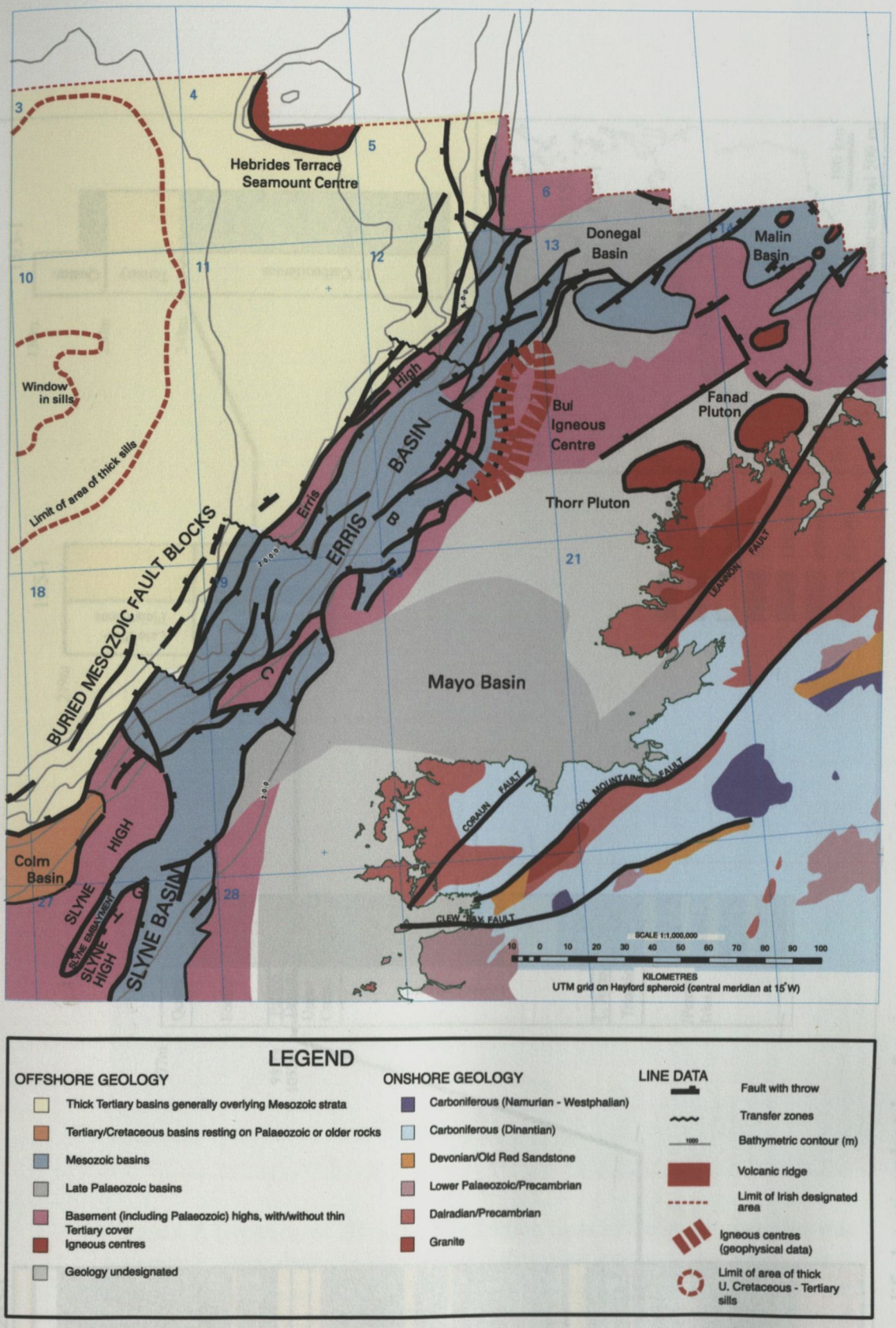


Figure 4.4. A north-trending section of WIRE 1and 3 aligned and interpreted by Klemperer *et al.* (1991). Reds are granites, blues are Carboniferous basins and green is Pre-Cambrian.



LEGEND

OFFSHORE GEOLOGY

- Thick Tertiary basins generally overlying Mesozoic strata
- Tertiary/Cretaceous basins resting on Palaeozoic or older rocks
- Mesozoic basins
- Late Palaeozoic basins
- Basement (including Palaeozoic) highs, with/without thin Tertiary cover
- Igneous centres
- Geology undesignated

ONSHORE GEOLOGY

- Carboniferous (Namurian - Westphalian)
- Carboniferous (Dinantian)
- Devonian/Old Red Sandstone
- Lower Palaeozoic/Precambrian
- Dalradian/Precambrian
- Granite

LINE DATA

- Fault with throw
- Transfer zones
- Bathymetric contour (m)
- Volcanic ridge
- Limit of Irish designated area
- Igneous centres (geophysical data)
- Limit of area of thick U. Cretaceous - Tertiary sills

Figure 4.5. Stuctural framework, basin boundaries and basic geology taken from Naylor *et al.* (1999). Each Quad. has a number which will be referred to in text for location. Map is over the study area.

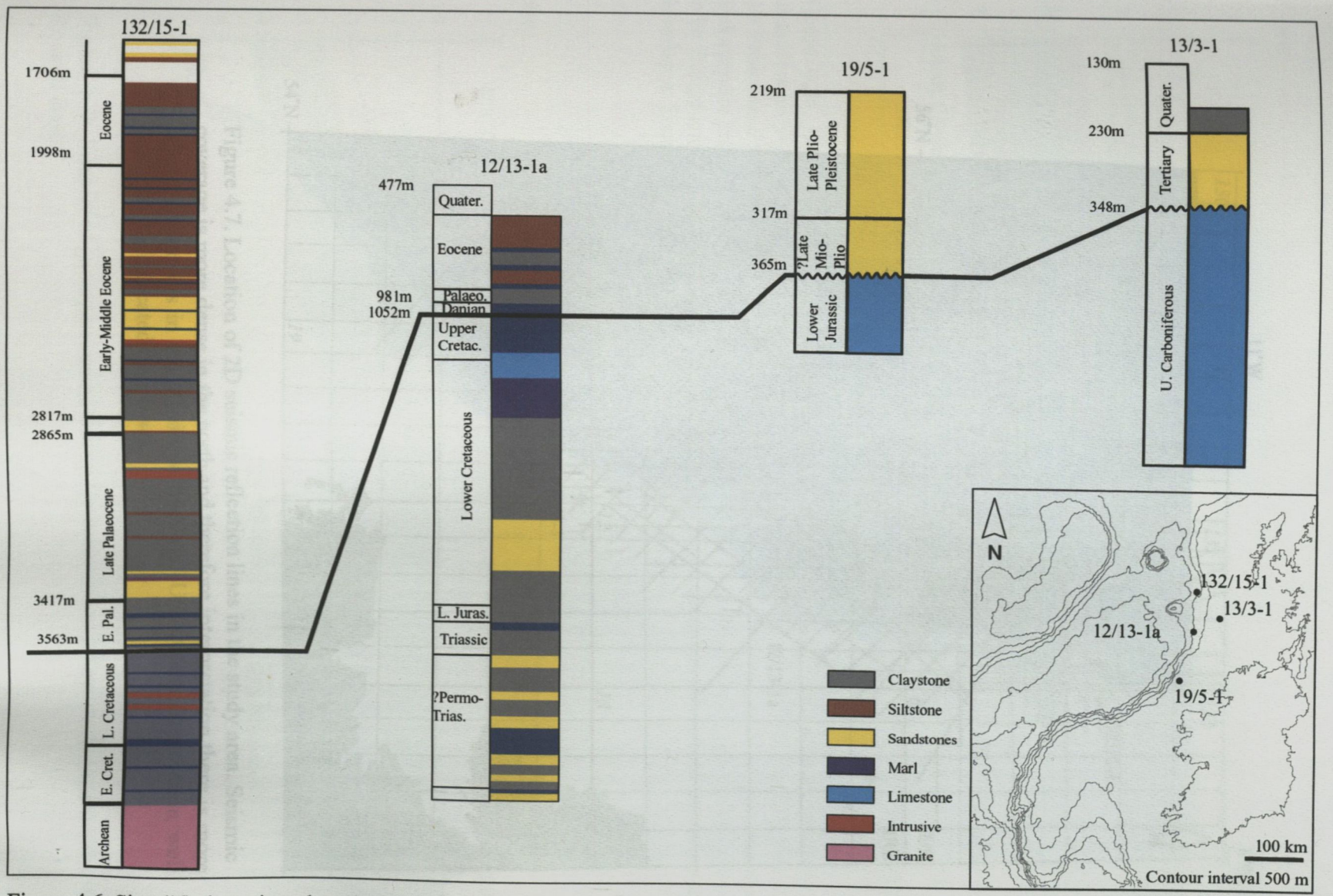


Figure 4.6. Simplified stratigraphy taken from composite well logs showing base Tertiary unconformity in heavy black line. Depths are given in metres below sea level.

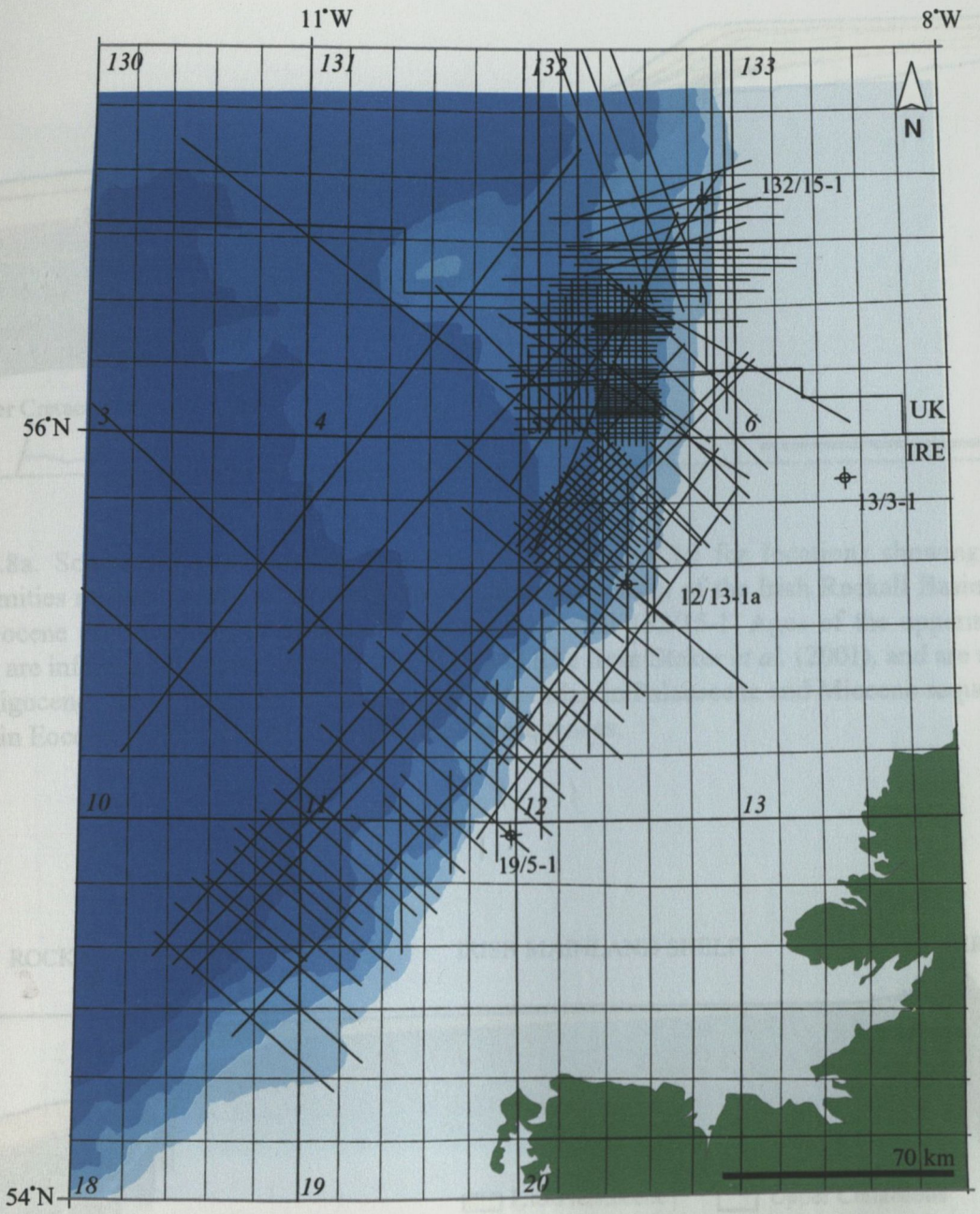


Figure 4.7. Location of 2D seismic reflection lines in the study area. Seismic coverage is more dense in the north and therefore interpretation there is more reliable. Numbers in italic indicate Irish and UK Quads. Exploration well locations are indicated by crosses.

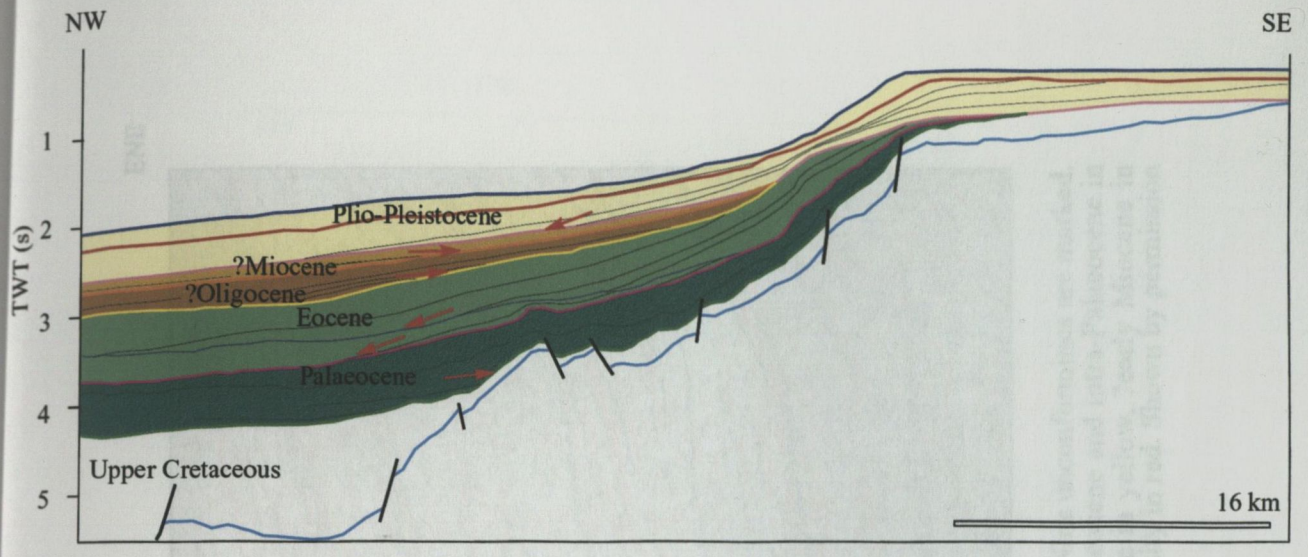


Figure 4.8a. Schematic cross section from Line 4 (see Fig. 4.10 for location) showing regional unconformities mapped in this study along the northeastern margin of the Irish Rockall Basin. Ages of the Palaeocene and Eocene packages are constrained by well 132/15-1. Ages of the uppermost three packages are inferred by correlation with RTa, RTb and RTc from Stoker *et al.* (2001), and are suggested to be ?Oligocene, ?Miocene and Plio-Pleistocene. Note onlap in Palaeocene and Miocene sequences and downlap in Eocene, ?Oligocene and Plio-Pleistocene sequences.

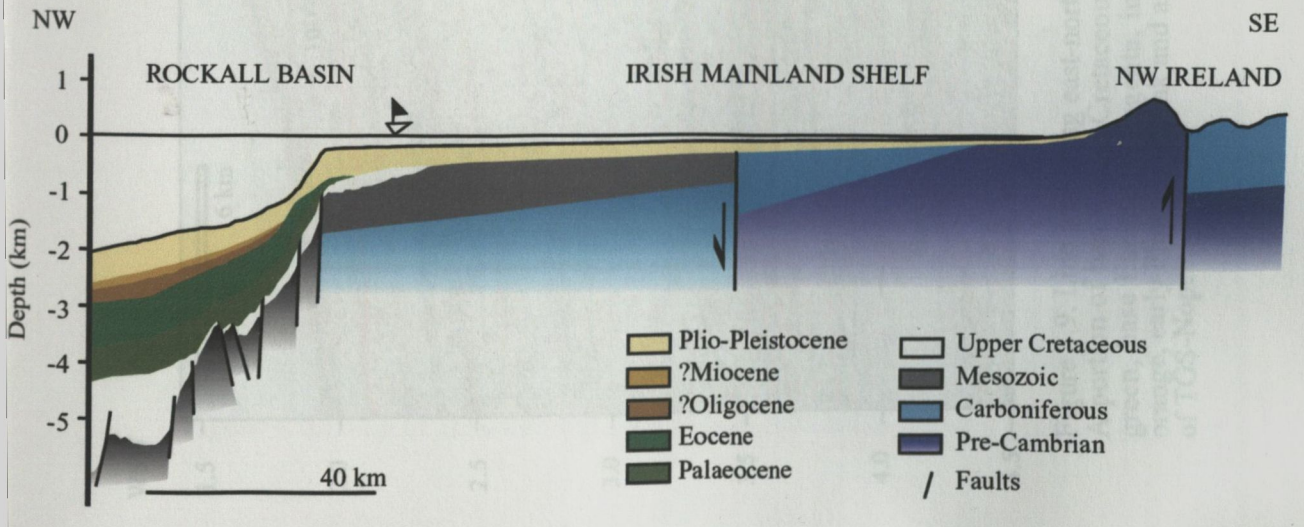


Figure 4.8b. Simplified geological cross-section from northwest Ireland to the northeast Irish Rockall Basin.

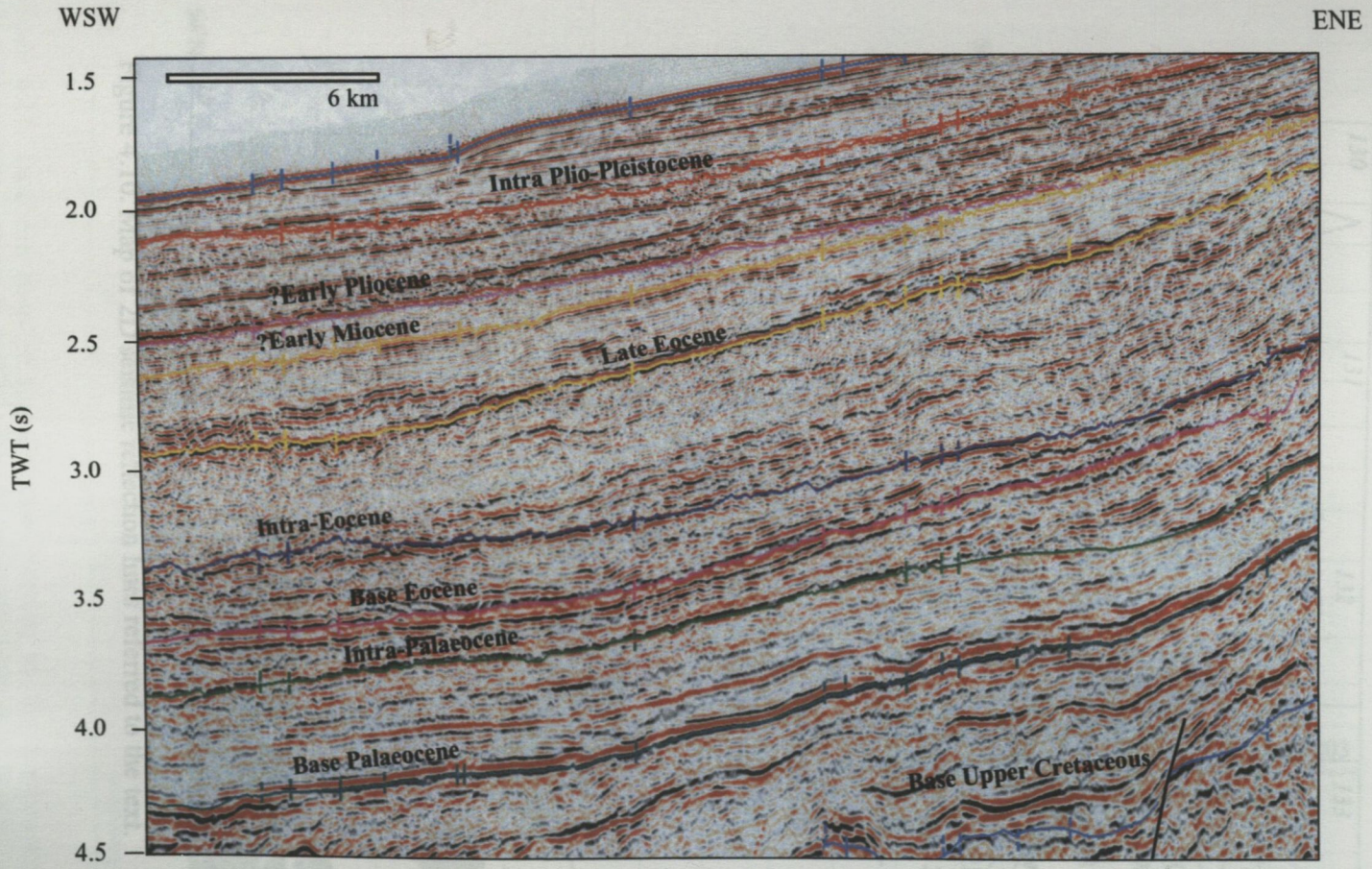


Figure 4.9. Line 1 trending east-northeast (see Fig. 4.10 for location). Nine unconformities are marked. A portion of base Upper Cretaceous unconformity in blue, base Palaeocene and intra-Palaeocene in green, base Eocene in magenta, intra-Eocene in blue, a late Eocene in yellow, ?early Miocene in orange, early Pliocene in pink and an intra Plio-Pleistocene unconformity in red. Shown by permission of TGS-Nopec.

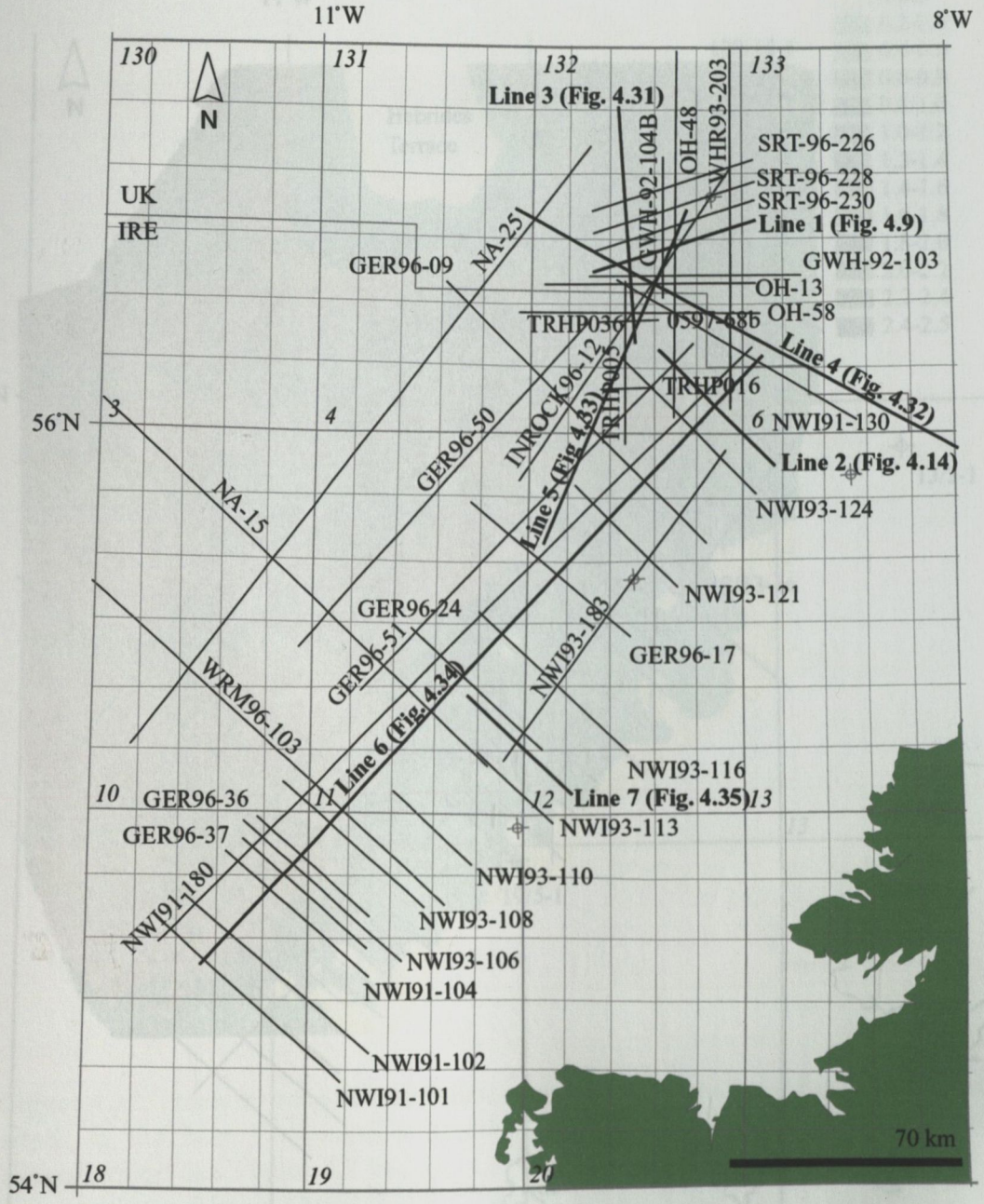


Figure 4.10. Map of 2D seismic reflection lines referred to the text.

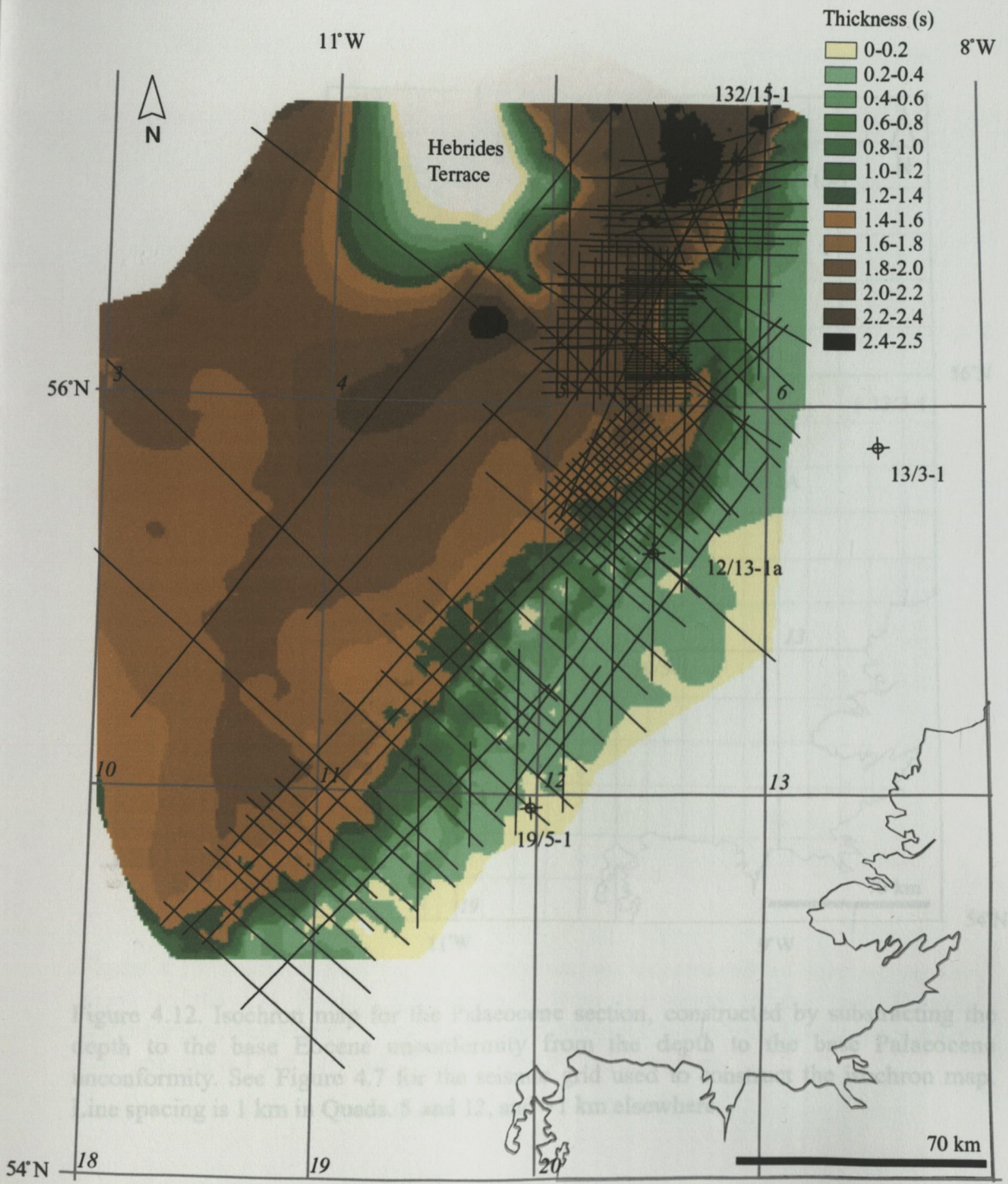


Figure 4.11. Isochron map of the Cenozoic section in the northeastern Rockall Basin substracting base Tertiary to seabed. Seismic reflection lines used to build the grid are shown by black lines. Also shown are the locations of wells that define the upper and lower limits of the Cenozoic package.

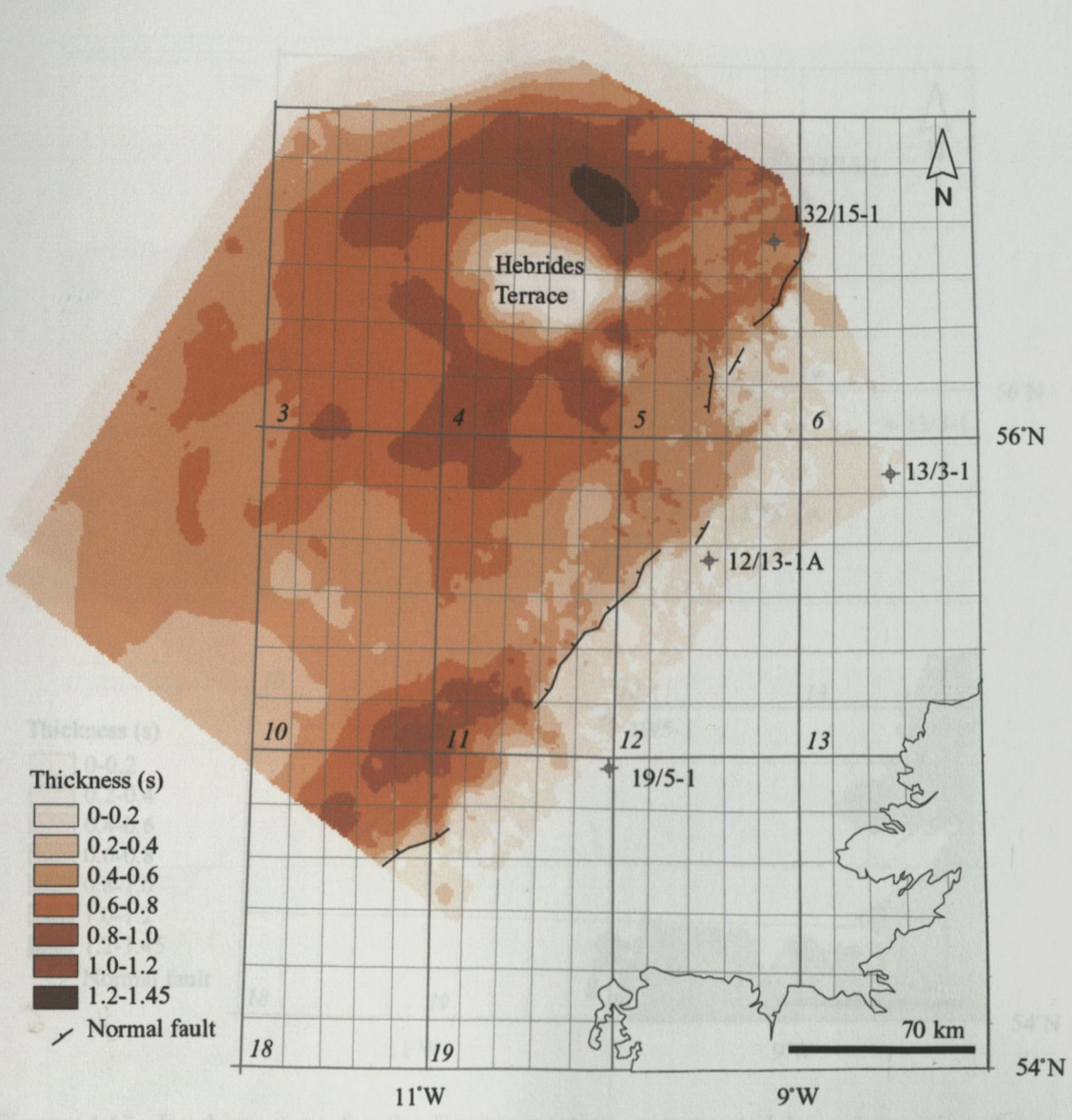


Figure 4.12. Isochron map for the Palaeocene section, constructed by substracting the depth to the base Eocene unconformity from the depth to the base Palaeocene unconformity. See Figure 4.7 for the seismic grid used to construct the isochron map. Line spacing is 1 km in Quads. 5 and 12, and >1 km elsewhere.

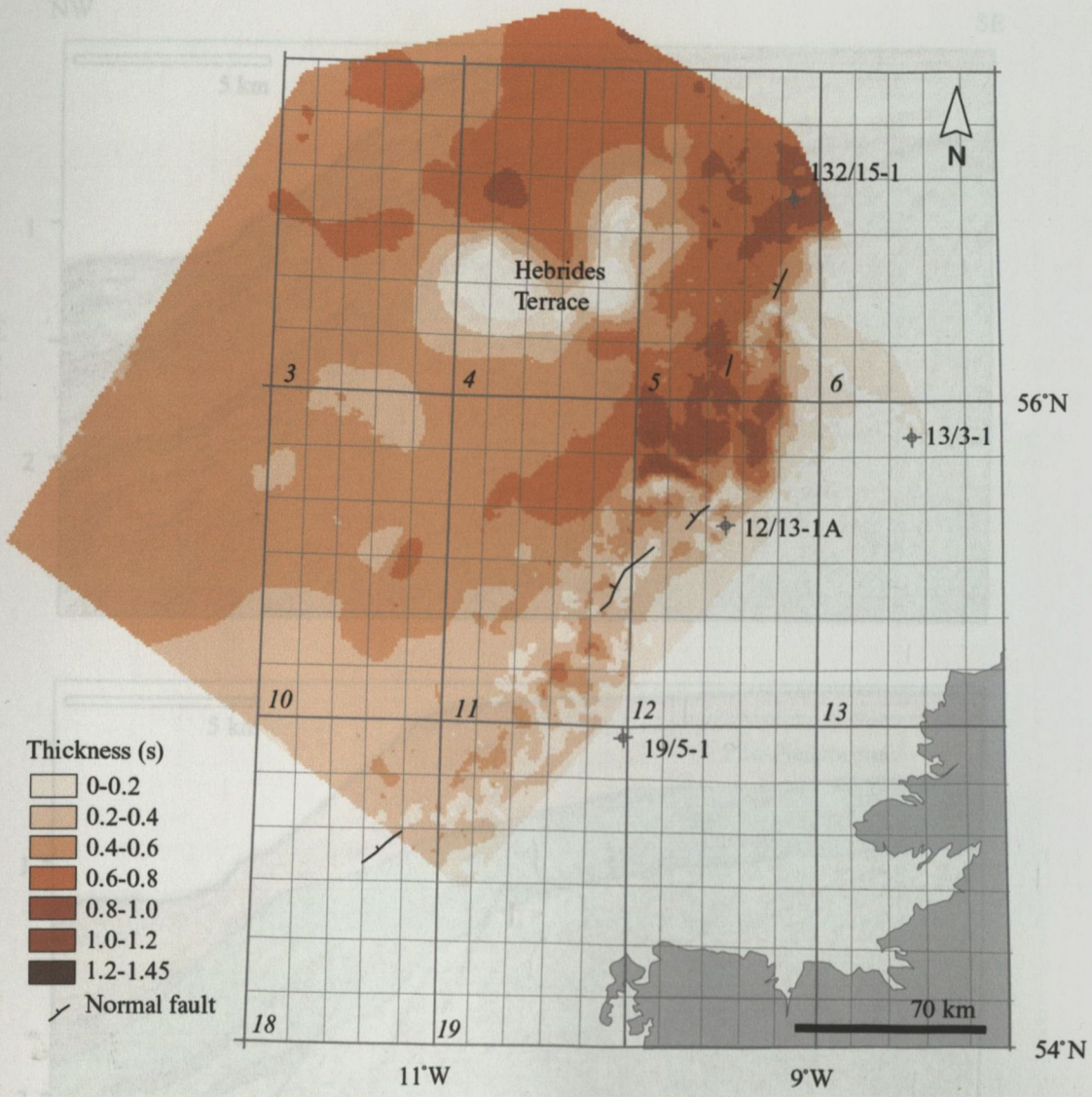


Figure 4.13. Isochron map for the Eocene section, constructed by substracting the depth to the late Eocene unconformity from the depth to the base Eocene unconformity. See Figure 4.7 for the seismic grid used to construct the isochron map. Line spacing is 1 km in Quads. 5 and 12, and >1 km elsewhere.

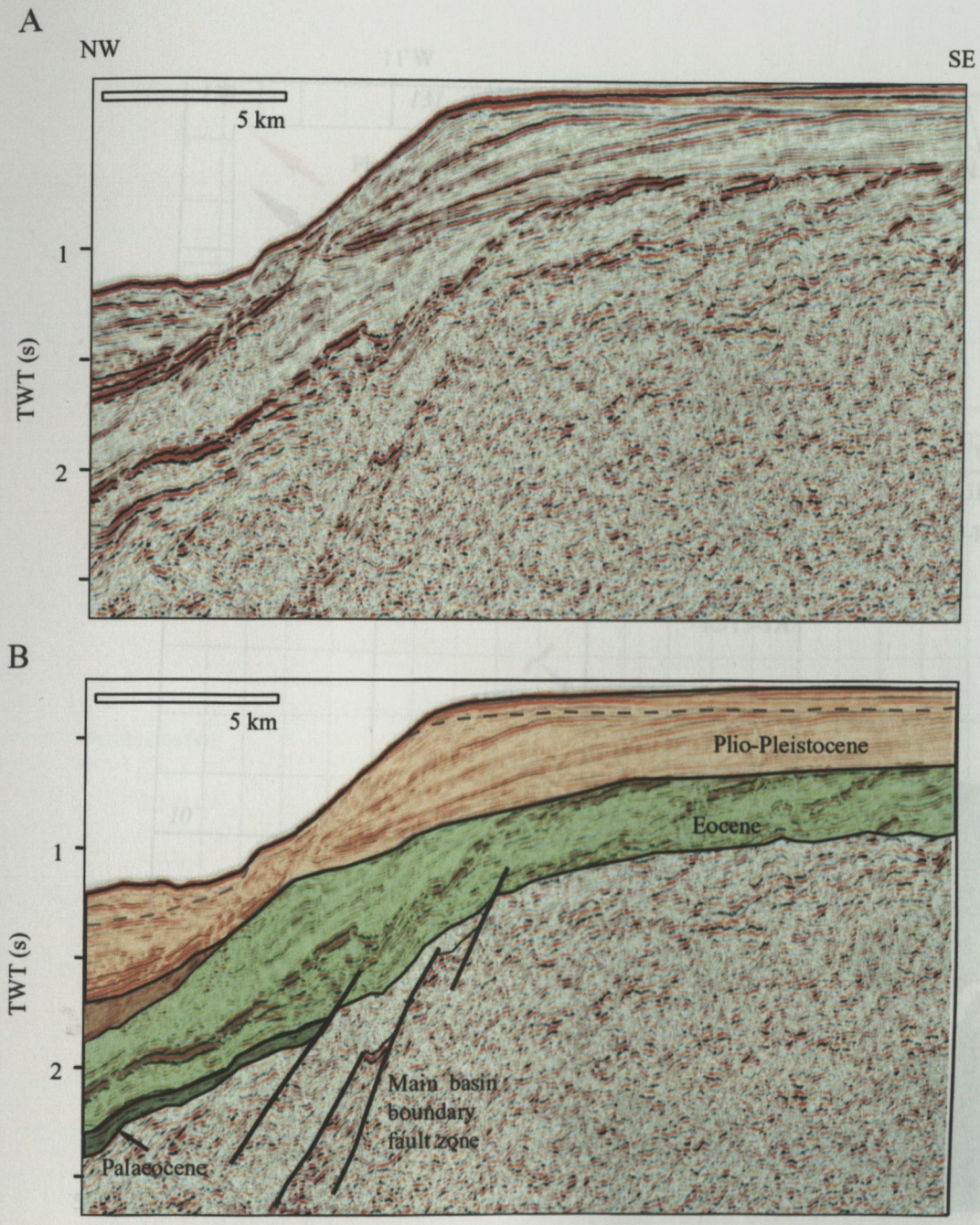


Figure 4.14. A, uninterpreted portion of Line 2 in the north of the study area, reproduced by permission of TGS-Nopec (see Fig. 4.10 for location). B, interpretation. Note progradation from southeast to northwest during the early Eocene and Plio-Pleistocene. Dashed line shows the top of the Plio-Pleistocene progradational wedge. Thin black lines are unconformity boundaries between the Cenozoic packages. Thick black lines are faults.

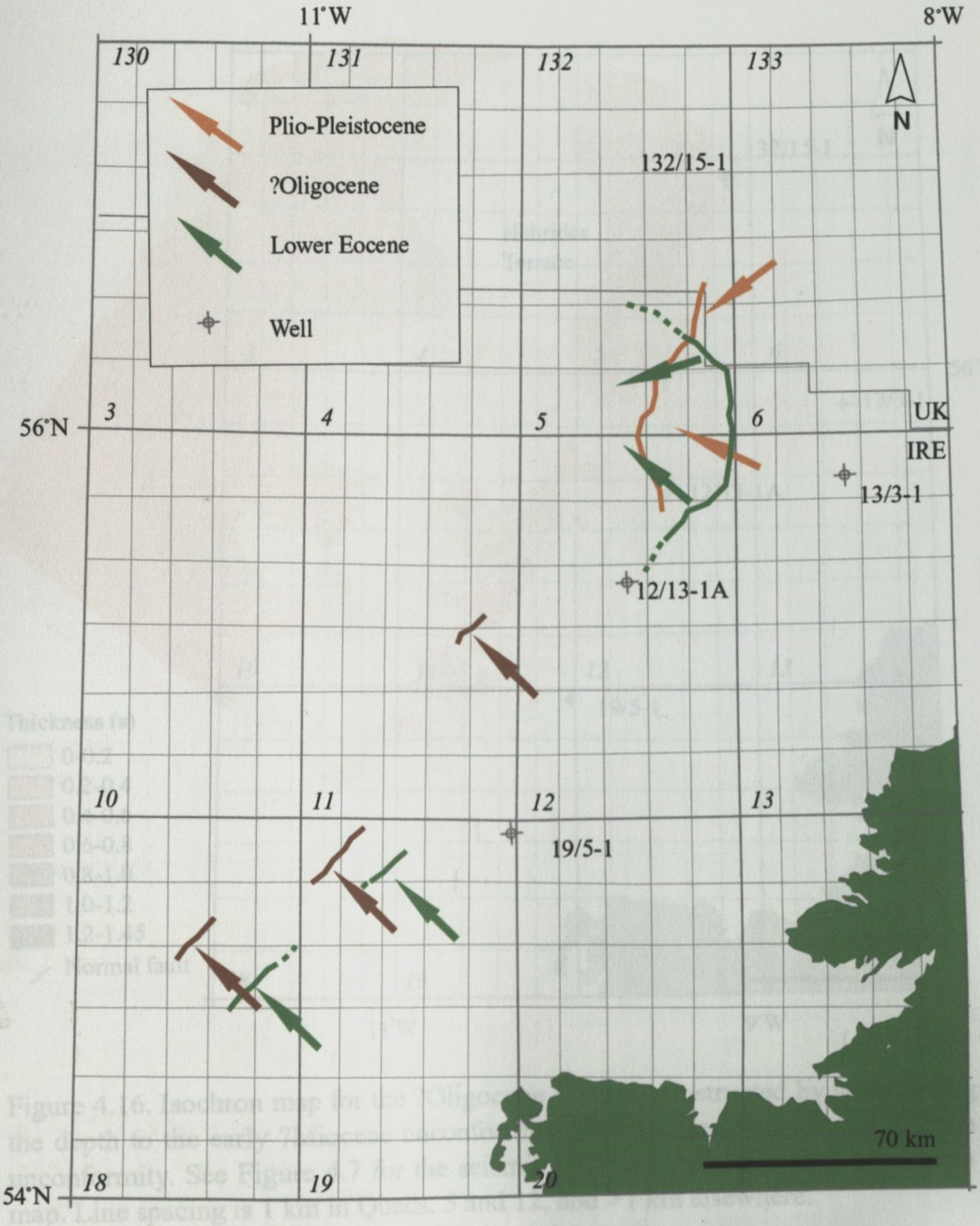


Figure 4.15. Cenozoic progradation directions based on interpretation of seismic reflection profiles. Arrows show approximate direction of progradation while thick lines show the approximate limits of progradation.

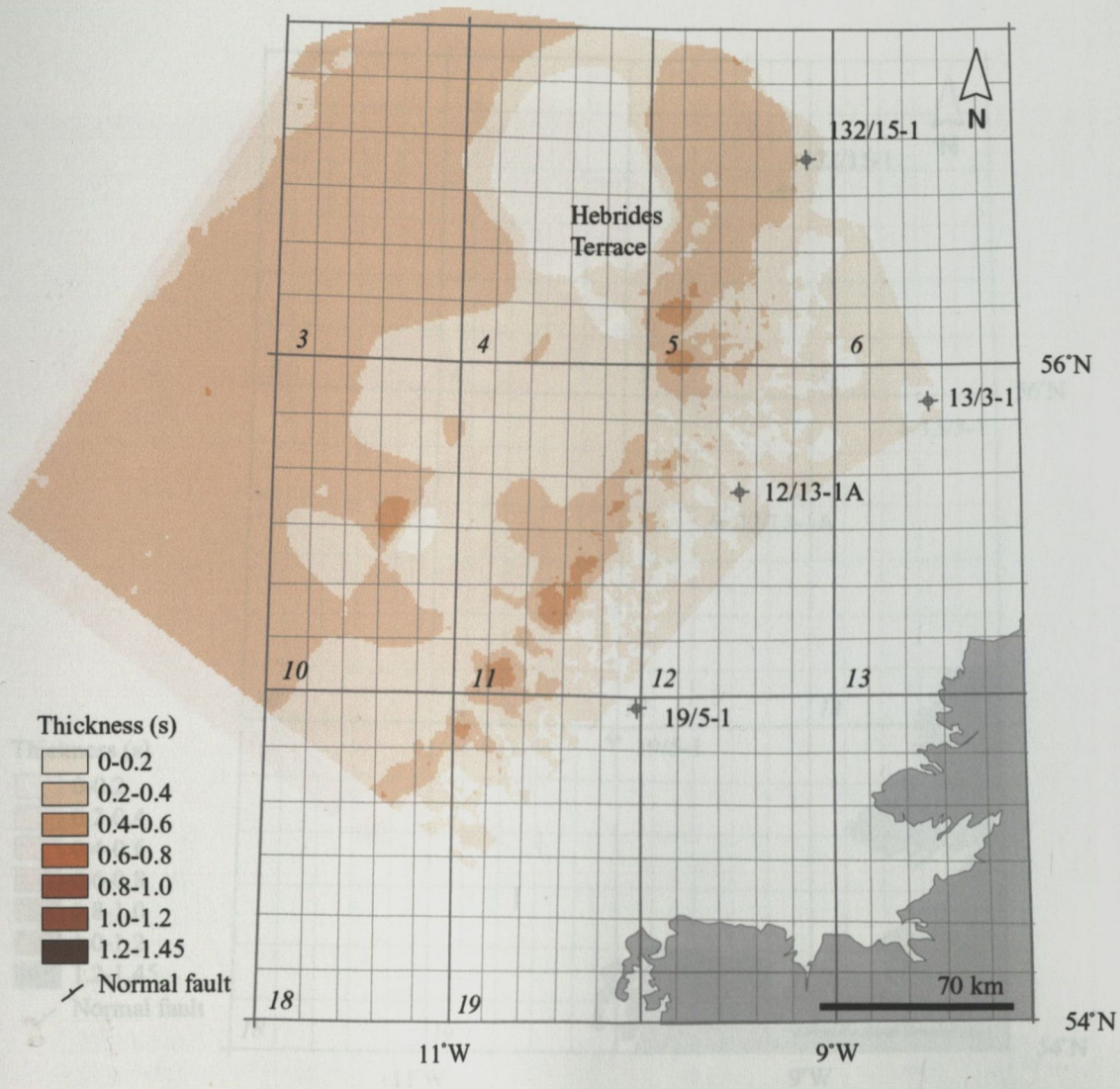


Figure 4.16. Isochron map for the ?Oligocene section, constructed by substracting the depth to the early ?Miocene unconformity from the depth to the late Eocene unconformity. See Figure 4.7 for the seismic grid used to construct the isochron map. Line spacing is 1 km in Quads. 5 and 12, and >1 km elsewhere.

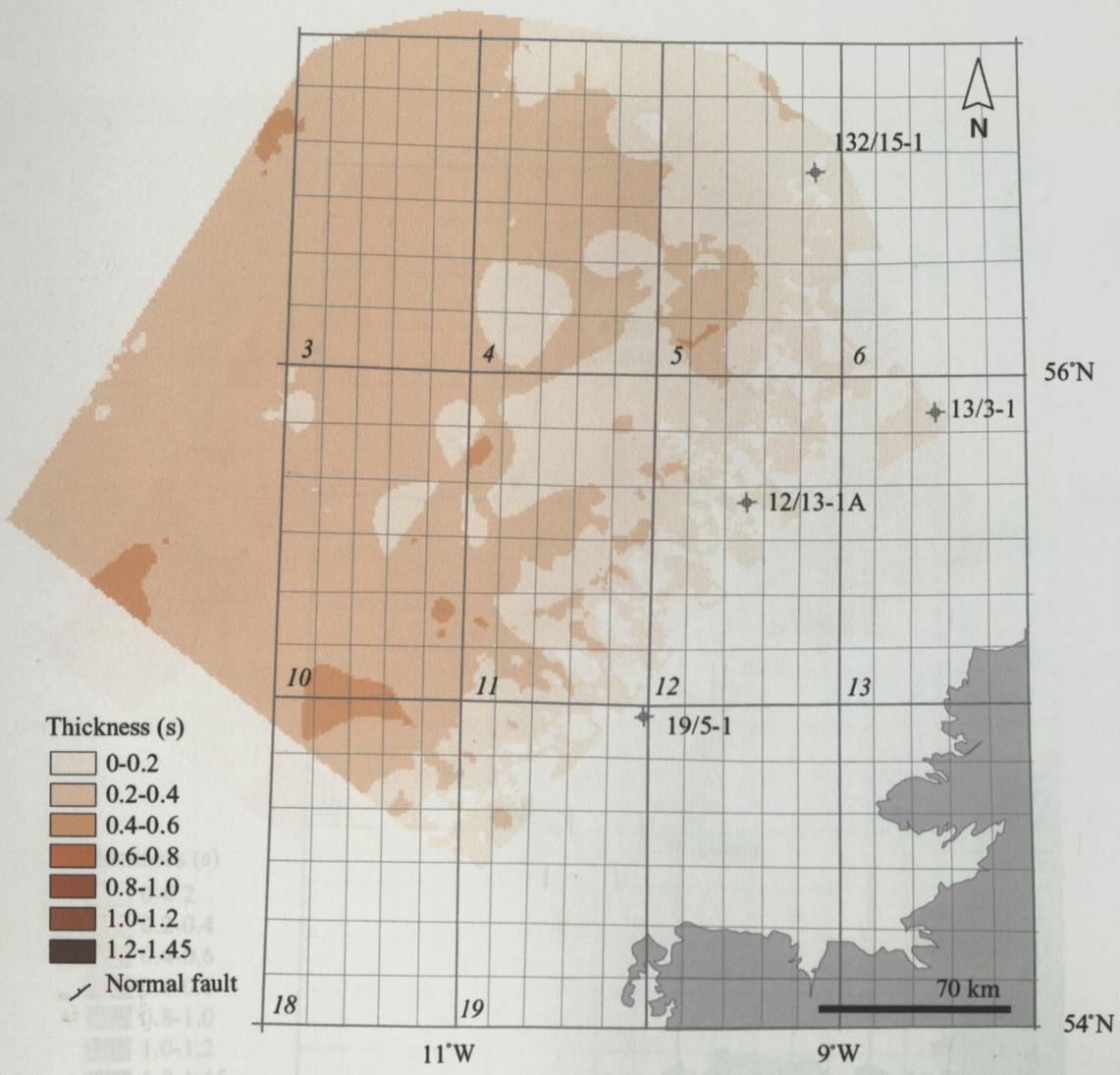


Figure 4.17. Isochron map for the ?Miocene section, constructed by substracting the depth to the base early Pliocene unconformity from the depth to the base ?Miocene unconformity. See Figure 4.7 for the seismic grid used to construct the isochron map. Line spacing is 1 km in Quads. 5 and 12, and >1 km elsewhere.

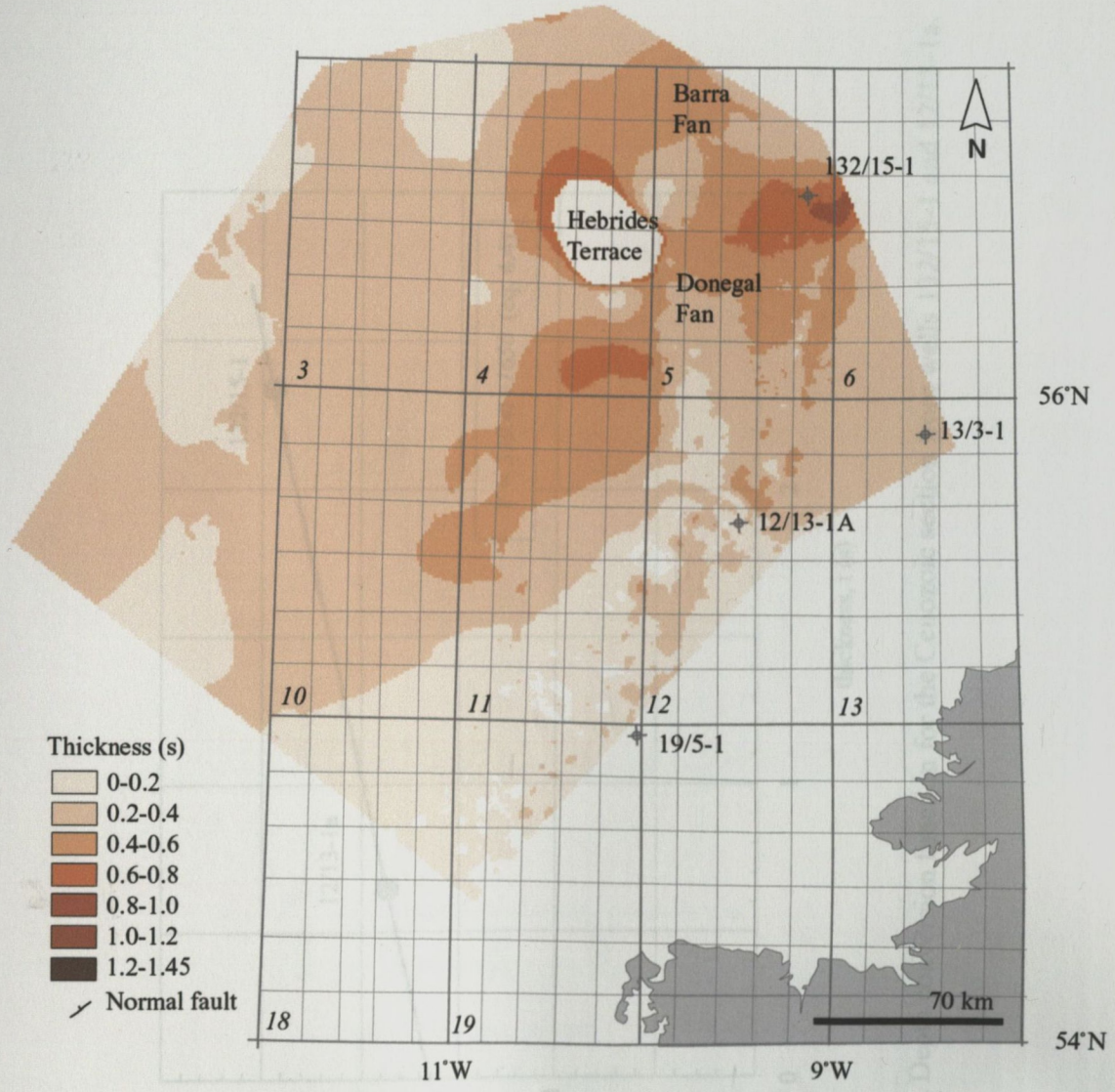


Figure 4.18. Isochron map for the Plio-Pleistocene section, constructed by substracting the depth to the seabed from the depth to the early Pliocene unconformity. See Figure 4.7 for the seismic grid used to construct the isochron map. Line spacing is 1 km in Quads. 5 and 12, and >1 km elsewhere.

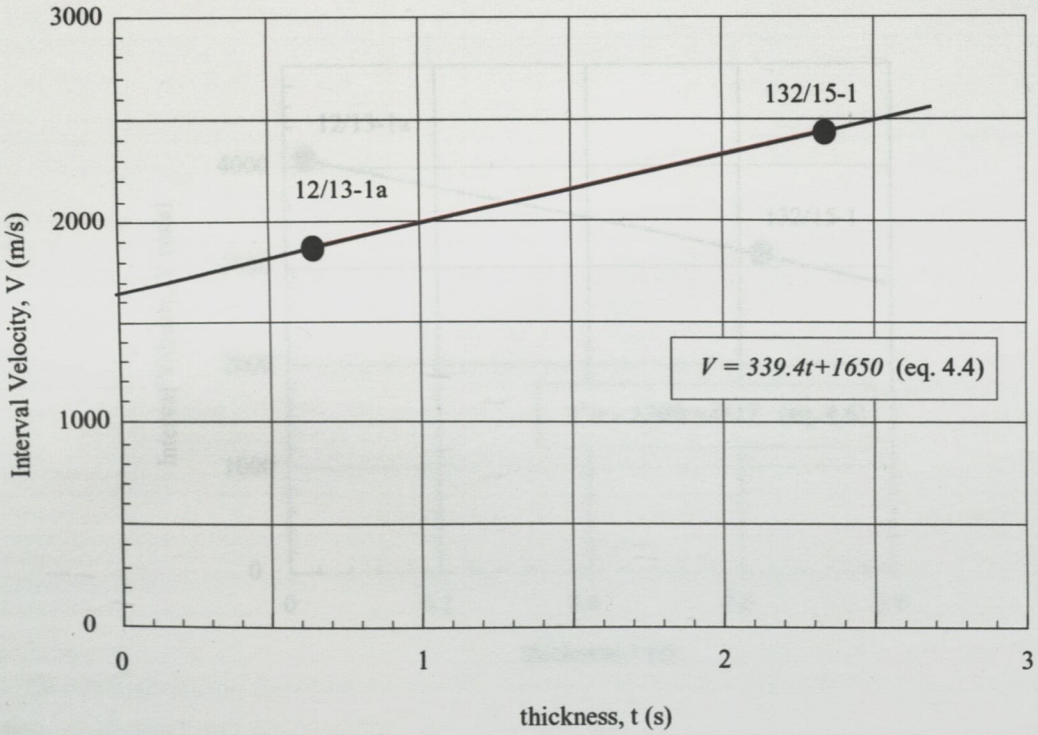


Figure 4.19. Depth conversion function for the Cenozoic section from wells 132/15-1 and 12/13-1a.

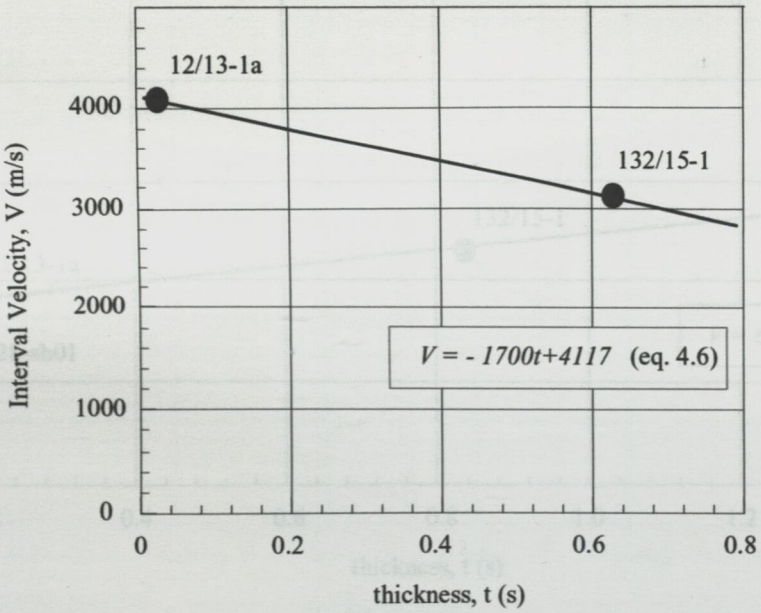


Figure 4.20. Depth conversion function for the Palaeocene section from wells 132/15-1 and 12/13-1a.

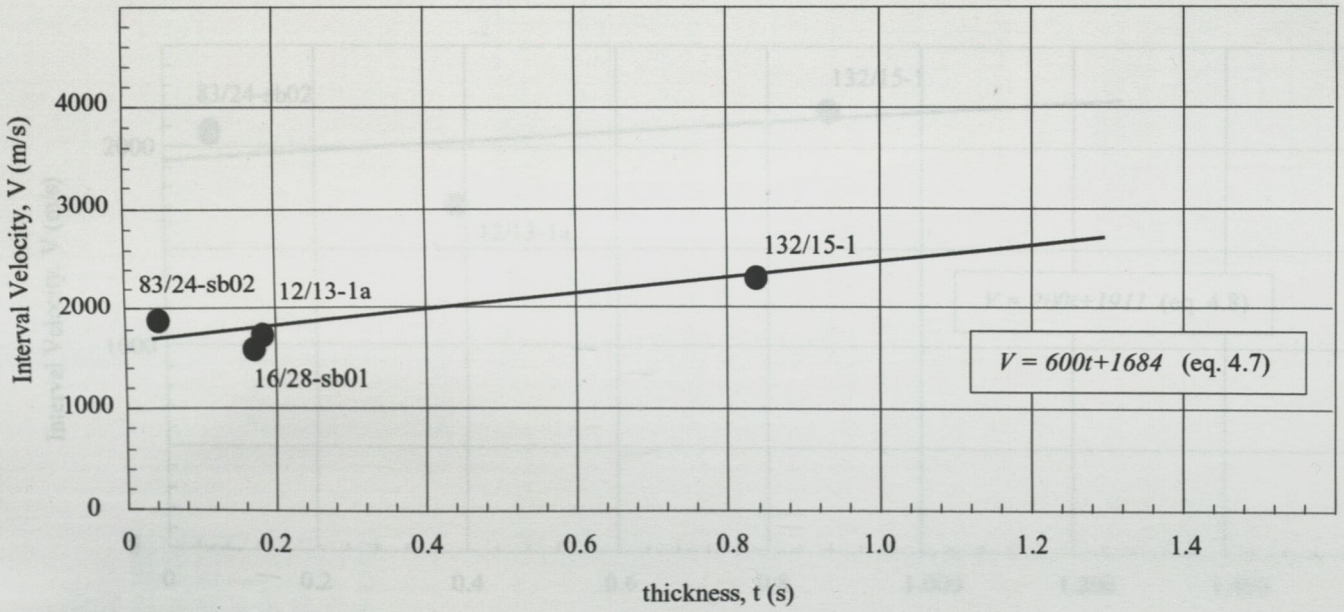


Figure 4.21. Depth conversion function for the Eocene section from wells 132/15-1 and 12/13-1a and shallow BGS borholes 16/28-sb01 and 83/24-sb02.

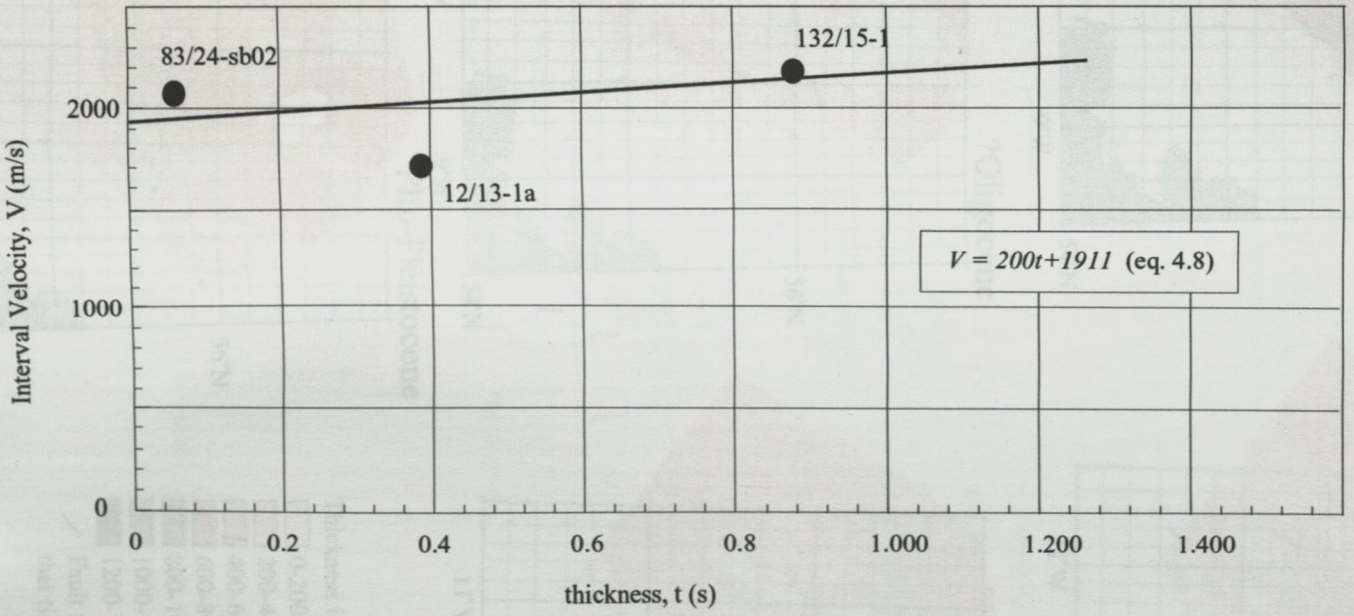


Figure 4.22. Depth conversion function for the post-Eocene section from wells 132/15-1 and 12/13-1a and shallow BGS borehole 83/24-sb02.

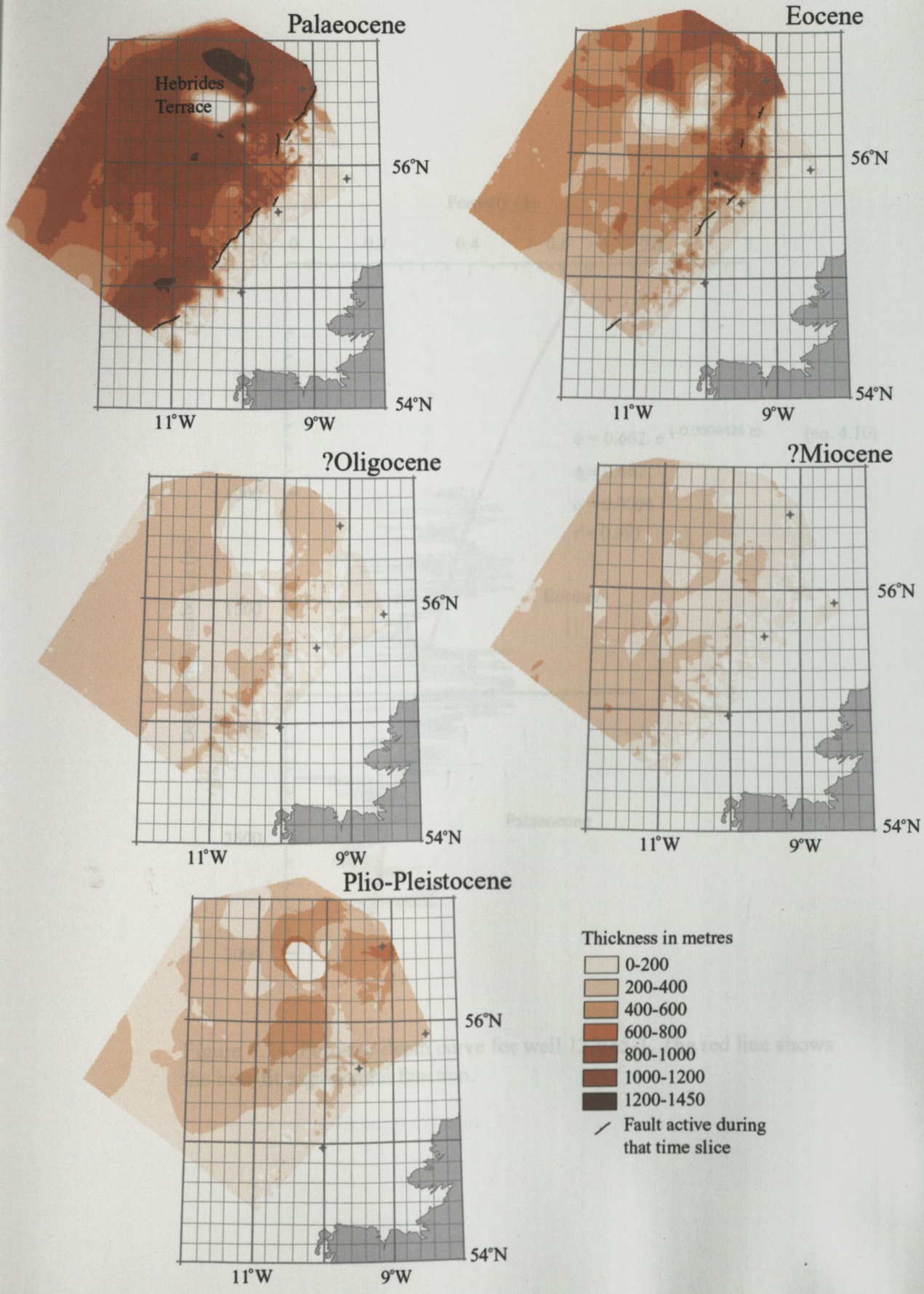


Figure 4.23. Isopach maps derived from isochrons using depth conversion functions in Table 4.10.

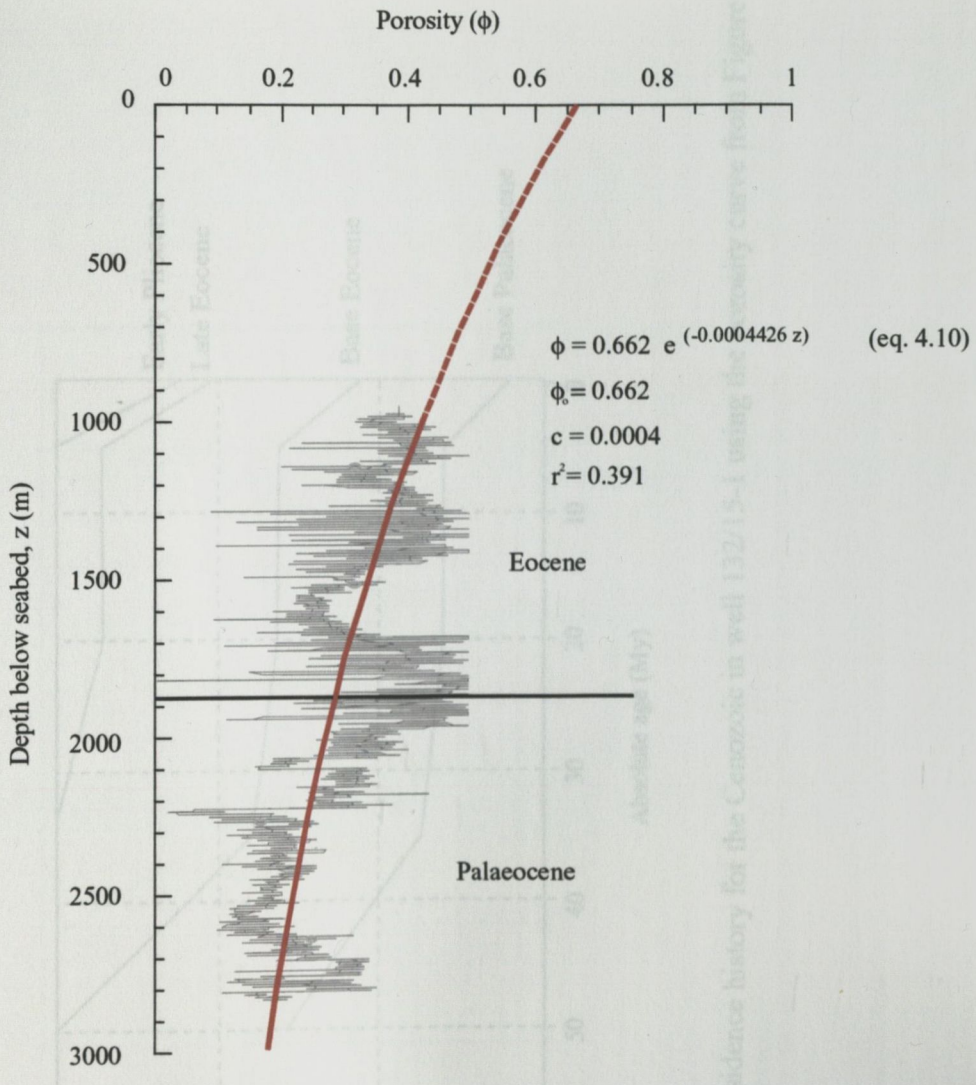


Figure 4.24. Porosity-depth curve for well 132/15-1. The red line shows the best-fit exponential function.

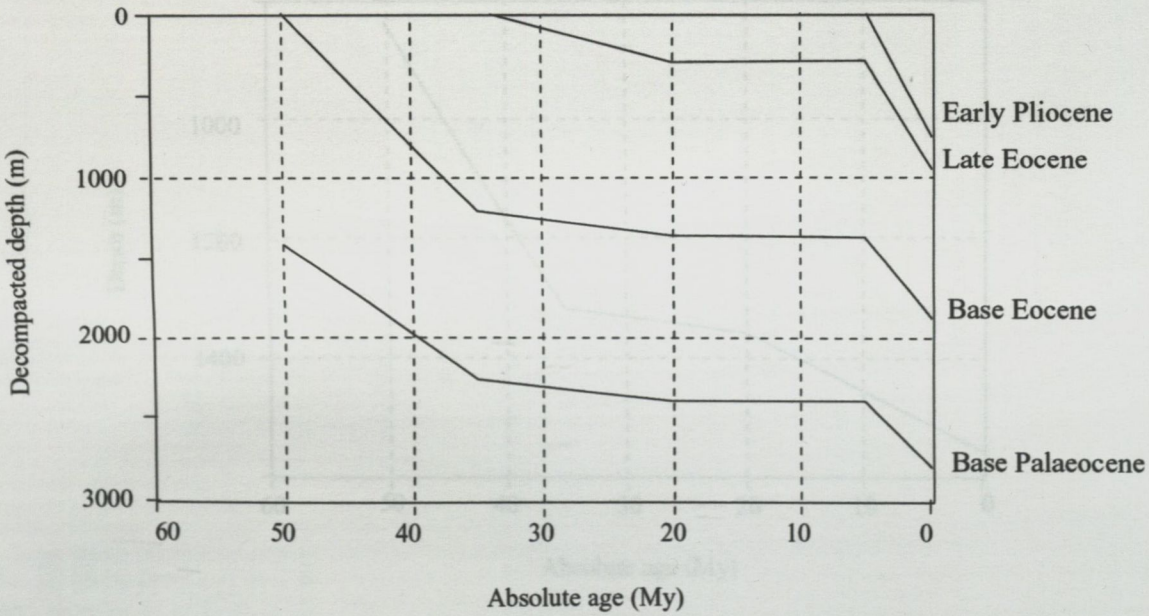


Figure 4.25. Decompacted subsidence history for the Cenozoic in well 132/15-1 using the porosity curve from Figure 4.24.

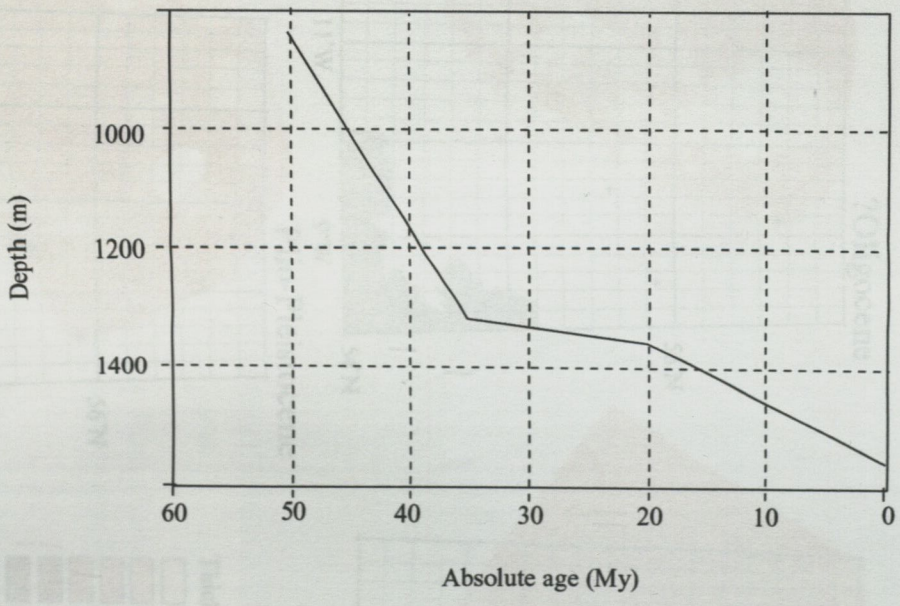


Figure 4.26. Tectonic subsidence during the Cenozoic for well 132/15-1, corrected for isosotasy but not corrected for palaeobathymetry and eustacy.

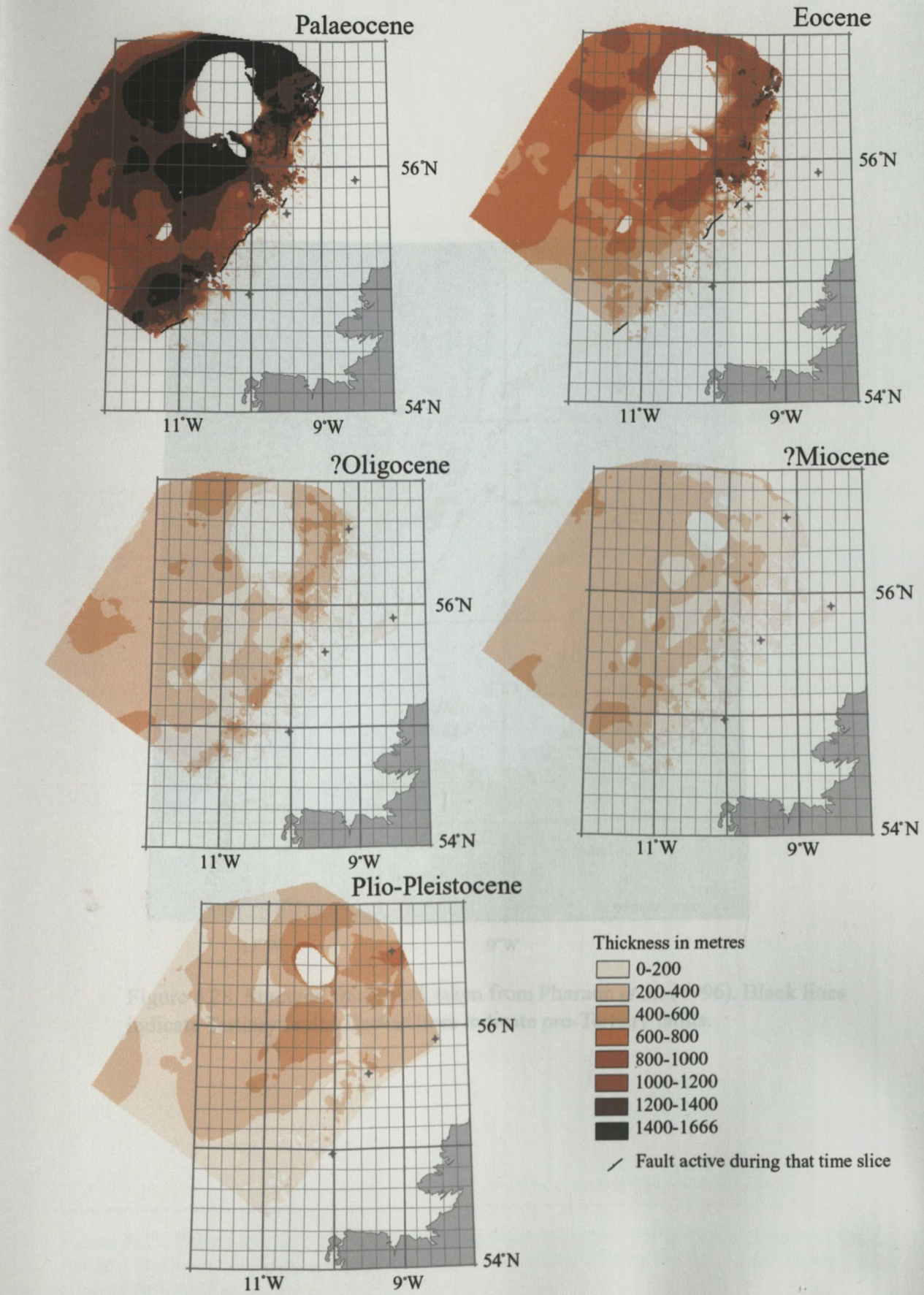


Figure 4.27. Decompacted isopach maps for the northeastern Irish Rockall Basin using porosity curve from Figure 4.24.

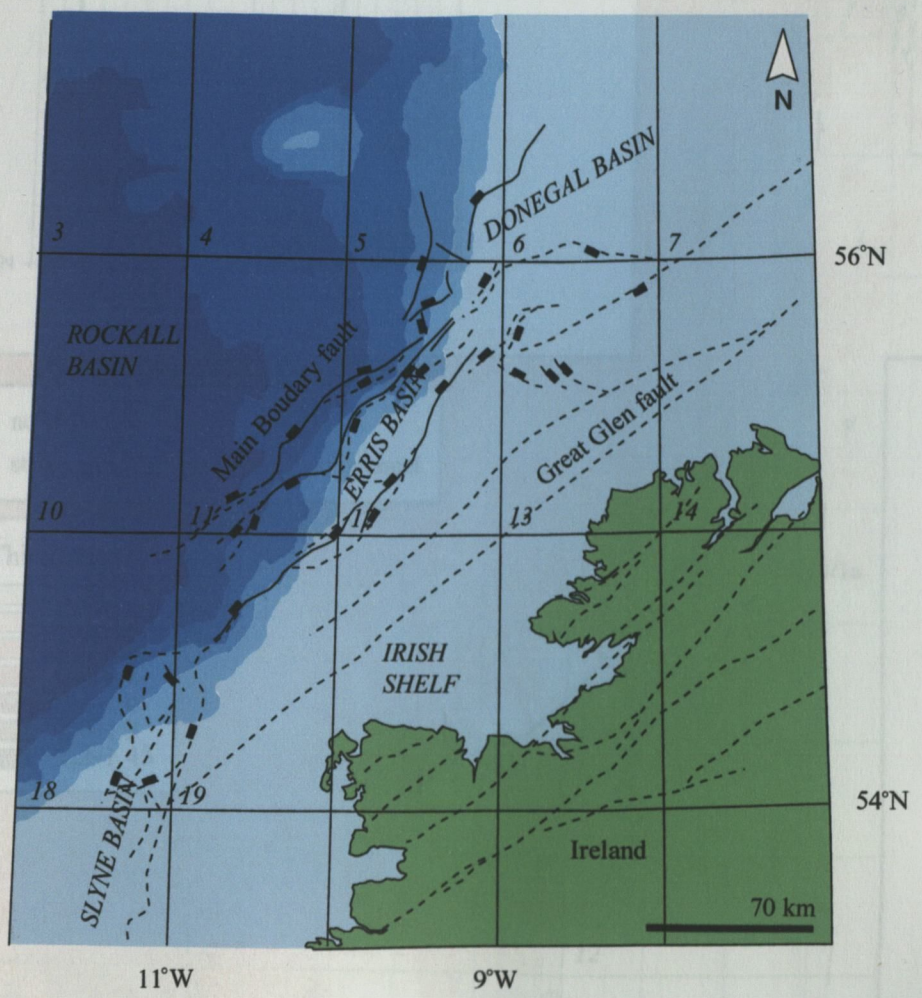


Figure 4.28. Stuctural framework taken from Pharaoh *et al.* (1996). Black lines indicate Tertiary faults. Dashed lines indicate pre-Tertiary faults.

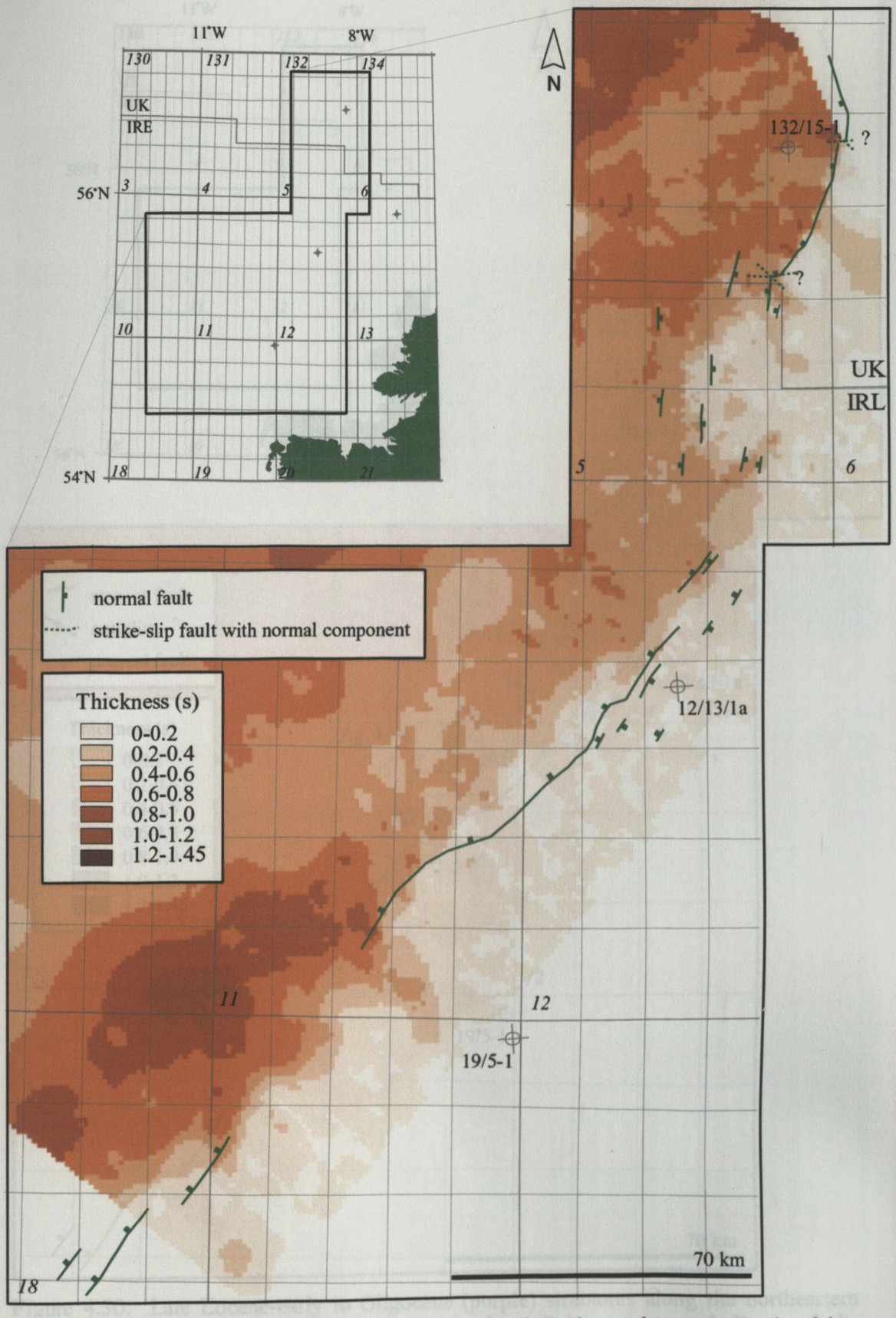


Figure 4.29. Palaeocene to early Eocene (green) faults along the northeastern margin of the Rockall Basin and Palaeocene isochron. Faults were mapped using the two-dimensional seismic dataset (Fig. 4.7).

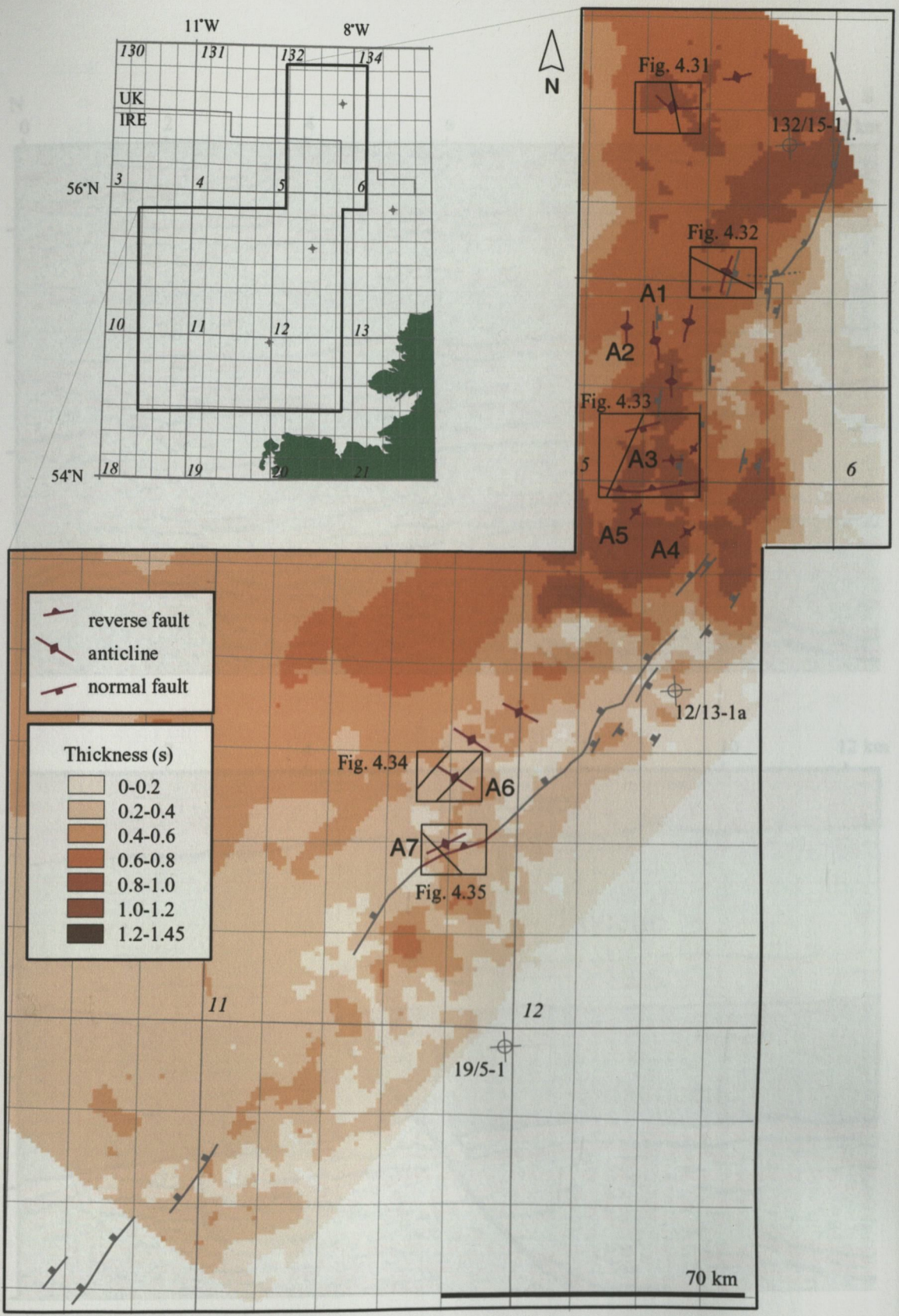


Figure 4.30. Late Eocene-early to Oligocene (purple) structures along the northeastern margin of the Irish Rockall Basin and Eocene isochron. Palaeocene to early Eocene faults are shown in grey. Structures were mapped using the two-dimensional seismic dataset (Fig. 4.7). Boxes show the location of detailed figures, and black lines show the position of seismic lines shown in the figures. A1, A2,...etc refers to anticlines mention in text.

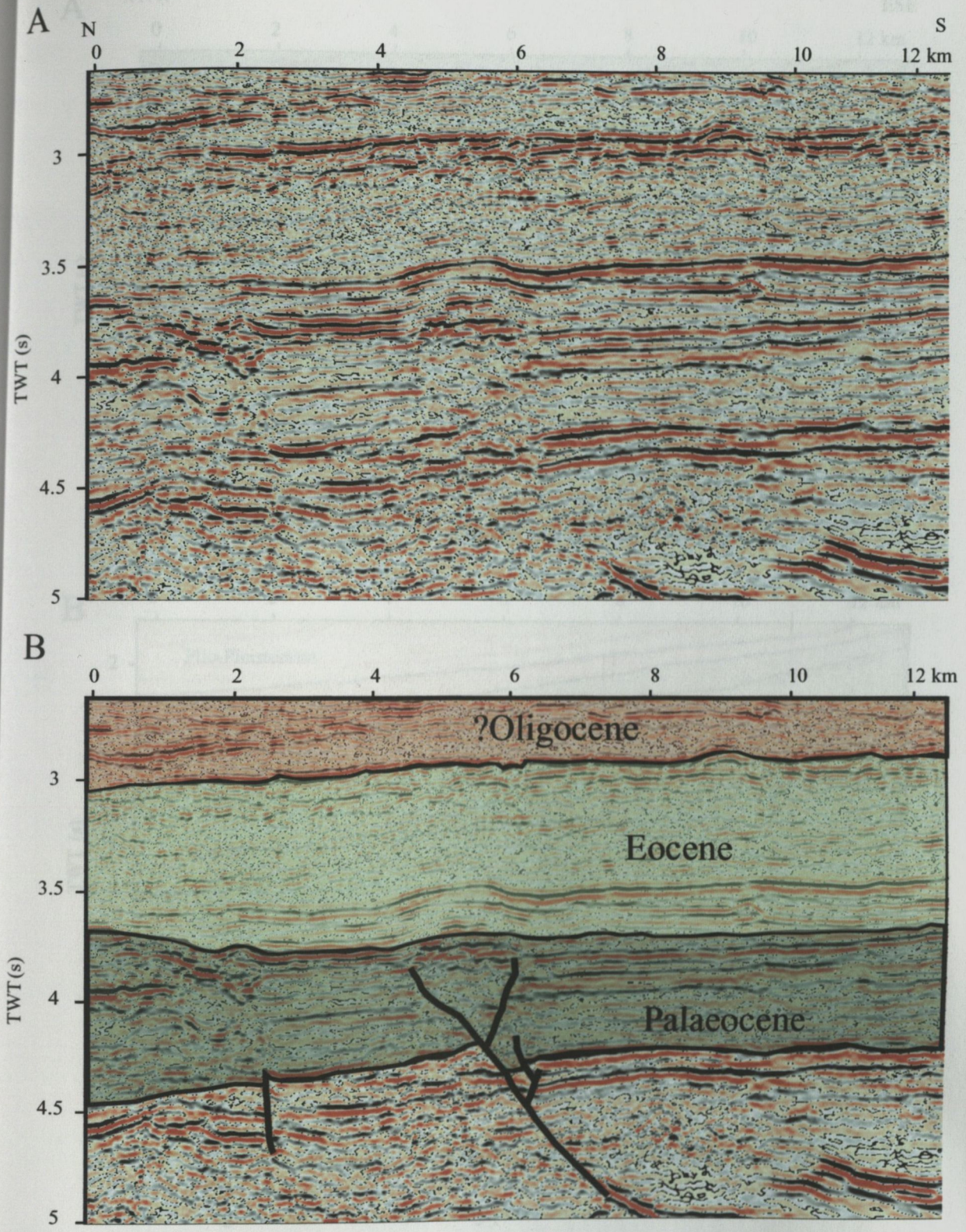


Figure 4.31. A, uninterpreted section of Line 3 north in the study area (see Fig. 4.30 or Fig. 4.10 for location). B, interpretation of a compresional structure. Shown by permission of TGS-Nopec.

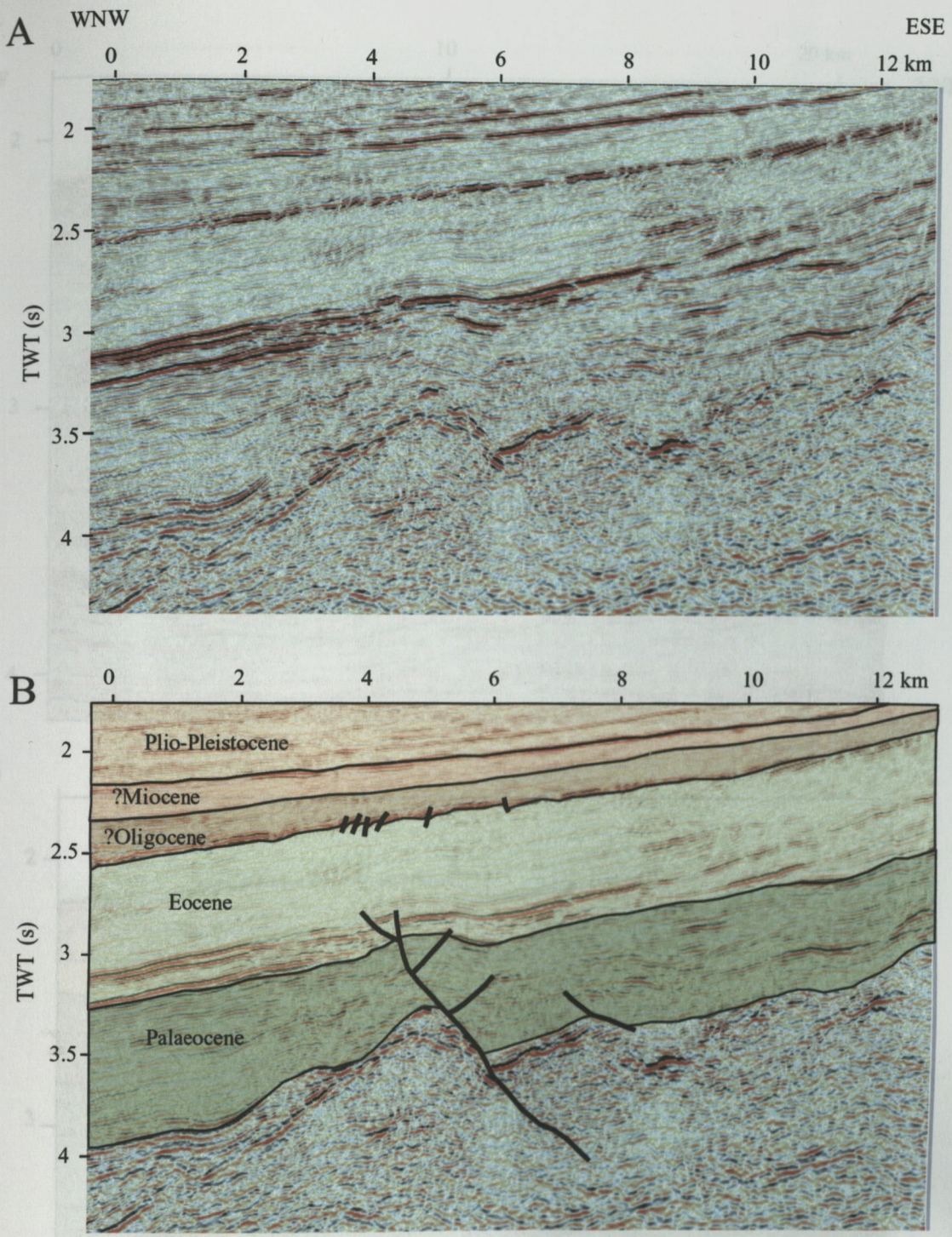


Figure 4.32. A, uninterpreted section of seismic Line 4 (see Fig. 4.30 or Fig. 4.10 for location). B, interpretation of a Palaeocene normal fault and upper Eocene to lower ?Oligocene anticline. Shown by permission of WesternGeco.

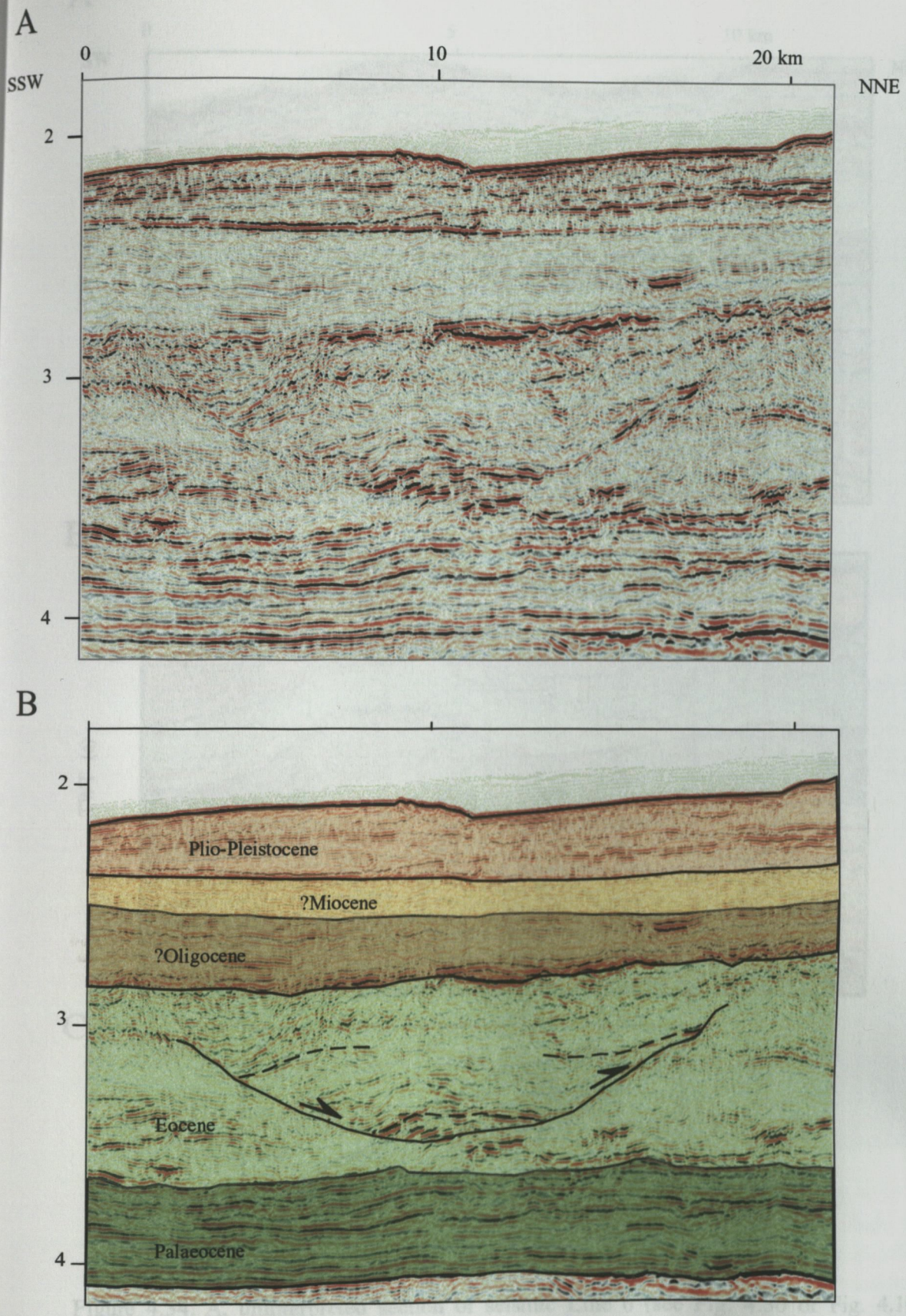


Figure 4.33. A, uninterpreted section of seismic Line 5 (see Figure 4.30 and Fig. 4.10 for location). B, interpretation of a large curved intra-Eocene surface as a slump 18 km wide. Shown by permission of WesternGeco.

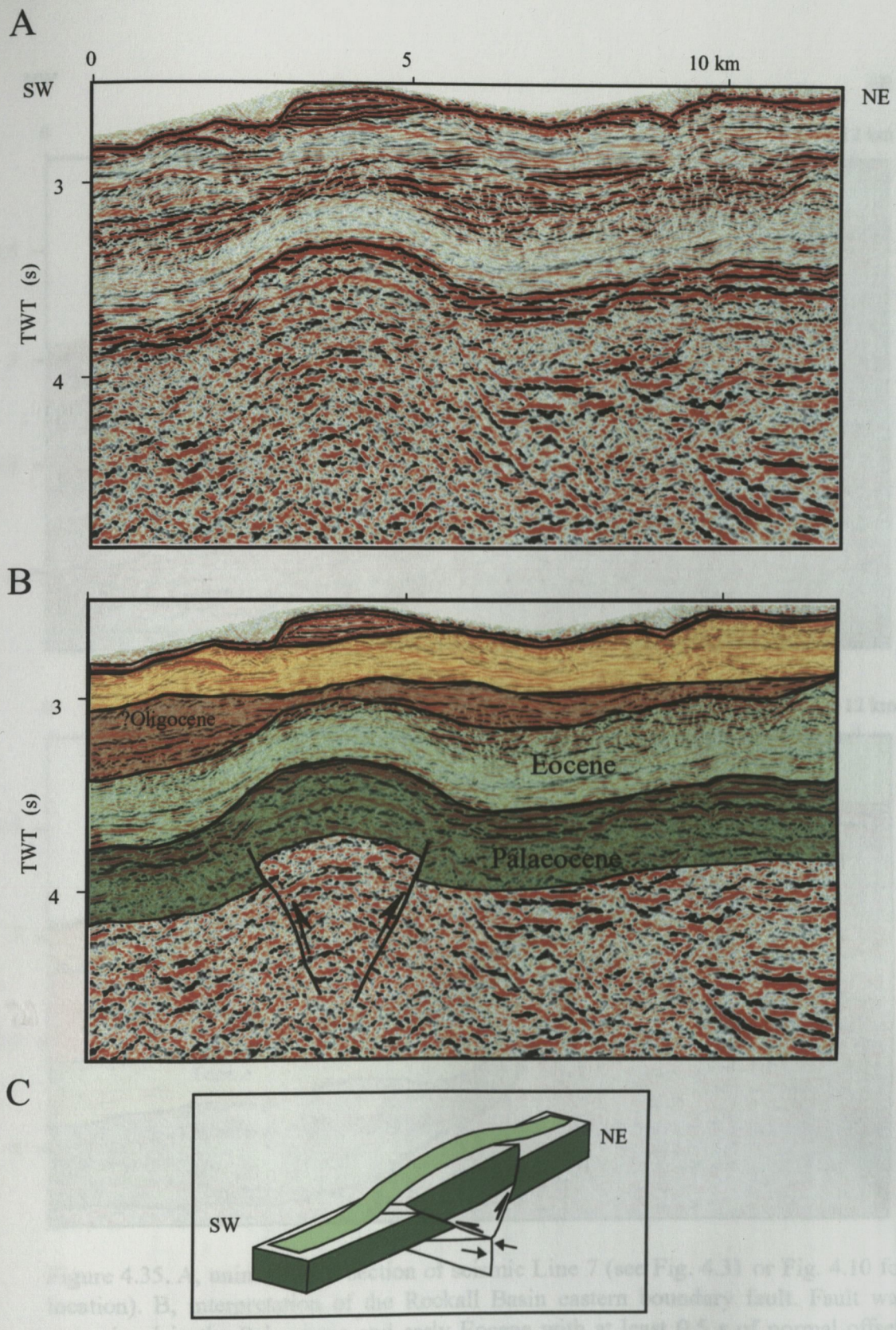


Figure 4.34. A, uninterpreted section of seismic Line 6 (see Fig. 4.30 or Fig. 4.10 for location). B, interpretation of a late Eocene or early ?Oligocene anticline with 300 ms of relief trending west-northwest and perpendicular to the basin margin. C, block diagram of interpreted stucture. Seismic line shown by permission of Veritas DGC Limited.

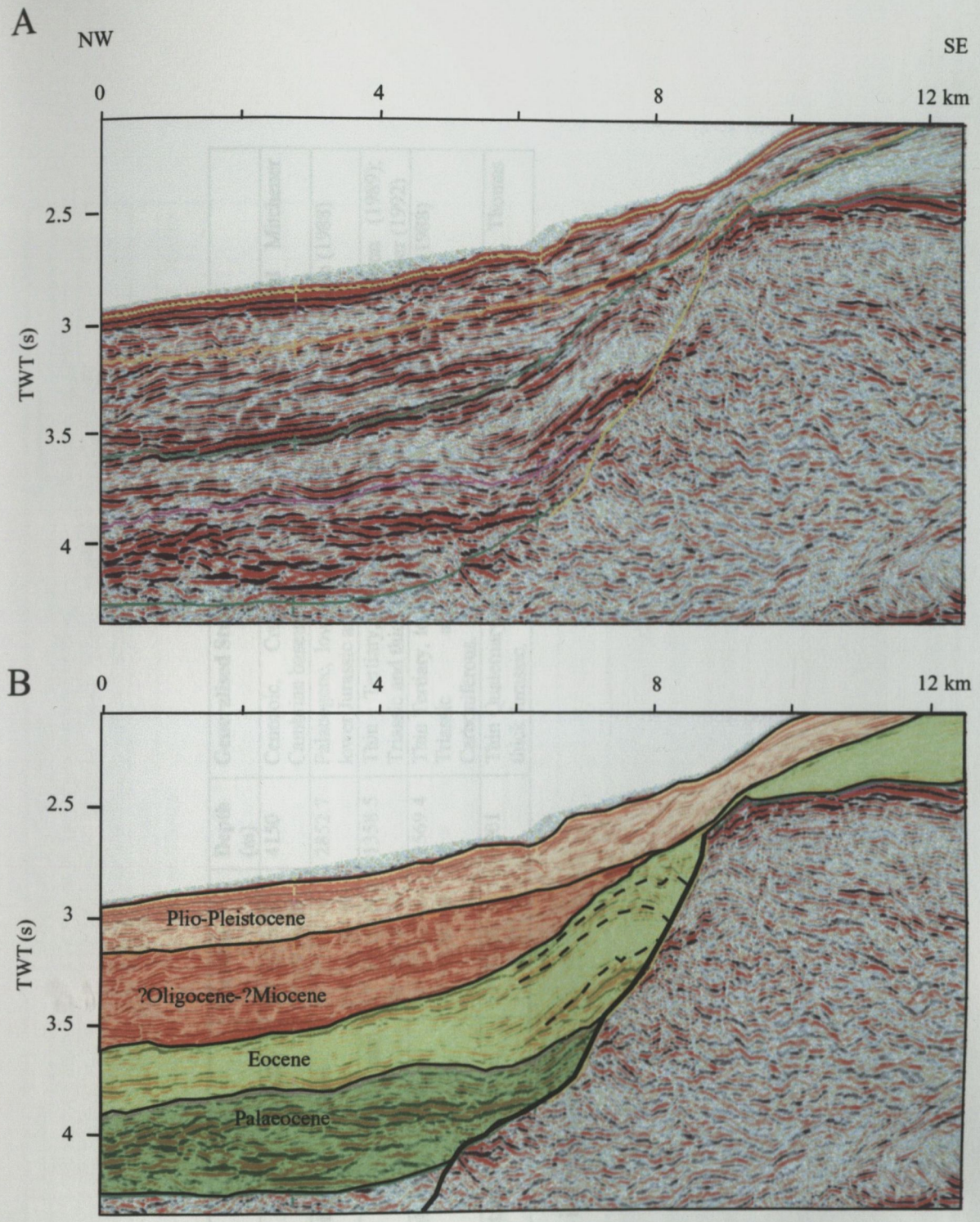


Figure 4.35. A, uninterpreted section of seismic Line 7 (see Fig. 4.31 or Fig. 4.10 for location). B, interpretation of the Rockall Basin eastern boundary fault. Fault was extensional in the Palaeocene and early Eocene with at least 0.5 s of normal offset. Deformation switched to compressional in the late Eocene. Shown by permission of TGS-Nopec.

Well	Date drilled & company	Basin	Location	Depth (m)	Generalised Stratigraphy	References
132/15-1 UK	1992, BP Plc.	UK Rockall	56° 36.45'N 09° 09.08'W	4150	Cenozoic, Cretaceous and Pre-Cambrian basement	Musgrove and Mitchener (1996)
12/13-1A IRE	1979, Amoco Ireland Exploration Co	Erris Basin	55° 37.03' N 09° 30.38' W	2852.7	Palaeogene, lower-upper Cretaceous, lower Jurassic and Permo-Triassic.	Tate and Dobson (1988)
13/3-1 IRE	1978 Texaco	Donegal Basin	55° 53.18' N 08° 30.08' W	1358.5	Thin Tertiary, Jurassic, Permo-Triassic and thick Carboniferous.	Tate and Dobson (1989); Murphy and Croker (1992)
19/5-1 IRE	1978 Amoco Ireland Exploration Co.	Erris Basin	54° 57.42' N 10° 02.00' W	2569.4	Thin Tertiary, lower Jurassic, Permo-Triassic and lower/upper Carboniferous.	Tate and Dobson (1988)
27/13-1 IRE	1981, Elf Aquitaine Ltd	Slyne Basin	53° 33.26' N 11° 24.37' W	2701	Thin Quaternary to Late Tertiary and thick Jurassic.	Scotchman and Thomas (1995)

Table 4.1. Exploration wells in the study area.

Wells	Location	Details of Tertiary section	References
UK163/6-1A	NE Rockall Basin	Sequence of Tertiary volcanics (1045 m)	Morton *et al.* (1988)
UK164/25-2	NE Rockall Basin	Middle/upper Miocene muds above shallow marine sands and muds with bioturbation	Egerton (1998)
DSDP 610	Southern Rockall Basin	Miocene to recent	Masson & Kidd (1986)
JOIDES	Hatton Rockall	Tertiary succession	Laughton *et al.* (1972); Naylor and Shannon (1982)
DSDP116	Hatton Basin	Oligocene to Mio-Pliocene ooze and chalk with chert (808 m) above upper Eocene carbonate ooze (46 m)	Naylor & Shannon (1982)
DSDP117	Hatton Basin	Oligocene cherty limestone and ooze (152 m) above lower Eocene ooze, sandstones and claystones (152 m)	Naylor & Shannon (1982)
BGS88/7, 7A	Hebrides Slope	Late Miocene-early Pliocene unconformity	Stoker *et al.* (1994)
BGS94/4	NW Rockall Basin	Upper Eocene/lower Oligocene mass-flow deposits	Stoker *et al.* (2001)
BGS94/1	W Rockall Basin	Upper Eocene deep marine limestones above early Late Eocene shallow marine mudstones and sandstones	Stoker *et al.* (2001)
ODP981	W Rockall Basin	Intra-Pliocene reflector	Jansen *et al.* (1995)
BGS83/20-sb01	SE Rockall Basin		Stoker (1999)
BGS83/24-sb02	SE Rockall Basin		Stoker (1999)
BGS11/20-sb01	NE Irish Rockall Basin		Stoker (1999)
BGS16/28-sb01	East Rockall Basin		Stoker (1999)

Table 4.2. Other well data controlling stratigraphy and age of Cenozoic sediments in the Rockall Basin.

Survey name	Year and Company
Inrock 96	1998, Spectrum-reprocessed
TRHP 98	1998, TFE-Proprietary
E0597	1999, TFE-Proprietary
E95IE07	1995, Enterprise
E97IE21	1997, Enterprise
DGER96	1996, Digicon
GWH92	1992, GECO-Prakla
NWI91	1991, Nopec
NWI93	1993, Nopec
WHR93	1993, Nopec
SRT96	1996, Nopec
M89-WB	1989, Mobile
INROCK96	1996, Spectrum
NA	1975-76, Western
OH	1975-76, Western

Table 4.3. Two-dimensional seismic surveys used in this study.

Geochronological scale	Age (My)	This work	Stoker *et al.* (2001)	Corfield *et al.* (1999)	van Weering *et al.* (1999)	Svaerdborg (1998)	Shannon *et al.* (1993)	Masson & Kidd (1986)	Miller and Tucholke (1983)
Plio-Pleistocene	5	Early Pliocene	C10	Intra Miocene	Upper Package: Drift development and slumps	Yellow Light Green	Base RT4	Yellow	R1
Miocene	20	Early ?Miocene	C20			Dark Green (Dark Green)	Base RT3	Purple Green	R2
Oligocene	30	Late Eocene	C30	Early Oligocene	Lower Package: Progradation and slumping	Blue	Base RT2	Brown	R4
Eocene	53	Base Eocene		Base Eocene					
Palaeocene	65	Base Tertiary		Intra Palaeocene Danian			RT1		

Table 4.4. Regional seismic reflections in the Rockall Basin mapped by different authors. Stoker *et al.* (2001) used nannoplankton from boreholes to date megasequences, and therefore have the most reliable time constraints. Other authors dated reflections based on projections to wells.

132/15-1	Depth below sea level (m)	Thickness (m)	Seismic TWT (s)	Thickness TWT (s)	Av. Velocity (m/s)	Inter. Velocity (m/s)
Seabed	707		0.961		1471	
		953		0.867		2198
?Late Eocene	1660		1.828		1816	
		933		0.836		2232
Base Eocene	2593		2.664		1946	
		944		0.618		3055
Base Tertiary	3537		3.282		2155	

12/13-1A	Depth below sea level (m)	Thickness (m)	Seismic TWT (s)	Thickness TWT (s)	Av. Velocity (m/s)	Inter. Velocity (m/s)
Seabed	480		0.660		1454	
		340		0.394		1726
?Late Eocene	820		1.054		1556	
		167		0.192		1739
Base Eocene	987		1.246		1584	
		71		0.035		4057
Base Tertiary	1058		1.281		1652	

19/5-1	Depth below sea level (m)	Thickness (m)	Seismic TWT (s)	Thickness TWT (s)	Av. Velocity (m/s)	Inter. Velocity (m/s)
Seabed	115		0.158		1457	
Holocene-Pleistocene		103		0.032		6477
	219		0.190		2303	
Pleistocene-Late Pliocene		98		0.224		874
	317		0.224		2827	
?L. Miocene-Pliocene		49		0.136		717
	365		0.360		2.030	

Table 4.5. Well data used for depth conversion taken from composite well logs and seismic lines tied into the wells. Interval (Inter.) and average (Av.) velocities are calculated dividing thickness in metres (m) by thickness in seconds (s).

132/15-1	Depth below sea level (m)	Thickness (m)	Seismic TWT (s)	Thickness TWT (s)	Av. Velocity (m/s)	Inter. Velocity (m/s)
Seabed	707		0.961		1471	
		2830		2.321		2438
B.Tertiary	3537		3.282		2155	

12/13-1A	Depth below sea level (m)	Thickness (m)	Seismic TWT (s)	Thickness TWT (s)	Av. Velocity (m/s)	Inter. Velocity (m/s)
Seabed	480		660		1454	
		578		621		1861
B. Tertiary	1058		1281		1651	

	Thickness TWT (s)	Thickness (m)	Interval Velocity (m/s)
Minimum value	0.001	1.605	1605
Maximum value	2.506	3009	2402

Table 4.6. Cenozoic section thicknesses in seconds and metres measured from wells 132/15-1 and 12/13-1a and seismic sections tied to the wells. The interval velocity for the Cenozoic section is calculated by dividing thickness in metres (m) by thickness in seconds (s). The average velocity to the base Tertiary unconformity and the seabed is also calculated. The third table shows the maximum and minimum thicknesses in seconds from the isochron map and the estimated maximum and minimum velocities used for depth converting, using the average velocity function calculated from the two wells (Fig. 4.20).

132/15-1	Depth below sea level (m)	Thickness (m)	Seismic TWT (s)	Thickness TWT (s)	Av. Velocity (m/s)	Inter. Velocity (m/s)
Base Eocene	2593		2.664		1946	
		944		0.618		3055
Base Tertiary	3537		3.282		2155	

12/13-1a	Depth below sea level (m)	Thickness (m)	Seismic TWT (s)	Thickness TWT (s)	Av. Velocity (m/s)	Inter. Velocity (m/s)
Base Eocene	987		1.246		1584	
		71		0.035		4057
Base Tertiary	1058		1.281		1651	

	Thickness TWT (s)	Thickness (m)	Interval Velocity (m/s)
Minimum value	0.001	2.057	4115
Maximum value	1.500	1154	1538

Table 4.7. Palaeocene section thicknesses in seconds and metres measured from wells 132/15-1 and 12/13-1a and seismic sections tied to the wells. The internal velocity for the Palaeocene section is calculated by dividing thickness in metres (m) by time in seconds (s) in one-way travel time. The average velocity to the base Tertiary unconformity and the base Eocene is also calculated. The third table shows the maximum and minimum thicknesses in seconds from the isochron map and the estimated maximum and minimum velocities used for depth converting, using the average velocity function calculated from the two wells (Fig. 4.21).

132/15-1	Depth below sea level (m)	Thickness (m)	Seismic TWT (s)	Thickness TWT (s)	Av. Velocity (m/s)	Inter. Velocity (m/s)
Late Eocene	1660		1.828		1816	
		933		0.836		2232
Base Eocene	2593		2664		1946	

12/13-1a	Depth below sea level (m)	Thickness (m)	Seismic TWT (s)	Thickness TWT (s)	Av. Velocity (m/s)	Inter. Velocity (m/s)
Late Eocene	820		1.054		1555	
		167		0.192		1739
Base Eocene	987		1.246		1584	

Borehole 83/24-sb02	Depth below sea level (m)	Thickness (m)	Seismic TWT (s)	Thickness TWT (s)	Av. Velocity (m/s)	Inter. Velocity (m/s)
Seabed	1566		2.086		1501	
		38		0.040		1906
Lower Eocene	1604		2.126		1509	

Borehole 16/28-sb01	Depth below sea level (m)	Thickness (m)	Seismic TWT (s)	Thickness TWT (s)	Av. Velocity (m/s)	Inter. Velocity (m/s)
Seabed	1465		1.956		1497	
		146		0.181		1612
Lower Eocene	1610		2.137		1507	

	Thickness TWT (s)	Thickness (m)	Interval Velocity (m/s)
Minimum	1	0.842	1685
Maximum	1101	1290	2344

Table 4.8. Eocene section thicknesses in seconds and metres measured from wells 132/15-1 and 12/13-1a, boreholes 83/24-sb02 and 16/28-sb01, and seismic sections tied to the wells. The interval velocity for the Palaeocene section is calculated by dividing thickness in metres (m) by thickness in seconds (s) OWT. The average velocity to the base Eocene unconformity and to late Eocene unconformity is also calculated. The last table shows the maximum and minimum thicknesses in seconds from the isochron map and the estimated maximum and minimum velocities used for depth conversion (Fig. 4.22).

132/15-1	Depth below sea level (m)	Thickness (m)	Seismic TWT (s)	Thickness TWT (s)	Av. Velocity (m/s)	Inter. Velocity (m/s)
Seabed	707		0.961		1471	
		953		0.867		2198
Late Eocene	1660		1.828		1816	

12/13-1a

12/13-1a	Depth below sea level (m)	Thickness (m)	Seismic TWT (s)	Thickness TWT (s)	Av. Velocity (m/s)	Inter. Velocity (m/s)
Seabed	480		0.660		1454	
		340		0.394		1725
Late Eocene	820		1.054		1555	

83/20-sb01	Depth below sea level (m)	Thickness (m)	Seismic TWT (s)	Thickness TWT (s)	Av. Velocity (m/s)	Inter. Velocity (m/s)
Seabed	1045		1.428		1463	
		86		0.082		2089
Miocene	1131		1.510		1497	

	Thickness TWT (s)	Thickness (m)	Interval Velocity (m/s)
Minimum	0.001	0.955	1911
Maximum	1.123	1199	2135

Table 4.9. Post-Eocene section thicknesses in seconds and metres measured from wells 132/15-1, 12/13-1a and borehole 83/24-sb02, and seismic sections tied to the wells. The interval velocity for the post-Eocene section is calculated by dividing thickness in metres (m) by thickness in seconds (s) in one-way travel time. The average velocity to the late Eocene unconformity and the seabed is also calculated. The last table shows the maximum and minimum thickness in seconds from the isochron map and the estimated maximum and minimum velocities used for depth conversion (Fig. 4.23).

Package	Interval Velocity functions (m/s)			Evidence from wells
	1) Entire Cenozoic	2) Prescribed post-late Eocene	3) Variable post-late Eocene	
Early Pliocene – Seabed	$V = 339t + 1650$	1800	$V = 200t + 1911$	132/15-1
Early Miocene – Early Pliocene		1900		12/13-1a
Late Eocene – Early Miocene		2000		83/24-sb02
Base Eocene – Late Eocene		$V = 600t + 1684$		16/28-sb01
Base Tertiary – Base Eocene		$V = -1700 + 4117$		

Table 4.10. Summary of velocity constant values and functions obtained from well evidence for the five different Cenozoic sedimentary packages.

Well 132/15-1	Depth from seabed to top of package (m)	Depth from seabed to base of package (m)	Thickness (m)	Age (My)
Plio-Pleistocene	0	767	767	0-5
?Miocene	767	767	0	5-20
?Oligocene	767	967	200	20-35
Eocene	967	1886	919	35-50
Palaeocene	1886	2830	944	50-60

Table 4.11. Depth from seabed to base and top of each sedimentary package. Thickness and age in well 132/15-1 are also given.

Decompacted depth from seabed to base of package	50 Ma	35 Ma	20 Ma	5 Ma	0 Ma
Plio-Pleistocene	0	0	0	0	767 m
Miocene	0	0	0	?	767 m
Oligocene	0	0	289 m	289 m	967 m
Eocene	0	1213 m	1388 m	1388 m	1886 m
Palaeocene	1417 m	2259 m	2403 m	2403 m	2830 m

Table 4.12. Decompacted depth below seabed in metres to the base of each package at various times in the past. The present day (0 Ma) depths to the base of each layer are given by the right-hand column. At 5 Ma the Plio-Pleistocene was not yet deposited. The Miocene section is missing in the well. At 20 Ma the Miocene and Plio-Pleistocene were not yet deposited and the Oligocene section was therefore uncompacted with a depth to its base of 289 m below seabed. At 35 Ma the base Eocene was at 1213 m below seabed. At 50 Ma the base Palaeocene was at 1417 m below seabed.

ϕ	50 Ma	35 Ma	20 Ma	5 Ma	0 Ma
Plio-Pleistocene					0.55
Miocene					-
Oligocene			0.6	0.5	0.45
Eocene		0.5	0.45	0.35	0.35
Palaeocene	0.45	0.35	0.3	0.25	0.25

Table 4.13. Backstripped porosity (ϕ) taken from porosity curve in well 132/15-1 (Fig. 4.25).

	50 Ma	35 Ma	20 Ma	5 Ma	0 Ma
Bulk density (kg/m^3)	1946	1968	2011		2054

Table 4.14. Bulk density of the entire sedimentary column calculated from Eq. 4.11.

	50 Ma	35 Ma	20 Ma	5 Ma	0 Ma
Subsidence	842	1320	1360		1550

Table 4.15. Backstripped tectonically-driven subsidence. The lack of wells drilled in the Rockall Basin allowed only a preliminary estimation of the tectonically-driven subsidence which has not been corrected for palaeobathymetry or eustacy.

	Mean thickness (m)	Duration (My)	Accumulation rates (m/My)
Plio-Pleist. (5 – 0 My)	254	5	51
?Miocene (23 – 5 My)	248	18	14
?Oligocene (36 – 23 My)	282	13	22
Eocene (53 – 36 My)	648	17	38
Palaeocene (66 – 53 My)	1205	13	93
Cenozoic (66-0)	1811	66	27

Table 4.16. Spatially-averaged accumulation rates in the northeastern Irish Rockall Basin taken from isopach maps in this study.

Chapter 5 Denudation, deposition and flexure on the northwestern Irish margin during the Cenozoic

5.1 Introduction

The northwestern Irish passive margin was characterised by onshore denudation and offshore sedimentation throughout the Cenozoic (Allen *et al.* in press). Offshore sedimentation is reflected by an almost complete Cenozoic succession three kilometres thick in the northeastern Rockall Basin (Chapter 4). On onshore northwestern Ireland no extensive Tertiary or Mesozoic deposits exist and bedrock is predominantly composed of Pre-Cambrian to Carboniferous rocks, suggesting at least some episodes of widespread denudation during the Cenozoic. The flexural effects of sedimentary loading due to offshore deposition and unloading due to onshore denudation will be explored in this chapter.

To quantify the magnitude of denudation several techniques can be used. Hillis (1995) used sonic velocities (a function of sedimentary compaction) from Mesozoic sediments to estimate approximately 1 km of Tertiary denudation in and around the United Kingdom. In Chapter 3 denudational estimates were given from a simple function proportional to present day relief (Anhert 1970; Summerfield 1991a). This method may well be unreliable when applied over long time scales.

Denudation is commonly estimated using forward modelling of apatite fission track data (Brown *et al.* 1994). Apatite fission track modelling is a thermochronological method that uses fission track parameters, such as the age and length of the apatite fission tracks, to estimate a palaeo-thermal history for a given sample (Gleadow *et al.* 1986; Duddy *et al.* 1988; Green 1988). It has been widely used in the British Isles (Bray *et al.* 1992; Green *et al.* 1999; Green 1986, 1989; Lewis *et al.* 1992), Ireland (Allen *et al.* in press; Green *et al.* 2000; Keeley *et al.* 1993; McCullogh 1993, 1994) and other passive margins such as southeastern Australia (Gallagher & Brown 1997), southern Norway (Rohrman *et al.* 1995) and northeast Greenland (Thomson *et al.* 1999).

The offshore Cenozoic depositional history and tectonic activity of northwestern Ireland was described in Chapter 4. The aim of this chapter is a comparison between the onshore and offshore Cenozoic denudational, depositional and flexural history in this region. First, the amount of denudation onshore will be estimated using apatite fission track modelling and compared with the amount of deposition offshore during the Cenozoic. Secondly, the flexural effect of sediment loading and erosional unloading will be calculated, assuming an elastic lithosphere with different values of rigidity overlying a viscous fluid.

Section 5.2 introduces apatite fission track analysis, and describes the basis for denudation estimates presented here and in other published work. Offshore well samples are modelled to calculate denudation around the margins of the northwestern Irish offshore basins during the Cenozoic.

In section 5.3, offshore denudation estimates are integrated with a larger database of denudation estimates from onshore Ireland (Allen *et al.* in press). The denudation histories for four time slices, Palaeocene, Eocene, Oligocene and post-Oligocene, are discussed.

Section 5.4 compares the rates and volumes of solid sediment denuded from onshore and the Irish Mainland Shelf with rates and volumes of sediment deposited in the northeastern Irish Rockall Basin.

Section 5.5 calculates the flexural response to this spatially-variable loading and unloading of the lithosphere over the last 65 My.

Similar studies involving denudation, deposition and flexure have been done for other passive margins, including the eastern US (Pazzaglia and Gardner 1994), eastern Africa (Clift and Lorenzo 1999), western South Africa (Gilchrist and Summerfield 1990), southern England (Watts *et al.* 2000) and the Scotian Basin, North America (Erickson 1993). Gilchrist and Summerfield (1990) used flexural models to show that the contrast in denudation rates in the flanks of rifted margins and adjacent coastal interiors results in marginal upwarps of up to 600 m; they explained variations in local relief by flexure. In the more topographically subdued middle US Atlantic passive

margin, Pazzaglia and Gardner (1994) calculated late Cenozoic flexural deformation driven by continental denudation and offshore deposition, with an onshore flexural uplift response that compares well with palaeotopography given by preserved fluvial terraces.

The northwestern Irish margin has onshore relief of up to 500 m, possible evidence of tectonic activity in the form of river knickpoints (Chapter 3), a Cenozoic denudation history given by apatite fission track analysis (Section 5.3), and a good offshore Cenozoic sedimentary record (Chapter 4). These factors make this area an ideal place to study the potential effects of flexural deformation.

5.2 Apatite fission track analysis

5.2.1 Introduction

The aim of this section is to present remodelled apatite fission track data from offshore wells in northwestern Ireland using the same technique as in Allen *et al.* (in press). This allows direct comparison between the resulting offshore thermal histories and those presented by Allen *et al.* (in press). Thermal histories for different time intervals during the Cenozoic will be taken from Allen *et al.* (in press) for onshore Ireland, and converted into denudational histories using a geothermal gradient constrained by offshore wells. Onshore and offshore denudational histories will be combined to compare later with basin deposition.

Apatite is a mineral usually found in sandstones, granites, igneous rocks and granitic gneisses. Fission tracks grow in apatite crystals by radioactive decay of uranium atoms (^{238}U). Fission track ages require an estimate of the relative abundance of the parent and daughter product (e.g., the number of ^{238}U atoms and the number of spontaneous fission tracks per unit volume). As the temperature increases the tracks become shorter (<14 μm) (anneal) till they disappear (total annealing) at ~125°C (Gleadow *et al.* 1986). If temperature decreases below 60°C tracks maintain their length and so, the maximum temperature the sample was under can be calculated.

Apatite fission track analysis allows determination of the magnitude of the maximum temperature of a sample and the time at which cooling from that maximum began. For a detailed description of the technique and laboratory studies on the response of apatite fission tracks to elevated temperatures see Green *et al.* (1989), Duddy *et al.* (1994) and Bray *et al.* (1992).

Fission track age is the time over which tracks have accumulated in the apatite crystal. It can be calculated by knowing the concentration of ^{238}U in the sample and the number of fission tracks. A sample that was never at temperatures higher than 60°C will show a fission track age equal to the time over which tracks accumulated. A sample that resided between 60-120°C for part of its thermal history will show partially annealed fission tracks. The fission track age will be reduced as tracks progressively shortened. When the sample is exposed to temperatures higher than 120°C the fission track age is reset to 0 My.

The distribution of track lengths contains information on when and how the sample cooled down. Samples for which the present temperature is also the maximum temperature, show symmetric, unimodal distributions in which tracks are equally annealed. The higher the temperature the greater the annealing and the smaller the fission track age. Samples that have resided in the partial annealing zone (palaeotemperatures between 120-60°C) typically yield a bimodal distribution with two populations of tracks: one set equally shortened by temperatures between 60-120°C and the other set of tracks formed during subsequent cooling. The fission track age will reflect the amount of track reduction shown by the shorter population. If the maximum palaeotemperature was greater than 120°C and if the sample was cooled rapidly and monotonically, then the fission track age relates directly to the time of cooling. Samples recording two periods of heating, being the first one greater than 120°C in intensity will show three distributions sets.

Forward modelling of fission track age and track length distribution yields constraints on the thermal history of a sample. Thermal history information is extracted from fission track data by fitting measured apatite fission track parameters through a variety of possible thermal-history scenarios. The modelling in this work was done

using a probabilistic approach, Monte Trax (Gallagher 1995), and is described in section 5.2.3.

The kinetic basis for fission track modelling (the rate at which tracks anneal) was established on mono-compositional apatites (Green 1989) on the basis of a series of laboratory experiments on Durango apatite (Green 1986; Laslett *et al.* 1987; Duddy *et al.* 1988). However, the kinetics of fission tracks in apatite in particular depend on apatite composition, particularly on the fluorine/chlorine ratio (Green *et al.* 1986, 1996). The model used in this work does not account for different apatite composition and a Durango apatite composition (fluorine/chlorine ratio of ~0.1) is assumed for all samples.

5.2.2 Previous Cenozoic apatite fission track studies in Ireland

Apatite fission track analysis has been used extensively as a thermo-chronological tool in the British Isles (Green 1986; Bray *et al.* 1992; Lewis *et al.* 1992; Green *et al.* 1993; Green *et al.* 1997) and in Ireland (McCullough 1993, 1994; Keeley *et al.* 1993; Green *et al.* 2000; Allen *et al.* in press).

Clift *et al.* (1998) used apatite fission track analyses and subsidence curves in offshore wells to predict 2.5 km of Cenozoic denudation in northwestern Britain, caused by igneous underplating (Clift and Turner 1998; Brodie and White 1995). Thomson *et al.* (1999) found thermal evidence for at least 2.5 km of denudation in northwestern Scotland, but attributed only 1 km of this to actual Cenozoic denudation with the rest being due to thermal effect of the Tertiary Igneous Complex. Evans (1997) suggested 2 km of erosion from the West Orkney Basin commencing in the latest Cretaceous/Early Tertiary.

McCullough (1993) analysed apatite samples from both onshore and offshore Ireland and found evidence for a period of elevated palaeo-temperatures in the Late Cretaceous to Early Tertiary (50-80 My). He assumed palaeo-geothermal gradients of 40 to 65°C km^{-1} and calculated 800 to 2000 m of denudation after maximum Late Cretaceous to Early Tertiary palaeo-temperatures were reached over Ireland (Table 5.1).

Green *et al.* (1999) found no evidence for elevated Early Tertiary heat flow west of the Shetland Islands, and suggested that palaeo-geothermal gradients at that time were similar to those of the present day (~30°C km^{-1}). In the same area they also found strong evidence for Late Tertiary uplift and erosion.

Green *et al.* (2000) analysed Irish onshore apatite samples, and suggested a complex Tertiary history of heating and cooling with probably two cooling events. The first event occurred at ~60 My, with maximum palaeo-temperatures ranging between 50-75°C; the second occurred at ~20 My, with maximum palaeo-temperatures between 40-50°C. At least one kilometre of erosion during the Early Tertiary can be assumed using a palaeo-geothermal gradient of 20 to 60°C km^{-1}.

Allen *et al.* (in press) integrated new onshore apatite fission track data with existing published (Keeley *et al.* 1993; McCullough 1993, 1994) and unpublished work. All data were remodelled using Monte Trax (Gallagher 1995) and details are given in Allen *et al.* (in press). They obtained denudation rates varying in time and space of 20 to 40 m/My during the Cenozoic. They assumed a palaeo-geothermal gradient of 22°C km^{-1}, based on the conclusion of Green *et al.* (1999) that Tertiary geothermal gradients were being similar to those in the present day. I used the same onshore database and added data from four offshore wells. I also estimated geothermal gradients based on well data. The Cenozoic denudation history was then modelled in time slices equivalent to the ages of the Irish Rockall Basin unconformities (Chapter 4).

5.2.3 Database and methods

Thirty-five onshore apatite fission track samples from northwestern Ireland were chosen from the database presented by Allen *et al.* (in press). The data were selected from an area bounded by Killary Harbour to the south and the border with Northern Ireland to the east. Details of sample locations and fission track parameters are given in Table 5.2, or for further detail see Allen *et al.* (in press).

Apatite fission track samples from wells 132/15-1, 19/5-1, 12/13-1a and 27/13-1, off northwestern Ireland, were also modelled. Each well has 4 to 6 samples at various depths. Fission track data and parameters were taken from unpublished Geotrack reports (Gibson 1997; Gibson 1996; Green 1993; Arne 1992, available to TotalFinaElf, Exploration, UK (Table 5.3). Samples were remodelled using the same thermal history model used by Allen *et al.* (in press), Monte Trax (Gallagher 1995), with the same parameters.

Monte Trax (Gallagher 1995) is a computer program that calculates a thermal history from apatite fission track parameters using a stochastic (optimisation) search procedure. The thermal history obtained is not necessarily unique and there may be other thermal histories that can match the data equally well (Gallagher 1995). Initial model runs incorporated the fission track annealing model of Laslett *et al.* (1987). This annealing model is based on laboratory annealing experiments performed on a mono-compositional Durango apatite with a fluorine/chlorine ratio of ~0.1 (Young *et al.* 1969). Extrapolation of the Laslett *et al.* (1987) Durango apatite model to geological time scales (10^6 to 10^7 y) predicts a partial annealing temperature range from ~60°C to ~110°C with an uncertainty of about 10°C.

One of the major limitations of the Laslett *et al.* (1987) model is that it does not predict sufficient annealing at temperatures less than ~60°C. It has been observed that volcanic or volcanogenic sediments that have undergone no significant post-eruption heating, have observed mean track lengths of 14 to 14.5 μm, while the Durango standard predicts them to be about 16 μm (e.g. Vrolijk *et al.* 1990). Consequently, thermal history simulations can be biased towards inferring rapid cooling from ~60°C to surface temperatures with consequent overestimates of recent denudation. Galbraith & Laslett (1993) developed a model that is more sensitive to temperatures <60°C but the model formulation was not applied to the Durango apatite data. K. Gallagher (pers. comm.) has adopted the Galbraith & Laslett (1993) model and has applied it to the Durango apatite data given by Green *et al.* (1986). The onshore samples were subsequently re-modelled using this modified annealing model, referred to here as Gallagher (in prep.). Relative to the Laslett *et al.* (1987) model, this revised model produces more annealing at lower temperatures, and thus yields lower cooling rates.

Monte Trax requires that the bounds for the thermal history be specified, although these constraints may be quite loose. Where possible, these bounds on the thermal history are based on geological data. The depositional history of wells was used to constrain the initial thermal history (e.g. Fig. 5.1). In this way the initial thermal history is much better constrained for the offshore samples than for those onshore and therefore the denudation estimates obtained are more reliable.

Once the initial thermal history is constrained, the observed fission track parameters (fission track age, mean track length, standard deviation and track length distribution) are entered. Monte Trax uses a probabilistic genetic algorithm approach (Gallagher 1995) to calculate the thermal history that best fits the observed parameters. With the genetic algorithm approach, the information gained by sampling is used to determine better-fitting models, and more models are selected for testing around these better models. This method finds in each calculated generation the best-fit models and uses these to re-calculate the next generation. 20 generations with 100 calculations in each generation were used to obtain the results presented here. For each sample the program was run 3 to 6 times in order to ensure that consistent results between runs were obtained.

5.2.4 Modelling of well samples

Thermal modelling of twenty-one sandstone samples from four wells off northwestern Ireland was done (Table 5.3). The geology of the drilled section above each sample was used to define an initial thermal history.

A depositional or surface temperature for sandstone samples of 10±10°C was assumed. As the sample gets buried temperature increases in proportion to the depth of burial and the palaeo-geothermal gradient. The well section above each sample gives the uncompacted depth of burial. The geothermal gradient is assumed to range between 20 to 40 °C km^{-1}.

Apatite crystals in sandstone can contain information on the inherited thermal history prior to the deposition of the rock if the buried sample did not reach temperatures higher than 120°C (total annealing) after deposition. I assumed that burial of samples

with Carboniferous stratigraphic ages during the Hercynian Orogeny (Late Carboniferous to Permian) resulted in post-burial temperatures higher than 120°C and therefore total annealing. For this reason samples with stratigraphic ages older than 300 My were not allowed to have an inherited thermal history prior to deposition in the modelling. Post-Permian samples (younger than 280 My) might not have reached 120°C during burial and were allowed in the modelling the freedom to have a pre-depositional thermal history.

Unconformities define periods of time during which the sample might have been buried and exhumed one or more times. The thermal model can be given the freedom to increase or decrease temperature during the unconformity time interval by increasing the number of time-temperature pairs. That is, the number of time and temperature ranges used to define the initial thermal history in the model. Carboniferous and pre-Carboniferous surface samples from onshore Ireland (Allen *et al.* in press) have no record of the post-Carboniferous geological and thermal history, whereas samples from offshore wells with a overlying stratigraphic section can help define with more confidence the initial and therefore the resultant thermal histories.

5.2.4.1 Well 19/5-1

Apatite fission track data from six sandstone samples, dated as Carboniferous to Lower Jurassic, were acquired from well 19/5-1 (Fig. 5.1). The samples range in depth from 430 to 2575 m below the seabed. Three unconformities are recognised in this well with section missing between 328 to 318 My, 305 to 256 My, and 195 to 5 My (Fig. 5.1). Stratigraphic ages come from the composite well log.

The ages of the samples, the age of the rocks below and above the unconformities and the thickness of section above each sample allow the reconstruction of an initial thermal history. Depth in metres was converted into temperatures assuming a range of palaeo-geothermal gradients between 20 and 40°C km^{-1}. This range was chosen by considering that geothermal gradients during the Cenozoic were similar to those in the present day (Green *et al.* 1999), although this might not have been the case for the Mesozoic. The procedure used will be explained for sample GC651-12 only, although

the same procedure applies to the rest of the samples analysed in this study. The initial thermal history was constrained in the following way (Table 5.4):

Sample GC651-12 with a stratigraphic age of 345±3 My, is assumed to be deposited at a surface temperature of 10±10°C. At 328 My, the sample was buried by 1323 m. The burial increased palaeo-temperature to 40±15°C assuming a geothermal gradient of 20 to 40°C km^{-1}.

An unconformity is recorded between 328-318 My. The model is allowed the freedom to continue burial of the sample after 328 My, within a temperature range of 80±40°C, followed by cooling at any time between 328 and 318 My. Only one period of cooling is allowed, therefore the model cannot undergo repeated heating and cooling cycles during this unconformity. At 318 My, temperatures are assumed to be the same as at 328 My (40±15°C). By 305 My, the sample was re-buried by 271 m of section. This burial increased the temperatures to 40±15°C.

Between 305 and 256 My, another period of erosion occurred. Therefore at 280±25 My, the sample is allowed a palaeo-temperature of 90±40°C, and cooling is allowed at any time between 280±25 My. At 256 My, the sample was buried just as much as it was at 305 My, and the temperature was therefore 48±15°C. By 195 My, deposition of 512 m of section increased the temperature to 63±15°C.

Between 195 and 5 My, an unconformity is recorded. Because of the long time elapsed during this unconformity, four phases of deposition and erosion are allowed in the model. Each phase can increase sample temperatures up to 80°C, but the minimum temperature must be 63±15°C, as the sample was always buried by at least 2106 m of section.

The procedure described above was followed for the rest of the samples in well 19/5-1 (GC651-10, GC651-8, GC651-4, GC651-3, GC651-1) and the initial thermal histories are summarised in Table 5.4.

The initial thermal history is then used to enter time temperature constraints in Monte Trax, shown as a series of black boxes in Figure 5.2. The program is then free to find

the best-fitting thermal history within the boundaries marked by the boxes. The distribution of observed confined track lengths in the sample is shown in the histogram of Figure 5.2. The blue curve plotted with the histogram is the predicted track length distribution calculated by Monte Trax on the basis of the best thermal history. The thermal history obtained is the one that best fits the track length data but is not necessarily the true one. The model was run from 3 to 6 times to ensure that consistent results were achieved, rather than random thermal histories.

Misfit values close to 1 (Fig. 5.2) fit the observed data very well, while misfits much less than 1 do not. With sample GC651-4, any initial thermal history always results in a bad misfit. Likewise, GC651-3 has consistent misfits of 0.6 and therefore is assumed to be unreliable. The rest of the samples, with misfits close to 1, are shown in Table 5.5. All or most of the modelled thermal histories obtained for each sample in different runs are consistent (Fig. 5.3), in that they suggest that a maximum temperature of 60-96°C were reached between 28 and 42 My (Table 5.5). This maximum thermal event coincides with the Oligocene to Miocene regional uplift and erosion of Chapman *et al.* (1999) based on 2D seismic evidence.

5.2.4.2 Well 12/13-1a

Well 12/13-1a has apatite fission track data sets from six sandstone samples. The well log shows that samples were taken at depths ranging from 2111 to 2774 m below seabed (Fig 5.4). Three samples are Permo-Triassic in age, and lie below two unconformities with section missing from 205 to 140 My, and 34 to 2 My. The other three samples are Cretaceous in age and lie between the unconformities. The distance from each sample to the two unconformities is measured (Fig. 5.4). The thickness of rock above each sample allows calculation of the increase in temperature due to sedimentary burial, again using a geothermal gradient of 20 to 40°C km^{-1}.

The age of each sample, the age of the rocks below and above the unconformities and the thickness of rock converted into degrees centigrade are used to reconstruct an initial thermal history (Table 5.6). The oldest stratigraphic age of the samples is 240±5 My. Because this post-dates the Hercynian Orogeny, a previous thermal history may be recorded in the apatite grains. The thermal history constraints used to model

these samples thus allow for an inherited thermal history with temperatures of 80±80 °C, during the period 300±150 My.

Time-temperature constraints are defined for the initial thermal history (Table 5.6) and are shown as black boxes in Figure 5.5. The program was run for six times on each sample to make sure consistent results were obtained. All modelled thermal histories had misfits of ~1, except for sample GC492-15 with misfits close to 0. Five samples show highly consistent thermal history results (Fig. 5.6). Maximum palaeo-temperatures appear to have been reached in the Middle Jurassic and late Oligocene (Fig. 5.6). All samples appear to have experienced a maximum Cenozoic temperature of 70 to 97°C at about 18 to 34 My (Table 5.7). There is no evidence of an earlier Tertiary high temperature event.

5.2.4.3 Well 132/15-1

Well 132/15-1 has apatite fission track data from four sandstone samples. The samples were taken between depths of 2475 to 3339 m below seabed and are Cretaceous in age (Fig. 5.7). An unconformity is present between rocks of 34±4 My and 30±2 My in age. The distance from each sample to the unconformity is measured (Fig. 5.7). Here again, the thickness of rock above each sample allows calculation of the thermal effects due to burial, using a geothermal gradient of 20 to 40°C km^{-1}.

The initial thermal history was reconstructed using the sedimentary thickness above each sample in the same way as in previous samples (see section 5.2.4.1) and is summarised in Table 5.8. The oldest stratigraphic age of the samples is 58.5±2.5 My. Because this post-dates the Hercynian Orogeny, a previous thermal history may be recorded in the apatite grains. Again, the thermal history constraints used to model these samples allow for an inherited thermal history, with temperatures of 80±80°C during the period 200±140 My.

Time-temperature constraints are shown as black boxes in Figure 5.8 and in more detail in Table 5.8. Sample GC564-4 resulted in misfits <<1, therefore the results are considered to be unreliable. The three other samples show misfits close to 1 and were run four times each to make sure consistent results were obtained (Table 5.9). Results

for those three samples, consistently show a maximum temperature of 38 and 112°C occurring from 31 to 36 My (Fig 5.9). This sudden increase in temperature during the late Eocene might be due to the thermal effect of widespread volcanism during the Palaeogene. Evidence of volcanic intrusives is found in the well stratigraphy (Fig. 4.6) during the late Palaeocene and early to middle Eocene. The presence of local igneous intrusions as late as 31 to 36 My may be the cause of anomalously high temperatures in the thermal histories of the samples.

5.2.4.4 Well 27/13-1

Well 27/13-1 has five sandstone samples, all Jurassic in age. An unconformity is present 450 m below seabed between rocks of 155 My and 2 My age (Fig. 5.10). Distance from each sample to the unconformity is measured (Fig. 5.10) and the thickness of rock above each sample allows calculation of the thermal effect due to burial, using a geothermal gradient of 20 to 40°C km^{-1}.

The initial thermal history is summarised in Table 5.10. The oldest stratigraphic age of the samples is 206±2 My. Because this post-dates the Hercynian Orogeny, a previous thermal history may be recorded in the apatite grains. Again, the thermal history constraints used to model these samples allow for an inherited thermal history, with temperatures of 80±80°C during the period 300±150 My.

Time-temperature constraints are shown as black boxes in Figure 5.11 and in more detail in Table 5.10. Sample GC375-4 resulted in misfits << 1, therefore the results are considered to be unreliable. The other four samples show misfits close to 1 and were run for eight times each to make sure consistent results were obtained (Table 5.11). Results for the four samples do not show the same consistency found in the samples from other wells (e.g. 12/13-1a). Samples in well 27/13-1 yielded fewer tracks than samples in other wells and that might partially explain the lack of consistency found. However, the results show a general cooling during the Tertiary, except for sample GC375-2 with a maximum temperature of 75-80°C at about 22-50 My (Fig. 5.12). Three of the samples modelled consistently show a cooling episode from about 80 to present day.

5.2.5 Summary

Well data allow general constraints to be placed on the thermal history for the Cenozoic. Consistent modelled thermal histories were obtained for each well, suggesting:

Maximum palaeo-temperature of 60 to 96°C was reached between 28 and 42 My in well 19/5-1.

Maximum palaeo-temperature of 70 to 97°C at about 34 to 18 My in well 12/13-1a, but there is no evidence for an earlier Tertiary high temperature event.

Maximum palaeo-temperature of 38 to112°C at 31 to 36 My in well 132/15-1. This sudden increase in temperature during the late Eocene might be due to the thermal effect of widespread volcanism during the Palaeogene.

Modelled samples for well 27/13-1 show a general cooling, suggesting uplift and erosion during the Cenozoic.

Modelling of offshore wells allows more reliable results on denudation than onshore, because of the preservation of a Mesozoic to Cenozoic sequence allows prediction of an initial thermal history and a geothermal gradient.

5.3 Denudation estimated from apatite fission track modelling

Denudation maps were built using the thermal histories obtained from apatite fission track modelling of well samples presented in the previous section, along with thermal histories for onshore samples obtained using the same method by Allen *et al.* (in press).

5.3.1 Methods

Once the thermal history is constrained for the Cenozoic, the net amount of denudation at any particular point is obtained by the following function:

$$Denudation = \frac{T_1 - T_2}{dT / dz} \qquad \text{(eq. 5.1)}$$

where T_1 and T_2 are the palaeo-temperatures at certain times taken from the thermal history [°C], and dT / dz is the palaeo-geothermal gradient [°C km^{-1}].

A series of palaeo-temperature estimates from apatite fission track analysis over a vertical range of depths can be used to reconstruct a palaeo-temperature profile through the preserved section and therefore the palaeo-geothermal gradient. Well data from offshore northwestern Ireland (Table 5.3) shows that the geothermal gradient for each well is constrained by apatite fission track data and vitrinite reflectance (Gibson 1997; Gibson 1996; Green 1993; Arne 1992). A best estimate of the Cenozoic geothermal gradient might be the mean of the geothermal gradient values for all wells, which is 27°C km^{-1}. Brown (1991) and Green at al. (1999) found no evidence for elevated Early Tertiary heat flows and geothermal gradient along the UK Atlantic margin. Therefore in this work, in order to estimate denudation from a thermal history, a constant value of 27°C km^{-1} throughout the Cenozoic is assumed for onshore data. For the offshore wells the own palaeo-geothermal gradients measured in each well were used (Table 5.3).

I have divided the Cenozoic into intervals according to the unconformities picked offshore in order to establish temporal relations between sediment denuded and sediment deposited. The intervals are Palaeocene (66-52 My), Eocene (52-36), Oligocene (36-23) and Miocene to present (23-0 My). Miocene and Plio-Pleistocene were not subdivided because of the uncertainties in the thermal model for the last few million years, which yield overestimates of the denudation (see section 5.2.3). Therefore it must be kept in mind that denudation results for the last 23 My might be overestimated.

Denudation was calculated using equation 5.1. Temperatures were taken from the thermal history modelled for each well. Each well has four to six samples, from which four to six thermal histories were obtained (see Figs. 5.3, 5.6, 5.9 and 5.12). As has been shown, the thermal histories modelled in each well are internally consistent, although not exactly the same. Therefore to estimate denudation from one thermal history, one must choose the modelled thermal history that best represents all the samples. The selection of the best representative thermal history for each well was based on minimum misfit, the greatest consistency between independent model runs and common peak temperatures with other samples modelled within the same well. Denudation estimates for each interval are given in Table 5.12, along with palaeo-temperatures and geothermal gradient values used.

5.3.2 Contouring method

Denudation maps for the entire Cenozoic as well as the Palaeocene, Eocene, Oligocene and Miocene to present intervals are presented in this section. The data set has a total of thirty-five onshore (Allen *et al.* in press) and four offshore samples. The data were contoured using ArcView software. An inverse distance weighted (IDW) interpolation scheme was used to produce a grid for each interval, with a cell size of 1 km^2. This method determines output cell values using a linear weighted combination of a set of sample points. The weight is a function of inverse distance. The input number of sample points was limited to 12, using the nearest neighbour method. A power parameter in the IDW interpolation controls the significance of the surrounding points upon the interpolated value, such that a higher power results in a smaller influence from distant points. The power used in the interpolation of the grids was 2. Since the IDW is a weighted average, the interpolated value cannot be greater then the highest or less than the lowest input (Watson and Philip 1985).

The resulting surface is an estimate of denudation as a continuous function of position, which at the same time preserves the existing data point values. This contouring method smoothes discontinuities in the original data.

5.3.2.1 Cenozoic denudation

Denudation for the Cenozoic is presented using both the Laslett *et al.* (1987) and the Gallagher (in prep.) annealing models (Fig. 5.13). The general pattern between the two models does not change much, although the magnitudes do vary. The Gallagher (in prep.) model is considered to be a better estimate for estimating Cenozoic denudations because it does not infer rapid cooling at temperatures lower than 60°C, therefore the magnitude of denudation is more subdued. In the following sections only denudation maps obtained with the Gallagher (in prep.) model will be presented and discussed.

Maximum Cenozoic denudation takes place in northern and western County Donegal, County Sligo and County Fermanagh (Fig. 5.13). Maximum magnitudes in these areas range from 1200 to 1600 m (Fig. 5.13A). In other onshore areas, denudation ranges between 800 to 1200 m. Well 12/13-1a and well 132/15-1 show net Cenozoic deposition, with a maximum of 400 m and 1500 m of burial respectively. The other wells show denudation ranging between 600 to 1400 m. This result compares well with the stratigraphy of the wells; wells 12/13-1a and 132/15-1 are the two wells drilled off western Ireland, where Cenozoic stratigraphy is better preserved, probably as a consequence of relatively low denudation compared with the basin margin and onshore Ireland. Overall, denudation seems to decrease towards the northwest (Rockall Basin) and to a lesser degree, towards the southwest (Porcupine Basin).

Mean denudation rates, averaged over the entire study area, are calculated by dividing the mean value of denudation during each time interval [m] by the duration of the interval [My] (Table 5.13). Calculated in this way, Cenozoic denudation rates in northwestern Ireland averaged in space and time are about 13 m My^{-1}.

5.3.2.1 Palaeocene denudation

Palaeocene denudation is subdued with a maximum of 860 m but an average of 120 m. A maximum denudation centre is located north of County Donegal and a minor one, south of County Mayo (Fig. 5.14). Apart from these centres, denudation during this interval was fairly uniform in onshore northwestern Ireland. Minor deposition

appears to have taken place locally north of County Mayo and Sligo. All the wells, except for 27/13-1, were under deposition. Modelling of apatite fission track data shows that 440 m were deposited in well 132/15-1 and 180 m in 12/13-1a. Approximately 700 m of Palaeocene sediments are preserved in well 132/15-1 and <100 m in 12/13-1a. Modelling of well 19/5-1 shows deposition of 240 m of sediment, while the stratigraphy of the well shows no Palaeocene sediments. These results indicate post-Palaeocene denudation of ~260 m in well 132/15-1, ~80 m in well 12/13-1a and, at least 240 m in well 19/5-1. Spatially-averaged denudation rates were about 9 m/My (Table 5.13).

5.3.2.2 Eocene denudation

During the Eocene, both the rate and magnitude of denudation and deposition increased considerably (Fig. 5.15). A maximum of 1270 m and average of 270 m were eroded. A major denudational centre, defined by three samples, was located in County Sligo and 800 to 1400 m of solid sediment was removed during this interval. North County Donegal provided a source of sediment as well, with denudation of up to 1000 m in the Eocene (Fig. 5.15). Three of the modelled wells show that deposition occurred in the Erris and Rockall Basins. Eocene sediments are preserved in the stratigraphy of well 12/13-1a and 132/15-1. Evidence of a progradational event of unknown environment near these two wells was shown in section 4.4.5, partially derived from a sedimentary source in northwestern Ireland. The stratigraphy of well 19/5-1 shows no evidence of Eocene sedimentation, contrary to the apatite fission track modelling results which suggest ~140 m of deposition. This may be explained by post-Eocene uplift and erosion of at least 140 m of sediment in the southern Erris Basin. The Slyne Basin appears to have undergone minor denudation during the Palaeocene and Eocene. No Tertiary sediments are preserved in well 27/13-1. Spatially-averaged Eocene denudation rates were 16 m My^{-1}, almost twice the Palaeocene value (Table 5.13). This increase in denudation rate might provide a local source for the Eocene progradation event found in seismic lines and explained in section 4.4.5.

5.3.2.3 Oligocene denudation

During the Oligocene the magnitude of denudation was relatively low compared with the rest of the Cenozoic, and denudation was more uniformly distributed across northwestern Ireland (Fig. 5.16). Although the maximum denudation recorded is 900 m, the mean value is only 110 m, given an overall spatially-averaged denudation rate of 8 m My^{-1}, the lowest in the Cenozoic (Table 5.13). Apatite fission track modelling indicates offshore deposition in the Erris Basin. No Oligocene sediments are preserved in the stratigraphy of the wells in the Erris Basin and this might be explained by post-Oligocene erosion. Post-Oligocene apatite fission track modelling suggests major denudation during Miocene to present time. Modelling of well 132/15-1 indicates Oligocene denudation, but as discussed in section 5.2.4.3 this might be a result of a heating event caused by local igneous activity at the end of the Eocene. The stratigraphy of well 132/15-1 shows overall deposition during the Oligocene.

5.3.2.4 Miocene to present denudation

From the Miocene to the present, the magnitude and rate of denudation increased considerably (Fig. 5.17). Maximum denudation during this interval is 1800 m in the Erris Basin, and the mean value is 360 m, the highest value obtained by modelling during the Cenozoic. Northern County Mayo underwent between 400 and 1000 m of erosion, while the Erris Basin lost from 600 to possibly 1800 m of solid sediment. This high denudation explains the lack of, or poor preservation of, Tertiary sediments in the Erris Basin, especially in well 19/5-1. Modelling of well 132/15-1 in the Rockall Basin appears to be the only area with deposition, as also shown by the stratigraphy of the well. Overall, the spatially-averaged denudation rate is 20 m My^{-1}, the highest obtained for the Cenozoic (Table 5.13).

5.3.4 Uncertainties of denudation maps

The precision of the denudation estimates must be discussed when interpreting denudation maps derived from apatite fission track modelling. First, the Laslett *et al.* (1987) annealing model can be biased towards inferring rapid, recent cooling from ~60°C to surface temperatures with consequent overestimates of the most recent

denudation rates. The Gallagher (in prep.) model leads to more annealing, particularly at lower temperatures. Secondly, apatite fluorine and chlorine composition probably varies in each sample, and the model used in this study considers a Durango mono-compositional apatite. However, the consistency found in the results obtained for the modelling of offshore wells indicates that the effects of this assumption are probably minor.

Allen *et al.* (in press) gave an uncertainty of about 400-500 m for their denudation estimates, based on various errors, and so spatial variations in the onshore denudation maps should be considered with this level of uncertainty in mind. Modelled thermal histories and palaeo-geothermal gradients for offshore samples are much better constrained, because the well section allows better definition of the initial thermal history and geothermal gradient, therefore denudation results are more reliable.

5.4 Denudation versus deposition

The denudation and deposition maps for the Palaeocene, Eocene, Oligocene and Miocene to present were mosaiced together to compare marginal denudation with basin deposition. Denudation maps are derived from apatite fission track modelling (section 5.2 and 5.3). Deposition maps are obtained from two-dimensional seismic interpretation (Chapter 4). Thickness of denudation and deposition are shown in metres (Figs. 5.18, 5.19, 5.20, 5.21, 5.22). The grids have 1 km resolution. Volumes of solid sediment eroded and deposited are also compared and patterns of possible sedimentary flow during the Cenozoic are considered.

5.4.1 Cenozoic denudation and deposition

The total volume of Cenozoic solid sediment in the portion of the northeastern Irish Rockall Basin contained by the study area is 104,400 km^3 (Table 5.14). The total volume of solid sediment denuded calculated from apatite fission track modelling is 50,800 km^3. The space and time-averaged Cenozoic depositional rate is 27 m My^{-1}, double the denudational rate of 13 m/My (Table 5.15). This implies that at most only half of the sediments deposited in the northeastern Irish Rockall Basin, could have been derived from onshore denudation in the northwest of Ireland. In reality it was

probably less because some of the denuded sediments was transported south or southwest to the Porcupine Basin.

The Cenozoic isopach map (Fig. 5.18) shows a depocentre of 3155 m around the Hebrides Seamount Terrace suggesting that it was providing sediments into the northern Irish Rockall Basin. Maximum denudation of 1578 m occurred in central northwestern Ireland. The two centres of maximum denudation and maximum deposition are at least 200 km apart, implying drainage systems of approximately this length. Northwestern Ireland was providing the Rockall Basin with approximately 50,800 km^3 of sediments, but another 53,200 km^3 are necessary to explain Cenozoic deposition in the northeastern Irish Rockall Basin.

Several studies have demonstrated using apatite fission track analysis and subsidence curves from well data, that maximum Cenozoic denudation within and around the British Isles occurred in western Scotland or to the north of the Rockall Basin (Evans 1997; White and Lovell 1997; Clift *et al.* 1998; Thomson *et al.* 1999). This implies that as well as Ireland, the western and northern UK margin also provided sediments into the basin. The lack of sedimentary balance might also imply regional reworking of sediments within the Rockall Basin by bottom current activity outside the study area.

5.4.2 Palaeocene denudation and deposition

Palaeocene erosion was moderate with surface-averaged denudation rates of 9 m/My (Table 5.15). However, surface averaged depositional rates are one of the highest in the Cenozoic with 90 m My^{-1}. This contrast might be partially an artefact of the high velocity applied while depth converting the Palaeocene, in other word, the thickness of the Palaeocene section may be over-estimated. Two sedimentary depocentres located in the north and south of the study area have thicknesses of up to 1200 m (Fig. 5.19). The total volume of Palaeocene solid sediment is 43,700 km^3, which is much greater than the 7,000 km^3 of onshore denudation (Table 5.14). A maximum denudation centre is located in northern County Donegal and possible a minor one in southern County Mayo. One can hardly relate moderate Palaeocene denudation onshore with the Palaeocene depocentre directly to the west of Donegal. It seems

unlikely that sediments in the northeastern Irish Rockall Basin had an Irish origin during this interval, and a sedimentary source from the western UK or possibly the uplifted Hebrides Terrace seems more reasonable because of its proximity. Early Tertiary igneous activity related to continental rifting caused regional uplift including the northern Rockall Basin (Brodie & White 1995). This surface uplift resulted in major denudation in northern Rockall and adjacent margins. This event might partially explain low denudation rates in Ireland but high sedimentation rates in the northeastern Rockall Basin.

5.4.3 Eocene denudation and deposition

During the Eocene denudation increased considerably across much of the northwestern Irish margin (Fig. 5.20). Northern Donegal still had high values of up to 800 m of denudation, but maximum denudation of 1300 m occurred in County Sligo. Surface-averaged denudation rates onshore are 16 m My^{-1}, much lower than the offshore Eocene accumulation rates of 38 m/My (Table 5.15). The total volume of Eocene solid sediment denuded in northwestern Ireland is 16,900 km^3 while the volume of Eocene sediment deposited in the northeast Irish Rockall Basin is 26,300 km^3 (Table 5.14).

The offshore depositional pattern changed considerably during this interval. A major sedimentary depocentre with a maximum thickness of 1300 m was located offshore northwestern Ireland. Evidence of northwest-directed progradation of unknown environment was shown in section 4.4.5 and this suggests a sediment source in northwestern Ireland. Although the volume of sediments and rates of denudation and deposition between onshore and offshore are somewhat unbalanced, the increase in deposition rate during the Eocene might explain progradational fans to the west of County Donegal. Low denudation in County Mayo is consistent with the thin Eocene isopach directly to the west (Fig. 5.20).

5.4.4 Oligocene denudation and deposition

In the Oligocene, both denudation and deposition became more spatially uniform and decreased in intensity (Fig. 5.21). North Donegal did not experience the same

magnitude of denudation as it did during the Palaeocene and Eocene. Volumes of sediment denuded in northwest Ireland during the Oligocene are 5,000 km^3 at surface-averaged rates of 7 m My^{-1}, while volumes of Oligocene sediments deposited in the northeast Irish Rockall Basin are 10,200 km^3 at rates of 22 m/My (Table 5.14, Table 5.15).

Offshore Oligocene deposition in the south of the study area is characterised by local progradational fans of unknown environment ~400 to 600 m thick. Clinoforms within the progradational fan dip to the northwest (section 4.4.6). There is no clear evidence for local onshore denudation to explain this progradational event (Fig. 5.21).

5.4.5 Miocene to present denudation and deposition

From the Miocene to present day, both denudation and deposition increased relative to the Oligocene and Eocene (Fig. 5.22). The total volume of sediment denuded is 22,000 km^3 with a spatially and temporally-averaged denudation rate of 20 m My^{-1}. The volume of sediments deposited is 25,300 km^3 at an average rate of 19 m/My (Table 5.14 and Table 5.15). Masson and Kidd (1986) pointed out that Cenozoic sedimentation rates decreased to about 15 m/My by Miocene times which compares well with the estimate in this works. Denudation and deposition compare quite well in terms of volumes and rates.

Denudation is highest in the south of the study area, northern County Mayo, and in the Erris Basin. Denudation rates are the highest in the Cenozoic and, within the limits of apatite fission track modelling explained in section 5.3.4, this might explain the lack of preservation of Tertiary sediments on the Irish Continental Shelf and onshore northwestern Ireland. Although erosion rates are high in the Erris Basin and Irish mainland, no progradational fans have been recognised near denudational centres, but they exist in the north of the study area (see section 4.4.8).

5.5 Flexure

5.5.1 Introduction

Lithospheric plates float on a viscous fluid called the mantle. When a load is applied to the upper crust, for example by an ice sheet, thrust sheet, or by sedimentation like in any basin, the lithosphere deflects as a function of time and space. If the lithosphere has no strength over geological time scales, there is no coupling between adjacent lithospheric blocks, then the lithosphere behaves like blocks of crust floating in a viscous mantle following Airy's isostatic model. The lithosphere in this case is not elastic, but rigid. The other end member on lithosphere mechanical behaviour when a load is applied, is that the lithosphere behaves elastically and has a non-zero internal strength (Watts and Ryan 1976; Watts 1989). In this case, the load applied to an elastic plate cause, widespread deformation, or deflection (Turcotte and Schubert 1982; Forsyth 1985).

The concept of elastic thickness (T_e) is introduced when one tries to estimate an effective elastic thickness that simulates the real elastic behaviour of the lithosphere. It is calculated by matching the observed deflection of the plate to the calculated deflection using gravity, topographic and seismicity data. The strength of the continental lithosphere and therefore the T_e is somehow controlled by its thermal state (Sahagian and Holland 1993), but also depends on variables such as, surface and subsurface loads, density variations, forces due to horizontal far-field stresses, bending moments (related to the plate curvature), a particular geometry of the basement, deflection of the Moho, and gravity anomalies.

Burov and Diament (1995) combined data from other authors to show that T_e in the continents has a wide range of values from 5 to 110 km. Maggi *et al.* (2000) showed that the elastic thicknesses of different foreland sedimentary basins range from 5 to 37 km.

In rifted basins the T_e seem to be smaller. Using admittance studies of free-air gravity anomalies some authors demonstrated that the elastic thickness of the lithosphere beneath the North Sea (Barton and Wood 1984) and beneath Scotland (Barton 1992)

is < 5 km. Wood *et al.* (1987) and Joy (1992) modelled basin subsidence of the Rockall Basin and the Central North Sea, respectively, assuming no lithospheric strength. Watts *et al.* (2000) concluded that a T_e of 10 km in southern England is necessary to explain the amplitude and wavelength of a tilted topographic surface. Nadin *et al.* (1999) modelled rifting on the Rockall Basin using a flexural cantilever model (Kusznir *et al.* 1991), obtaining an elastic thickness of 3 km, based on best fit to both basin structure and gravity anomalies. Ongoing research, using satellite gravity and bathymetric data, suggests an effective elastic thickness varying from 10 km onshore northwestern Ireland to 14 km in the Rockall Basin (Daly *et al.* 2001).

All these variable results lead to doubts about the significance of continental T_e estimates. Bellingham and White (2000) argue that the elastic thickness of sedimentary basins is much lower than has been previously suggested.

In view of the wide range of elastic thicknesses used in the Rockall Basin and the variability in space and time, this work uses several T_e values. It is likely that the lithosphere in the northwestern Irish continental margin was weak during rifting in the Cretaceous yielding values of T_e of ~3 km (Wood *et al.* 1987; Nadin *et al.* 1999) but thermal cooling during the Cenozoic may have increased T_e to up to 10 km or more (Daly *et al.* 2001). Flexural modelling is presented using various elastic thicknesses of 3, 10, 20 and 30 km. The results will be compared with present day basin unconformities and onshore topography.

The potential for onshore rock uplift and offshore subsidence due to sedimentary loading and erosional unloading on the northwestern Irish margin, will be assessed in a flexural model along three northwest-oriented cross sections. The flexural response to sedimentary loading and unloading has been calculated in several passive margins such as the US Atlantic margin using T_e of 40 km (Pazzaglia and Gardner 1994), western South Africa using various T_e of 7.5 km, 15 km and, 22.5 km (Gilchrist and Summerfield 1990) and southern England with T_e of 10 km (Watts *et al.* 2000).

5.5.2 Methods

The flexural response due to loading, whether positive or negative was determined by a one-dimensional model, following the theory of elastic-plate bending (Hetenyi, 1974). Flexure of a marginal basin is modelled here as the bending of an infinite linear elastic plate caused by an irregular load along a given profile.

The elastic thickness along the profile is assumed to be uniform. This assumption might be unrealistic at first view, as flexural rigidity varies laterally (Lyon-Caen et al 1985). However, Daly *et al.* (2001) have shown, using gravity and bathymetry data that, the elastic thickness of the lithosphere in the northwestern Irish margin varies from 10 km onshore northwestern Ireland to 14 km in the Rockall Basin, therefore the variation is not that great.

The equations in this study were taken from Jordan (1981) and Hetenyi (1974). Hetenyi (1974) derived the equation describing subsidence of a point *j*, located a distance *x* from the origin, on an infinite elastic beam buoyed by a fluid substratum, in this case, the mantle, due to load *i* of magnitude *h* and width 2*a* (Fig. 5.23). If that point load *i* is centred at a distance *s* away from the origin, the deflection *w* of point *j* will be:

$$w_j = \frac{h_i \lambda}{2K}(\exp(-\lambda a))(\cos \lambda a + \sin \lambda a) \qquad \text{(eq. 5.2)}$$

The term λ includes both the buoyancy of the mantle beneath the crust and the flexural rigidity of the lithosphere. Sedimentation is assumed to keep pace with subsidence, so that the hydrostatic restoring force K is determined by sediment/air replacing mantle $(\rho_m - \rho_a)g$. For selected values of flexural rigidity:

$$\lambda = \left(\frac{(\rho_m - \rho_a)g}{4D}\right)^{1/4} \qquad \text{(eq. 5.3)}$$

where ρ_m and ρ_a are densities of mantle (3300 kg m^{-3}) and air (1.29 kg m^{-3}) respectively, and g is 9.78 m sec^{-2}. Flexural rigidity D is given by:

$$D = \frac{EH^3}{12(1-\nu^2)} \qquad \text{(eq. 5.4)}$$

where E is Young's modulus (7 10^{10} kg $m^{-1}s^{-2}$), ν is Poisson's ratio (0.15) and H is the effective elastic thickness of the plate. The elastic thickness of the plate is not well-constrained, and therefore different values will be applied and compared. For a selected value of elastic thickness (H), D and λ are calculated.

Integration of equation 5.2 over the entire load profile, composed of a set of point load elements I, and over all subsiding points J, yields to three equations for the flexural response (Jordan 1981).

When j is to the left of i, subsidence w_{ij} is given by:

$$w_{ij} = \frac{-h}{2}\frac{(\rho_s - \rho_a)}{(\rho_m - \rho_a)}[\ \exp((-\lambda)(-x+s-a))\cos((\lambda)(-x+s-a)) \qquad \text{(eq. 5.5)}$$
$$-\exp((-\lambda)(-x+s+a))\cos((\lambda)(-x+s+a))\ ]$$

If j is below i:

$$w_{ij} = \frac{-h}{2}\frac{(\rho_s - \rho_a)}{(\rho_m - \rho_a)}[2 - \exp((-\lambda)(x-s+a))\cos((\lambda)(x-s+a)) \qquad \text{(eq. 5.6)}$$
$$-\exp((-\lambda)(-x+s+a))\cos((\lambda)(-x+s+a))\ ]$$

If j is to the right of i:

$$w_{ij} = \frac{h}{2}\frac{(\rho_s - \rho_a)}{(\rho_m - \rho_a)}[\ \exp((-\lambda)(x-s+a))\cos((\lambda)(x-s+a)) \qquad \text{(eq. 5.7)}$$
$$-\exp((-\lambda)(x-s-a))\cos((\lambda)(x-s-a))\ ]$$

ρ_s is the density of the load, in this case the density of the sediment in the Rockall Basin. A data set describing each load profile consists of a row vector, I elements

long, with each element containing the height h of the load at that point (Fig. 5.23). The elements are 1 km across. Each load profile was treated individually.

To compute the subsidence of each 1 km-wide response element 1 to J on a cross section due to load element h_i, the position of an element *j* relative to the load element *i* was determined (Fig. 5.23), and subsidence w_{ij} found from the appropriate equation (eq. 5.5, 5.6, or 5.7). This w_{ij} was added to the subsidence at *j* due to all preceding load elements. The subsidence w_{ij} was then computed for the $j + 1$ response element.

After all J elements were analysed for load element *i*, the $i + 1$ load element was input and subsidence w_I caused by it determined, until all I load elements were considered. The flexural model was written in Matlab (Appendix 8).

5.5.3 Flexural response in the northwestern Irish margin

The one-dimensional flexural model was applied to three northwest-trending sections going from northwestern Ireland to the northeastern Irish Rockall Basin (A-A', B-B' and C-C' in Fig. 5.24). Northwest-trending sections were chosen because one of the aims of this study is to investigate whether Cenozoic deposition in the Rockall Basin and margin denudation has had a flexural uplift effect on the present-day northwestern Irish topography. The sections are 355 km long and are overlain on the denudation and deposition map in Fig. 5.24 to show the magnitudes of the depositional and erosional loads. Different models were run using elastic thickness of 3, 10, 20 and 30 km.

5.5.3.1 Model results: flexural subsidence

The flexural subsidence or negative deflection in the Rockall Basin due to the entire Cenozoic load varies by an order of hundreds of metres using different elastic thicknesses, but the general shape of the profile remains similar (Fig. 5.24). Flexural subsidence is greatest in the northern-most profile (A-A'), with 1300 to 2200 m of deflection, as a consequence of maximum sediment thicknesses in the Rockall Basin. The central profile (B-B') shows deflections of 1100 to 2000 m, depending on the elastic thickness. Profile C-C' shows flexural subsidence of 1500 to 1900 m. The

magnitudes of the flexural subsidence caused by Cenozoic sedimentation using T_e of 30, 20, or 10 km do not explain present the day-position of the base Tertiary, which is approximately 4500 m below the sea level (Fig. 5.25). Even using a T_e as low as 3 km, the flexural subsidence is at most 2000 m (Fig. 5.26). This implies that there was pre-existing basinal topography before Cenozoic deposition began, or there has been non-flexural subsidence of the basin floor, or both.

Figure 5.25 shows the deflection at different times in the Cenozoic along the northern profile (A-A', see Fig. 5.24 for location), using a T_e of 10 km (Daly *et al.* 2001). This profile contains the areas of maximum denudation and deposition for the total Cenozoic, and therefore it also has the maximum magnitudes of Cenozoic deflection. However, the locations of the sedimentary and denudational maxima vary in space and time. I compare the expected deflection of the base Tertiary surface throughout the Cenozoic with the present day depth of the Cenozoic unconformities and the magnitude of the loads (Fig. 5.25). The plate is assumed to be horizontal at 66 Ma and deflection is 0 m before Palaeocene deposition (Fig. 5.25). This assumption is not correct because significant bathymetry existed in the Rockall Basin at 66 Ma after Cretaceous rifting as shown by onlap of Upper Cretaceous and Palaeocene marine sediments onto the basin margin. For this reason, the flexural results must be treated as estimates of depth change and not as absolute depths, as the deflections have not been corrected for palaeobathymetry or eustacy. Palaeobathymetry and eustacy in the Rockall Basin are poorly constrained because of the lack of well data.

Figure 5.25 shows that at base Eocene time (at 53 Ma), the Rockall Basin in profile A-A' had undergone a flexural subsidence of up to 700 m due to Palaeocene sedimentation and denudation (Fig. 5.25). This result is possibly overestimated as a consequence of poor velocity constraints for the Palaeocene during depth conversion. At late Eocene time (at 36 Ma), flexure due to loading of Eocene sediments was up to 600 m. This result is partially due to loading during sedimentary progradation in the Eocene. The Palaeocene and Eocene were times of maximum flexural subsidence as a consequence of rapid sedimentation in the Rockall Basin. From the late Eocene to ?Miocene, the deflection due to loading is only 200 m, and from ?Miocene to present day, it is 400 m.

The total Cenozoic deflection is ~1900 m using a T_e of 10 km (Fig. 5.25). The present-day position of the base Tertiary is located about 4500 m below sea level (Fig. 5.25). Flexural subsidence using a T_e of 10 km can only account for 1900 m of basin subsidence, so another 2600 m of non-flexurally driven subsidence, or initial palaeobathymetry, or both are needed to explain the much deeper present-day position of the base Tertiary.

With a T_e of 3 km, the flexural subsidence results change only by a couple of hundred metres, still not enough to explain the present-day depths to the Cenozoic unconformities (Fig. 5.26). This result implies that, independent of the elastic thickness used in the flexural model, less than 40% of the Cenozoic subsidence in the Rockall Basin is due to sedimentary loading. Thermal and tectonic subsidence during extension of the basin, water loading, and palaeobathymetric data must be added to the flexural subsidence obtained in this model. The backstripped subsidence curve calculated by isostasy for well 132/15-1 in Chapter 4 (Table 4.15) estimated a tectonically and thermally driven subsidence not corrected for palaeobathymetry and eustacy of 1500 m for the whole Cenozoic. Substracting the present day position of base Tertiary (4500 m) by the flexurally driven subsidence (2000 m) and by the tectonically and thermally driven subsidence (1500 m), one obtains an estimate of 1000 m of the bathymetry in the early Palaeocene and changes in sea level. Substracting the present day position of the base Eocene (3500 m) by the flexurally driven subsidence (1400 m) (Fig. 5.26) and by the tectonically and thermally driven subsidence (842 m) (Table 4.15), one obtains an estimate of 1258 m needed to explain the present day position of the early Eocene horizon caused by a pre-existing bathymetry together with changes in sea level. Substracting the present day position of base ?Oligocene (2500 m) by the flexurally driven subsidence (700 m) and by the tectonically and thermally driven subsidence (1320 m), one obtains an estimate of 480 m of extra subsidence or changes in sea level to explain the present day position of the early Oligocene horizon. Substracting the present day position of base ?Miocene (2250 m) by the flexurally driven subsidence (500 m) and by the tectonically and thermally driven subsidence (1360 m), one obtains an estimate of 390 m of extra subsidence or changes in sea level.

5.5.3.2 Model results: flexural uplift

The flexural response of the total Cenozoic load across the three profiles shows maximum rock uplift during the Cenozoic of 700 to 1100 m, depending on the value of elastic thickness used (3, 10, 20 or 30 km) (Fig. 5.24). The position of the maximum rock uplift does not vary much laterally unless the elastic thickness is reduced to less than 10 km (Fig. 5.24). These results are the accumulated deflection for the Cenozoic and do not necessarily explain the present day topography as topography is controlled by other factors such as tectonic uplift and differential erosion. Figures 5.25 and 5.26 show how a denudation of up to 1400 m and sedimentation of up to 2500 m, results in onshore flexural uplift of up to 1000 m.

Using a T_e of 3 km, the deflection explains slightly the present day topography in profiles A-A' and B-B' (Fig. 5.24), suggesting low T_e for the Irish crust. The total Cenozoic sedimentation and marginal denudation might partially explain the maximum elevation of the northwestern Irish topography using T_e of 10, 20 or 30 km (Fig. 5.24). Tectonic relative uplift might have also play a role on formation of topography in northwestern Ireland, but the flexural response to onshore denudation and offshore deposition in the Rockall Basin has contributed to mountain formation.

Deposition in the Rockall Basin can trigger more denudation onshore Ireland by marginal flexural uplift considering the lithosphere behaves elastically. Cenozoic sedimentation and denudation in northwestern Ireland can trigger up to 1000 m of flexural uplift. This uplift can partially be reflected in the present day topography, by its elevation and maybe by small topographic or fluvial vertical offsets as shown by knickpoints in Chapter 3.

Palaeocene sedimentation and denudation produced a positive deflection onshore Ireland of less than 300 m (Fig. 5.27) independent of the elastic thickness used. This value is partially controlled by the low denudation values onshore northwestern Ireland and partially by the high sedimentation thicknesses in the Rockall Basin. This flexural uplift may have induced later Eocene onshore denudation and sedimentation in the Rockall Basin. During the Eocene, due to the local higher onshore denudational and the related depositional centres in the form of progradational fans in the northern

part of the study area, Eocene flexural uplift increases to up to 500 m in profiles A-A' and B-B' (Fig. 5.28). In the Oligocene low overall denudation and deposition reduces the flexural uplift response to 200 m maximum (Fig. 5.29). From the Miocene to present, the magnitude of denudation and offshore sedimentation increased, and therefore the flexural uplift response is up to 500 m using a T_e of 3 km.

5.5.3.3 Model results: uplift and subsidence rates

Basin subsidence rates due to sedimentary loading for each time interval in the Cenozoic are obtained by dividing the maximum flexural subsidence by the duration of the time interval and are given on Table 5.16. Maximum subsidence rates are maximum in the Palaeocene (54 mMy^{-1}) and decrease to 35 mMy^{-1} in the Eocene, to 15 mMy^{-1} in the ?Oligocene and to 17 mMy^{-1} in the ?Miocene to present.

Marginal rock uplift rates due to sedimentary unloading or denudation for each time interval in the Cenozoic are obtained in the same way and are given on Table 5.17. Maximum uplift rates are 12 mMy^{-1} in the Palaeocene, 20 mMy^{-1} in the Eocene, 8 mMy^{-1} in the ?Oligocene and 13 mMy^{-1} in the ?Miocene to present.

These results are controlled by the amount of denudation and deposition occurred in the northwestern Irish continental margin during the Cenozoic.

5.6 Conclusions

(1) Fission track modelling of samples from four wells offshore northwestern Ireland allows a reliable, but very spatially limited, estimate of the Cenozoic thermal history of the northwestern Irish offshore basins. Modelling of various samples in each well results in consistently similar Cenozoic thermal histories. However samples within different wells show different thermal histories. Well 19/5-1 reached temperatures of 60 to 96°C between 28 and 42 My. Well 12/13-1a reached temperatures of 70 to 97°C at about 18 to 34 My. Well 132/15-1 reached temperatures of 38 to 112°C during 31 to 36 My. Well 27/13-1 shows a general cooling trend during the Cenozoic.

(2) Conversion of Cenozoic thermal histories to denudation estimates was done using a geothermal gradient of 27°C km^{-1}, based on well data. Well 12/13-1a and well 132/15-1 show net Cenozoic deposition, with a maximum of 400 m and 1500 m of burial respectively. Wells 19/5-1 and 27/13-1 show net Cenozoic denudation ranging between 600 to 1400 m.

(3) During the Cenozoic 50,800 km^3 of sediment were denuded from northwestern Ireland with temporally and spatially averaged surface denudation rate of 13 mMy^{-1}. Over the same time interval, 104,400 km^3 of sediment were deposited in the northeastern Irish Rockall Basin at an average rate of 27 mMy^{-1}.

(4) The Eocene is characterised by an increase in marginal denudation onshore and in the Erris Basin, which coincides with a progradational phase of unknown environment in the northeastern Irish Rockall Basin. The post-Oligocene is characterised by another increase in margin denudation, which might explain the lack of preservation of Tertiary sediments in onshore Ireland, Slyne and Erris basins.

(5) Cenozoic flexure caused by sedimentary loading and unloading gives rise to to rock uplift in the Irish Shelf and onshore northwestern Ireland of 700 m using a T_e of 30 km and up to 1000 m using a T_e of 3 km. Therefore at least 700 m of the Cenozoic topography might be explained by flexure.

(6) Flexural subsidence using T_e as low as 3 km can account only for 2100 m of basin subsidence, but another 2600 m of non-flexurally driven subsidence, palaeobathymetry or changes in sea level, are needed to explain the present day depths to the base Tertiary and intra-Cenozoic unconformities.

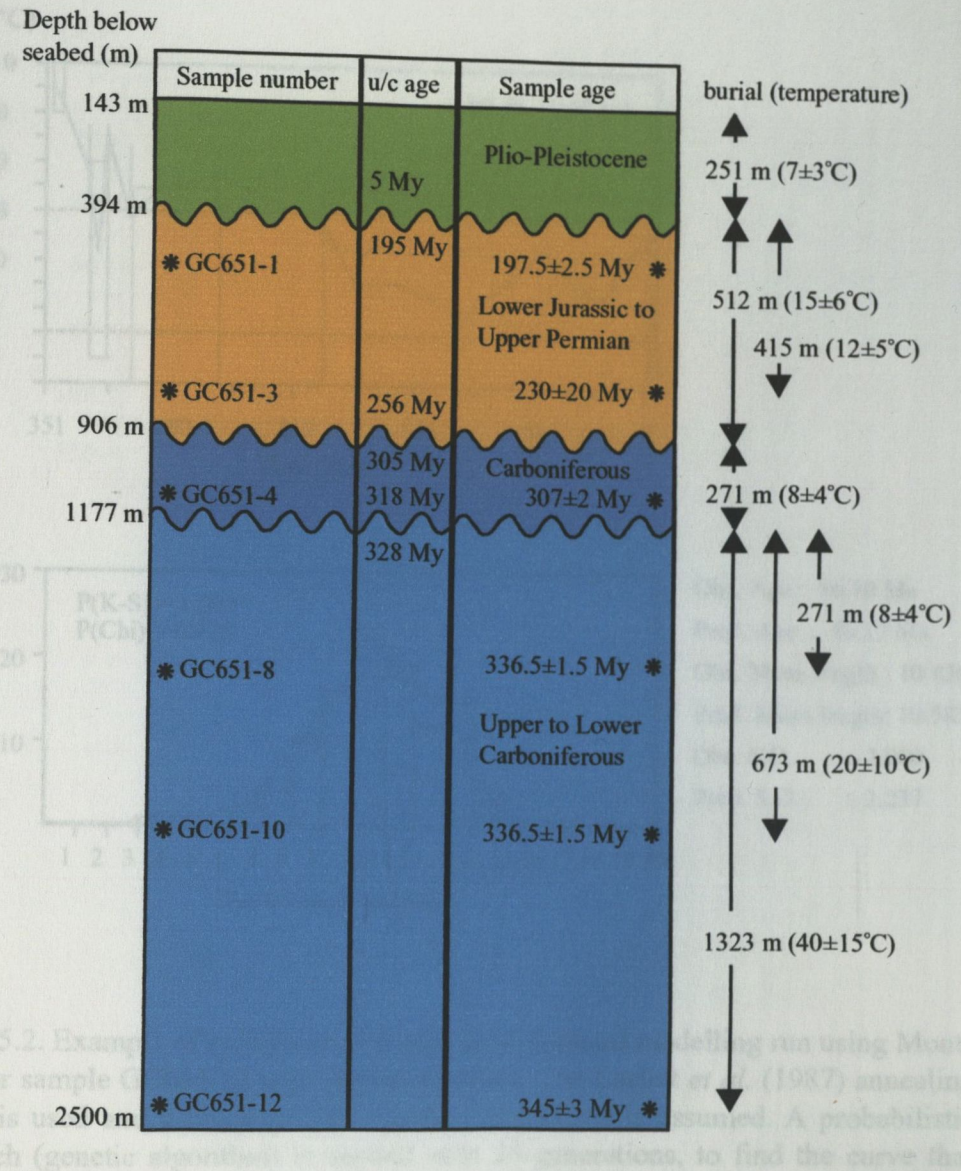


Figure 5.1. Composite well log for well 19/5-1, showing, sample number, position of the sample (✱), depth to unconformities, age of sediments below and above unconformities and age of the samples taken from Gibson (1997). Vertical arrows show thicknesses from sample to unconformity, used to estimate the thermal effect due to sedimentary burial. A geothermal gradient of 20-40°C/km yields an equivalent temperature with an error given in brackets.

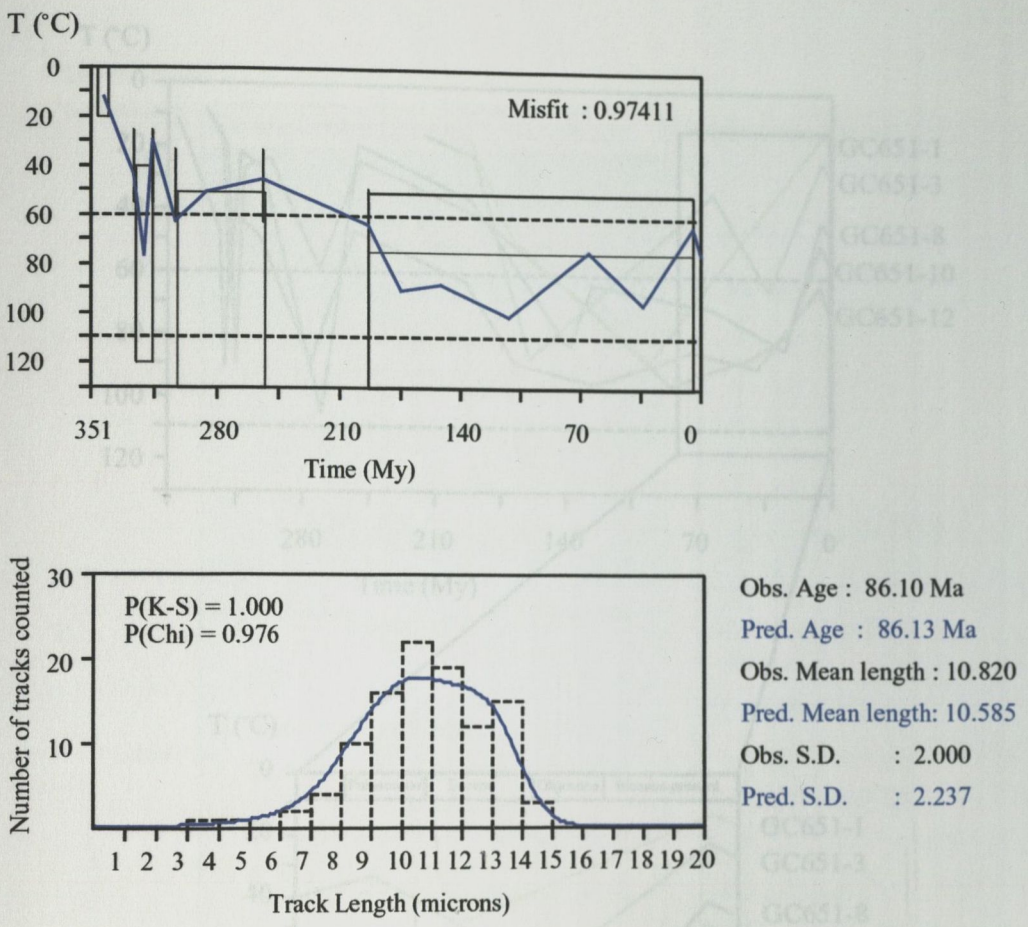


Figure 5.2. Example of an individual fission track forward modelling run using Monte Trax for sample GC651-12 with minimum misfit. The Laslett *et al.* (1987) annealing model is used and a Durango-type apatite composition is assumed. A probabilistic approach (genetic algorithm) is applied with 20 generations, to find the curve that best fits the observed track length data (histogram in black). The modelled thermal history, shown in the top panel in blue, is the one that best fits the observed data, but it is not the only one possible. Horizontal dashed lines in the top panel show the boundaries of the apatite partial annealing zone and, black boxes show boundaries of the initial thermal history confined by geological data.

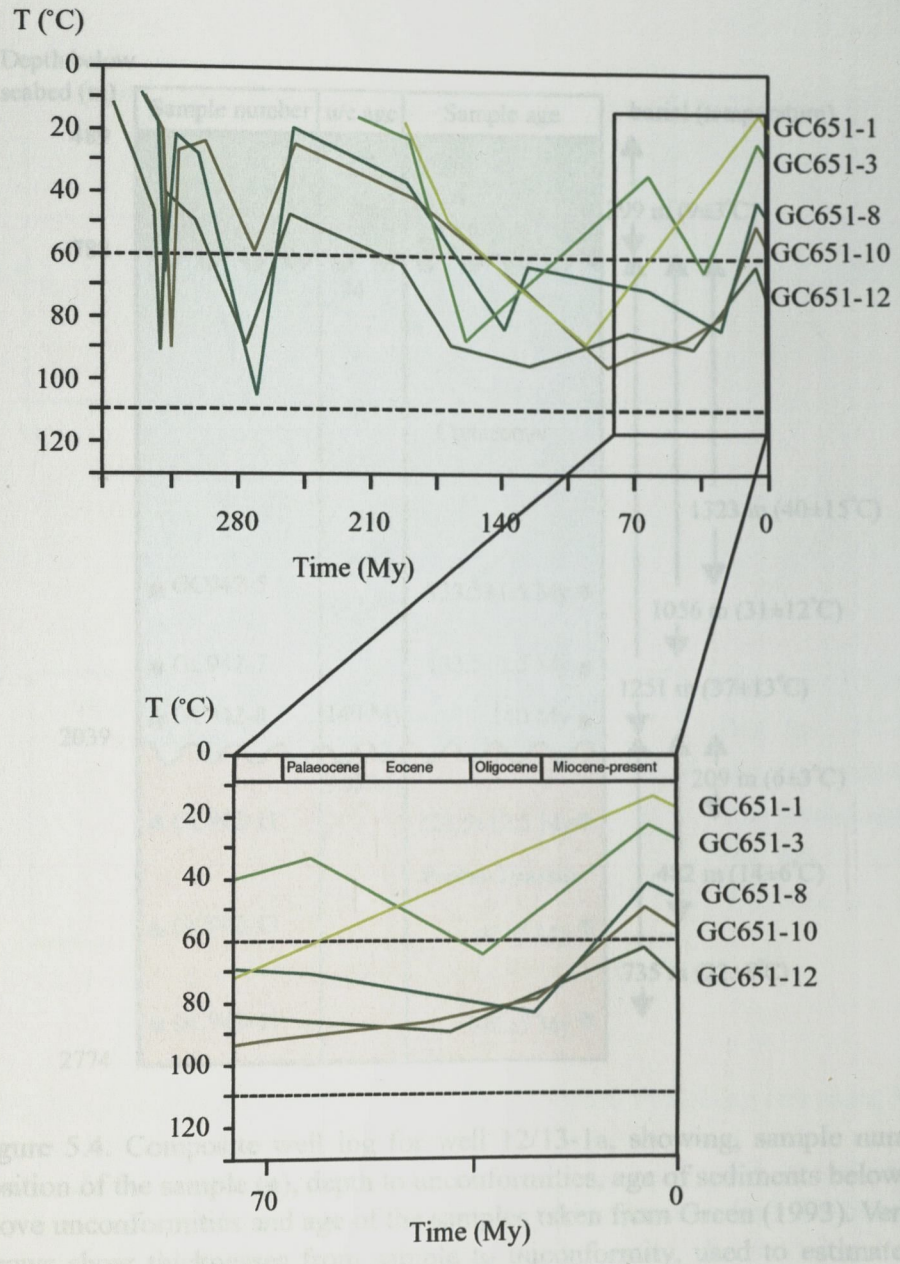


Figure 5.3. Modelled thermal history for well 19/5-1. See text for explanation of modelling method. Dashed lines are boundaries of the apatite partial annealing zone. A close up view of the Cenzoic thermal history is also shown.

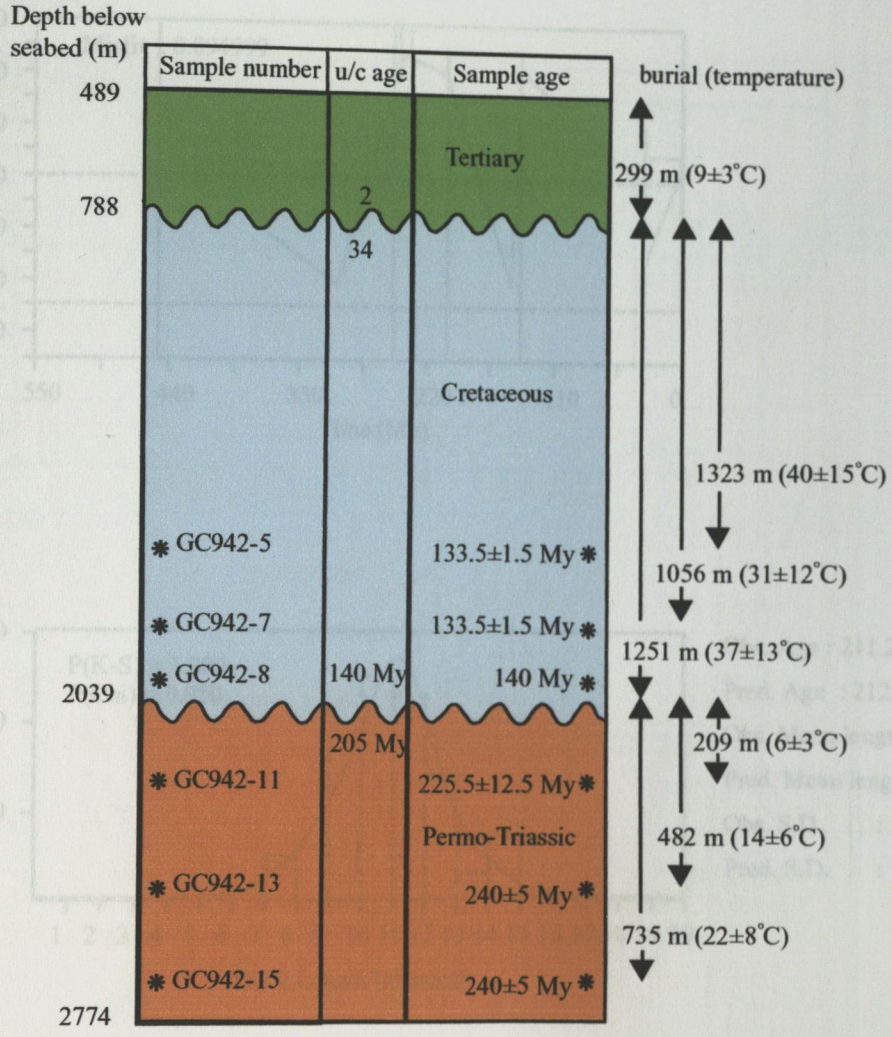


Figure 5.4. Composite well log for well 12/13-1a, showing, sample number, position of the sample (✱), depth to unconformities, age of sediments below and above unconformities and age of the samples taken from Green (1993). Vertical arrows show thicknesses from sample to unconformity, used to estimate the thermal effect due to sedimentary burial. A geothermal gradient of 20-40 °C/km yields an equivalent temperature with an error given in brackets.

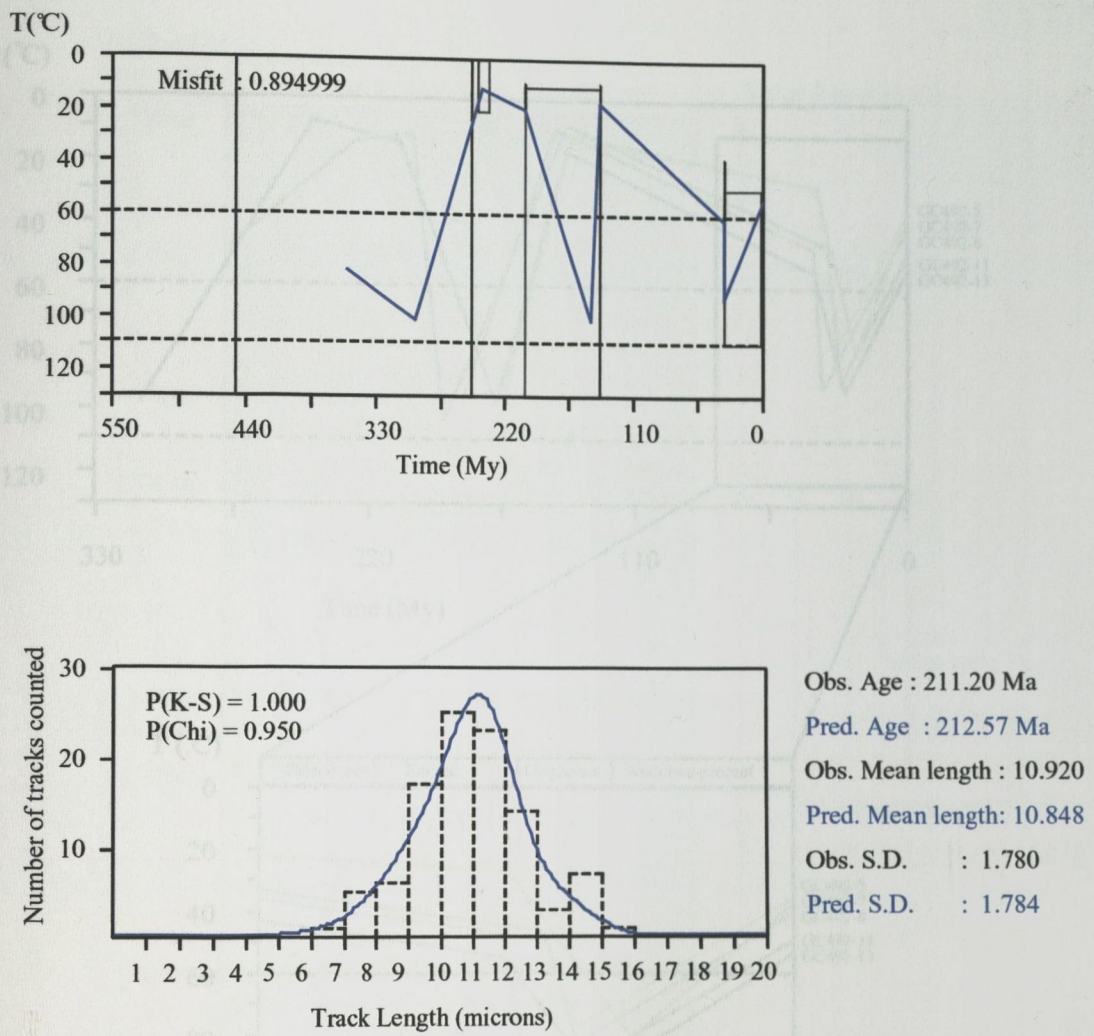


Figure 5.5. Example of an individual fission track forward modelling run using Monte Trax for sample GC942-13 with minimum misfit. The Laslett *et al.* (1987) annealing model is used and a Durango-type apatite composition is assumed. A probabilistic approach (genetic algorithm) is applied with 20 generations, to find the curve that best fits the observed track length data (histogram in black). The modelled thermal history, shown in the top panel in blue, is the one that best fits the observed data, but it is not the only one possible. Horizontal dashed lines in the top panel show the boundaries of the apatite partial annealing zone and, black boxes show boundaries of the initial thermal history confined by geological data.

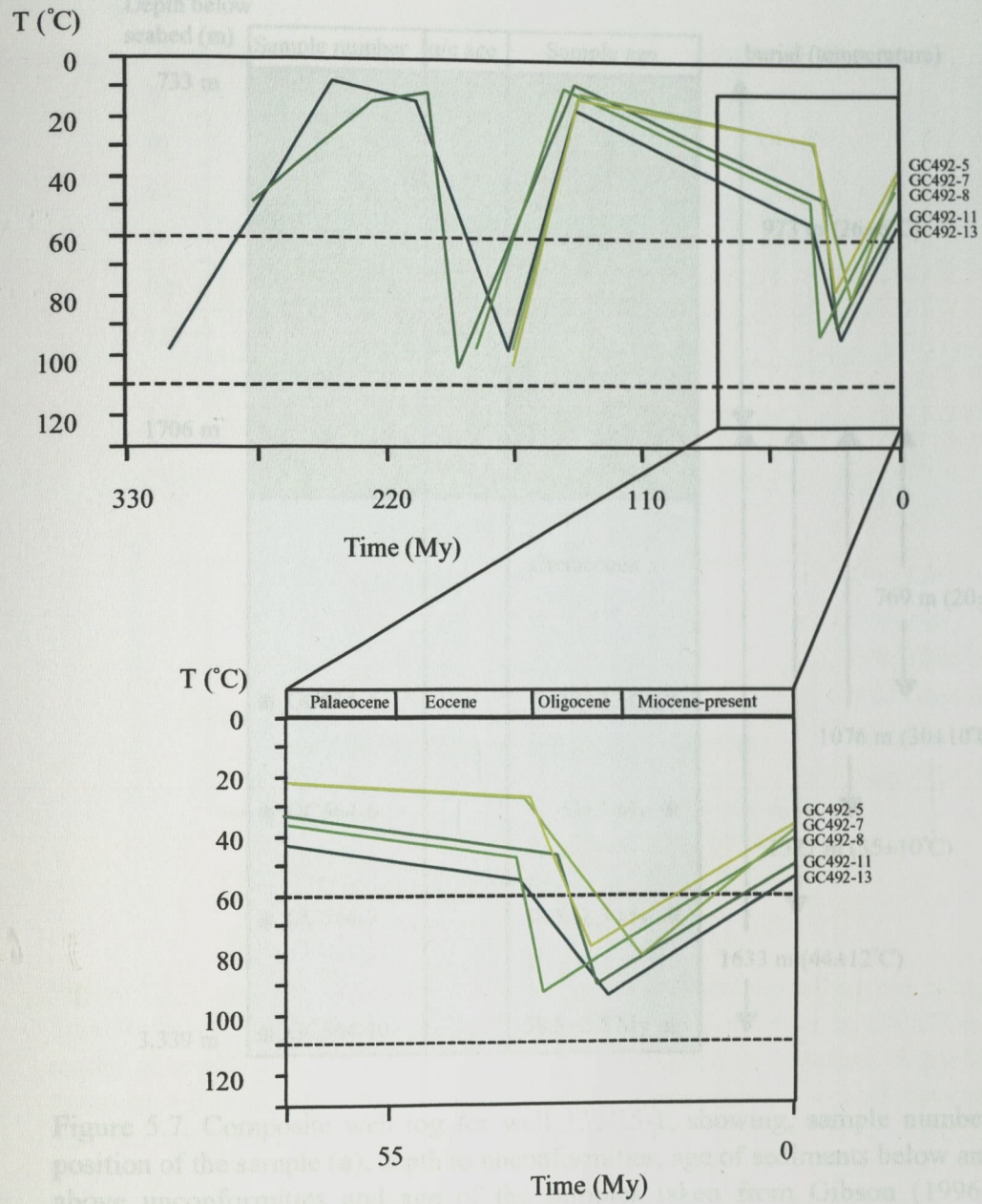


Figure 5.6. Modelled thermal history for well 12/13-1a. See text for explanation of modelling method. Dashed lines are boundaries of the apatite partial annealing zone. A close up view of the Cenzoic thermal history is also shown.

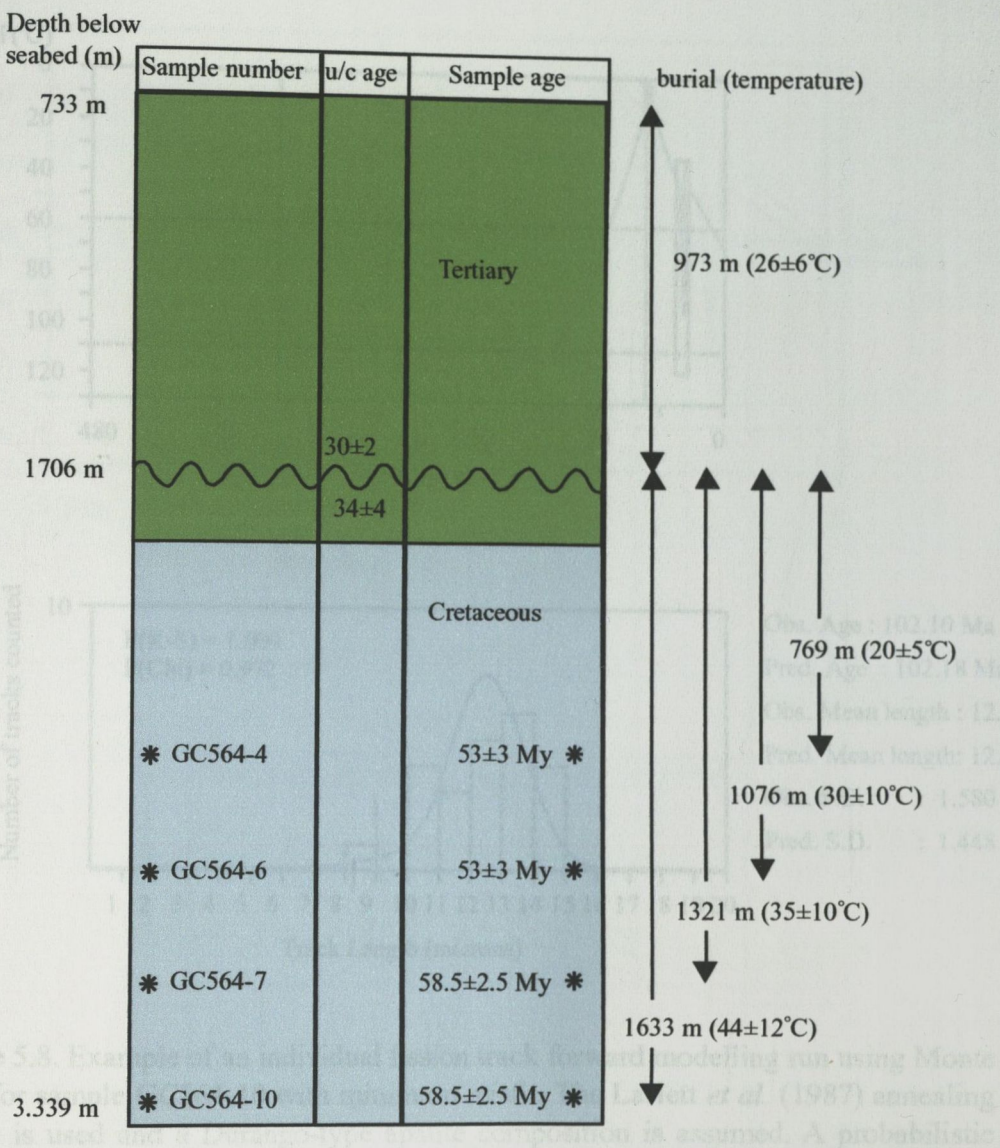


Figure 5.7. Composite well log for well 132/15-1, showing, sample number, position of the sample (*), depth to unconformities, age of sediments below and above unconformities and age of the samples taken from Gibson (1996). Vertical arrows show thicknesses from sample to unconformity, used to estimate the thermal effect due to sedimentary burial. A geothermal gradient of 20-40°C/km yields an equivalent temperature with an error given in brackets.

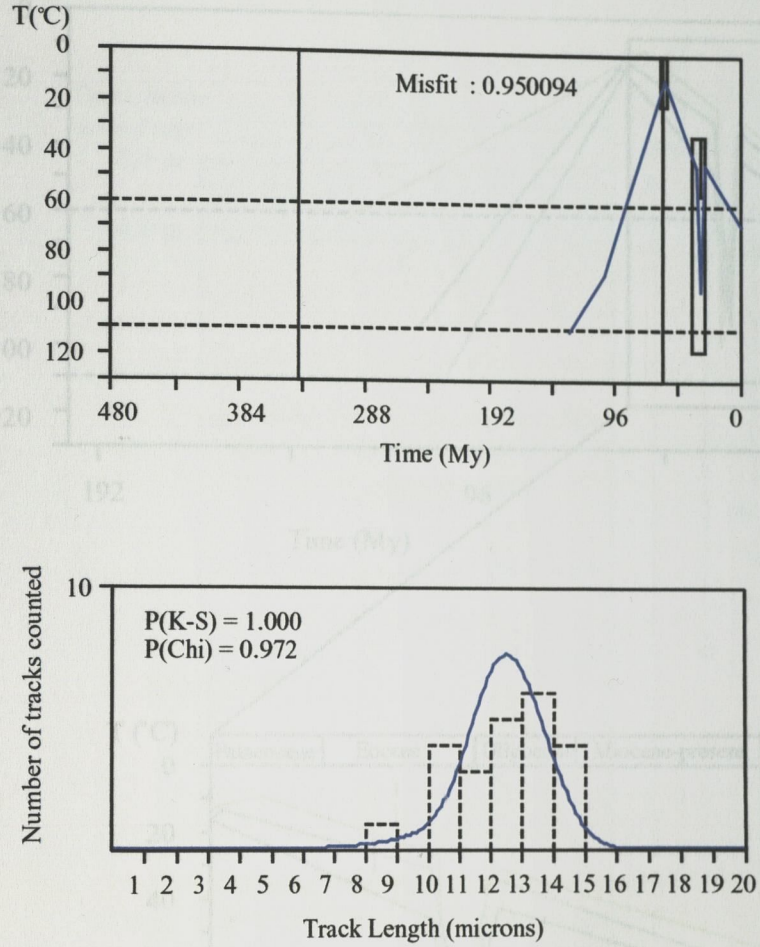


Figure 5.8. Example of an individual fission track forward modelling run using Monte Trax for sample GC564-10 with minimum misfit. The Laslett *et al.* (1987) annealing model is used and a Durango-type apatite composition is assumed. A probabilistic approach (genetic algorithm) is applied with 20 generations, to find the curve that best fits the observed track length data (histogram in black). The modelled thermal history, shown in the top panel in blue, is the one that best fits the observed data, but it is not the only one possible. Horizontal dashed lines in the top panel show the boundaries of the apatite partial annealing zone and, black boxes show boundaries of the initial thermal history confined by geological data.

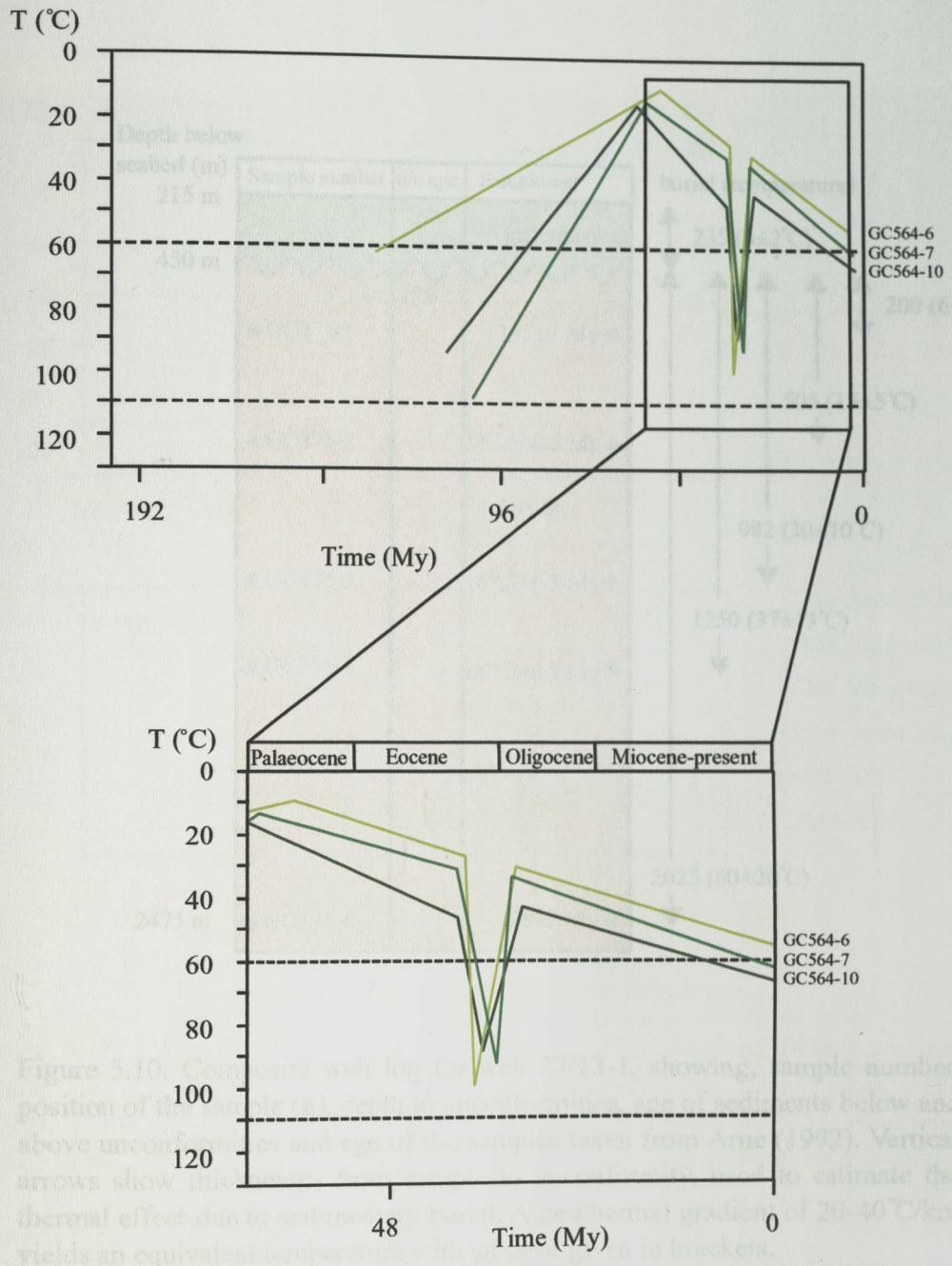


Figure 5.9. Modelled thermal history for well 132/15-1. See text for explanation of modelling method. Dashed lines are boundaries of the apatite partial annealing zone. A close up view of the Cenzoic thermal history is also shown.

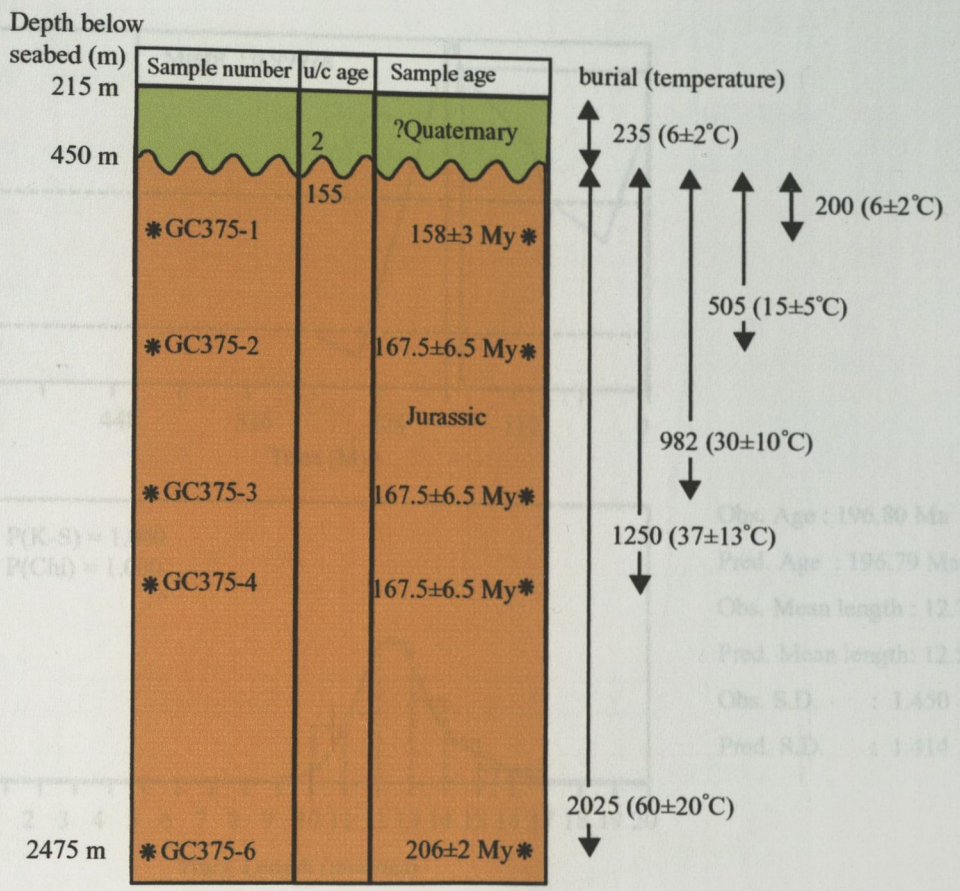


Figure 5.10. Composite well log for well 27/13-1, showing, sample number, position of the sample (✱), depth to unconformities, age of sediments below and above unconformities and age of the samples taken from Arne (1992). Vertical arrows show thicknesses from sample to unconformity, used to estimate the thermal effect due to sedimentary burial. A geothermal gradient of 20-40 °C/km yields an equivalent temperature with an error given in brackets.

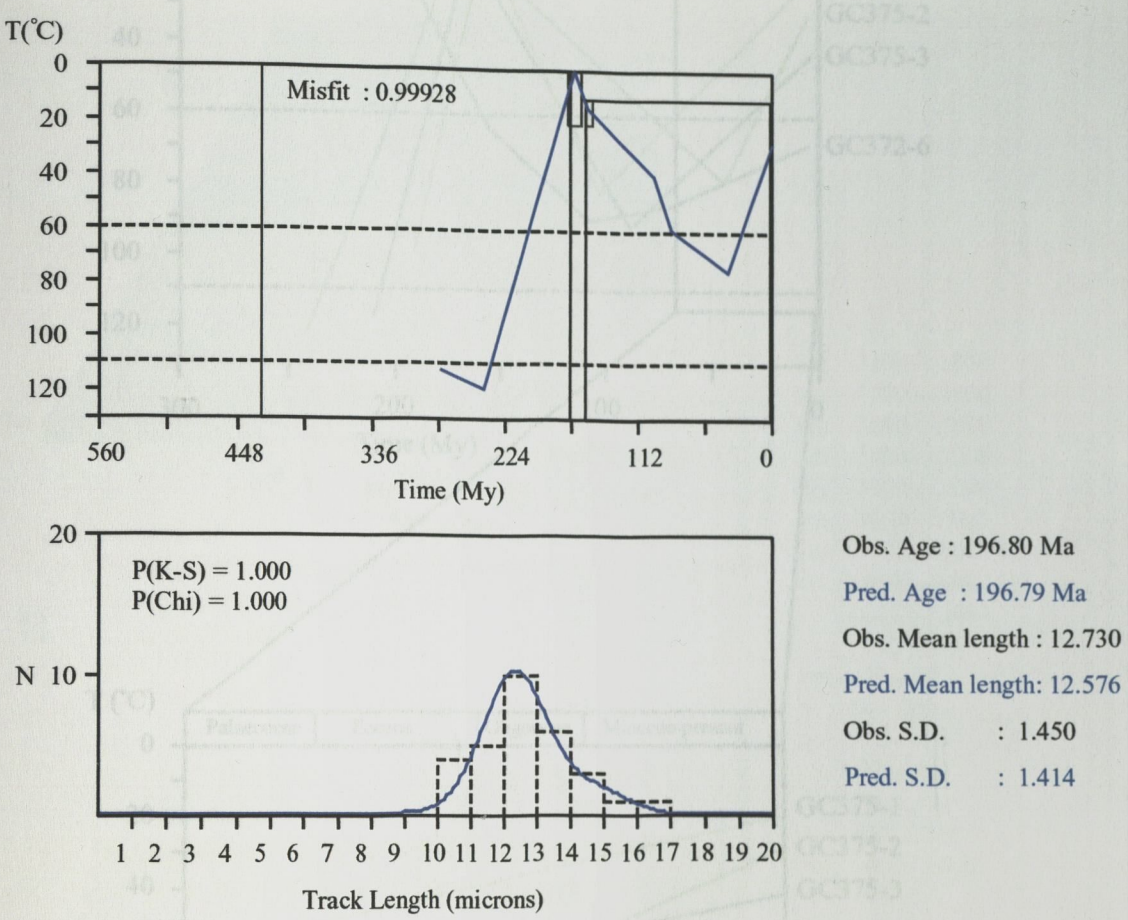


Figure 5.11. Example of an individual fission track forward modelling run using Monte Trax for sample GC375-2 with minimum misfit. The Laslett *et al.* (1987) annealing model is used and a Durango-type apatite composition is assumed. A probabilistic approach (genetic algorithm) is applied with 20 generations, to find the curve that best fits the observed track length data (histogram in black). The modelled thermal history, shown in the top panel in blue, is the one that best fits the observed data, but it is not the only one possible. Horizontal dashed lines in the top panel show the boundaries of the apatite partial annealing zone and, black boxes show boundaries of the initial thermal history confined by geological data.

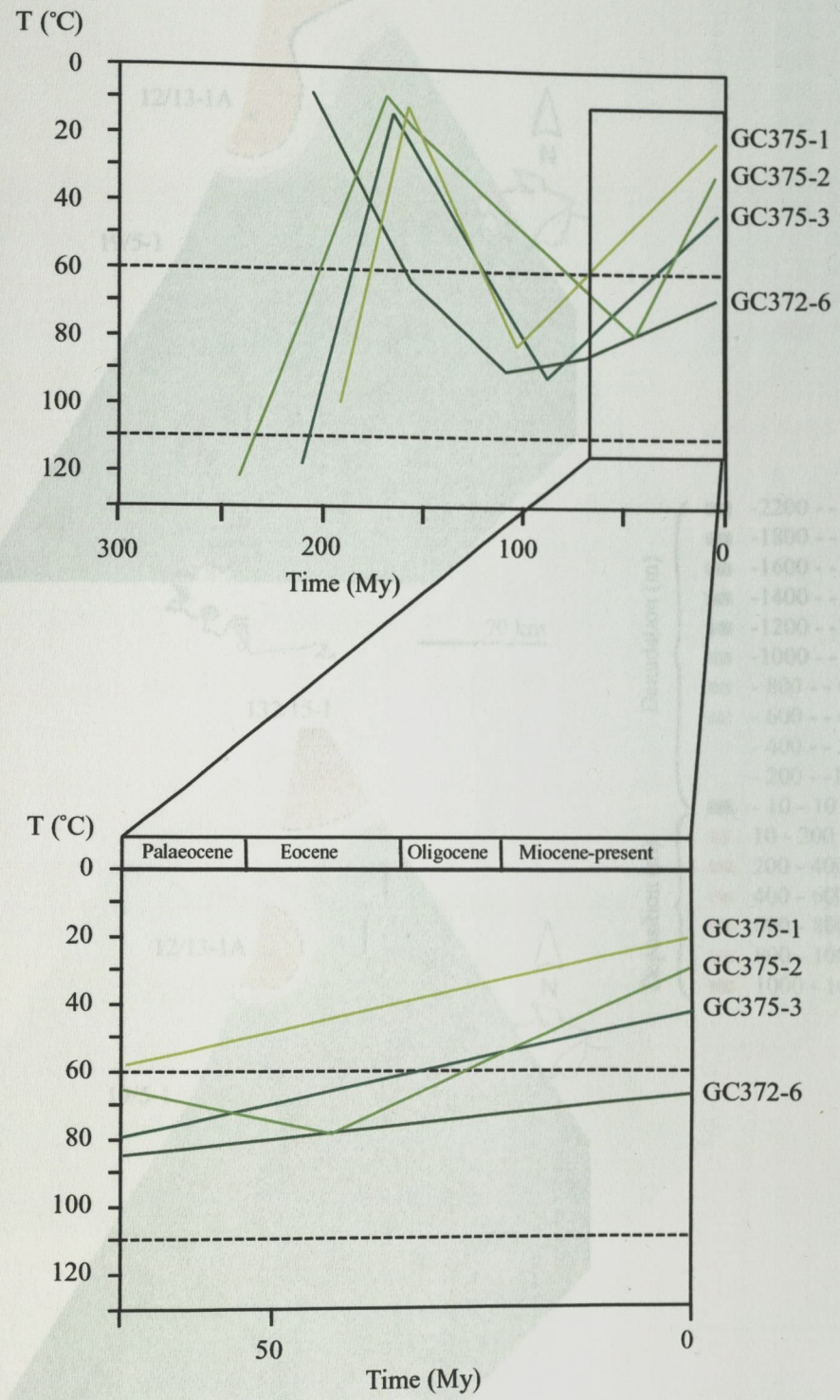


Figure 5.12. Modelled thermal history for well 27/13-1. See text for explanation of modelling method. Dashed lines are boundaries of the apatite partial annealing zone. A close up view of the Cenzoic thermal history is also shown.

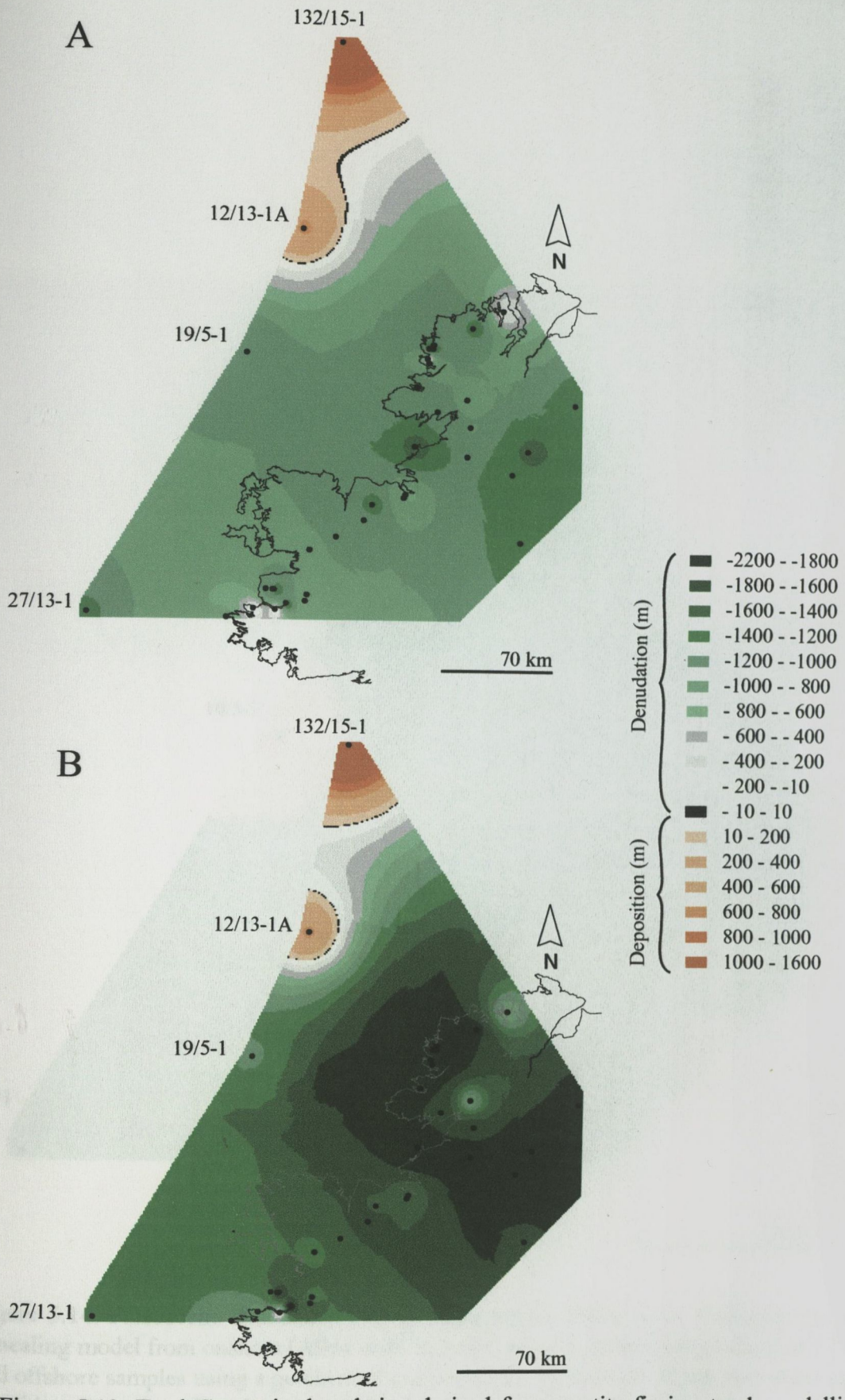


Figure 5.13. Total Cenozoic denudation derived from apatite fission track modelling from onshore (Allen *et al.* in press.) using a geothermal gradient of 27 °C/km and offshore samples using a geothermal gradient given by the well. Black dots show sample localities. Coastline of northwestern Ireland is shown for orientation. A, denudation using annealing model based on Gallagher (*in prep.*) annealing model. B, denudation using Laslett *et al.* (1987) annealing model.

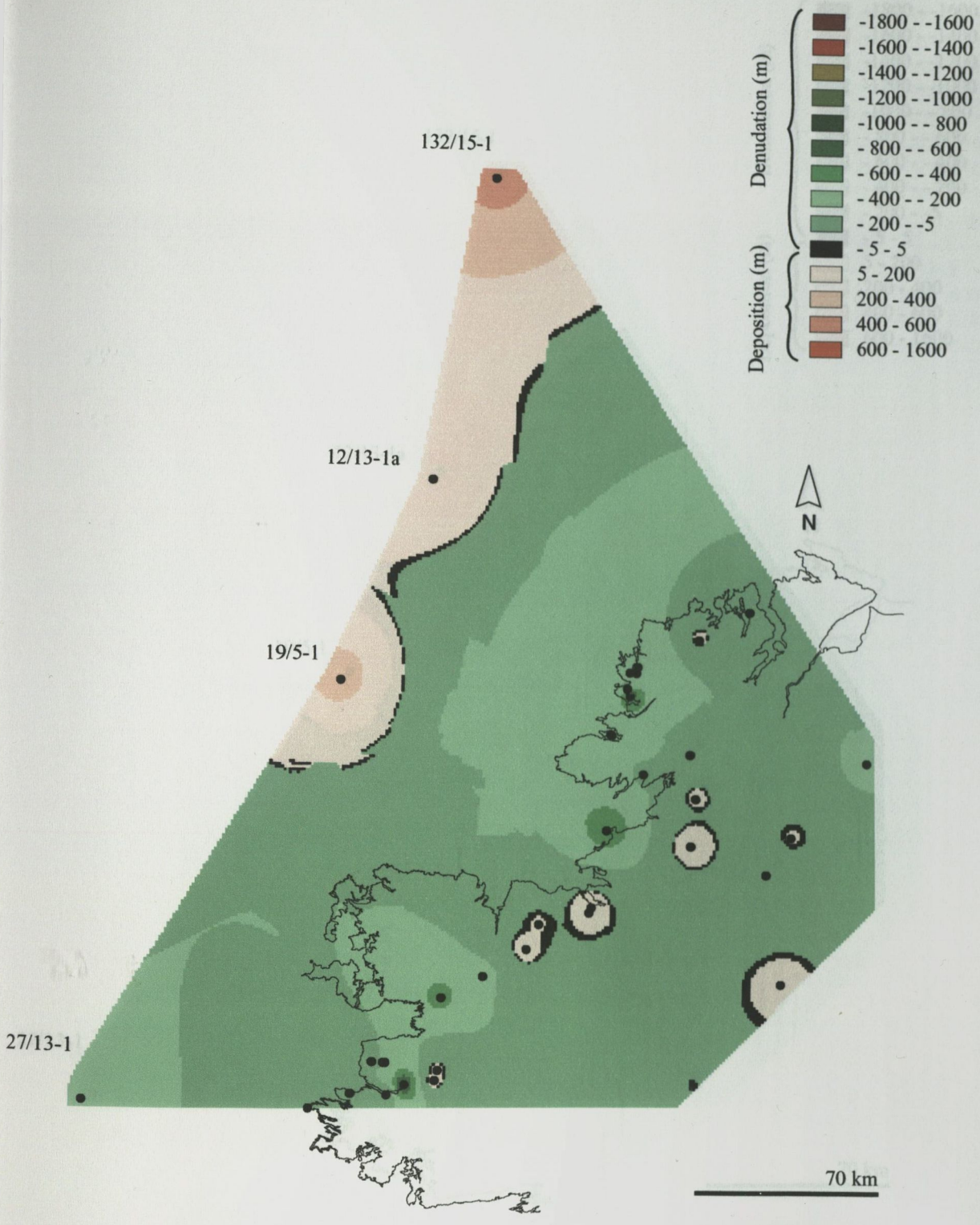


Figure 5.14. Palaeocene denudation derived from apatite fission track Gallagher (*in prep.*) annealing model from onshore (Allen *et al.* in press) using a geothermal gradient of 27°C/km and offshore samples using a geothermal gradient given by the well. Black dots show sample localities. Coastline of northwestern Ireland is shown for orientation.

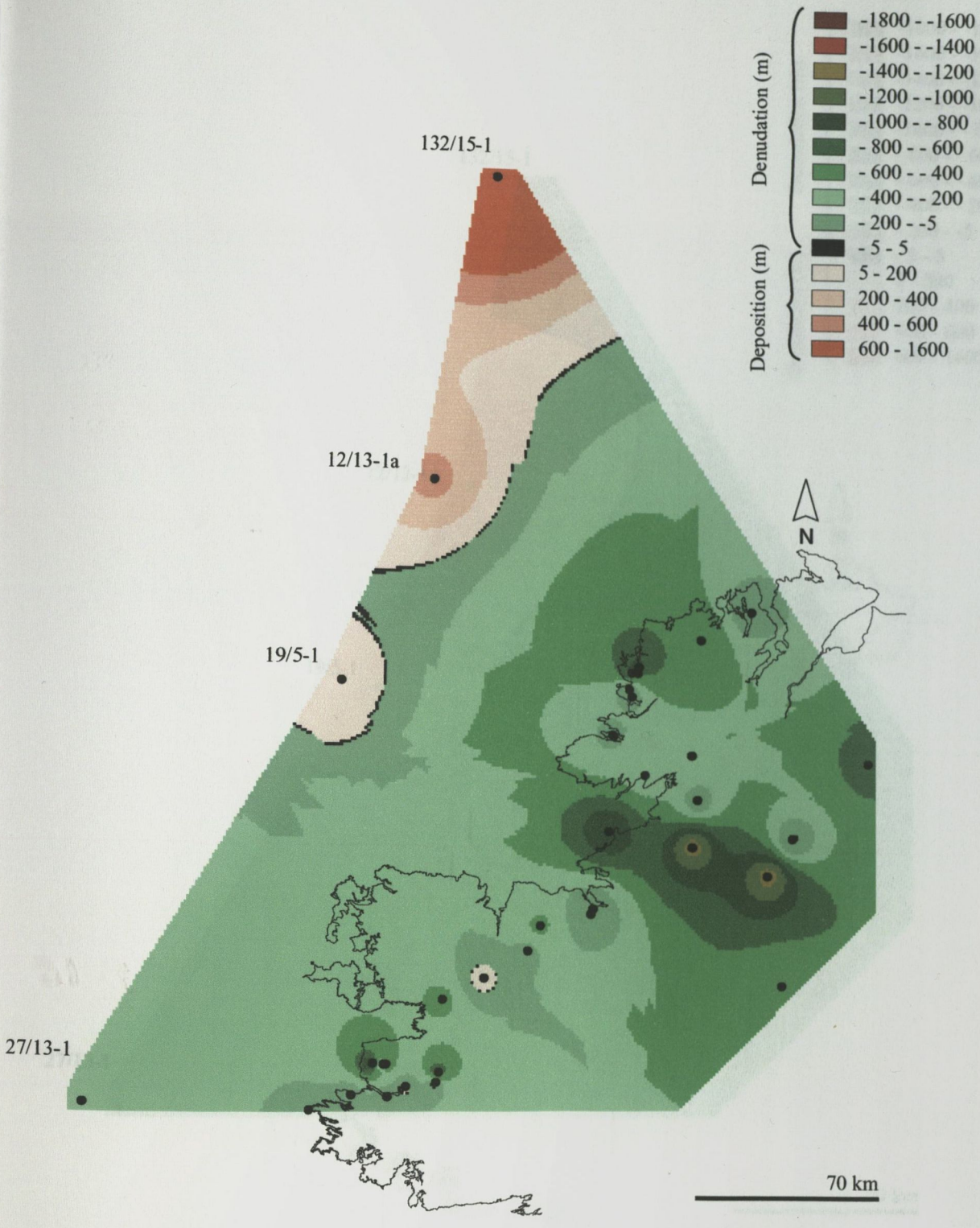


Figure 5.15. Eocene denudation derived from apatite fission track Gallagher (*in prep.*) annealing model from onshore (Allen *et al.* in press.) using a geothermal gradient of 27 °C /km and offshore samples using a geothermal gradient given by the well. Black dots show sample localities. Coastline of northwestern Ireland is shown for orientation.

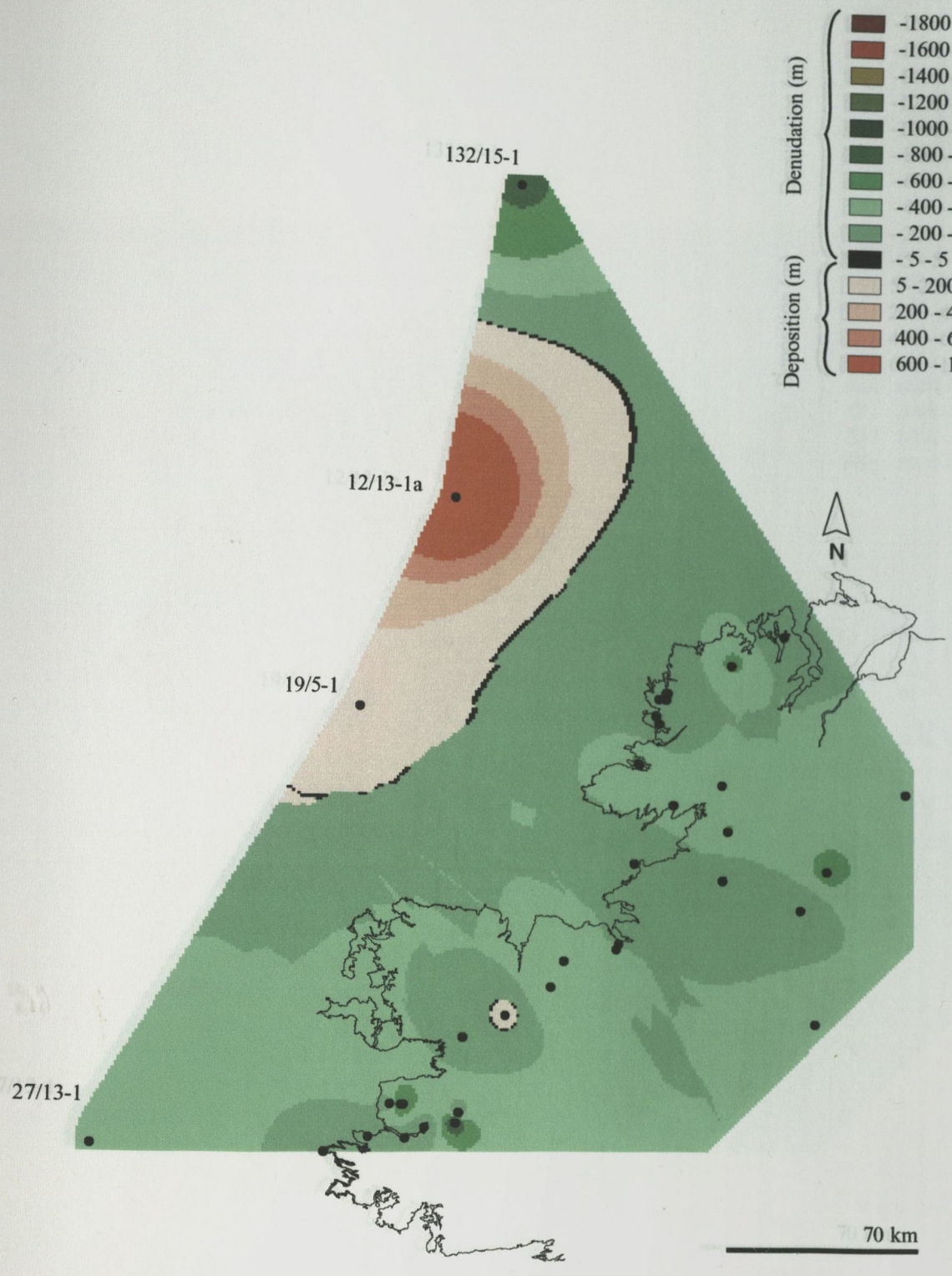


Figure 5.16. Oligocene denudation derived from apatite fission track Gallagher (*in prep.*) annealing model from onshore (Allen *et al.* in press.) using a geothermal gradient of 27 °C/km and offshore samples using a geothermal gradient given by the well. Black dots show sample localities. Coastline of northwestern Ireland is shown for orientation.

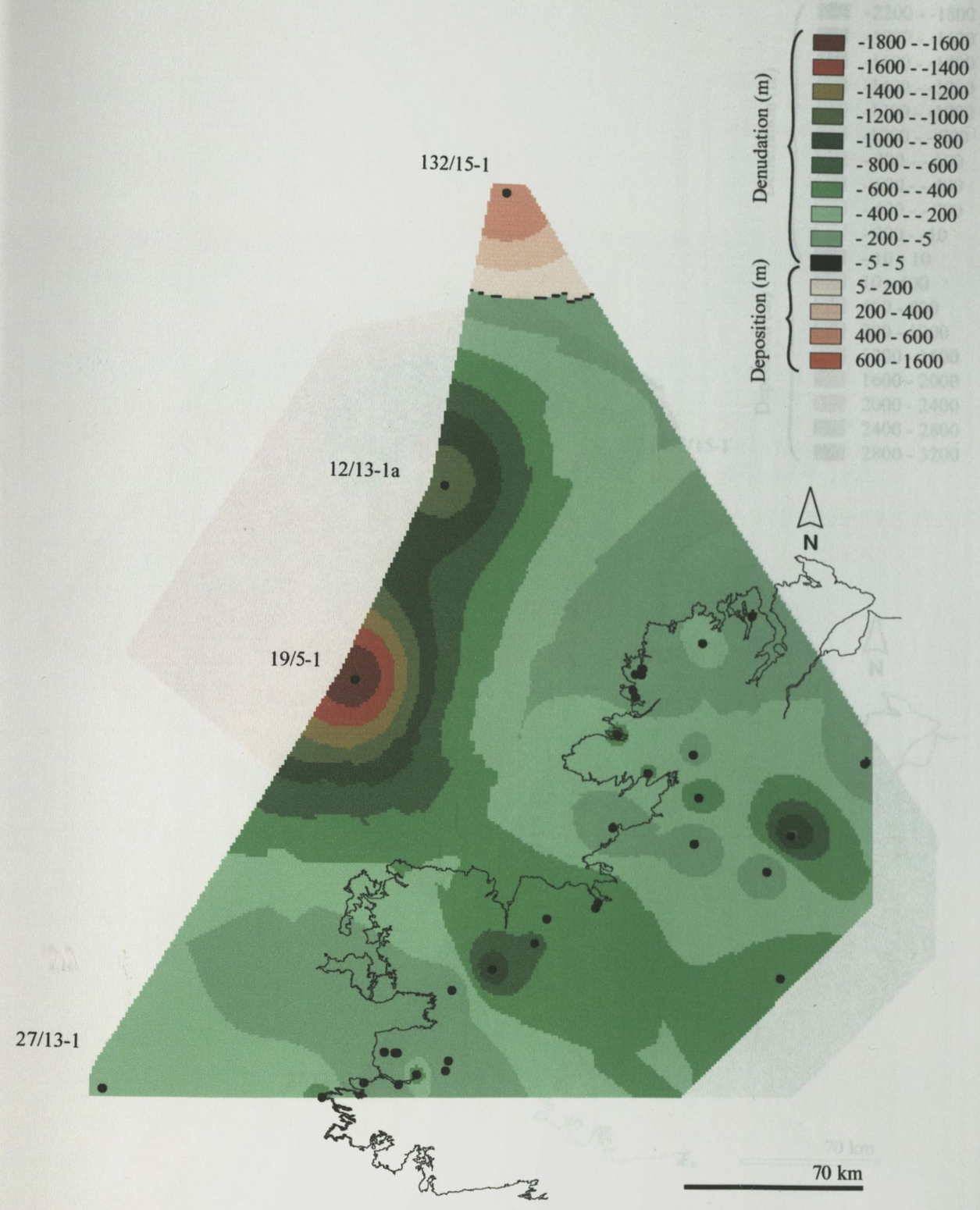


Figure 5.17. Miocene to present denudation derived from apatite fission track Gallagher (*in prep.*) annealing model from onshore (Allen *et al.* in press.) using a geothermal gradient of 27 C /km and offshore samples using a geothermal gradient given by the well. Black dots show sample localities. Coastline of northwestern Ireland is shown for orientation.

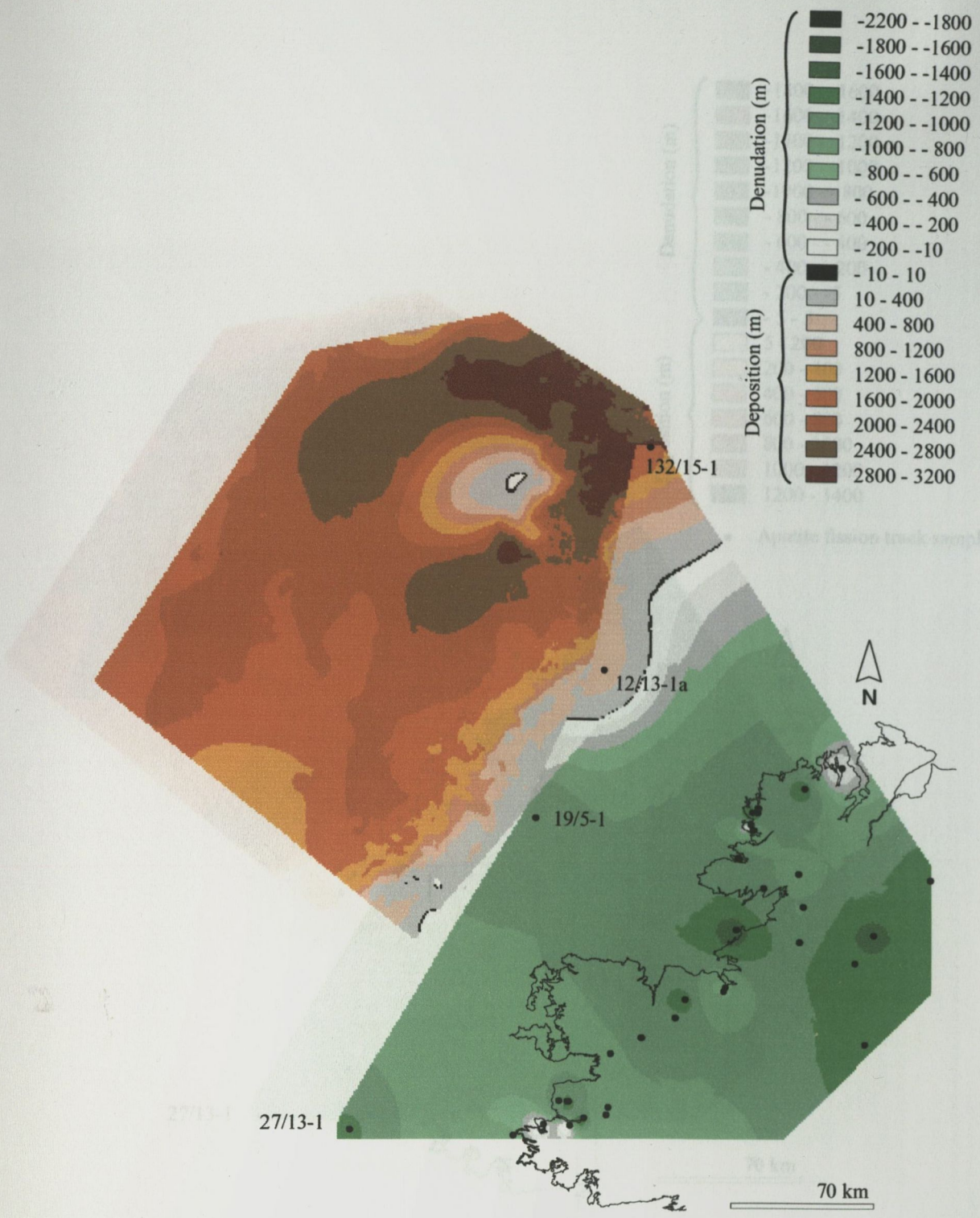


Figure 5.18. Mosaic of onshore denudation and offshore deposition during the Cenozoic. Overlapping area between denudation and deposition maps shows the mismatch between the two different databases.

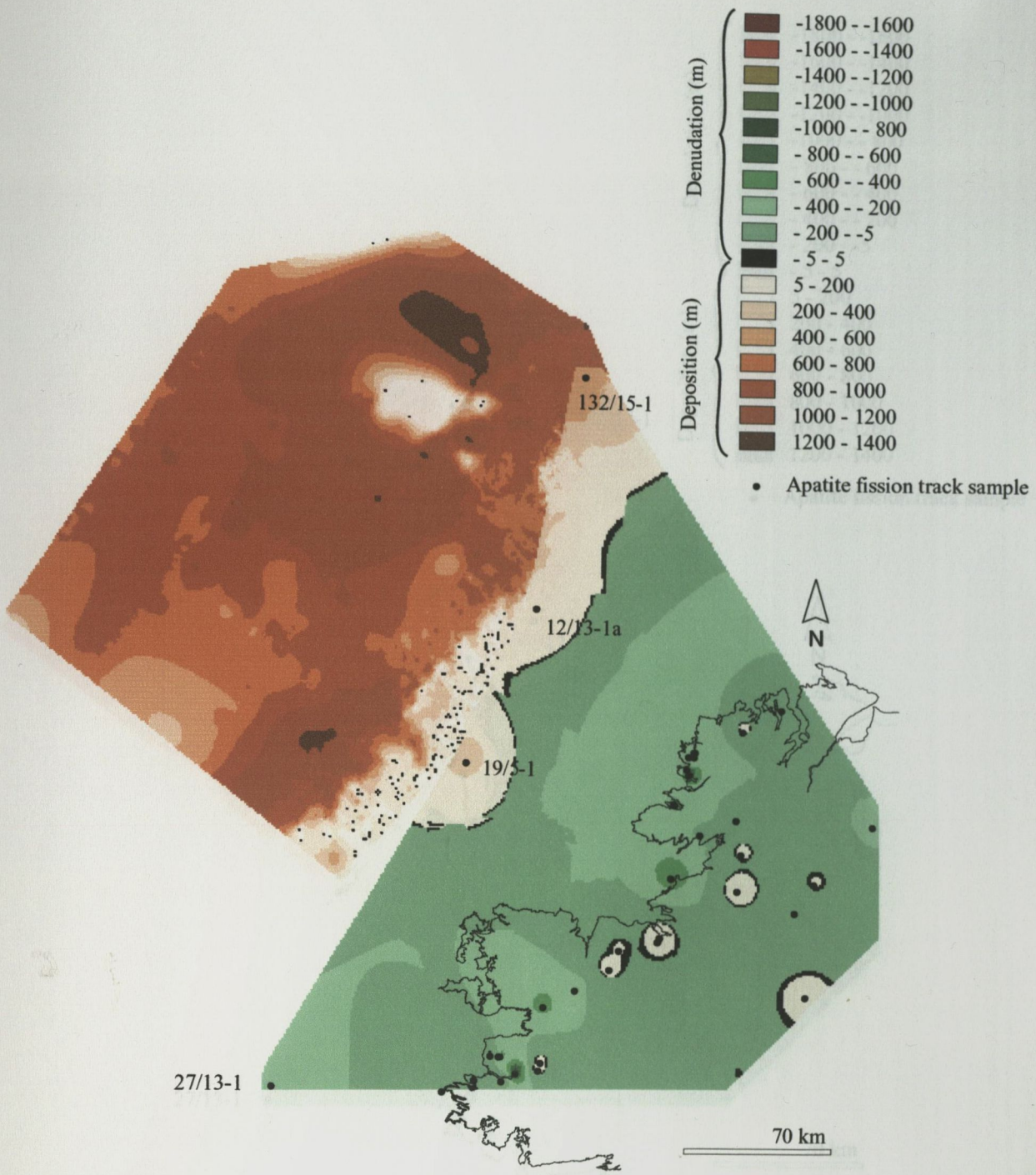


Figure 5.19. Mosaic of onshore denudation and offshore deposition during the Palaeocene. Overlapping area between denudation and deposition maps shows the mismatch between the two different databases.

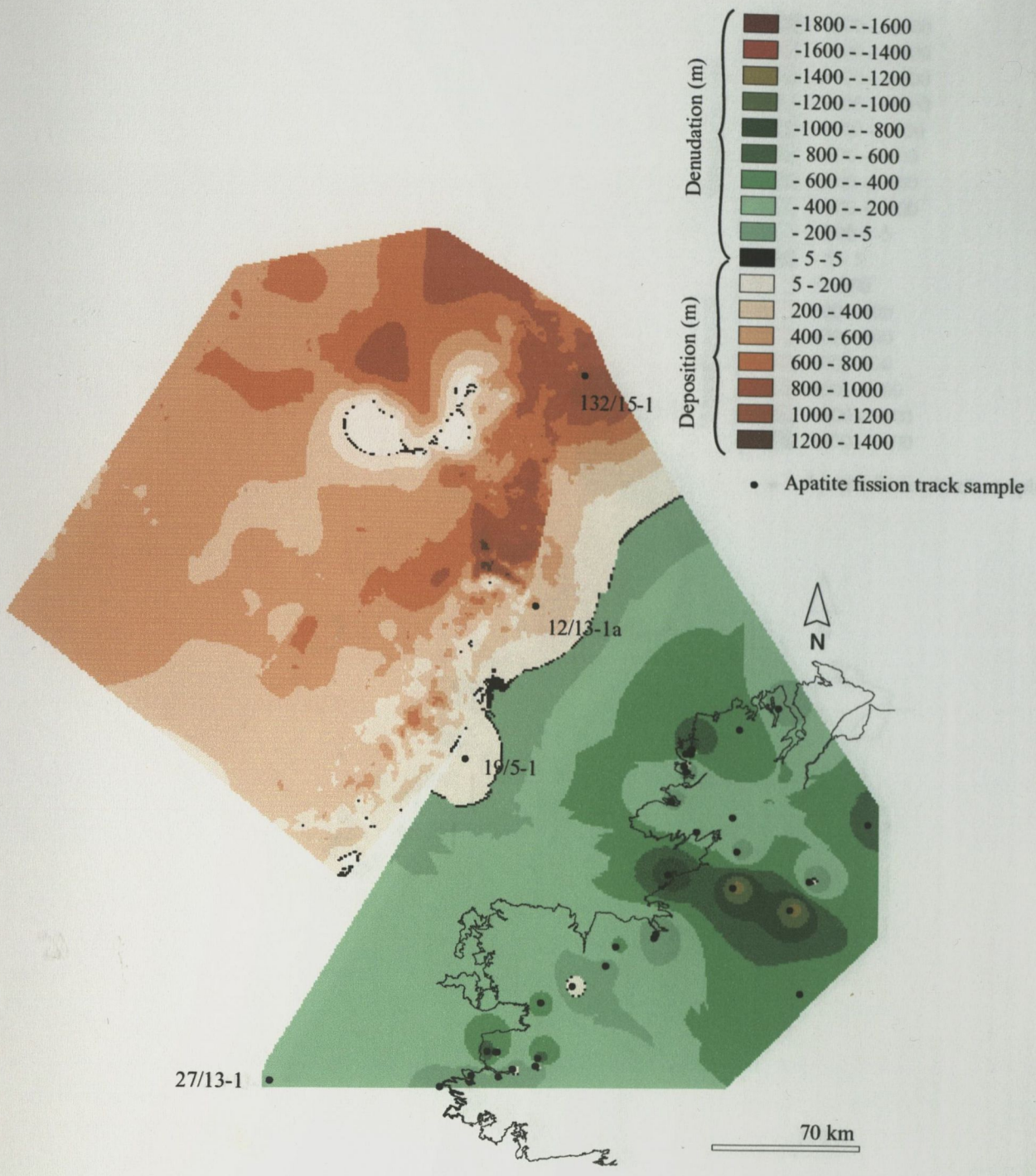


Figure 5.20. Mosaic of onshore denudation and offshore deposition during the Eocene. Overlapping area between denudation and deposition maps shows the mismatch between the two different databases.

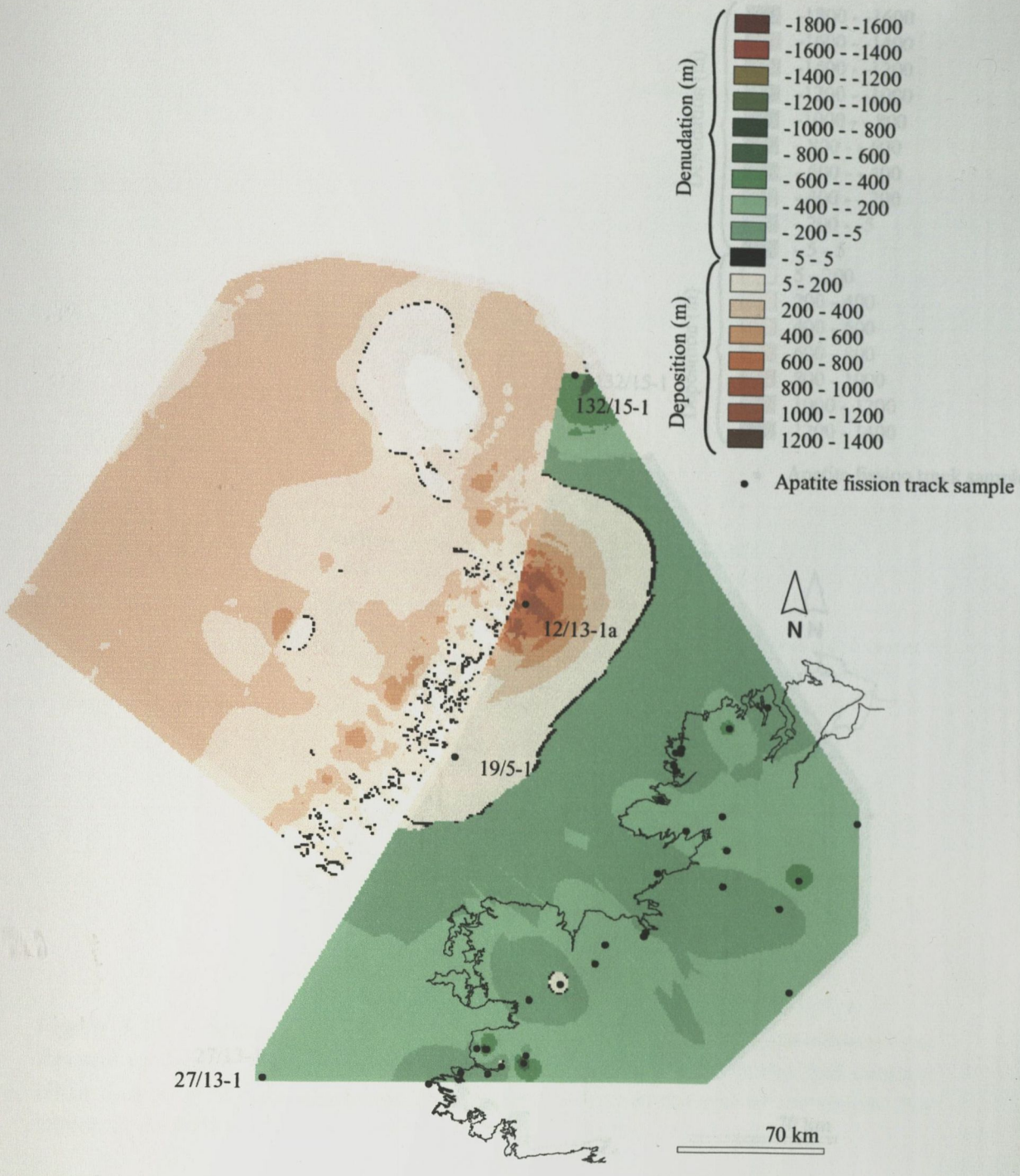


Figure 5.21. Mosaic of onshore denudation and offshore deposition during the Oligocene. Overlapping area between denudation and deposition maps shows the mismatch between the two different databases.

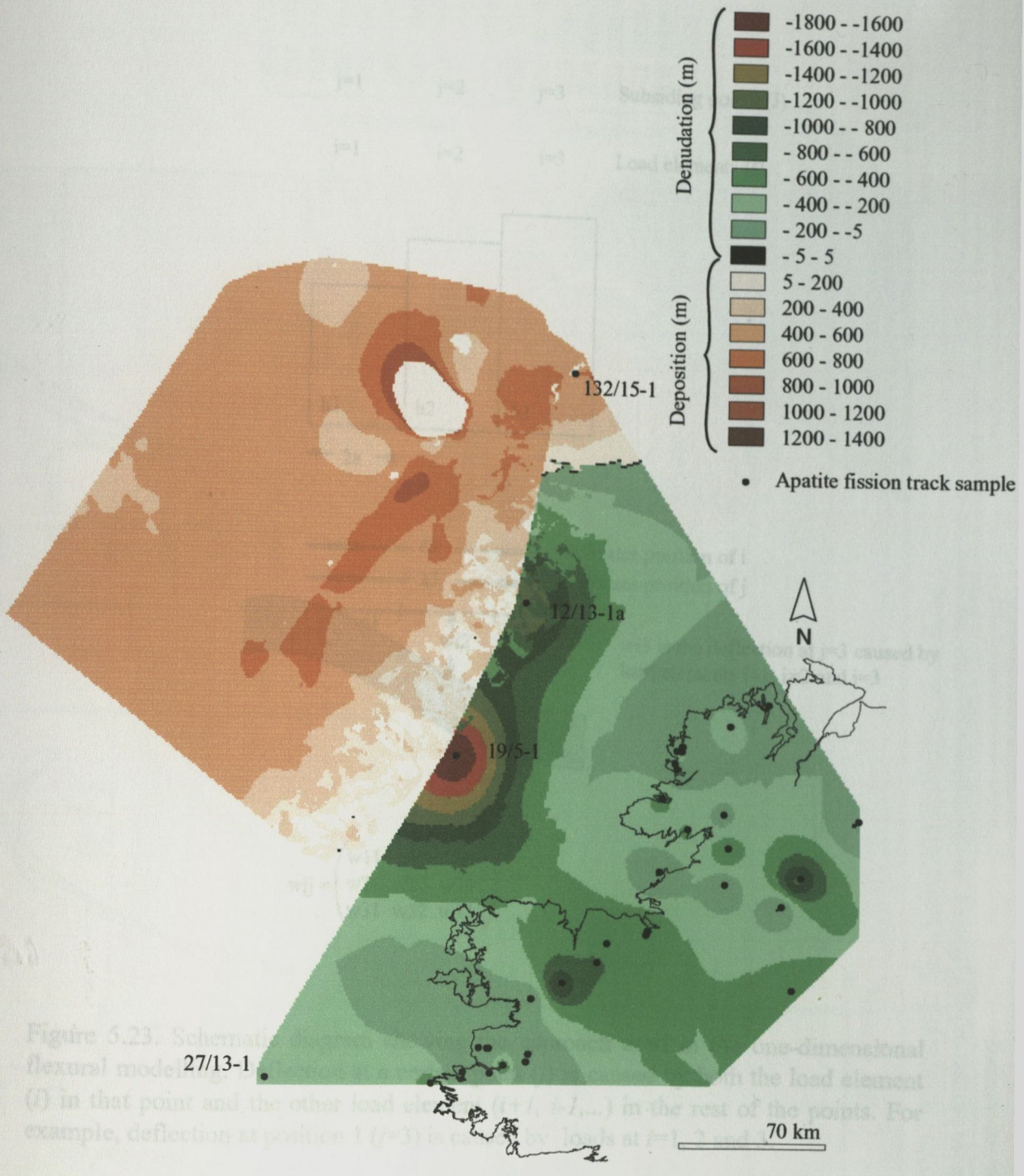


Figure 5.22. Mosaic of onshore denudation and offshore deposition during the Miocene to present. Overlapping area between denudation and deposition maps shows the mismatch between the two different databases.

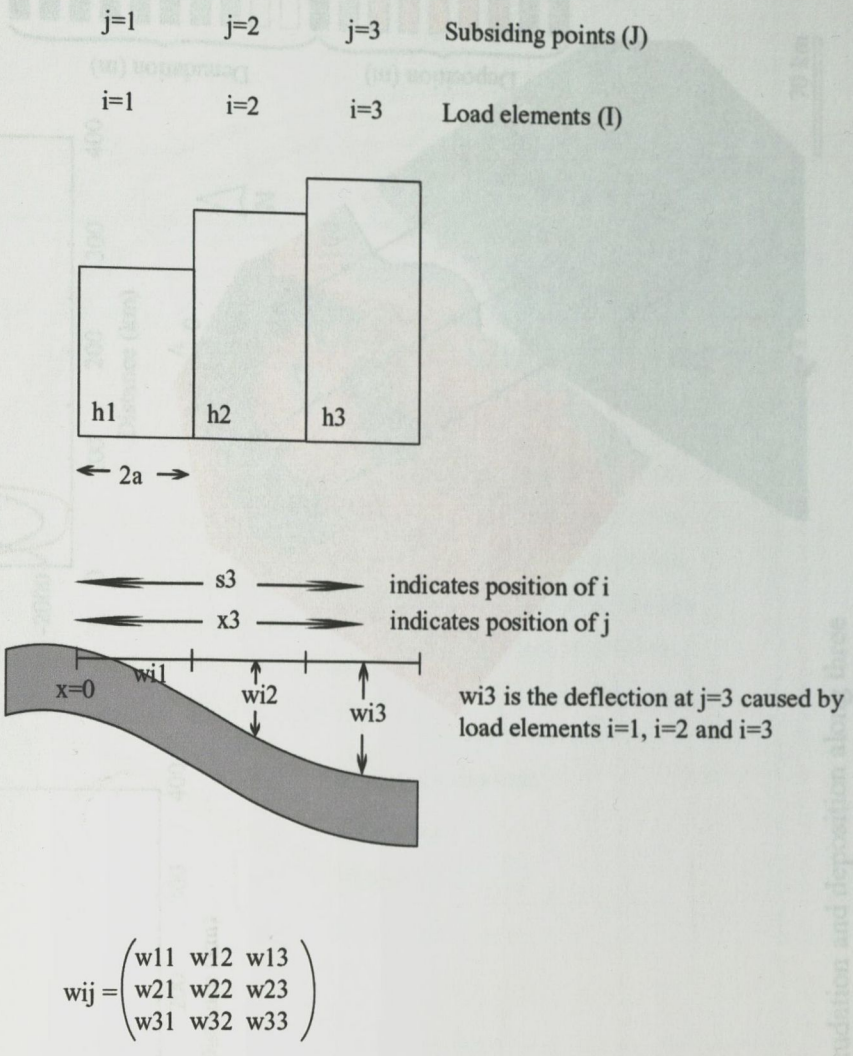


Figure 5.23. Schematic diagram showing the approach used in the one-dimensional flexural modelling. Deflection at a certain point (*j*) is caused by both the load element (*i*) in that point and the other load element (*i+1, i-1,...*) in the rest of the points. For example, deflection at position 1 (*j*=3) is caused by loads at *i*=1, 2 and 3.

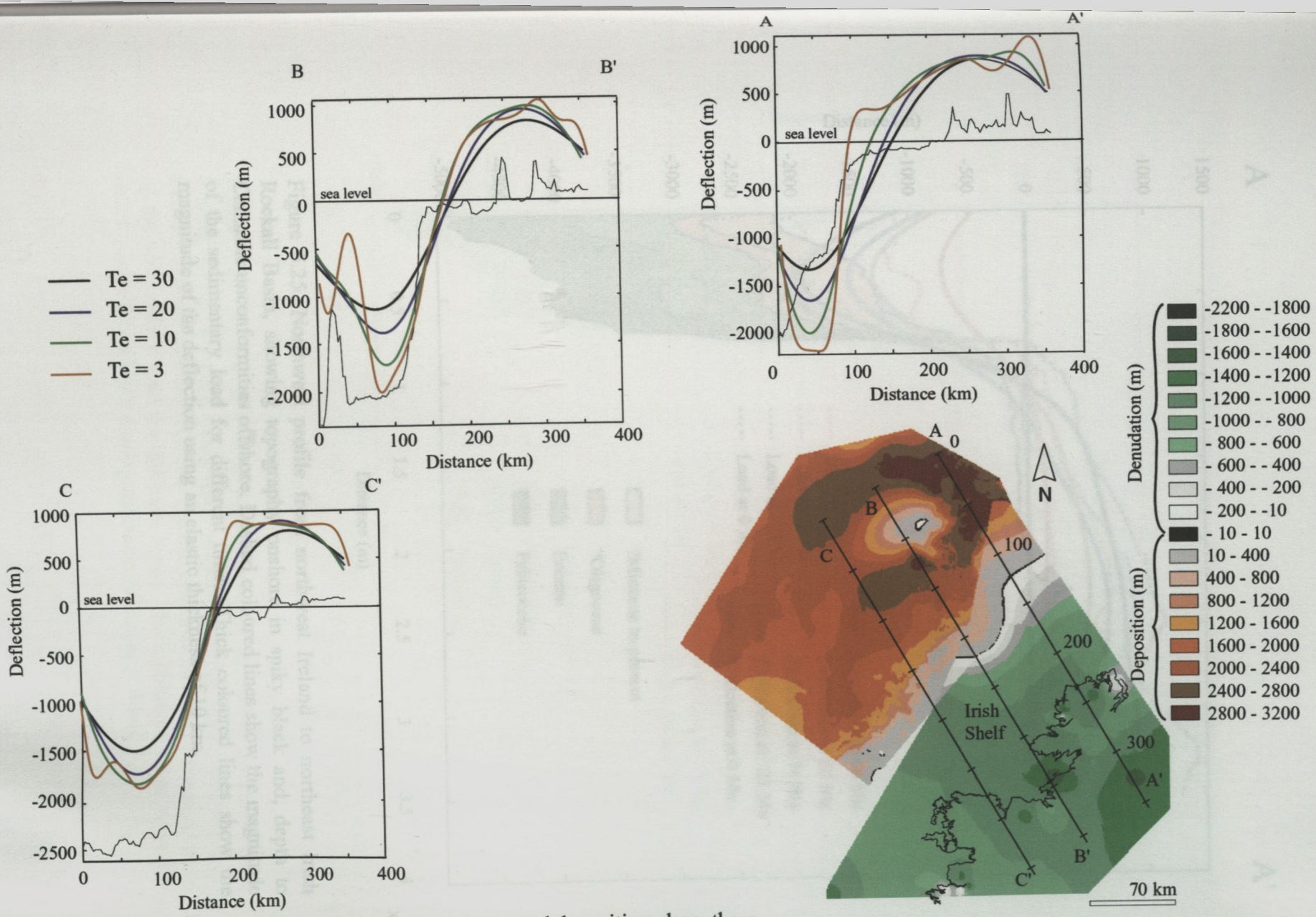


Figure 5.24. Flexural response to Cenozoic denudation and deposition along three profiles in the northwest Irish margin using different elastic thicknesses (Te). Thin line shows bathymetry and topography.

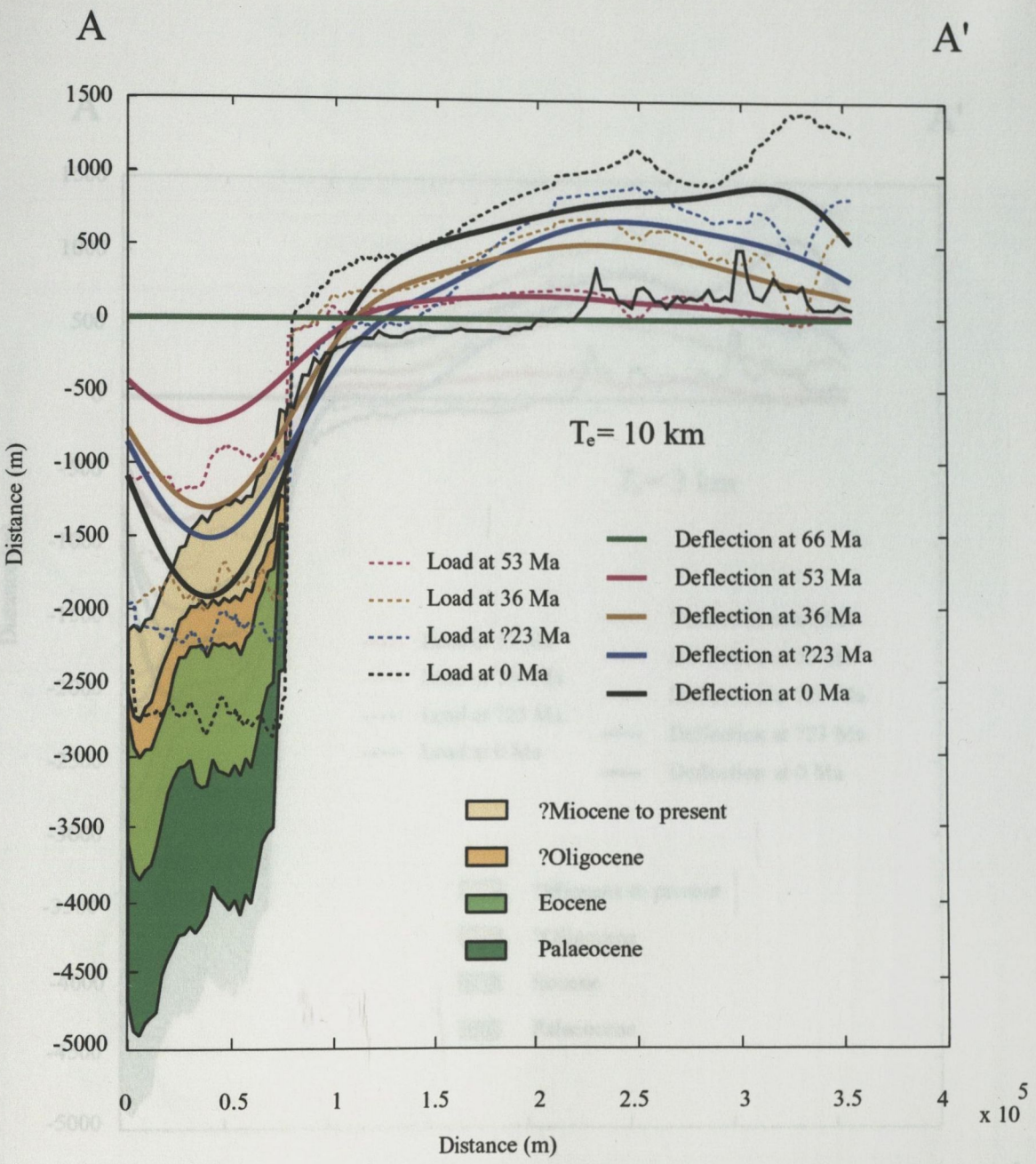


Figure 5.25. Northwest profile from northwest Ireland to northeast Irish Rockall Basin, showing topography onshore in spiky black and, depth to Cenozoic unconformities offshore. Dashed coloured lines show the magnitude of the sedimentary load for different times. Thick coloured lines show the magnitude of the deflection using an elastic thickness of 10 km.

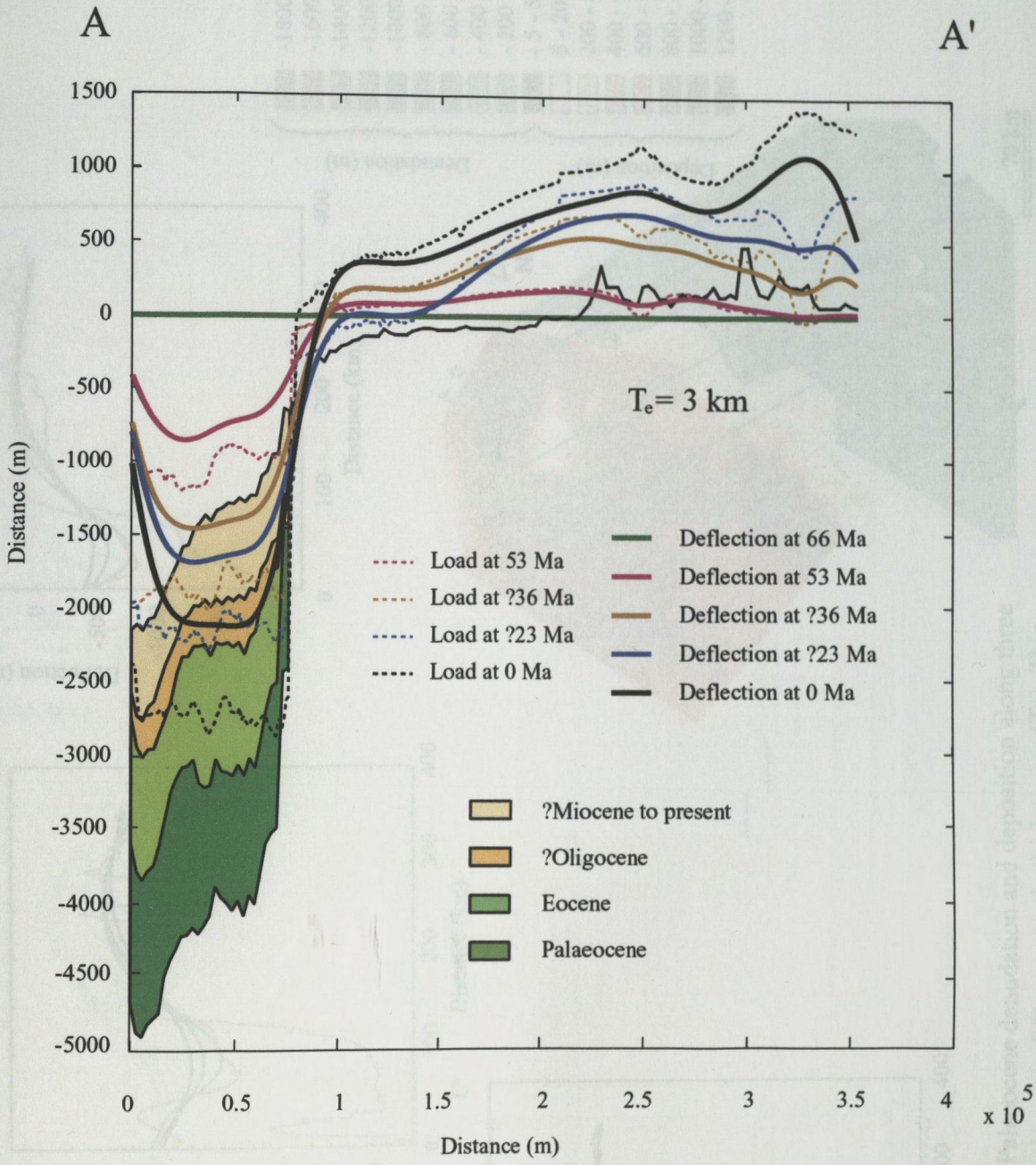


Figure 5.26. Northwest profile from northwest Ireland to northeast Irish Rockall Basin, showing topography onshore in spiky black and, depth to Cenozoic unconformities offshore. Dashed coloured lines show the magnitude of the sedimentary load for different times. Thick coloured lines show the magnitude of the deflection using an elastic thickness of 3 km.

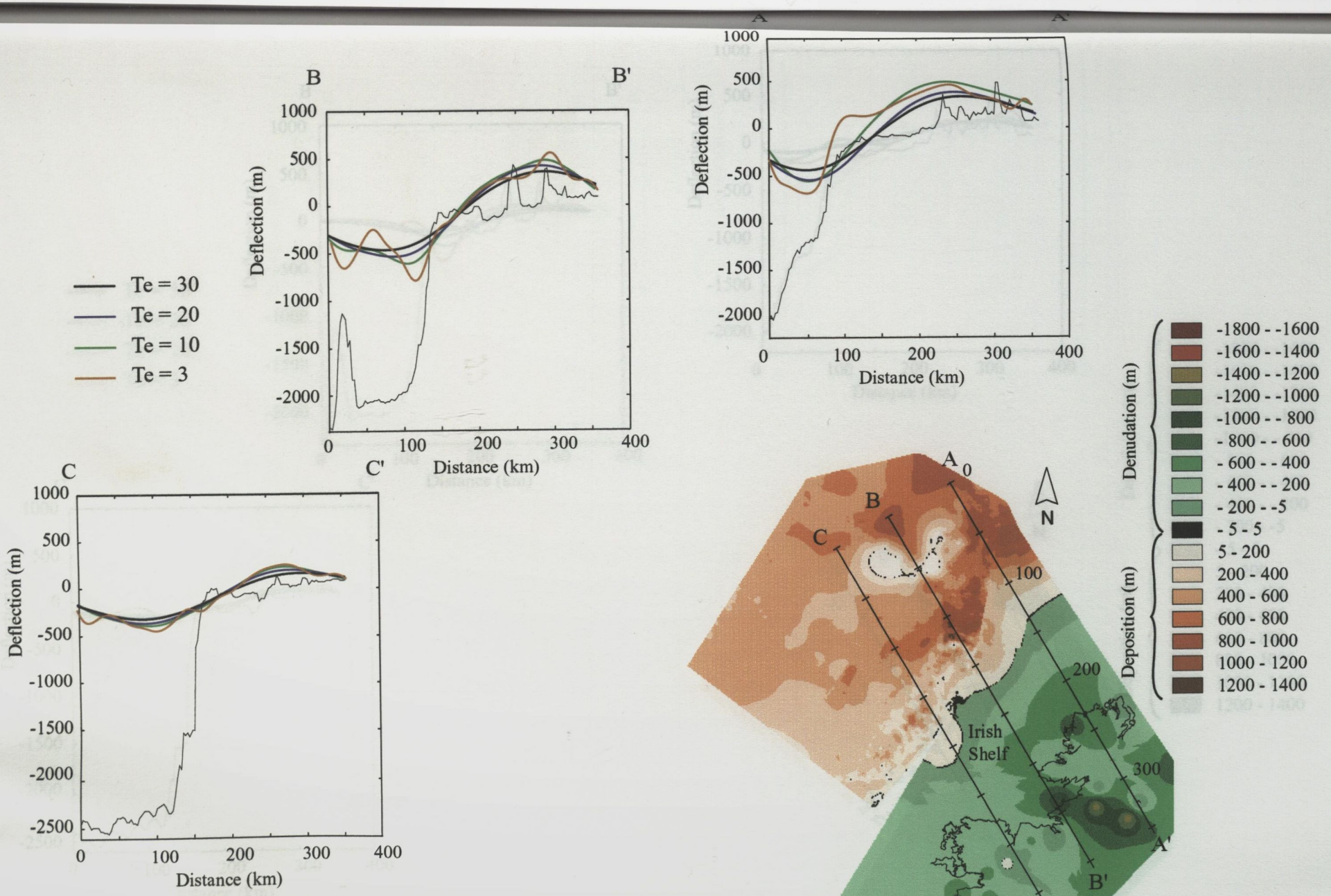


Figure 5.28. Flexural response to Eocene denudation and deposition along three profiles in the northwest Irish margin using different elastic thicknesses (Te). Thin line shows bathymetry and topography.

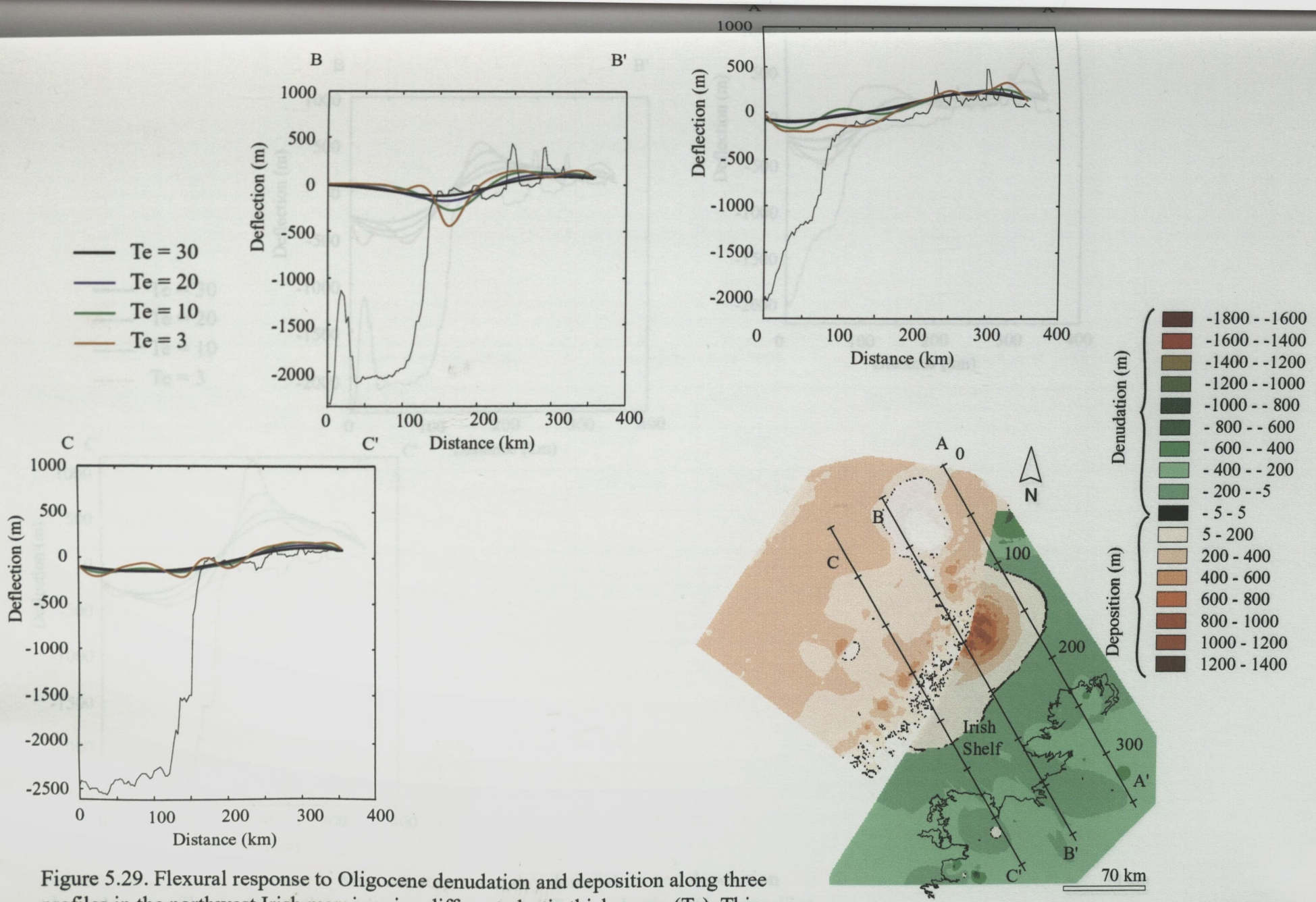


Figure 5.29. Flexural response to Oligocene denudation and deposition along three profiles in the northwest Irish margin using different elastic thicknesses (Te). Thin line shows bathymetry and topography.

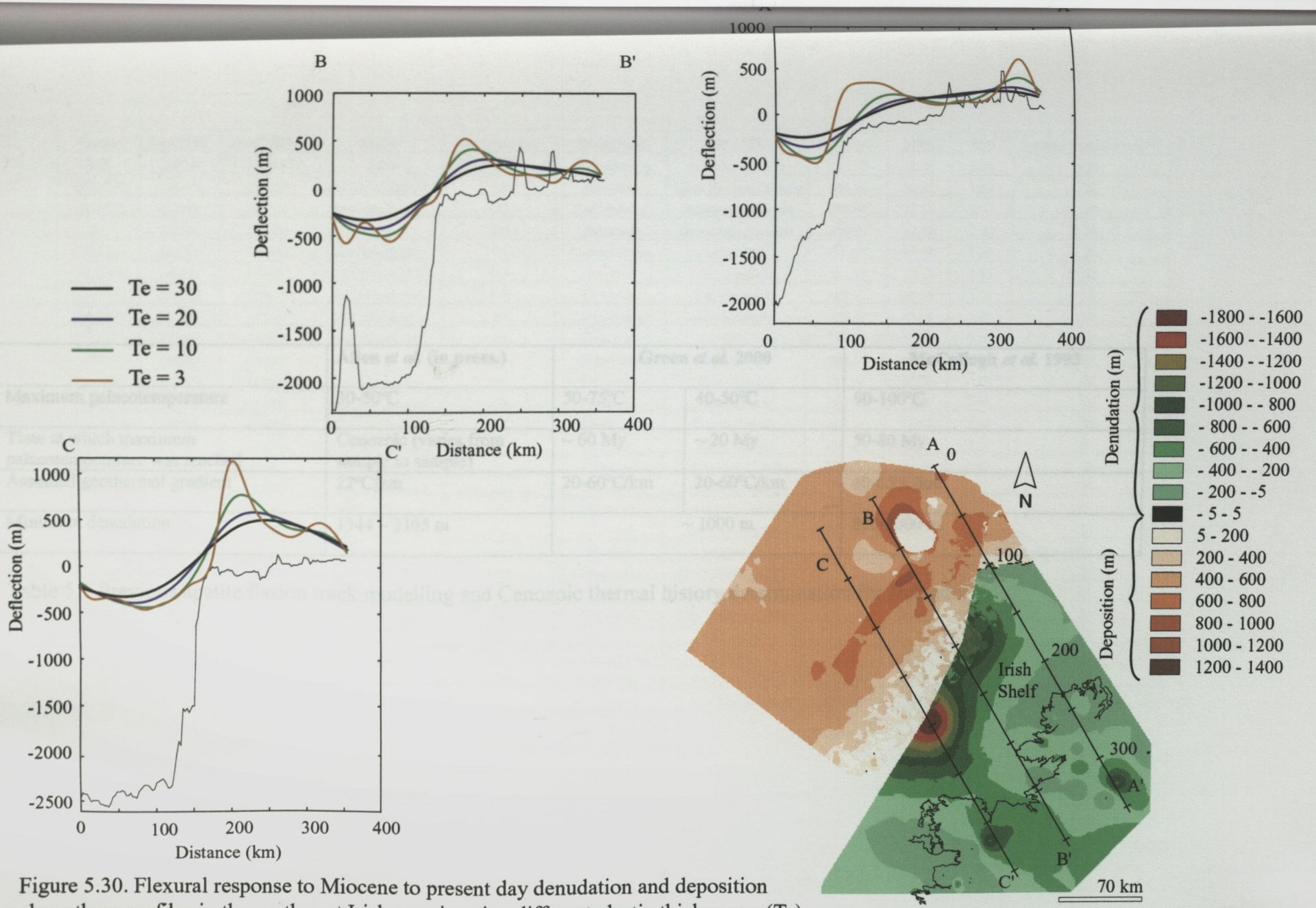


Figure 5.30. Flexural response to Miocene to present day denudation and deposition along three profiles in the northwest Irish margin using different elastic thicknesses (Te). Thin line shows bathymetry and topography.

	Allen *et al.* (in press.)	Green *et al.* 2000		McCullogh *et al.* 1993
Maximum palaeotemperature	30-50°C	50-75°C	40-50°C	90-100°C
Time at which maximum palaeotemperature was reached	Cenozoic (varies from sample to sample)	~ 60 My	~ 20 My	50-80 My
Assumed geothermal gradient	22°C/km	20-60°C/km	20-60°C/km	40-65°C/km
Minimum denudation	1344 – 2165 m	~ 1000 m		800-2000 m

Table 5.1 Previous apatite fission track modelling and Cenozoic thermal history determination for Ireland.

Sample	EASTING	NORTHING	Source	Elevation (m)	Statigraphy	LOCALITY	AFT age	MTL	SDV	Present temperature °C
BS1	185098	374943	Tulip	0	Carboniferous	Barnesmore Gap	143.37	12.75	1.70	20
C062277	206198	427751	McCulloch (unpub)	50	Devonian	Main Donegal Granite	159.25	12.41	1.65	20
C380251	237998	425126	McCulloch (93)	195	PreCambrian	Dalradian Basement	300.91	12.85	2.37	20
F1	202500	385400	Tulip	100	Devonian	Barnesmore Granite	189.69	12.84	1.77	20
G222329	122200	332903	McCulloch (93)	0	Carboniferous	Killala Bay	55.42	13.74	1.45	20
G402145	140199	314490	McCulloch (93)	165	Devonian	Ox Mountains	154.81	12.55	1.53	20
G450237	145002	323669	McCulloch (93)	195	Devonian	Ox Mountains	169.41	12.48	1.54	20
G710579	171002	357937	McCulloch (93)	10	Carboniferous	Mullaghmore	166.15	12.45	1.92	20
G725933	172501	393324	McCulloch (93)	10	Devonian	Ardara Granite	181.04	12.49	1.56	20
GL	105900	270800	Tulip	82	Ordovician	Partry Mts	200.69	12.55	2.77	20
Gleadow1	182497	417986	Gleadow (unpub)	40	Devonian	Thorr Granite	187.46	12.25	2.15	20
Gleadow2	183002	417984	Gleadow (unpub)	60	Devonian	Thorr Granite	200.63	12.25	2.04	20
Gleadow3	179999	415992	Gleadow (unpub)	72	Devonian	Rosses Granite	197.11	11.92	2.15	20
Gleadow4	182501	415759	Gleadow (unpub)	55	Devonian	Thorr Granite	187.46	12.25	2.15	20
Gleadow5	178998	409875	Gleadow (unpub)	25	Devonian	Trawenagh Granite	193.73	12.24	2.42	20
Gleadow6	179999	407310	Gleadow (unpub)	28	Devonian	Trawenagh Granite	180.11	12.32	2.27	20
Gleadow8	173002	411361	Gleadow (unpub)	10	Devonian	Trawenagh Granite	175.28	12.36	1.88	20
Gleadow9	86002	273976	Gleadow (unpub)	175	Devonian	Corvock Granite	124.26	12.27	2.36	20
H302411	230198	341137	McCulloch (93)	80	Silurian	near Eniskillen	176.05	12.32	2.07	20
H397547	239698	354678	McCulloch (93)	190	Devonian	SE of Trillick (B80)	177.32	11.49	1.67	20
L810743	81003	274323	McCulloch (93)	74	Devonian	Cregganbaun	152.10	12.89	1.99	20
L935657	93497	265672	McCulloch (93)	29	Ordovician	N of Leenane (N59)	152.33	12.65	1.81	20
LE	104900	267000	Tulip	247	Ordovician	Partry Mts	271.23	12.43	2.12	20
MT1	184980	378454	Tulip	20	Carboniferous	Milltown	190.85	12.35	2.33	20
OM1	164223	327635	Tulip	100	Caledonian	Ox Mountains	153.95	12.79	1.40	20
OM2	123383	304852	Tulip	11	Caledonian	Pontoon Bridge	154.75	13.27	1.31	20

Table 5.2. Apatite fission track samples taken from Allen *et al.* (in press.).

Sample	Easting	Northing	Reference	Depth bsl (m)	Statigraphic age	Well	AFT age	error	MTL	error	SDV	P T	GG	Track length distribution (μm)																			
														1	2	3	4	5	6	7	8	9	10	11	12	13	14	15	16	17	18	19	20
GC564-4	132592	569388	Gibson (1996)	-2475	56-50	132/15-1	222.20	23.1	12.76	0.14	1.35	48	32											8	20	29	28	12	1		1	1	1
GC564-6	132592	569388	Gibson (1996)	-2782	56-50	132/15-1	178.30	34.3	11.93	0.59	2.13	55	32								1			4	3	1	1	3					
GC564-7	132592	569388	Gibson (1996)	-3027	61-56	132/15-1	91.00	25.3	12.99	0.69	1.83	61	32											1	1	1	2	1	1				
GC564-10	132592	569388	Gibson (1996)	-3339	61-56	132/15-1	102.10	25.4	12.45	0.33	1.58	68	32									1		4	3	5	6	4					
GC564-13	132592	569388	Gibson (1996)	-3524	65-60	132/15-1	39.50	19.3				72	32																				
GC564-23	132592	569388	Gibson (1996)	-4095	2700	132/15-1	1.20	0.6				85	32																				
GC651-1	69382	371433	Gibson (1997)	-507	200-195	19-5/1	177.90	38.3	12.09	0.66	2.18	20	20.5									1	1	3		2	1	2	1				
GC651-3	69382	371433	Gibson (1997)	-809	250-210	19-5/1	276.50	16.6	12.26	0.17	1.83	28	20.5					1			1	3	9	11	20	28	25	16	3				
GC651-4	69382	371433	Gibson (1997)	-1074	309-305	19-5/1	256.30	19.3	12.68	0.33	1.88	36	20.5								1		3	1	5	8	9	4	1		1	3	
GC651-8	69382	371433	Gibson (1997)	-1448	338-335	19-5/1	197.70	19.3	10.90	0.24	1.56	46	20.5								1	3	8	9	12	2	5	1				
GC651-10	69382	371433	Gibson (1997)	-1859	338-335	19-5/1	132.30	9.5	10.57	0.26	2.60	57	20.5		1			1	4	2	9	10	10	16	15	15	9	8	1				
GC651-12	69382	371433	Gibson (1997)	-2507	348-342	19-5/1	86.10	14.2	10.82	0.19	2.00	75	20.5				1	1		2	4	10	16	22	29	12	15	3					
GC492-2.1	117344	458951	Green (1993)	-1013		12/13-1a						17	27																				
GC492-5	117344	458951	Green (1993)	-1724	135-132	12/13-1a	137.90	19.9	12.95	0.31	1.61	36	27										1	2	7	2	7	6	3				
GC492-7	117344	458951	Green (1993)	-1844	135-132	12/13-1a	236.30	17.1	11.76	0.21	2.09	39	27		1			2				3	6	14	20	28	17	7	2				
GC492-8	117344	458951	Green (1993)	-1995	144-135	12/13-1a	221.90	18.8	11.31	0.23	2.17	42	27			1		1		2	1	6	7	11	26	17	13	1	3				
GC492-11	117344	458951	Green (1993)	-2248	235-210	12/13-1a	242.10	31.7	11.19	0.17	1.73	48	27				1			1	1	6	14	18	28	21	9	3	1				
GC492-13	117344	458951	Green (1993)	-2521	245-235	12/13-1a	211.20	23.1	10.92	0.18	1.78	54	27							1	5	6	17	25	23	14	3	7	1				
GC492-15	117344	458951	Green (1993)	-2774	245-235	12/13-1a	190.00	12.5	11.10	0.22	2.19	60	27			1		2			1	8	18	17	18	21	9		2	1		1	
GC375-1	-15995	236284	Arne (1992)	-650	161-155	27/13-1	200.40	24.7	12.68	0.38	2.27	19	27						1			1	1	2	9	6	5	8	2				
GC375-2	-15995	236284	Arne (1992)	-955	174-161	27/13-1	196.80	19.4	12.73	0.27	1.45	27	27											4	5	10	6	3	1	1			
GC375-3	-15995	236284	Arne (1992)	-1432	174-161	27/13-1	154.20	16.2	11.86	0.24	2.09	40	27							1		4	10	15	14	11	9	8	2	3			
GC375-4	-15995	236284	Arne (1992)	-1700	174-161	27/13-1	152.70	26.5	10.68	0.53	3.10	47	27		2							5	6	5	3	8	1	3			1		
GC375-5	-15995	236284	Arne (1992)	-2262	195-187	27/13-1	23.90	8.8				62	27																				
GC375-6	-15995	236284	Arne (1992)	-2475	208-204	27/13-1	129.20	101	10.93	0.39	0.78	67	27										1	1	2								

Table 5.3. Apatite fission track data from samples in four offshore wells taken from Gibson (1996), Green (1993), Arne (1992), Gibson (1997). Depth of samples are taken from cuttings and is therefore an approximation; AFT age is apatite fission track age; MTL is mean track length; SDV is the standard deviation; P.T is the present day temperature; G.G is the geothermal gradient.

	Time (My)	Temp (°C)	Geological evidence
GC651-12	345±3	10±10	stratigraphic age
	328	40±15	burial of 1323 m (40°C)
	323±5	80±40	unconf. Min temp 40°C
	318	40±15	burial of 1323 km (40°C)
	305	48±15	burial of +271 m (+8°C)
	280±25	90±40	unconf. Min temp 48°C
	256	48±15	burial of 1594 m (48°C)
	195	63±15	burial of +512 m (+15°C)
	100±95	90±40	unconf. Min. temp of 50°C
	100±95	90±40	unconf. Min. temp of 50°C
	100±95	90±40	unconf. Min. temp of 50°C
	100±95	90±40	unconf. Min. temp of 50°C
	100±95	90±40	unconf. Min. temp of 50°C
	5	63±5	burial of 2006 m (63°C)
	0	75	present day temperature
GC651-10	336.5±1.5	10±10	stratigraphic age
	328	20±10	burial of 673 m (20°C)
	323±5	70±50	unconf. Min temp 20°C
	318	20±10	burial of 673 m (20°C)
	305	28±10	burial of +271 m (+8°C)
	280±25	80±50	unconf. Min temp 28°C
	256	28±10	burial of 944 m (28°C)
	195	43±10	burial of +512 m (+15°C)
	100±95	80±40	unconf. Min. temp of 40°C
	100±95	80±40	unconf. Min. temp of 40°C
	100±95	80±40	unconf. Min. temp of 40°C
	100±95	80±40	unconf. Min. temp of 40°C
	100±95	80±40	unconf. Min. temp of 40°C
	100±95	80±40	unconf. Min. temp of 40°C
	5	50±5	burial of 1456 m (50°C)
	0	57	present day temperature
GC651-8	336.5±1.5	10±10	stratigraphic age
	328	18±10	burial of 271 m (+8°C)
	323±5	70±50	unconf. Min temp of 18°C
	318	18±10	burial of 271 m (18°C)
	305	26±10	burial of +271 m (+8°C)
	280±25	70±50	unconf. Min temp 26°C
	256	26±10	burial of 542 m (26°C)
	195	41±10	burial of +512 m (+15°C)
	100±95	80±40	unconf. Min temp of 41°C
	100±95	80±40	unconf. Min temp of 41°C
	100±95	80±40	unconf. Min temp of 41°C
	100±95	80±40	unconf. Min temp of 41°C
	100±95	80±40	unconf. Min temp of 41°C
	5	41±5	burial of 1054 m (41°C)
	0	46	present day temperature

	Time (My)	Temp (°C)	Geological evidence
GC651-4	400±100	80±80	possible inheritance
	400±100	80±80	possible inheritance
	307±2	10±10	stratigraphic age
	280±25	70±50	unconf. Min temp of 18°C
	256	18±10	burial of 168 m (+5°C)
	195	33±10	burial of +512 m (+15°C)
	100±95	80±50	unconf. Min temp of 33°C
	100±95	80±50	unconf. Min temp of 33°C
	100±95	80±50	unconf. Min temp of 33°C
	100±95	80±50	unconf. Min temp of 33°C
	100±95	80±50	unconf. Min temp of 33°C
	5	33±3	burial of 680 m (30°C)
	0	36	present day temperature
GC651-3	350±100	80±80	possible inheritance
	350±100	80±80	possible inheritance
	230±20	10±10	stratigraphic age
	195	22±10	burial of 0.415 (+12°C)
	100±95	70±50	unconf. Min temp of 22°C
	100±95	70±50	unconf. Min temp of 22°C
	100±95	70±50	unconf. Min temp of 22°C
	100±95	70±50	unconf. Min temp of 22°C
	100±95	70±50	unconf. Min temp of 22°C
	5	22±5	burial of 415 m (+12°C)
	0	28	present day temperature
GC651-1	300±100	80±80	possible inheritance
	300±100	80±80	possible inheritance
	197.5±2.5	10±10	stratigraphic age
	100±95	70±60	unconf. Min temp of 10°C
	100±95	70±60	unconf. Min temp of 10°C
	100±95	70±60	unconf. Min temp of 10°C
	100±95	70±60	unconf. Min temp of 10°C
	100±95	70±60	unconf. Min temp of 10°C
	5	10±10	erosion in unconf.
	0	20	present day temperature

Table 5.4. Reconstruction of the initial thermal history of each sample from the geology of well 19/5-1. The temperature of each sample is given at different times. When the sample was at the surface (e.g. unconformity, time of deposition) a temperature of 10±10°C is assumed. A geothermal gradient of 20-40°C was used to do the conversion from meters to temperatures.

Sample	$Time_1$ (My)	$Temp_1$ (°C)	$Time_2$ (My)	$Temp_2$ (°C)	$Time_3$ (My)	$Temp_3$ (°C)
GC651-12			31-42	88-96		
GC651-10			32-42	85-91	60-65	89-104
GC651-8	12-18	79-82	28-39	82-92	68	87
GC651-3			26-47	60-71		
GC651-1	16	62				

Table 5.5. Summarised maximum palaeo-temperatures reached for each sample in well 19/5-1. Each sample was modelled between three and six times and all or most of the resulted thermal histories modelled show maximum palaeo-temperatures ranges at the time ranges indicated in the table for three possible different events.

	Time (My)	Temp (°C)	Geological evidence
GC942-15	350±100	80±80	possible inheritance
	350±100	80±80	possible inheritance
	240±5	10±10	stratigraphic age
	205	22±8	burial of 735 m (22°)
	172.5±32.5	70±50	unconf. Min temp of 22°C
	140	22±8	burial of 735 m (22°)
	34	59±13	burial of +1251 m (+37°C)
	18±16	90±30	unconf. Min temp of 59°C
	0	60	present day temperature
GC942-13	350±100	80±80	possible inheritance
	350±100	80±80	possible inheritance
	240±5	10±10	stratigraphic age
	205	14±6	burial of 482 m (14°C)
	172.5±32.5	70±60	unconf. Min temp of 14°C
	140	14±6	burial of 482 m (14°C)
	34	51±13	burial of +1251 m (+37°C)
	18±16	80±30	unconf. Min temp of 51°C
	0	54	present day temperature
GC942-11	350±130	80±80	possible inheritance
	350±130	80±80	possible inheritance
	222.5±12.5	10±10	stratigraphic age
	205	6±3	burial of 209 m (6°C)
	172.5±32.5	70±60	unconf. Min temp of 10°C
	140	6±30	burial of 209 m (6°C)
	34	43±13	burial of +1251 m (+37°C)
	18±16	80±40	unconf. Min temp of 43°C
	0	48	present day temperature

	Time (My)	Temp (°C)	Geological evidence
GC942-8	300±150	80±80	possible inheritance
	300±150	80±80	possible inheritance
	140	10±10	stratigraphic age
	34	37±13	burial of +1251 m (+37°C)
	18±16	80±40	unconf. Min temp of 37°C
	0	42	present day temperature
GC942-7	300±160	80±80	possible inheritance
	300±160	80±80	possible inheritance
	133.5±1.5	10±10	stratigraphic age
	34	31±12	burial of 1056 m (31°C)
	18±16	70±40	unconf. Min temp of 31°C
	0	39	present day temperature
GC942-5	300±160	80±80	possible inheritance
	300±160	80±80	possible inheritance
	133.5±1.5	10±10	stratigraphic age
	34	28±10	burial of 936 m (28°C)
	18±16	70±40	unconf. Min temp of 28°C
	0	36	present day temperature

Table 5.6. Reconstruction of the initial thermal history of each sample from the geology of well 12/13-1a. The temperature of each sample is given at different times. When the sample was at the surface (e.g. unconformity, time of deposition) a temperature of 10±10°C is assumed. A geothermal gradient of 20-40°C was used to do the conversion from meters to temperatures.

Sample	$Time_1$ (My)	$Temp_1$ (°C)
GC492-13	25-33	91-97
GC492-11	18-33	90-92
GC492-8	29-33	84-94
GC492-7	19-30	81-89
GC492-5	24-34	79-80

Table 5.7. Summarised maximum palaeo-temperatures reached for each sample in well 12/13-1a. Each sample was modelled six times and all or most of the resulted thermal histories modelled show maximum palaeo-temperatures ranges at the time ranges indicated in the table.

	Time (My)	Temp (°C)	Geological evidence
GC564-10	200±140	80±80	possible inheritance
	200±140	80±80	possible inheritance
	58.5±2.5	10±10	stratigraphic age
	34±4	44±12	burial of 1633 m
	33±5	75±43	unconf. Min temp of 32°C
	30±2	44±12	burial of 1633 m
	0	68	present day temperature
GC564-7	200±140	80±80	possible inheritance
	200±140	80±80	possible inheritance
	58.5±2.5	10±10	stratigraphic age
	34±4	35±10	burial of 1321 m
	33±5	75±50	unconf. Min temp of 25°C
	30±2	35±10	burial of 1321 m
	0	61	present day temperature
GC564-6	200±150	80±80	possible inheritance
	200±150	80±80	possible inheritance
	53±3	10±10	stratigraphic age
	34±4	30±10	burial of 1076 m
	33±5	70±50	unconf. Min temp of 20°C
	30±2	30±10	burial of 1076 m
	0	55	present day temperature
GC564-4	200±150	80±80	possible inheritance
	200±150	80±80	possible inheritance
	53±3	10±10	stratigraphic age
	34±4	20±5	burial of 769 m
	33±5	70±55	unconf. Min temp of 15°C
	30±2	20±5	burial of 769 m
	0	48	present day temperature

Table 5.8. Reconstruction of the initial thermal history for each sample from the geology of well 132/15-1. The temperature of each sample is given at different times. When the sample was at the surface (e.g. unconformity, time of deposition) a temperature of 10±10°C is assumed. A geothermal gradient of 20-40°C was used to do the conversion from meters to temperatures.

Sample	$Time_1$ (My)	$Temp_1$ (°C)
GC564-10	31-36	90-103
GC564-7	32-34	38-112
GC564-6	31-34	73-111

Table 5.9. Summarised maximum palaeo-temperatures reached for each sample in well 132/15-1. Each sample was modelled four times and all or most of the resulted thermal histories modelled show maximum palaeo-temperatures ranges at the time ranges indicated in the table.

	Time (My)	Temp (°C)	Geological evidence
GC375-6	300±130	80±80	possible inheritance
	300±130	80±80	possible inheritance
	206±2	10±10	stratigraphic age
	155±3	60±20	burial of 2025 m (60°C)
	80±78	80±40	unconf. Min temp of 40°C
	0	67	present day temperature
GC-375-4	300±130	80±80	possible inheritance
	300±130	80±80	possible inheritance
	167.5±6.5	10±10	stratigraphic age
	155±3	37±13	burial of 1250 m
	80±78	80±50	unconf. Min temp of 24°C
	0	47	present day temperature
GC375-3	300±130	80±80	possible inheritance
	300±130	80±80	possible inheritance
	167.5±6.5	10±10	stratigraphic age
	155±3	30±10	burial of 982 m
	80±78	70±50	unconf. Min temp of 20°C
	0	40	present day temperature
GC375-2	300±130	80±80	possible inheritance
	300±130	80±80	possible inheritance
	167.5±6.5	10±10	stratigraphic age
	155±3	15±5	burial of 505 m
	80±78	70±60	unconf. Min temp of 10°C
	0	27	present day temperature
GC375-1	300±130	80±80	possible inheritance
	300±130	80±80	possible inheritance
	158±3	10±10	stratigraphic age
	155±3	15±5	burial of 2000 m
	80±78	70±60	unconf. Min temp of 10°C
	0	19	present day temperature

Table 5.10. Reconstruction of the initial thermal history for each sample from the geology of well 27/13-1. The temperature of each sample is given at different times. When the sample was at the surface (e.g. unconformity, time of deposition) a temperature of 10±10°C is assumed. A geothermal gradient of 20-40°C was used to do the conversion from meters to temperatures.

Sample	Time$_1$ (My)	Temp$_1$ (°C)	Time$_2$ (My)	Temp$_2$ (°C)	Time$_3$ (My)	Temp$_3$ (°C)
GC375-6	13-14	92-94				
GC375-3					74-99	86-93
GC375-2			22-50	75-80		

Table 5.11. Summarised maximum palaeo-temperatures reached for each sample in well 27/13-1. Each sample was modelled eight times and all or most of the resulted thermal histories modelled show maximum palaeo-temperatures ranges at the time ranges indicated in the table.

	Palaeocene (66 – 54 My)	Eocene (52 – 36 My)	Oligocene (36 – 24 My)	Miocene to present (24 – 0 My)
19/5-1 sample GC651-4	T_{start} 70°C T_{end} 75°C dT/dz 20.5 °C km^{-1} Δz -0.240 km	T_{start} 75°C T_{end} 78°C dT/dz 20.5 °C km^{-1} Δz -0.150 km	T_{start} 78°C T_{end} 82°C dT/dz 20.5 °C/km Δz -0.240 km	T_{start} 82°C T_{end} 46°C dT/dz 20.5 °C/km Δz 1.760 km
12/13-1a sample GC492-13	T_{start} 43°C T_{end} 48°C dT/dz 27 °C/km Δz -0.180 km	T_{start} 48°C T_{end} 60°C dT/dz 27 °C/km Δz -0.440 km	T_{start} 60°C T_{end} 90°C dT/dz 27 °C/km Δz -1.110 km	T_{start} 90°C T_{end} 60°C dT/dz 27 °C/km Δz 1.110 km
132/15-1 sample GC564-10	T_{start} 18°C T_{end} 32°C dT/dz 32 °C/km Δz -0.440 km	T_{start} 32°C T_{end} 70°C dT/dz 32 °C/km Δz -1.190 km	T_{start} 70°C T_{end} 50°C dT/dz 32 °C/km Δz 0.620 km	T_{start} 50°C T_{end} 68°C dT/dz 32 °C/km Δz -0.560 km
27/13-1 sample GC375-3	T_{start} 80°C T_{end} 72°C dT/dz 27 °C/km Δz 0.300 km	T_{start} 72°C T_{end} 62°C dT/dz 27 °C/km Δz 0.370 km	T_{start} 62°C T_{end} 55°C dT/dz 27 °C/km Δz 0.260 km	T_{start} 55°C T_{end} 47°C dT/dz 27 °C/km Δz 0.300 km

Table 5.12. Denudation in kilometres (Δz) for each well in the different time intervals calculated using eq. 5.1. The well sample with the modelled misfits ~1 was used as best representative. The palaeo-geothermal gradient taken from AFT and VT data for each well in Geotrack reports was used (Table 5.3). Negative values indicate deposition and positive values indicate denudation.

	Mean thickness (m)	Duration (My)	Denudation Rate (m/My)
Miocene to present (23 – 0 My)	360	18	20
Oligocene (36 – 23 My)	110	13	8
Eocene (53 – 36 My)	270	17	16
Palaeocene (66 – 53 My)	120	13	9
Cenozoic (66 – 0 My)	870	66	13

Table 5.13. Spatially and temporally-averaged denudation rates for the northwestern Irish continental margin, derived from apatite fission track modelling.

	Volume of solid sediment denuded (km^3)	Volume of solid sediment deposited (km^3)	
Pliocene to Pleistocene (2-0)	22,000	14,300	25,300
?Miocene to Pliocene (23-2 My)		11,000	
?Oligocene (36-23 My)	5,000	10,200	
Eocene (53-36 My)	16,900	26,300	
Palaeocene (66-53 My)	7,000	43,700	
Cenozoic (66-0 My)	50,800	104,400	

Table 5.14. Volumes of solid sediment deposited in the northeastern Rockall Basin and denuded off northwestern Ireland.

	Denudation rates (m/My)	Accumulation rates (m/My)	
Plio-Pleist. (5 – 0 My)	20	51	19
?Miocene (23 – 5 My)		14	
?Oligocene (36 – 23 My)	8	22	
Eocene (53 – 36 My)	16	38	
Palaeocene (66 – 53 My)	9	93	
Cenozoic (66 – 0 My)	13	27	

Table 5.15. Comparison between spatially and temporally-averaged denudation and deposition rates [m/My] taken from apatite fission track modelling and seismic interpretation respectively.

	Palaeocene (66-53 My)	Eocene (53-36 My)	?Oligocene (36-23 My)	?Miocene to present (23-0 My)
Flexural subsidence (m)	700	600	200	400
Subsidence rate (m/My)	54	35	15	17

Table 5.16. Maximum subsidence rates during the Cenozoic due to sedimentary loading in the Rockall Basin using T_e of 10 km.

	Palaeocene (66-53 My)	Eocene (53-36 My)	?Oligocene (36-23 My)	?Miocene to present (23-0 My)
Flexural uplift (m)	150	350	100	300
Uplift rate (m/My)	12	20	8	13

Table 5.17. Maximum uplift rate during the Cenozoic due to sedimentary loading in the Rockall Basin using T_e of 10 km.

Chapter 6 Conclusions and discussion

6.1 Conclusions

- Many of the present-day river systems in northwestern Ireland are out of equilibrium and their profiles contain knickpoints up to 60 m. Some of these knickpoints are clearly due to differential erodibility between adjacent lithologies, particularly where rivers cut across metadolerite intrusions, Dalradian quartzites and Ordovician sandstones.

- Other knickpoints in northwestern Ireland do not appear to be controlled by bedrock lithology, and occur in several rivers flowing across the same fault. In these cases knickpoint formation is very likely to be due to a structural control, and possibly by Cenozoic tectonic activity on that particular fault. However, preferential erosion along an existing but inactive fault zone cannot be ruled out.

- A regional morphometric and lithological analysis concludes that the topography of northwestern Ireland cannot be explained entirely by differential erosion due to lithology only and a partial structural control is suggested.

- Movement on a number of faults was inferred from a combination of evidence from river knickpoints, morphological anomalies, abrupt and non-lithologically controlled gradients in relief and wind gaps, including the Leannan, Gweebarra, Barneslough, Aghla, Kittyfannan, Eglish-Belshade, Laghy, Glenade, Glencar, Ox Mountains, Bangor and Erriff faults. These faults trend northeast, east and northwest. Most of the northeast-trending faults seem to have been down thrown to the northwest.

- The Cenozoic succession in the Rockall Basin is conformable in the basin centre and thins unconformably (through both onlap and downlap) onto the basin margins over about 30 km of horizontal distance. Palaeocene and ?Miocene packages are seen onlapping onto their respective basal surfaces. Eocene,

?Oligocene and Plio-Pleistocene packages locally downlap onto their basal unconformities.

- During the Palaeocene a major depocentre developed in the northwest of the study area, both north and south of the Hebrides Terrace Seamount. There was also a local depocentre in the southwest of the study area. Total accumulation rates, averaged over the study area were 93 m My^{-1}.

- Early Eocene sand progradation of unknown sedimentary environment was common in the northeastern Irish Rockall Basin in both the north and the south of the study area, suggesting that Ireland, as well as Scotland, was providing sediments to the basin. A depocentre in the northwestern side of the study area has up to 1470 m of Eocene sediment, where the margin changes trend from north to northeast.

- Discontinuous normal faults are mapped along the main basin boundary fault in the northeastern Irish Rockall Basin offsetting base Tertiary to base Eocene reflectors. Base Tertiary offsets are on the order of hundreds of metres while base Eocene offsets are only a few tens of metres. Within the study area, normal offsets seem to increase in magnitude to the south.

- During the late Eocene to early Oligocene, tectonic inversion and major subsidence took place in the Rockall Basin. Late Eocene to early Oligocene compression is expressed as east, north and east-northeast trending anticlines that apparently developed in a transpressional regime. Some of these anticlines were formed by reactivation of older north-northeast trending normal faults. This event was coeval and compatible with southeast-directed North Atlantic ridge push.

- The post-late Eocene unconformity is a markedly angular boundary that erodes upper Eocene sediments, whilst post-upper Eocene sediments onlap onto it. The ?Oligocene isochron map shows small local sediment depocentres adjacent to and downslope of the basin margin with progradation of unknown environment, suggesting local sediment input from the Irish continental margin during post-late

Eocene time. The post-late Eocene and pre-Pliocene isopach maps show a decrease in accumulation rates from 38 m/My in the Eocene to 22 and 14 m/My in the ?Oligocene and ?Miocene, respectively.

- Basinal reflections of presumed ?Miocene age onlap onto the ?lower Miocene unconformity. This package can be visualised as a sedimentary wedge pinching out northeastwards.

- Plio-Pleistocene accumulation rates are relatively high, at up to 51 m My^{-1}. During this time a deltaic progradational phase took place in the north of the study area, with sediment input from Scotland and to a lesser extent, from Ireland. Two separate progradational events are separated by a local intra Plio-Pleistocene unconformity.

- Fission track modelling of samples from four wells offshore northwestern Ireland allows a reliable, but very spatially limited, estimate of the Cenozoic thermal history of the northwestern Irish offshore basins. Modelling of various samples in each well results in consistently similar Cenozoic thermal histories. However samples within different wells show different thermal histories. Well 19/5-1 reached temperatures of 60 to 96°C between 28 and 42 My. Well 12/13-1a reached temperatures of 70 to 97°C at about 18 to 34 My. Well 132/15-1 reached temperatures of 38 to 112°C between 31 to 36 My. Well 27/13-1 shows a general cooling trend during the Cenozoic.

- Conversion of Cenozoic thermal histories to denudation estimates was done using a geothermal gradient of 27°C km^{-1}, based on well data. Well 12/13-1a and well 132/15-1 show net Cenozoic deposition, with up to 400 m and 1500 m of burial, respectively. Wells 19/5-1 and 27/13-1 show net Cenozoic denudation ranging between 600 to 1400 m.

- During the Cenozoic 50,800 km^3 of sediment were denuded from northwestern Ireland with temporally and spatially averaged surface denudation rate of 13 mMy^{-1}. Over the same time interval, 104,400 km^3 of sediment were deposited in the northeastern Irish Rockall Basin at an average rate of 27 m My^{-1}.

- The Eocene is characterised by an increase in marginal denudation onshore and in the Erris Basin, which coincides with a progradational phase of unknown environment in the northeastern Irish Rockall Basin. The post-Oligocene is characterised by another increase in marginal denudation, which might explain the lack of preservation of Tertiary sediments in onshore Ireland, and in the Slyne and Erris Basins. Local marginal progradation of unknown environment during the Oligocene might be related to this increase in denudation.

- Cenozoic flexure caused by sedimentary loading and unloading gave rise to a maximum of 700 m of rock uplift on the Irish Shelf and onshore northwestern Ireland using a T_e of 30 km and up to 1000 m using a T_e of 3 km. Therefore at least 700 m of the Cenozoic onshore uplift might be explained by flexure.

- Flexural deflection using a T_e as low as 3 km can account for 2100 m of Cenozoic basin subsidence, but another 2600 m of thermal or tectonic subsidence, palaeobathymetry or changes in sea level, are needed to explain the present day depths to the base Tertiary and intra-Cenozoic unconformities.

6.2 Discussion

It is trivial to think that resistant lithologies in any landscape will survive erosion better than less resistant ones. However, the landscape in a passive margin such as the northwestern Irish margin during the Cenozoic is under the effect of many processes such as tectonic activity due to continental rifting and oceanic ridge push, variable climate conditions and sea level, differential erosion and flexural compensation. All of these factors together contribute to the formation of a landscape. The mountains in northwestern Ireland result from a combination of all these processes.

Topographic scarps such as those formed on the southern side of the Blue Stack Mountains and the Nephin Beg Mountains coincide with large contrasts in lithological resistance, although lithological contrasts do not totally explain the topography. Study of the elevation distribution of a single formation allowed areas where the topography cannot simply be explained by lithological changes to be located. However, intra-

formational lithological changes and joint and fracture patterns might also play a role in landscape formation but this has not been considered in this work.

River knickpoints are found along several streams crossing the Boundary Fault, on the southern side of the Blue Stack Mountains, but again lithological differences are difficult to discount in this area. In other cases knickpoints are found within the same lithological formation, and knickpoint formation due to differential erosion can be discriminated against. In those cases knickpoints are assumed to form due to a structural control. However, the influence of bedrock strength properties imparted by jointing and fracturing in knickpoint formation and on escarpment retreat has not been considered and might be an important factor (Weissel and Seidl 1997).

The combined evidence of river knickpoints in several catchments, morphological anomalies, non-lithologically controlled high relief and wind gaps across a fault is here taken to suggest Cenozoic movement on that fault. The maximum relief of structurally controlled river knickpoints is 60 m. If they are indeed tectonically controlled, one can argue that maximum fault displacements of 60 m occurred along some of the northwestern Irish onshore faults since establishment of the present catchment system. Glacial erosion may have enhanced knickpoints leading to an overestimate of displacement. Conversely, the fluvial system tends to reach equilibrium through time retreating the knickpoint vertically and horizontally, leading to an underestimate of the original maximum displacement. It seems likely that, if Cenozoic displacements have occurred on faults in northwestern Ireland, total relative displacements have been on the order of, at most, several hundred metres. This estimate is constrained as much by the present distribution of elevation and relief as by catchment morphology.

One can only vaguely attempt to date fault activity by knickpoint migration since the knickpoints were formed. Structurally controlled knickpoints in northwestern Ireland have retreated from the position of the fault to the present day maximum curvature of the knickpoint by a maximum of 2 km of horizontal distance measured along the river profiles. Assuming that the structurally controlled knickpoints were generated by Cenozoic fault activity, and assuming a rate of knickpoint migration, estimation of the most recent fault displacement is potentially feasible. In Hawaiian basalts, rates of

knickpoint migration are about 2 km/My (Burbank and Anderson 2001). It seems likely, following Clayton and Shamoon's (1998) scale of resistance for British rocks, that Eocene basalts are less resistant to erosion than the Dalradian and Carboniferous Formations. Weissel and Seidl (1997) inferred an average rate of large-scale knickpoint retreat and therefore escarpment retreat in eastern Australia of 2 km My^{-1}, independent of lithology. Other workers have considered that escarpments on passive margins propagate inland at a rate of 1 km My^{-1}. Applying rates of knickpoint migration of 1 to 2 km/My gives a first-order approximation for the time at which fault activity in northwestern Ireland may have ceased on the order of a several million years ago. It is thus possible, within very large error bars, to suggest that these faults were active during the Plio-Pleistocene.

The isostatic or flexural effect of unloading and loading by ice and sediment during the last two million years might be responsible for this subdued tectonic activity. The topography, where tectonically controlled, might be due to the combination of accumulated flexural uplift during the Cenozoic caused by denudation onshore Ireland and sedimentation in the offshore basins west of Ireland.

Relief-derived denudation rate estimates were calculated using a very simplistic formula that ignores the influences of climate and tectonic displacement and includes all the complexity of denudational processes into the single measure of relief. Relief can be a useful tool to measure denudation over unknown periods of time (Ahnert 1970; Summerfield 1991). Denudation rate estimates derived from thermochronology may also have large uncertainties (see Section 5.3.4), particularly in the choice of palaeo-geothermal gradients in converting temperatures to depths and in the possible influence of hydrothermal fluids (Brown and Summerfield 2000), but they do at least constrain the timing of cooling and therefore denudation. Modelling of offshore wells allows more reliable results on denudation than onshore, because the preservation of a Mesozoic to Cenozoic sequence allows prediction of an initial thermal history and a geothermal gradient. Combining independent evidence helps to minimise errors and achieve a more realistic approach. Low values of relief in the Ox Mountains and the Blue Stack Mountains imply lower denudation rates than in other upland areas in northwestern Ireland over time periods possibly as long as 66 My, as shown by the fission track-derived denudation rates.

The Cenozoic isopach maps in the northeastern Irish Rockall Basin, yield first-order information on the probable source regions for the Cenozoic sediment. Isopach maps in the southern part of the study area must be treated with caution because of the lack of well control, resulting in large uncertainties in the age control on Cenozoic surfaces. Isopach maps of the northern area are better constrained by both well and seismic data. The discrepancy between Palaeocene volumes of sediment denuded and deposited (Table 5.15) might be partially related to the lack of control on the seismic velocity of this section. However, another possibility might be that Early Tertiary igneous activity related to continental rifting caused regional surface uplift increasing from south to north, including the northern Rockall Basin (Brodie & White 1995). This surface uplift resulted in major denudation in the northern Rockall Basin and adjacent margins, and sedimentation in the south. This event might partially explain low denudation rates in Ireland but high sedimentation rates in the northeastern Rockall Basin during the Early Tertiary. Generally, Cenozoic sediment volumes deposited in the northeastern Irish Rockall Basin are twice as large as the volume of material denuded from northwestern Ireland. This may be indirect evidence of a Cenozoic drainage system extending far beyond northwestern Ireland to the east and northeast and contributing significant amounts of sediment to the northeastern Rockall Basin. Eocene denudation in northwestern Ireland can only account for half of the sedimentation in the Rockall Basin. However, the relative increase in onshore denudation might be partially responsible for the coeval offshore sand progradation northwest of Ireland.

Deposition in the Rockall Basin may have triggered greater denudation of onshore Ireland by marginal flexural rock uplift. The flexural model results are directly related to the onshore estimates of denudation and offshore deposition. Cenozoic sedimentation and denudation in northwestern Ireland could have triggered up to 1000 m of flexural uplift. This uplift is partly reflected in the present day topography, by its elevation and maybe by small topographic or fluvial vertical offsets. However, tectonic uplift and denudation must be added to the flexural uplift, to obtain the final topography.

Mainly northeast-oriented structures have been recognized to be active in the Cenzoic in both the onshore and offshore. Offshore normal faults with offsets in the order of hundreds of metres were active in the Palaeocene and early Eocene. Using an Andersonian strain-stress conversion, one can suggest an approximately northwest extension direction for the Palaeocene to early Eocene. This extension direction has been suggested by Doré *et al.* (1999) in other basins further north along the northwestern European plate. Late Eocene to early Oligocene transpression is recognised in the northeastern Irish Rockall Basin and might be attributed to a southeast-directed ridge push. However, the strain might also be enhanced by the Alpine closure between Africa and Europe at this time (Zoback 1992; Müller *et al.* 1992). This Late Eocene to early Oligocene transpression cannot be related to any particular sedimentary or denudational pattern.

6.3 Future work

Now that the magnitude of the flexural subsidence in the Rockall Basin has been constrained, a better undestanding of the subsidence caused by thermal cooling, sea level changes and palaeobathymety are needed to fully describe the Cenozoic evolution of the Rockall Basin. For this one would need more well data in the Rockall Basin.

An analysis of the effect of fractures and intraformational discontinuities on the topography would be useful to discriminate river knickpoints and high relief caused by fault activity from those caused by differential erosion within fractured zones. Field structural mapping of those onshore faults located in this study would be useful to investigare and corroborate recent tectonic activity. However, Cenozoic structural mapping in areas of pre-Mesozoic bedrock is always uncertain.

Appendixes

Appendix 1 Procedure for preparation of sediment samples for pollen analysis

The use of a spike for absolute frequency analysis requires a modified procedure involving exact volume preparations.

1. Record sample number, site, location, and sediment type on preparation sheet or in a preparation log book.

2. Make a smear of raw sediment in water on a microscope slide, and examine it for inorganic material (note size of particles, mineralogy, presence of diatoms, sponge spicules, chrysophyte cysts, and other siliceous microfossils) and organic material such as cellular fragments, fungal hyphae, algae, chitin, and charcoal fragments (note size of fragments and composition). Record these observations and estimate the frequency of the various components on a five point scale (abundant, frequent, occasional, rare, absent). Alternatively use the sediment description of Troels-Smith, 1955.

3. If the sediment is calcareous:
Transfer 1-2 cm^3 of sediment to be labelled boiling tube and slowly add *c.* 10 cm^3 10% hydrochloric acid (HCl). Note this solution is caustic. Wear protective equipment When effervescence stops, place tube in boiling water bath and stir until effervescence again stops.
If sediment is highly calcareous, it will be necessary to centrifuge, decant, and repeat this step with fresh 10% HCl to ensure removal of all carbonates. If the tube threatens to froth over, reduce the foam with a squirt of acetone, away from any open flame. Centrifuge1 and decant. It is essential to remove all calcium carbonate if stage 9 is to be followed, otherwise insoluble calcium fluoride will be formed.

4. Wash with distilled water, centrifuge, decant. Repeat at least twice.

5. If the sample is non-calcareous : Transfer 1-2 cm^3 of sediment to a labelled boiling tube and add *c.* 10 cm^3 of 10% NaOH. Note this solution is caustic. Wear protective equipment. Place in a boiling water bath for no more than 2-5 minutes, and stir occasionally. Record the darkness of the supernatant, as a measure of the degree of humification of the sample.

6. Sieving: If sediment contains much coarse mineral material or organic debris, strain and wash it through a fine sieve (about 120□m mesh) into a plastic centrifuge tube. Wash the residue on the screen thoroughly with a jet of distilled water. Centrifuge and decant the NaOH. Place the coarse residues trapped in the mesh screen in a labelled petri dish, and examine with a binocular microscope for seeds, fruit, moss remains, etc.

7. Wash at least five times with distilled water until no trace of brown colour remains in the

1 The centrifuging stage requires spinning at 3,000 rpm for 5 minutes. Carefully decant the supernatant. When working with acid/alkali solutions use the centrifuge in the fume cupboard. When decanting spent HF pour it into a labelled plastic bottle for specialist disposal

supernatant. When washing, gently stir the sediment in the bottom of the tube before adding water, thereby preventing the formation of lumps.

8. Wash with 10% HCl, centrifuge, and decant. Note this solution is caustic. Wear protective equipment

9. If the sediment contains much mineral matter, treat with 60% hydrofluoric acid (HF) using either one of the two alternatives below. Only handle HF in the fume cupboard and with full protective equipment (see above)

a) Hot HF. In the fume cupboard, add *c.* 10-15 cm^3 HF (wear correct protective clothing, face mask, rubber apron and gloves).

Stir with polyethylene rods, and place the centrifuge tubes in a boiling water bath for between *c.* 30 minutes and 2 hours. Stir occasionally. Remove the tubes from the water bath and add 95% methanol (to reduce specific gravity) to within 2 cm of the rim of the tube. Stir to mix well, and centrifuge. Carefully decant the HF (in the fume cupboard) into labelled plastic bottles for specialist disposal. If clay or silt remains, repeat.

b) Cold HF. In the fume cupboard, add *c.* 25 cm^3 HF (wear correct protective clothing, face mask, rubber apron and gloves). Leave in the fume cupboard for at least 8 hours (usually overnight), and stir occasionally. Stir, centrifuge, and decant. If silt or clay remains, repeat.

10. When all of the HF has been decanted half fill the tube with 10% HCl, and place in a boiling water bath for *c.* 15 minutes to remove colloidal silicates and silicofluorides. Centrifuge while still hot and decant. If much mineral residue remains, repeat the wash with hot 10% HCl one or more times. Generally continue this until the supernatant loses its yellow colour.

11. (seldom used -see P.Coxon) If the sediment contains much pyrite or related sulphide compounds, such as hydrotroilite, melnikovite, and marasite (Vallentyne, 1963), add *c.* 10 cm^3 10% nitric acid, and place in a boiling water bath for no more than 2 minutes. Centrifuge and decant. Note this solution is caustic. Wear protective equipment

12. Wash once with distilled water, centrifuge, and decant.

13. Stir, add *c.* 10 cm^3 glacial acetic acid, stir, centrifuge and decant. Note this solution is caustic. Wear protective equipment

14. Add 9 cm^3 acetic anhydride and 1 cm^3 concentrated sulphuric acid (wear complete protective clothing including rubber gloves and face mask). Stir. Place tube in boiling water bath for 2 minutes stirring once after 1 minute. Remove tube and fill with glacial acetic acid. Stir. Centrifuge and decant.
Note this solution is very caustic. Wear full protective equipment

15. Stir, add *c.* 10 cm^3 glacial acetic acid, stir, centrifuge, and decant. This removes the soluble

cellulose acetate products of acetolysis. Note this solution is caustic. Wear protective equipment

16. Stir, add *c.* 10cm^3 distilled water. Stir, centrifuge and decant.

17. Stir, add *c.* 9 cm^3 distilled water and 1 cm^3 10% NaOH to obtain the correct pH for subsequent staining. Test with indicator paper that the pH is *c.*7 (Faegri, 1936). Stir, centrifuge and decant.

18. Stir, add 1 or 2 drops of aqueous safranin (or base fuchsin), stir and add *c.* 10 cm^3 distilled water. Stir, centrifuge and decant.

19. Stir, add *c.* 10 cm^3 tertiary butyl alcohol (TBA -also called 2-methylpropan-2-ol check), stir, centrifuge and decant. Use the TBA in a fume cupboard. Avoid contact with the skin.

20. Wash sediment into a labelled vial with TBA using a Pasteur pipette. Stir, cork vial, gently centrifuge and decant.

21. Add silicone oil (2000ccs viscosity) equal in amount to the sediment in the vial, stir, and leave uncorked (but covered with a tissue, for 3-4 days in a drawer before counting.

22. Prepare a slide for counting by thoroughly stirring the residue in a vial, and by placing a small drop of the residue on the centre of a clean slide. It is convenient to do this over a guide square the size of the coverglass to be used (generally 24mm x 24mm). Add silicone oil if necessary to achieve the desired pollen concentration. The drop should be smeared out to each corner of the square and back again until it is evenly and thinly distributed over the whole area. Any coarse material should be moved with a clean needle and fine forceps. Add a no. 0 coverslip (use square coverslips, to minimise the effect of non - random pollen distribution on the slide (Brookes and Thomas, 1976). It is convenient to lightly tack the corners of the coverslip with nail polish. Aim to prepare slides between 15 to 20µm in thickness, so that they are as thin as possible to permit the most effective use of high resolution apochromatic objectives and yet without causing excessive compression and resultant changes in pollen size (Cushing, 1961).

Time spent in careful mounting and the choice of a good mounting medium help in producing consistent results in pollen analysis and reduce the amount of labour necessary to make them. Because detailed pollen analysis requires complete quantitative records of all fossil pollen and spores, the quantitative analysis should be as unbiased as possible, and the slides should permit ideal microscopic observation. It is important for both measurement and for identification of critical and /or deteriorated pollen that the orientation of individual grains can be changed during routine analysis. Of all the mounting media so far used, silicone oil most of all fulfils these requirements.

Appendix 2 Matlab program on decompaction of well 132/15-1

```
% The following program does the decompaction of well 132/15-1
%code modified from Allen and Allen (1990)
% calculations are done in km, but data should be entered in m and results will be in m
%define variables
zb = [967 1886 2830];%depth to base of each layer
zt = [767 967 1886];          %depth to top of each layer
zb=zb/1000.0;
zt=zt/1000.0;
T = zb - zt;
times=3;
units=3;
Nzt=zeros(units,times);       %decompacted depth to top
Nzb=zeros(units,times);       %decompacted depth to base
PHIo = 0.66;
c = 0.44;
Ratio=PHIo/c;

%operate
for j = 1:times;  %times at which we decompact
  for i = j:units;        %sedimentary layers we decompact
      if i==j
            Nzt(i,j)=0; %removing the first layer the new top depth is 0
      else
            Nzt(i,j)=Nzb(i-1,j);
      end         %the new depth to the top equals the new depth to base at the last j
%solution
      A=exp(-c*zt(i))-exp(-c*zb(i));
      B=exp(-c*Nzt(i,j));
      Right=Nzt(i,j)+T(i)-(Ratio*A)+(Ratio*B);
      Nzb(i,j)=1.0;                    %start iterating with 1 km
      Left=Nzb(i,j)+(Ratio*exp(-c*Nzb(i,j)));
      while Left<0.9999*Right | Left>1.0001*Right
            if Left>1.0001*Right
            Nzb(i,j)=Nzb(i,j)-abs(Right-Left);
            elseif Left<0.9999*Right
            Nzb(i,j)=Nzb(i,j)+abs(Right-Left);
            else Left>0.9999*Right
            end
  Left=Nzb(i,j)+(Ratio*exp(-c*Nzb(i,j)));
      end
  end
end
```

Appendix 3 Matlab program on decompaction of the Cenozoic of the Rockall Basin

The following program does the decompaction of isopach maps from the northeast Irish Rockall Basin using data well 132/15-1.

```
%decompaction code modified from Allen and Allen (1990)
%program to decompact the Rockall Trough (2D unconformities + time)
%zb matrixes are depth to base of layer

% load zb_plio zb_mio zb_oli zb_eo zb_pal  %must be already defined no data values = 0
zt_mio=zb_plio;
zt_oli=zb_mio;
zt_eo=zb_oli;
zt_pal=zb_eo;

zt=cat(3,zt_mio,zt_oli,zt_eo,zt_pal);          % unconformity matrix in 3D for the top
zb=cat(3,zb_mio,zb_oli,zb_eo,zb_pal);          % unconformity matrix in 3D for the base
zb=zb/1000.0;                                  %converts into kilometers
zt=zt/1000.0;
T = zb - zt;                                   %Thickness

times=4;                                       %number of times decompacting
units=4;                                       %number of layers decompacting
ymax=326;                                      %y horizontal coordinate
xmax=309;                                      %x horizontal coordinate
Nzt=zeros(xmax,ymax,units,times);              %defines new decompacted matrix (top)
Nzb=zeros(xmax,ymax,units,times);
PHIo = 0.66;                                   %taken from well 132/15-1
c = 0.44;
Ratio = PHIo/c;

%operate

for y=1:ymax;
 for x=1:xmax;
        for j = 1:times;
        for i = j:units;
                if i==j                        %because we put the top of the sequence
                                               %at 0

                Nzt(x,y,i,j)=0;
                else
                Nzt(x,y,i,j)=Nzb(x,y,i-1,j);   %make the top=last base
                end

%solution to Nzb iterating
```

```
A=exp(-c*zt(x,y,i))-exp(-c*zb(x,y,i));          %from zt and zb that we know
B=exp(-c*Nzt(x,y,i,j));                         %we know Nzt
Right=Nzt(x,y,i,j)+T(x,y,i)-(Ratio*A)+(Ratio*B); %Right=Left

Nzb(x,y,i,j)=1.0;                               %start iterating with
                                                %1km to calculate Nzb
Left=Nzb(x,y,i,j)+(Ratio*exp(-c*Nzb(x,y,i,j)));

 while Left<0.9999*Right | Left>1.0001*Right    % | means or
       if Left>1.0001*Right
       Nzb(x,y,i,j)=Nzb(x,y,i,j)-abs(Right-Left);
       elseif Left<0.9999*Right
       Nzb(x,y,i,j)=Nzb(x,y,i,j)+abs(Right-Left);
       else Left>0.9999*Right
       end

 Left=Nzb(x,y,i,j)+(Ratio*exp(-c*Nzb(x,y,i,j)));
 end
end
end
```

Appendix 4 Matlab program on flexure of the Rockall Basin

The following program simulates the flexure of a plate based on Hetenyi (1974).

```
%Constants are:

a = 500;                %width of half a column in m
xaxis = 0:2*a:499000;          %x axis for plotting purposes
ROm = 3300;             %density of mantle in kg/m3  10 km deep
ROa = 1.29;             %density of air in kg/m3
ROs = 2500;             %density of sedimentary column
g = 9.78;               %m/sec2
POISSON = 0.15;         %range value for a gnessic plate (0.04-0.15)
YOUNG = 0.7e11;         %range value for a gneissic plate (0.04-0.7 in Pa or kg/m*s2)
H = 30000;              %elastic thickness of plate in m
D = YOUNG*(H^3)/(12*(1-(POISSON^2)));          %flexural rigidity in kgm2/sec2 or Nm
LAMBDA = ((ROm - ROa)*g/(4*D))^0.25;
Q = (ROs - ROa)/(2*(ROm - ROa));

%the density of the different sedimentary columns is the same
%Variables are
        eo_prof;                %height of each sed. column in i in m

%Start operating
for i = 1:341;
        for j = 1:341;
        s = a*(2*i-1);  %distance from 0 to i in m
        x = a*(2*j-1);  %distance from 0 to j in m
    if  j<i;
        K1 = LAMBDA*(-x+s-a);
        K2 = LAMBDA*(-x+s+a);
        w(i,j) = -eo_prof(i)*Q*((exp(-K1)*cos(K1)-exp(-K2)*cos(K2)));
  elseif j==i;
        K3 = LAMBDA*(x-s+a);
        K4 = LAMBDA*(-x+s+a);
        w(i,j) = -eo_prof(i)*Q*(2-(exp(-K3)*cos(K3))-(exp(-K4)*cos(K4)));
  elseif j>i;
        K5 = LAMBDA*(x-s+a);
        K6 = LAMBDA*(x-s-a);
        w(i,j) = eo_prof(i)*Q*(exp(-K5)*cos(K5)-exp(-K6)*cos(K6));
  end;
end
end
W = sum(w);
plot(xaxis,W)
```

References

AHNERT, F. 1970. Functional relationships between denudation, relief and uplift in large mid-latitude drainage basins. *American Journal of Science*, **268**, 243-63.

AHNERT, F. 1996. Introduction to geomorphology. Arnold, London, 173p.

ALLEN, P. A. & ALLEN, J. R. 1990. Basin analysis; principles and applications. Blackwell Science, UK, 451p.

ALLEN, P. A., BENNETT, S. D., CUNNINGHAM, M. J. M., CARTER, A., GALLAGHER, K., LAZZARETTI, E., GALEWSKY, J., DENSMORE, A. L., PHILLIPS, W. E. A., NAYLOR, D. & SOLLA HACH, C. (in press). The Post-Variscan thermal and denudation history of Ireland. *In:* DORÉ, A. G. (ed) *The Exhumation of the Circum-Atlantic Margins.* Geological Society, Special Publication.

ALSOP, G. I. 1992. Late-Caledonian sinistral displacement across the Leannan fault system, Northwest Ireland. *Geological Journal*, **27**, 119-125.

ANDERTON, R., BRIDGES, P. H., LEEDER, M. R. & SELLWOOD, B. W. 1979. *A Dynamic Stratigraphy of the British Isles; a study in crustal evolution.* George Allen & Unwin Ltd., UK, 301p.

ARMISHAW, J. E., HOLMES, R. W. & STOW, D. A. V. 1998. Morphology and sedimentation on the Hebrides Slope and Barra Fan, NW UK continental margin. *In:* STOKER, M. S., EVANS, D. & CRAMP, A. (eds) *Geological Processes on Continental Margins: Sedimentation, Mass Wasting and Stability.* Geological Society, London, Special Publications, **129**, 81-104.

ARNE, D. C. 1992. Apatite fission track analysis of six samples from well 27/13-1 west of Ireland. Geotrack report 375. Geotrack International Ltd., Australia. Unpublished report.

AUSTIN, B. 2001. Neogene stratigraphic framework of northeast Rockall Region. RSG Project 005. RSG/PIP Contract Number: C21-133-1.

BADLEY, M. E. 2001. Late ?Tertiary faulting, footwall uplift and topography in western Ireland. *In:* SHANNON, P. M, HAUGHTON, P. D. W. & CORCORAN, D. V. (eds) *The Petroleum*

Geology of Ireland's Offshore Basins. Geological Society of London, Special Publications, **188**, 201-207.

BALDAUF, J. G. 1986. Biostratigraphic and palaeoceanographic interpretation of lower and middle Miocene sediments, Rockall Plateau region, North Atlantic Ocean. *In:* RUDDIMAN, W. F., KIDD, R. B. & THOMAS, E. *ET AL.* (eds) *Initial Reports of the Deep Sea Drilling Project*, **94**. US Government Printing Office, Washington DC, 1033-1043.

BARTON, P. J. & WOOD, R. 1984. Tectonic evolution of the North Sea basin: crustal stretching and subsidence. *Geophysical Journal of the Royal Astronomical Society,* **79**, 987-1022.

BARTON, P. J. 1992. LISPB revisited: a new look under the Caledonides of northern Britain. *Geophysical Journal International*, **110**, 371-391.

BELLINGHAM, P. & WHITE, N. 2000. A general inverse method for modelling extensional sedimentary basins. *Basin Research*, **12**, 219-226.

BENNETT, S. D. & PHILLIPS, W. E .A. (in press). Onshore Tertiary tectonics of west and northwest Ireland using dykes as palaeostress indicators. *In:* SANDERS, I. (ed.) *Abstracts of the 44th Annual Irish Geological Research Meeting.* Irish Journal of Earth Science.

BGS/GEOTEAM 1996. A preliminary study of the structure and the geology of the western margin of the Irish Rockall Trough.

BISHOP, P. & GOLDRICK, G., 2000. Geomorphological evolution of the East Australian continental margin. *In:* SUMMERFIELD, M. A. (ed) *Geomorphology and Global Tectonics*. John Wiley & Sons Ltd., UK, 225-254.

BOLDREEL, L. O. & ANDERSEN, M. S. 1993. Late Palaeocene to Miocene compression in the Faroe-Rockall area. *In:* PARKER, J. R. (ed.) *Petroleum Geology of Northwest Europe: Proceedings of the 4th Conference.* Geological Society, London, 1025-1034.

BOLDREEL, L. O. & ANDERSEN, M. S. 1998. Tertiary compressional structures on the Faroe-Rockall Plateau in relation to Northeast Atlantic ridge-push and Alpine foreland stresses. *Tectonophysics*, **300**, 13-28.

BOTT, M. H. P, ARMOUR, A. R. HIMSWORTH, E. M, MURPHY, T. & WYLIE, G. 1979. An explosion seismology investigation of the continental margin west of the Hebrides, Scotland, at 58 degrees N, Crustal properties across passive margins. Tectonophysics, **59**, 217-231.

BRADSHAW, R. H. W. 2001. The Littletonian Warm Stage – post 10,000 BP. *In:* HOLLAND, C. H. (ed) *The Geology of Ireland*. Dunedin Academic Press, Edinburgh, UK, 429-442.

BRAY, R.J., GREEN, P.F. & DUDDY, I.R. 1992. Thermal history reconstruction using apatite fission track analysis and vitrinite reflectance: a case study from the UK East Midlands and Southern North Sea. *In:* HARDMAN R.F.P (ed) *Exploration Britain: Geological Insights for the Next Decade.* Geological Society Special Publication, **67**, 3-25.

BRODIE, J. & WHITE, N. 1994. Sedimentary basin inversion caused by igneous underplating: Northwest European continental shelf. *Geology*, **22**, 147-150.

BRODIE, J. & WHITE, N. 1995. The link between sedimentary basin inversion and igneous underplating. *In:* BUCHANAN, J. G. & BUCHANAN, P. G. (eds) *Basin Inversion*, Geological Society Special Publication, **88**, 21-38.

BROWN, R. W. 1991. Discussion on thermal and tectonic history of the East Midlands shelf (onshore UK) and surrounding regions assessed by apatite fission track analysis. *Journal of the Geological Society, London*, **148**, 785-787.

BROWN, R. W. & SUMMERFIELD, M. A. 1997. Some uncertainties in the derivation of rates of denudation from thermochronologic data. *Geomorphic processes/landscape evolution. Earth Surface Processes and Landforms*, **22**, 239-248.

BROWN, R. W., GALLAGHER, K., GLEADOW, A. J. W. & SUMMERFIELD, M. A. 2000. Morphotectonic evolution of the South Atlantic margins of Africa and South America. *In:* SUMMERFIELD, M. A. (ed) *Geomorphology and Global Tectonics*. John Wiley & Sons Ltd., UK, 255-281.

BROWN, R. W., SUMMERFIELD, M. A. & GLEADOW, A. J. W. 1994. Apatite fission track analysis: its potential for the estimation of denudation rates and implications for models of long-term landscape development. *In:* KIRKBY, M. J. (ed) *Process Models and Theoretical Geomorphology*. John Wiley & Sons Ltd. UK, 23-53.

BULL, J. M. & MASSON, D. G. 1996. The southern margin of the Rockall Plateau: stratigraphy, Tertiary volcanism and plate tectonic evolution. *Journal of the Geological Society, London*, **153**, 601-612.

BURBANK, D. W. & ANDERSON, R. S. 2001. Tectonic Geomorphology. Oxford: Blackwell Science, 274p.

BUROV, E. B. & DIAMENT, M. 1995. The effective elastic thickness (T_e) of the continental lithosphere: what does it mean? *Journal of Geophysical Research*, **100**, 3905-3929.

BYRNE, M. & O'DWYER, S. 1994. Mineral Deposits of Ireland. Map scale 1:1000 000. Dublin, Geological Survey of Ireland.

CHAPMAN, T. J., BROKS, T. M., CORCORAN, D. V., DUNCAN, L. A. & DANCER, P. N. 1999. The structural evolution of the Erris Trough, offshore Northwest Ireland, and implications for hydrocarbon generation. *In:* FLEET, A. J. & BOLDY, S. A. R. (eds) *Petroleum Geology of Northwest Europe; Proceedings of the 5th Conference*. Geological Society, London, 455-469.

CHARLESWORTH, J. K. 1924. The glacial geology of the Northwest of Ireland. *Proccedings of the Irish Royal Academy,* **32-40**, 174-314.

CHARLESWORTH, J. K. 1928. The glacial geology of north Mayo and west Sligo. *Proccedings of the Irish Royal Academy,* **38B**, 100-115.

CHASE, C. G. 1992. Fluvial land sculpting and the fractal dimension of topography. *Geomorphology*, **5**, 39-57.

CLARKE, B. 1999. Palaeocene sedimentation offshore Scotland. European Union of Geosciences, Journal of Conference Abstracts, **4**, 331.

CLARKE, B. 2000. The Palaeocene and early Eocene evolution of northern Britain and its offshore basins. *In:* DORÉ, A. G. (ed.) The Exhumation of the Circum-Atlantic Margins. Geological Society, Special Publication (abstract).

CLAYTON, G. & COXON, P. 1999. Spore and pollen biostratigraphy. *In:* JONES, T.P. & ROWE, N.P. (eds) *Fossil Plants and Spores: Modern Techniques.* Geological Society, London, UK, 225-229.

CLAYTON, K. & SHAMOON, N. 1998. A new approach to the relief of Great Britain: II. A classification of rocks based on relative resistance to denudation. *Geomorphology*, **25**, 155-171.

CLIFT, P. D. 1999. The thermal impact of Palaeocene magmatic underplating in the Faeroe-Shetland-Rockall region. *In:* FLEET, A. J. & BOLDY, S. A. R (eds) *Petroleum Geology of Northwest Europe; Proceedings of the 5th Conference*, **5**, 585-593.

CLIFT, P. D. & LORENZO, J. M. 1999. Flexural unloading and uplift along the Côte d'Ivoire-Ghana Transform Margin, equatorial Atlantic. *Journal of Geophysical Research*, **104**, 25,257-25,274.

CLIFT, P. D. & TURNER, J. 1998. Palaeogene igneous underplating and subsidence anomalies in the Rockall-Faeroe-Shetland area. *Marine and Petroleum Geology*, **15**, 223-243.

CLIFT, P. D., CARTER, A. & HURFORD, A. J. 1998. The erosional and uplift history of NE Atlantic passive margins: constraints on a passing plume. *Journal of the Geological Society, London,* **155**, 787-800.

CLIFT, P. D., CARTER, A. & HURFORD, A. J. 1998. The erosional and uplift history of NE Atlantic passive margins: constraints on a passive plume. *Journal of the Geological Society, London*, **155**, 787-800.

COCKBURN, H. A. P., BROWN, R. W., SUMMERFIELD, M. A. & SEIDL, M. A. 2000. Quantifying passive margin denudation and landscape development using a combined fission-track thermochronology and cosmogenic isotope analysis approach. *Earth and Planetary Science Letters,* **179**, 429-435.

COLE, J. E. & PEACHEY, J. 1999. Evidence for pre-Cretaceous rifting in the Rockall Trough: an analysis using quantitative plate tectonic modelling. *In:* FLEET, A. J. & BOLDY, S. A. R. (eds) *Petroleum Geology of Northwest Europe: Proceedings of the 5th Conference*. Geological Society, London, 359-370.

COLHOUN, E. 1968. The glacial geomorphology of the Sperrin Mountains and adjacent areas in Co. Tyrone, Co. Londonderry and Co. Donegal, Northen Ireland. PhD thesis, Department of Geography, Queen's University of Belfast.

COLHOUN, E. A. 1971. The glacial stratigraphy of the Sperrin Mountains and its relation to the glacial stratigraphy of northwest Ireland. *Proceedings of the Irish Royal Academy*, **71B**, 37-52.

COOPER, M. R., JOHNSTON, T. P., LEGG, I. C., MITCHELL, W. I. & REAY, D. M. 1997. Solid Geology Map of Northern Ireland (Second Edition). 1:250,000. Keyworth, Nottingham; British Geological Survey.

CORFIELD, S., MURPHY, N. & PARKER, S. 1999. The structural and stratigraphic framework of the Irish Rockall Trough. *In:* FLEET, A. J. & BOLDY, S. A. R. (eds) *Petroleum Geology of Northwest Europe: Proceedings of the 5th Conference*. Geological Society, London, 407-420.

COXON, P. & BROWNE, P. 1991. Glacial deposits of Southwest Ireland. *In:* EHLERS, J., GIBBARD, P. L. & ROSE, J. (eds) *Glacial Deposits in Great Britain and Ireland*. Geol. Landesamt, Hamburg, 355-365.

COXON, P. & CLAYTON, G. 1999. Light microscopy of fossil pollen and spores. *In:* JONES, T.P. & ROWE, N.P. (eds). *Fossil Plants and Spores: Modern Techniques*. Geological Society, London, UK, 47-51.

COXON, P. & COXON C. 1997. Pliocene or pre-Pliocene landsurface in Co. Galway. *In:* WIDDOWSON, M. (ed) *Palaeosurfaces: Recognition, reconstruction and palaeoenvronmental interpretation.* Geological Society, Special Publication, **120**, 37-55.

COXON, P. & FLEGG, A. M. 1987. A late Pliocene/early Pleistocene deposit at Pollnahallia, near Headford, County Galway. *Proceedings of the Royal Irish Academy*, **87**, 15-42.

CROCKER, P. F. & SHANNON, P. M. 1987. The evaluation and hydrocarbon prospectivity of the Porcupine Basin, offshore Ireland. *In:* BROOKS, J. & GLENNIE, K. W. (eds) *Petroleum Geology of NW Europe.* Graham and Trotman, London, 633-642.

CUNNINGHAM, G. A. & SHANNON, P. M. 1997. The Erris Ridge: a major geological feature in the NW Irish offshore basins. *Journal of the Geological Society, London*, **154**, 503-508.

CUNNINGHAM, M. 2000. Mesozoic-Tertiary tectonics of SE Ireland and genetic link to offshore extensional basins. PhD Thesis, Trinity College Dublin, Ireland.

DALY, J. S. 2001. Precambrian. *In:* HOLLAND, C. H. (ed) *The Geology of Ireland*. Dunedin Academic Press, Edinburgh, UK, 7-45.

DALY, E., BROWN, C. & EBINGER, C. 2001. Flexural rigidity and crustal structure across the Irish Atlantic margin using satellite gravity and bathymetry data. *Ireland's Deep-Water Frontier: Results from the Petroleum Infrastructure Program: Extended Abstracts*, 56-58.

DALY, J. S., HEAMAN, L. M., FITZGERALD, R. C., MENUGE, J. F. & MORTON, A. C. 1995. Geochronological and isotopic constrains on the age and crustal evolution of the crystalline basement in Western Ireland and Rockall. *In:* CROKER, P. F. & SHANNON, P. M. (eds) *The Petroleum Geology of Ireland's Offshore Basins*. Geological Society, London, Special Publication, **93**, 433-434.

DANCER, P. N., ALGAR, S. T. & WILSON, I. R., 1999. Structural evolution of the Slyne Trough. *In:* FLEET, A. J. & BOLDY, S. A. R. (eds.) *Petroleum geology of Northwest Europe; Proceedings of the 5th Conference*. Geological Society, London, 445-453.

DAVIES, G. L. 1970. The enigma of the Irish Tertiary. *In:* STEPHENS, N. & GLASSCOCK, R. E. (eds) *Irish Geographical Studies.* Queen's University of Belfast, Department of Geography, 1-16.

DEAN, K. MCLACHLAN, K. & CHAMBERS, A. 1999. Rifting and the development of the Faroe-Shetland Basin. *In:* FLEET, A. J. & BOLDY, S. A. R. (eds.) *Petroleum Geology of Northwest Europe; Proceedings of the 5th Conference*. Geological Society, London, 533-544.

DEWEY, J. F. 2000. Cenozoic tectonics of western Ireland. *Proceedings of the Geologists' Association*, **111**, 291-306.

DEWEY, J. F., AND MCKERROW, W. S. 1963. An outline of the geomorphology of Murrisk and north-west Galway. *Geological Magazine*, **100**, 260-275.

DINGLE, R. V., MEGSON, J. B. & SCRUTTON, R. A. 1982. Acoustic stratigraphy of the sedimentary succession west of Porcupine Bank, NE Atlantic Ocean; a preliminary account. *Marine Geology*, **47**, 17-35.

DOBSON, M. R., EVANS, D. & WHITTINGTON, R. 1975. The offshore extension of the Loch Gruinart fault, Islay. *Scottish Journal of Geology*, 2, 23-35.

DOLAN, J. F. 1986. The relationships between the "R2" seismic reflector and a zone of abundant detrital and authigenic smectites, Deep Sea Drilling Project Hole 610, Rockall Plateau region, North Atlantic. *In:* RUDDIMAN, W. F., KIDD, R. B. & THOMAS, E. *et al. Initial Reports of the Deep Sea Drilling Project, 94*. US Government Printing Office, Washington DC, 1109-1105.

DORÉ, A. G. & LUNDIN, E. R. 1996. Cenozoic compressional structures on the NE Atlantic margin: nature, origin and potential significance for hydrocarbon exploration. *Petroleum Geoscience*, **2**, 299-311.

DORÉ, A. G. & LUNDIN, E. R. 1997. A tectonic model for the Norwegian passive margin with implications for the NE Atlantic: Early Cretaceous to break-up. *Journal of the Geological Society, London*, **154**, 545-550.

DORÉ, A. G. 1992. Synoptic palaeogeography of the Northeast Atlantic seaway: late Permian to Cretaceous. *In:* PARNELL, J. (ed) *Basins on the Atlantic Seaboard*. Geological Society, London, Special Publication, **62**, 421-446.

DORÉ, A. G., LUNDIN, E. R. JENSEN, L. N., BIRKELAND, Ø., ELIASSEN, P. E. & FICHLER, C. 1999. Principal tectonic events in the evolution of the northwest European Atlantic margin. *In:* FLEET, A. J., BOLDY, S. A. R. (eds) *Petroleum Geology of Northwest Europe: Proceedings of the 5th Conference*. Geological Society, London, 41-61.

DUDDY, I. R., GREEN, P. F., BRAY, R. J. & HEGARTY, K. A., 1994. Recognition of the thermal effects of fluid flow in sedimentary basins. *In:* PARNELL, J. (ed) *Geofluids; Origin, Migration and Evolution of Fluids in Sedimentary Basins*. Geological Society Special Publications, **78**, 325-345.

DUDDY, I. R., GREEN, P. F. & LASLETT, G. M., 1988. Thermal annealing of fission tracks in apatite; 3, Variable temperature behaviour. *Chemical Geology; Isotope Geoscience Section*, **73**, 25-38.

DURY, G.H. 1964. Aspects of the geomorphology of Slieve League Peninsula, Donegal. *Proceedings of the Geologists' Association*, **75**, 445-459.

EGERTON, P. D. 1998. Seismic characterisation of Palaeogene depositional sequences: northeast Rockall Trough. *In:* STOKER, M. S., EVANS, D. & CRAMP, A. (eds) *Geological Processes on Continental Margins: Sedimentation, Mass Wasting and Stability*. Geological Society, Special Publications, **129**, 217-228.

ELDHOLM, O., KARASIK, A. M. & REKSNES, P. A. 1990. The North American Plate boundary. *In:* GRANTZ, A., JOHNSON, L., SWEENEY, J. F. (eds) *The Arctic Ocean Region. The Geology of North America*. Geological Society of America, Boulder, US, 171-184.

EMELEUS, C. H. & PRESTON, E. A. 1969. Field excursion guide: Tertiary volcanic rocks of Ireland. Queen's University of Belfast.

EMERY, D. & MYERS, K. 1996. *Sequence Stratigraphy.* Blackwell Science, UK, 297p.

ENGLAND, R. W. & HOBBS, R. W. 1997. The structure of the Rockall Trough imaged by deep seismic reflection profiling. *Journal of the Geological Society, London,* **154**, 497-502.

ENGLAND, R. W. 1995. Westline: a deep near-normal incidence reflection profile across the Rockall Trough. *In:* CROKER, P. F. & SHANNON, P. M. (eds) *The Petroleum Geology of Ireland's Offshore Basins.* Geological Society, Special Publication, **93**, 423-427.

ERICKSON, S. G. 1993. Sedimentary loading, lithospheric flexure, and subduction initiation at passive margins. *Geology*, **21**, 125-128.

EVANS, D. J. 1997. Estimates of the eroded overburden and the Permian-Quaternary subsidence history of the area west of Orkney. *Scottish Journal of Geology*, **33**, 169-182.

FALVEY, D. A. & MIDDLETON, M. F. 1981. Passive continental margins: evidence for a pre-breakup deep crustal metamorphic subsidence mechanism. *In: Colloquium on Geology of Continental Margins, Oceanologica Acta,* **4**, 103-114.

FARRINGTON, A. 1929. The pre-glacial topography of the Liffey Basin. *Proceedings of the Royal Irish Academy*, **368**, 148-170.

FLINN, D. 1992. The history of the Walls Boundary Fault, Shetland; the northward continuation of the Great Glen Fault from Scotland. *Journal of the Geological Society, London*, **149**, 721-726.

FORSYTH, D. W. 1985. Subsurface loading and estimates of flexural rigidity of continental lithosphere. *Journal of Geophysical Research*, **90**, 623-632.

FORTREY, R. A. & COCKS, L. R. M. 1988. Arenig to Llandovery faunal distributions in the Caledonides. *In:* HARRIS, A. L. & FETTES, D. J. (eds) *The Caledonian-Appalachean orogen.* Geological Society, London, Special Publication, **38**, 233-246.

GALBRAITH, R. F. & LASLETT, G. M. 1993. Statistical models for mixed fission track ages. *Nuclear Tracks*, **21**, 459-470.

GALLAGHER, K. & BROWN, R. 1997. The onshore record of passive margin evolution. *Journal of the Geological Society, London*, **154**, 451-457.

GALLAGHER, K. 1995. Evolving thermal histories from fission track data. *Earth and Planetary Science Letters*, **136**, 421-435.

GEOFFROY, L., BERGERAT, F. & ANGELIER, J. 1996. Brittle tectonism in relation to the Palaeogene evolution of the Tulean/NE Atlantic domain: a study in Ulster. *Geological Journal*, **31**, 259-269.

GEORGE, T. N. 1967. Landform in Ulster. *Scottish Journal of Geology*, **3**, 413-48.

GIBSON, H. J. 1996. Thermal history reconstruction of wells 132/15-1 and 164/25-2, located west of Scotland, using apatite fission track analysis and vitrinite reflectance.Geotrack report 564A. Geotrack International Ltd., Australia. Unpublished report.

GIBSON, H. J. 1997. Thermal history reconstruction in west of Ireland well 19/5-1 using apatite fission track analysis and vitrinite reflectance. Geotrack report 651. Geotrack International Ltd., Australia. Unpublished report.

GILCHRIST, A. R. & SUMMERFIELD, M. A. 1990. Differential denudation and flexural isostasy in formation of rifted-margin upwarps. *Nature*, **346**, 739-742

GILCHRIST, A. R. & SUMMERFIELD, M. A. 1991. Denudation, isostasy and landscape evolution. *Earth Surface Processes and Landforms*, **16**, 555-562.

GLEADOW, A. J. W. & BROWN, R. W. 2000. Fission-track thermochronology and the long-term denudational response to tectonics. *In:* SUMMERFIELD, M. A. (ed) *Geomorphology and Global Tectonics*. John Wiley & Sons Ltd., UK, 57-75.

GLEADOW, A. J. W., DUDDY, I. R., GREEN, P. F. & LOVERING, J. F. 1986. Confined track lengths in apatite: a diagnostic tool for thermal history samples. *Contributions to Mineralogy and Petrology*, **94**, 405-415.

GOLDRICK, G. & BISHOP, P. 1995. Differentiating the roles of lithology and uplift in the steepening of bedrock river long profiles; an example from southeastern Australia. *Journal of Geology*, **103**, 227-231.

GÓMEZ BALLESTEROS R. 1999. West of Ireland- Erris, Slyne & Porcupine Basins. Tectonic-Sedimentary Synthesis Study. Unpublished MSc. Thesis, Institute Français du Pétrole, France.

GRAHAM, J. R., LEAKE, B. E. & RYAN, P. D. 1985. The Geology of South Mayo. 1:63,360 map. University of Glasgow.

GREEN, P. F, HEGARTY, K. A. & DUDDY, I. R. 1996. Compositional influences on fission track annealing in apatite and improvement in routine application of AFTA®. *American Association of Petroleum Geologists, Abstracts with Program*, A. 56.

GREEN, P. F. 1988. The relationship between track shortening and fission track age reduction in apatite: combined influences of inherent instability, annealing anisotropy, length bias and system calibration. *Earth and Planetary Science Letters*, **89**, 335-352.

GREEN, P. F. 1989. Thermal and tectonic history of the East Midlands Shelf (onshore UK) and surrounding regions assessed by apatite fission track analysis. *Journal of the Geological Society, London*, **146**, 755-773.

GREEN, P. F. 1993. Thermal history reconstruction in Erris Trough well 12/13-1a using apatite fission track analysis and vitrinite reflectance. Geotrack report 492. Geotrack International Ltd., Australia. Unpublished report.

GREEN, P. F., DUDDY, I. R. & BRAY, R. J. 1997. Variation in thermal history styles around the Irish Sea and adjacent areas: implications for hydrocarbon occurrence and tectonic evolution. *In:* MEADOWS, N.S, TRUEBLOOD, S.P., HARDIMAN, M. & COWAN, G. (eds) *Petroleum Geology of the Irish Sea and Adjacent Areas*, Geological Society Special Publication, **124**, 73-93.

GREEN, P. F., DUDDY, I. R. HEGARTY, K. A. & BRAY, R. J. 1999. Early Tertiary heat flow along the UK Atlantic margin and adjacent areas. *In:* FLEET, A. J. & BOLDY, S. A. R. (eds) *Petroleum Geology of Northwest Europe: Proceedings of the 5th Conference.* Geological Society, London, 349-357.

GREEN, P. F., DUDDY, I. R., BRAY, R. J. & LEWIS, C. L. E. 1993. Elevated palaeotemperatures prior to Early Tertiary cooling throughout the UK region: implications for hydrocarbon generation. *In:* PARKER, J. R. (ed) *Petroleum Geology of Northwest Europe: Proceedings of the 4th Conference*, Geological Society, London, 1067-1074.

GREEN, P. F., DUDDY, I. R., GLEADOW, A. J. W., TINGATE, P. R. & LASLETT, G. M. 1986. Thermal annealing of fission tracks in apatite 1. A qualitative description. *Chemical Geology (Isotope Geoscience Section),* **59**, 237-253.

GREEN, P. F., DUDDY, I. R., HEGARTY, K. A., BRAY, R. J., SEVASTOPULO, G. D., CLAYTON G., & JOHNSTON, D. 2000. The post-Carboniferous evolution of Ireland: evidence from Thermal History Reconstruction. *Proceedings of the Geologists' Association*, **111**, 307-320.

GREEN, P.F. 1986. On the thermo-tectonic evolution of Northern England: evidence from fission track analysis. *Geological Magazine*, **123**, 493-506.

HACK, J. T. 1960. Interpretation of erosional topography in humid temperate climate. *American Journal of Science*, **258**, 80-97.

HACK, J. T. 1973. Stream profile analysis and stream gradient index. *Journal of Research of the US Geological Survey,* **1**, 421-429.

HAQ, B. U. 1987. Cenozoic sea level reconstructions. *Science*, **235**, 1156-1167

HAQ, B. U., HARDENBOL, J. & VAIL, P. R. 1987. The new chronostratigraphic basis of Cenozoic and Mesozoic sea level cycles. *In:* ROSS, C. A. & HAMAN, D. (eds.) *Timing and Depositional History of Eustatic Sequences; Constraints on Seismic Stratigraphy*. Special Publications - Cushman Foundation for Foraminiferal Research, **24**, 7-13.

HARNEY, S., LONG, C. B. & MACDERMOT, C. V. 1996. Geology of Sligo-Leitrim. Sheet 7, 1:100,000. Dublin, Geological Survey of Ireland.

HAUGHTON, P. D. W. & AMY, L. 2000. Interim sedimentological report on shallow borehole cores: 11/20-sb01, 16/28-sb01, 83/20-sb01 and 83/24-sb02. Technical Report for Rockall Studies Group, RSG Project 97/28.

HAUSER, F., O'REILLY, B. M., JACOB, A. W., SHANNON, P. M., MAKRIS, J. & VOGT, U. 1995. The crustal structure of the Rockall Trough; differential stretching without underplating. *Journal of Geophysical Research,* **100**, 4097-4116.

HETENYI, M., 1974. *Beams on Elastic Foundation: Theory with Applications in the Fields of Civil and Mechanical Engineering*. Ann Arbor, University of Michigan Press, 255p.

HILLIS, R. R. 1995. Regional Tertiary exhumation in and around the United Kingdom. *In:* BUCHANAN, J. G. & BUCHANAN, P. G. (eds) *Basin Inversion.* Geological Society, Special Publications, **88**, 167-190.

HINZ, K., ELDHOLM, O., BLOCK, M. & SKOGSEID, J. 1993. Evolution of North Atlantic volcanic continental margins. *In:* PARKER, J. R. (ed) *Petroleum Geology of Northwest Europe; Proceedings of the 4th Conference.* Geological Society, London, 901-913.

HITCHEN, K., MORTON, A. C., MEARNS, E. W., WHITEHOUSE, M. & STOKER, M. S. 1997. Geological implications from geochemical and isotopic studies of Upper Cretaceous and lower Tertiary igneous rocks around the northern Rockall Trough. *Journal of the Geological Society, London*, **154**, 517-521.

HOLMES, A. J., GRIFFITH, C. E. & SCOTCHMAN, I. C. 1999. The Jurassic petroleum system of the West of Britain Atlantic margin – an integration of tectonics, geochemistry and basin modelling. *In:* FLEET, A. J. & BOLDY, S. A. R. (eds.) *Petroleum Geology of Northwest Europe; Proceedings of the 5th Conference.* Geological Society, London, 1351-1365.

HOLMES, R., LONG, D. & DODD, L. R. 1998. Large scale debrites and submarine landslides on the Barra fan, west Britain. *In:* STOKER, M. S., EVANS, D. & CRAMP, A. (eds) *Geological Processes on Continental Margins: Sedimentation, Mass Wasting and Stability.* Geological Society, London, Special Publications, **129**, 67-79.

HOWE, J. A., STOKER, M. S. & STOW, D. A. V. 1994. Late Cenozoic sediment drift complex, northeast Rockall Trough, North Atlantic. *Paleoceanography*, **9**, 989-999.

HURTREZ, J. E. & LUCAZEAU, F. 1999. Lithological control on relief and hypsometry in the Herault drainage basin (France). *Comptes Rendus de l'Academie des Sciences*, Serie II. *Sciences de la Terre et des Planetes*, **328**, 687-694.

HUTTON, D. H. W. 1982. A tectonic model for emplacement of the Main Donegal Granite, NW Ireland. *Journal of the Geological Society of London*, **139**, 615-631.

JACOB, A. W. B. 1993. Seismic hazard in Ireland. *In:* MCGUIRE, R. K. (ed) *The Practice of Earthquake Hazard Assessment.* Dublin Institute for Advanced Studies, Ireland, 150-152.

JACOB, A. W. B., SHANNON, P. M., MAKRIS, J., HAUSER, F., VOGT, U. & O'REILLY, B. M. 1995. An overview of the results of the RAPIDS seismic project, North Atlantic. *In:* CROCKER, P. F. & SHANNON, P. M. (eds) *The Petroleum Geology of Ireland's Offshore Basins.* Geological Society, London, Special Publications, **93**, 429-431.

JAKOVIDES, J. 2000. Biostratigraphic review of the Tertiary sequences from: UK Rockall Trough well 132/15-1, Erris Trough well 12/13-1, and the shallow boreholes 11/20-Sb01, 16/20-Sb01, 83/20-Sb01, 83/24-Sb01 and 83/24-Sb02, Irish Rockall Trough. Rockall Studies Group. Project 00/4. Project number: 441/00.

JANSEN, E., RAYMO, M., BLUM, P. 1996. 3. Sites 980/981. *In:* JANSEN, E., RAYMO, M., BLUM, P. *Proceedings ODP, Initial Reports*. College Station, TX (Ocean Drilling Program), **162**, 49-90.

JENNINGS, J. N. 1972. The age of Canberra landforms. *Journal of the Geological Society of Australia*, **19**, 371-378.

JOPPEN, M. & WHITE, R. S. 1990. The structure and subsidence of Rockall Trough from two-ship seismic experiments. *Journal of Geophysical Research*, **95**, 19821-19837.

JORDAN, E. T. 1981. Thrust loads and foreland basin evolution, Cretaceous, western United States. *American Association of Petroleum Geology Bulletin*, **65**, 2506-2520.

JOY, A. M. 1992. Estimation of Cenozoic water depths in the Western Central Graben, UK North Sea, by subsidence modelling. *In:* HARDMAN, R. F. P (ed) *Exploration Britain: Geological Insights for the Next Decade*. Geological Society Special Publication, **67**, 107-125.

KEELEY, M.L., LEWIS, C.L.E., SEVASTOPULO, G.D., CLAYTON, G. & BLACKMORE, R. 1993. Apatite fission track data from southeast Ireland: implications for post-Variscan burial history. *Geological Magazine*, **130**, 171-176.

KENNEDY, W. Q. 1946. The Great Glen fault. *Quarterly Journal of the Geological Society of London*, **405**, 41-76.

KERR, A., SUGDEN, D. E. & SUMMERFIELD, M. A. 2000. Linking tectonics and landscape development in a passive margin setting; the Transantarctic Mountains. *In:* SUMMERFIELD, M. A. (ed). *Geomorphology and Global Tectonics*, John Wiley & Sons Ltd., 303-319.

KERR, I. 1987. Basement/cover structural relationships in the North Antrim area, Ireland. Unpublished Ph.D. thesis, Department of Geology, Queen's University of Belfast.

KLEMPERER, S. L., RYAN, P. D. & SNYDER, D. B. 1991. A deep seismic reflection transect across the Irish Caledonides. *Journal of the Geological Society, London*, **148**, 149-164.

KNOTT, S. D., BURCHELL, M. T., JOLLEY, E. J. & FRASER, A. J. 1993. Mesozoic to Cenozoic plate reconstruction of the North Atlantic and hydrocarbon plays of the Atlantic margins. *In:* PARKER, J. R. (ed.) *Petroleum Geology of Northwest Europe: Proceedings of the 4th Conference.* Geological Society, London, 953-974.

LAMBECK, K. 1996. Glaciation and sea-level change for Ireland and the Irish Sea since Late Devisian.Midlandian time. *Journal of the Geological Society, London*, **153**, 853-872.

LASLETT, G.M., GREEN, P.F., DUDDY, I.R. & GLEADOW, A.J.W. 1987. Thermal annealing of fission tracks in apatite, 2: A quantitative analysis. *Chemical Geology*, **65**, 1-13.

LAUGTHON, A. S., BERGGREN, W. A, BENSON, R. N., DAVIES, T. A., FRANZ, U, MUSICH, L. F., PERCH-NIELSEN, K., RUFFMAN, A. S., VAN HINTE, J. E. & WHITMARSH, R. B. 1972. *Initial Reports of the Deep Sea Drilling Project,* US Government Printing Office, Washington, **12**, 3-7.

LEEDAL, G. P. & WALKER, G. P. L. 1954. Tear faults in the Barnesmore area, Donegal. *Geological Magazine*, **91**, 116-120.

LEWIS, C.L.E., GREEN, P.F., CARTER, A. & HURFORD, A.J. 1992. Elevated K/T palaeotemperatures throughout Northwest England: three kilometres of Tertiary erosion? *Earth and Planetary Science Letters*, **112**, 131-145.

LIFTON, N. A. & CHASE, C. G. 1992. Tectonic, climatic and lithologic influences on landscape fractal dimension and hypsometry; implications for landscape evolution in the San Gabriel Mountains, California. *Geomorphology*, **5**, 77-114.

LONDALE, P. & SHOR, A. 1979. The oblique intersection of the Mid-Atlantic Ridge with Charlie-Gibbs transform fault. *Tectonophysics*, **54**, 195-209.

LONG, C. B., MCCONNELL, B. J. & ALSOP G. I. 1999. Geology of South Donegal. Sheet 3 and part of Sheet 4, 1:100,000. Geological Survey of Ireland.

LUNDIN, E. R. & DORÉ, A. G. 1997. A tectonic model for the Norwegian passive margin with implications for the NE Atlantic; Early Cretaceous to break-up. *Journal of the Geological Society, London*, **154**, 545-550.

LYON-CAEN, H., MOLNAR, P. & SUÁREZ, G. 1985. Gravity anomalies and flexure of the Brazilian shield beneath the Bolivian Andes. *Earth Planetary Science Letters*, **75**, 81-92.

MAGGI, A., JACKSON, J. A., MCKENZIE, D. & PRIESTLEY, K, 2000. Earthquake focal depths, effective elastic thickness, and the strength of the continental lithosphere. *Geology*, **28**, 495-498.

MAKRIS, J., GINZBURG, A., SHANNON, P. M., JACOB, A. W. B., BEAN, C. J. & VOGT, U. 1991. A new look at the Rockall region, offshore Ireland. *Marine and Petroleum Geology*, **8**, 410-416.

MASSON, D. G. & KIDD, R. B. 1986. Revised Tertiary stratigraphy of the southern Rockall Trough. *Initial Reports of the Deep Sea Drilling Project*, **80**, 1115-1139.

MAX, M. D. & BARKER, P. L. 1978. The westward extension of the Leannan fault of Donegal and its bearing on the Great Glen fault system. *Geological Magazine*, **115**, 215-218.

MAX, M. D. & RIDDIHOUGH, R. P. 1975. Continuation of the Highland Boundary fault in Ireland. *Geology*, **3**, 206-210.

MAX, M. D., LONG, C. B. & MACDERMOT C.V. 1992. Bedrock geology of North Mayo. Sheet 6, 1:100 000. Dublin, Geological Survey of Ireland.

MAYER, L. 2000. Application of digital elevation models to macro scale tectonic geomorphology. *In:* SUMMERFIELD, M. A. (ed) *Geomorphology and Global Tectonics*, John Wiley & Sons Ltd.., UK, 15-27.

MCCABE, A. M., KNIGHT, J. & MCCARRON, S. G. 1999. Ice-flow stages and glacial bedforms in north central Ireland; a record of rapid environmental change during the last glacial termination. *Journal of the Geological Society, London*, **156**, 63-72.

MCCONNELL, B. J. & LONG, C. B. 1997. Geology of North Donegal. Sheet 1 and part of Sheet 2, 1:100,000. Dublin, Geological Survey of Ireland.

McCULLOGH, A. A. 1993. Apatite fission track results from Ireland and the Porcupine basin and their significance for the evolution of the North Atlantic. *Marine and Petroleum Geology*, **10**, 572-591.

McCULLOGH, A. A. 1994. Low temperature thermal history of eastern Ireland: effects of fluid flow. *Marine and Petroleum Geology*, **11**, 389-399.

MEGSON, J. B. 1987. The evolution of the Rockall Trough and implications for the Faeroe-Shetland Trough. *In:* BROOKS, J. & GLENNIE, K. (eds) *Petroleum Geology of North West Europe.* Graham and Trotman Ltd., London, 653-655.

MERRITTS, D. J. & HESTERBERG, T. 1994. Stream networks and long-term surface uplift in the New Madrid seismic zone. *Science*, **265**, 1081-1084.

MERRITTS, D. J. & VINCENT, K. R. 1998. Geomorphic response of coastal streams to low, intermediate and high rates of uplift, Mendocino triple junction region, northern California. *Geological Society American Bulletin*, **101**, 1373-1388.

MILLER, G. 1990. Fracturing in the NW Carboniferous basin, Ireland. Unpublished Ph.D. thesis, Queen's University of Belfast.

MILLER, J. A., MATTHEWS, D. H. & ROBERTS, D. G. 1973. Rock of Grenville age from Rockall Bank. *Nature*, **246**, 61.

MILLER, J. R. 1991. The influence of bedrock geology on knickpoint development and channel-bed degradation along downcutting streams in south-central Indiana. *Journal of Geology*, **99**, 591-605.

MILLER, K. G. & TULCHOLKE, B. E. 1983. Development in Cenozoic abyssal circulation south of the Greenland Scotland Ridge. *In:* M. P. H. BOTT, S. SAXOV, M. TALWANI & J. THIEDE (eds) *Structure and Development of the Greenland Scotland Ridge.* Plenum, New York, 549-589.

MILLER, K. G. 1982. Cenozoic benthic foraminifera; case histories of paleoceanographic and sea-level changes. *In:* BUZAS, M. A. & SEN GUPTA, B. K. (eds.) *Foraminifera; notes for a short course.* Studies in Geology (Knoxville), **6**, 107-126.

MITCHELL, G. F. 1980. The search for Tertiary Ireland. *Journal of Earth Science, Royal Dublin Society*, **3**, 13-33.

MITCHELL, G. F. 1981. Other Tertiary events. *In:* Holland, C. H. (ed) *A Geology of Ireland.* Scottish Academic Press, Edinburgh, 231-234.

MITCHUM, R. M., JR., VAIL, P. R. & THOMPSON, S. 1977. III, Seismic stratigraphy and global changes of sea level; Part 2, The depositional sequence as a basic unit for stratigraphic analysis. *In:* PAYTON, C. E. (ed) *Seismic Stratigraphy; Applications to Hydrocarbon Exploration.* Memoir - American Association of Petroleum Geologists, **26**, 53-62.

MOHR, P. 1986. Possible Late Pleistocene faulting in Iar (West) Connacht, Ireland. *Geological Magazine,* **123**, 545-552.

MOHR, P. 2000. Late Palaeozoic and Palaeocene magmatic intrusion levels in West Connacht and inferences for palaeotopography. *Proceedings of the Geologists' Association*, **111**, 337-343.

MORTON, A. C., DIXON, J. E., FITTON, J. G., MACINTYRE, R. M., SMYTHE, D. K. & TAYLOR, P. N. 1988. Early Tertiary volcanic rocks in Well 163/6-1A, Rockall Trough. *In:* MORTON, A. C. & PARSON, L. M. (eds) *Early Tertiary Volcanism and the Opening of the NE Atlantic.* Geological Society, London, Special Publications, **39**, 293-308.

MURPHY, N. J. & CROKER, P. F. 1992. Many play concepts seen over wide area in Erris, Slyne troughs off Ireland. *Oil and Gas Journal*, **90**, 92-97.

MUSGROVE, F. W. & MITCHENER, B. 1996. Analysis of the pre-Tertiary rifting history of the Rockall Trough. *Petroleum Geoscience*, **2**, 353-360.

MUSSETT, A. E., DAGLEY, P. & SKELHORN, R. R. 1988. Time and duration of activity in the British Tertiary igneous province. *In:* MORTON, A. C. & PARSON, L. M. (eds) *Early Tertiary Volcanism and the Opening of the NE Atlantic.* Geological Society, London, Special Publications, **39**, 337-348.

MÜLLER, B., ZOBACK, M. L. & FUCHS, K. 1992. Regioanl patterns of tectonic stress in Europe. *Journal of Geophysical Research*, **97**, 11783-11803.

NADIN, P. A., HOUCHEN, M. A. & KUSZNIR, N. J. 1999. Evidence for pre-Cretaceous rifting in the Rockall Trough: an analysis using quantitative 2D structural/stratigraphic modelling. *In:* FLEET, A. J. & BOLDY, S. A. R. (eds) *Petroleum Geology of Northwest Europe: Proceedings of the 5th Conference.* Geological Society, London, 371-378.

NAYLOR, D. & ANSTEY, N. A. 1987. A reflection seismic study of the Pocupine Basin, offshore west Ireland. *Irish Journal of Earth Science*, **8**, 187-210.

NAYLOR, D. & SHANNON, P. M., 1982. *Geology of Offshore Ireland and West Britain*. Graham and Trotman Ltd., London, 161p.

NAYLOR, D. 1992. The post-Variscan history of Ireland. *In:* PARNELL, J. (ed) *Basins on the Atlantic Seaboard: Petroleum Geology, Sedimentology and Basin Evolution*. Geological Society, London, Special Publications, **62**, 255-75.

NAYLOR, D. 1998. Irish shorelines through geological time. *John Jackson Lecture, Royal Dublin Society, Occasional papers in Irish Science and Technology*, **17**, 1-20.

NAYLOR, D., SHANNON, P. M. & MURPHY, N. 1999. Irish Rockall Basin region - a standard nomenclature system. Petroleum Affairs Division, Special Publication 1/99.

NOLAN, C. & WILSON, I. 1999. Northeast Irish Rockall; assessing geological risk in a deepwater, frontier province. *American Association of Petroleum Geologists Bulletin*, **83**, 1330.

NUNNS, A.G. 1983. Plate tectonic evolution of the Greenland-Scotland Ridge and surrounding regions. *In:* BOTT, M. H. P., SAXOV, S. M., TALWANI, M. & THIEDE, J. (eds) *Structure and Development of the Greenland-Scotland Ridge; New Methods and Concepts*. NATO Advanced Research Institute/Plenum Press, New York, 661-678.

O'DRISCOLL, D., HOLCOMBE, B. B., ROSE, P. T. & JONES, D. J. 1995. Cretaceous and Tertiary unconformities in the Atlantic margin basins. *In:* CROCKER, P. F. & SHANNON, P. M. (eds) *The Petroleum Geology of Ireland's Offshore Basins*. Geological Society Special Publication, **93**, 341.

O'REILLY, B. M., HAUSER, F., JACOB, B. A. W., SHANNON, P. M. 1996. The lithosphere below the Rockall Trough: wide-angle seismic evidence for extensive serpentinisation. *Tectonophysics*, **225**, 1-23.

O'REILLY, B. M., HAUSER, F., JACOB, B. A. W., SHANNON, P. M., MAKRIS, J. & VOGT, U. 1995. The transition between the Erris and the Rockall basins: new evidence from wide-angle seismic data. *Tectonophysics*, **241**, 143-163.

O'REILLY, B. M., READMAN, P. W. & HAUSER, F. 1998. Lithospheric structure across the western Eurasian plate from a wide-angle seismic and gravity study: evidence for a regional thermal anomaly. *Earth and Planetary Science Letters*, **156**, 275-280.

OMRAN, M. A. 1990. Geophysical studies in the Hebrides Terrace Seamount area. PhD thesis. University College of Wales, Aberystwyth.

PARNELL, J. 1991. Hydrocarbon potential of Northern Ireland: Part 1. Burial histories and source rock potential. *Journal of Petroleum Geology*, **14**, 65-78.

PARNELL, J., CAREY, P. F., GREEN, P., DUNCAN, W. 1999. Hydrocarbon migration history, west of Shetland; integrated fluid inclusion and fission track studies. *In:* FLEET, A. J. & BOLDY, S. A. R. (eds) *Petroleum Geology of Northwest Europe; Proceedings of the 5th Conference.* Geological Society, London, 613-625.

PAZZAGLIA, F. J. & GARDNER, T. W. 1994. Late Cenozoic flexural deformation of the middle U.S. Atlantic passive margin. *Journal of Geophysical Research*, **99**, 12,143-12,157.

PAZZAGLIA, F. J. & GARDNER, T. W. 2000. Late Cenozoic landscape evolution of the US Atlantic passive margin; insights into a North American Great Escarpment. *In:* Summerfield, M. A. (ed) *Geomorphology and Global Tectonics*. John Wiley & Sons Ltd., 283-302.

PAZZAGLIA, F. J., GARDNER, T. W. & MERRITTS, D. J. 1998. Bedrock fluvial incision and longitudinal profile development over geologic time scales determined by fluvial terraces. *In:* Tinkler K. J. & Wohl E. E. (eds) *Rivers over Rock: Fluvial Processes in Bedrock Channels.* American Geophysical Union. Geophysical Monograph, **107**, 207-235.

PHARAOH, T. C., MORRIS, J. H., LONG, C. B. & RYAN, P. D. 1996. *Tectonic Map of Britain, Ireland and Adjacent Areas*, Keyworth, Nottingham, British Geological Survey, 1:1.500,000.

PHILLIPS, W. E. A. 2001. The Grampian Orogeny. *In:* HOLLAND, C. H. (ed) *The Geology of Ireland.* Dunedin Academic Press, Edinburgh, UK, 47-71.

PITCHER, W. S. & BERGER, A. R. 1972. *The Geology of Donegal; a Study of Granite Emplacement and Unroofing*. Wiley Interscience, New York, 435p.

PRESTON, J. 2001. Tertiary igneous activity. *In:* HOLLAND, C. H. (ed) *The Geology of Ireland.* Dunedin Academic Press, Edinburgh, UK, 353-373.

READMAN, P. W., O'REILLY, B. M. & MURPHY, T. 1997. Gravity gradients and upper-crustal tectonic fabrics, Ireland. *Journal of the Geological Society, London,* **154**, 817-828.

REFFAY, A. 1966. Problemes morphologiques dan la peninsule du sud-ouest du Donegal. *Rev. Geogr. Alpine,* **54**, 287-311.

RINALDO, A., DIETRICH, W. E., RIGON, R., VOGEL, G. K. & RODRÍGUEZ-ITURBE, I. 1995. Geomorphical signatures of varying climate. *Nature*, **374**, 632-635.

RITCHIE, J. D. & HITCHEN, K. 1996. Early Paleogene offshore igneous activity to the Northern of the UK and its relationship to the North Atlantique Igneous Province. *In:* KNOX, R., W. O. B., CORFIELD, R. M. & DUNAY, R. E. (eds) *Correlation of the Early Paleogene in Northwest Europe*. Geological Society, Special Publication, **10**, 63-78.

RITCHIE, J. D., GATLIFF, R. W. & RICHARDS, P. C. 1999. Early Tertiary magmatism in the offshore NW UK margin and surrounds. *In:* FLEET, A. J. & BOLDY, S. A. R. (eds) *Petroleum Geology of Northwest Europe; Proceedings of the 5th Conference.* Geological Society, London, 573-584.

ROBERTS, A. M. & HOLDSWORTH, R. E. 1999. Linking onshore and offshore structures; Mesozoic extension in the Scottish Highlands. *Journal of the Geological Society, London*, **156**, 1061-1064.

ROBERTS, D. G. 1974. Structural development of the British Isles, the continental margin and the Rockall Plateau. *In:* BURK, C. A. & DRAKE, C. L. (eds) *The Geology of Continental Margins.* Springer-Verlag, US, 343-359.

ROBERTS, D. G. 1975. Tectonic and stratigraphic evolution of the Rockall Plateau and Trough. *In:* WOODLAND, A. W. (ed) *Petroleum and the Continental Shelf of North-west Europe.* Applied Science Barking, 77-91.

ROBERTS, D. G. 1989. Basin inversion in and around the British Isles. *In:* COOPER, M. A. & WILLIAMS, G. D. (eds) *Inversion Tectonics*. Geological Society, London, Special Publication, **44**, 131-150.

ROBERTS, D. G., GINZBERG, A., NUNN, K. & MCQUILLIN, R. 1988. The structure of the Rockall Trough from seismic refraction and wide-angle reflection measurements. *Nature*, **332**, 632-635.

ROBERTS, D. G., MASSON, D. G. & MILES, P. R. 1981. Age and structure of the southern Rockall Trough; new evidence. *Earth and Planetary Science Letters*, **52**, 115-128.

ROBESON, D., BURNETT, R. D. & CLAYTON, J. 1988. The upper Palaeozoic Geology of the Porcupine, Erris and Donegal Basins, offshore Ireland. *Irish Journal of Earth Science*, **9**, 153-175.

ROHRMAN, M., VAN DER BEEK, P., ANDRIESSEN, P. & CLOETINGH, S. 1995. Meso-Cenozoic morphotectonic evolution of southern Norway: Neogene domal uplift inferred from apatite fission track thermochronology. *Tectonics*, **14**, 704-718.

ROSENBLOOM, N. A. & ANDERSON, R. S. 1994. Hillslope and channel evolution in a marine terraced landscape, Santa Cruz, California. *Journal of Geophysical Research*, **99**, 14,013-14,029.

ROWLEY, E. & WHITE, N. 1998. Inverse modelling of extension and denudation in the East Irish Sea and surrounding areas. *Earth and Planetary Science Letters*, **161**, 57-71.

SCHMIDT, K. M. & MONTGOMERY, D. R. 1995. Limits to relief. *Science*, **270**, 617-620.

SCHUMM, S. A. 1963. The disparity between present rates of denudation and orogeny. *US Geological Survey Prof. Paper*, **454-H**, 13p.

SCLATER, J. G. & CHRISTIE, P. A. F. 1980. Continental stretching: an explanation of the post-mid-Cretaceous subsidence in the North Sea Basin. *Journal of Geophysical Research*, **85**, 3711-3739.

SCOTCHMAN, I. C. & THOMAS, J. R. W. 1995. Maturity and hydrocarbon generation in the Slyne Trough, Northwest Ireland. *In:* CROKER, P. F. & SHANNON, P. M. (eds) *The Petroleum Geology of Ireland's Offshore Basins.* Geological Society, London, Special Publication, **93**, 385-411.

SELBY, M. J. 1980. A rock mass strength classification for geomorphic purposes; with tests from Antarctica and New Zealand. *Zietschrift für Geomorphologie*, **24**, 31-51.

SEVASTOPULO, G. D. & WYSE JACKSON, P. N. 2001. *In:* HOLLAND, C. H. (ed) *The Geology of Ireland.* Dunedin Academic Press, Edinburgh, UK, 241-288.

SHANNON, P. M. 1991. The development of Irish offshore sedimentary basins. *Journal of the Geological Society, London,* **148**, 181-189.

SHANNON, P. M., JACOB, A. W. B, MAKRIS, J, O'REILLY, B., HAUSER, F. & VOGT, U. 1995. Basin development and petroleum prospectivity of the Rockall and Hatton region. *In:* CROCKER, P. F. & SHANNON, P. M. (eds) *The Petroleum Geology of Ireland's Offshore Basins*. Geological Society, London, Special Publication, **93**, 435-457.

SHANNON, P. M., JACOB, A. W. B., MAKRIS, J., O'REILLY, B., HAUSER, F. & VOGT, U. 1994. Basin evolution in the Rockall region, North Atlantic. *First Break,* **12**, 515-522.

SHANNON, P. M., JACOB, A. W. B., O'REILLY, B. M., HAUSER, F., READMAN, P. W. & MAKRIS, J. 1999. Structural setting, geological development and basin modelling in the Rockall Trough. *In:* FLEET, A. J. & BOLDY, S. A. R. (eds) *Petroleum Geology of Northwest Europe: Proceedings of the 5th Conference*. Geological Society, London, 421-431.

SHANNON, P. M., MOORE, J. G., JACOB, A. W. B. & MAKRIS, J. 1993. Cretaceous and Tertiary basin development west of Ireland. *In:* PARKER, J. R. (ed) *Petroleum Geology of Northwest Europe: Proceedings of the 4th Conference*. Geological Society, London, 1057-1066.

SMALL, E. E. & ANDERSON, R. S. 1998. Pleistocene relief production in Laramide mountain ranges, western United States. *Geology*, **26**, 123-126.

SMYTHE, D. K. 1989. Rockall Trough-Cretaceous or Late Palaeozoic?. *Scottish Journal of Geology,* **25**, 5-43.

STEWART, M. HOLDSWORTH, R. E. & STRACHAN, R. E. 1999. Structure and early kniematic history of the Great Glen fault zone, Scotland. *Tectonics*, **18**, 326-342.

STILLMAN, C. J. 2001. Caledonian igneous activity. *In:* HOLLAND, C. H. (ed) *The Geology of Ireland*. Dunedin Academic Press, Edinburgh, UK, 145-178.

STOKER, M. S. 1995. The influence of glacigenic sedimentation on slope-apron development on the continental margin off Northwest Britain. *In:* SCRUTTON, R. A., STOKER, M. S., SHIMMIELD, G. B. & TUDHOPE, A. W. (eds) *The Tectonics, Sedimentation and Palaeoceanography of the North Atlantic Region*, **90**, 159-177.

STOKER, M. S. 1997. Mid- to late Cenozoic sedimentation on the continental margin off NW Britain. *Journal of the Geological Society, London*, **154**, 509-515.

STOKER, M. S. 1998. Sediment-drift development on the continental margin of NW Britain. In: Stoker, M. S., Evans, D. & Cramp, A. (eds) *Geological Processes on Continental Margins, Sedimentation, Mass-wasting and Stability.* Geological Society, London, Special Publication, **129**, 229-254.

STOKER, M. S. 1999. Irish Rockall Shallow Drilling Stratigraphic Summary. British Geological Survey Technical Report W3/99/2C.

STOKER, M. S., HITCHEN, K. & GRAHAM, C. C. 1993. United Kingdom offshore regional report: the geology of the Hebrides and West Shetland shelves, and adjacent deep-water areas. HMSO for the British Geological Survey, London.

STOKER, M. S., LESLIE, A. B., SCOTT, W. D., BRIDEN, J. C., HINE, N. M., HARLAND, R., WILKINSON, I. P., EVANS, D. & ARDUS, D. A. 1994. A record of late Cenozoic stratigraphy, sedimentation and climate change from the Hebrides slope, NE Atlantic Ocean. *Journal of the Geological Society, London*, **151**, 235-249.

STOKER, M. S., VAN WEERING, T. C. E. & SVAERDBORG, T. 2001. A mid- to late Cenozoic tectonostratigraphic framework for the Rockall Trough. *In:* SHANNON, P. M., HAUGHTON, P. & CORCORAN, D. (eds), *The Petroleum Geology of Ireland's Offshore Basins.* Geological Society of London, Special Publications, **188**, 411-438.

STOW, D. A. V. & HOLBROOK, J. A. 1984. Hatton Drift Contourites, northeast Atlantic, Deep Sea Drilling Project leg 81. *Initial Reports Deep Sea Drilling Project*, **81**, U. S. Government Printing Office, Washington, D. C., 695-699.

SUMMERFIELD, M. A. 1991A. *Global Geomorphology; an Introduction to the Study of Landforms*. Longman Science and Technology, UK, 537p.

SUMMERFIELD, M. A. 1991B. Sub-aerial denudation of passive margins: regional elevation versus local relief models. *Earth and Planetary Science Letters*, **102**, 460-469.

SVAERDBORG, T. 1998. A study of the Eocene to Recent deposits in the Rockall Trough, continental margin of the Northeast Atlantic Ocean: processing and interpretation of reflection seismic data. MSc. Thesis, University of Aarhus.

SYNGE, F. M. 1963. The glaciation of the Nephin Beg range, Co. Mayo. *Irish Geography*, **4**, 397-403.

SYNGE, F. M. 1979. Quaternary glaciation in Ireland. *Quaternary Newsletter*, **28**, 1-18.

TATE, M. P. 1993. Structural framework and tectono-stratigraphic evolution of the Porcupine Seabight Basin, offshore western Ireland. *Marine and Petroleum Geology*, **10**, 95-123.

TATE, M. P., DODD, C. D. & GRANT, N. T. 1999. The Northeast Rockall Basin and its significance in the evolution of the Rockall-Faeroes/East Greenland rift system. *In:* FLEET, A. J. & BOLDY, S. A. R. (eds) *Petroleum Geology of Northwest Europe; Proceedings of the 5th Conference*. Geological Society, London, 391-406.

TATE, M. P. & DOBSON, M. R. 1988. Syn- and post-rift igneous activity in the Porcupine Seabight Basin and adjacent continental margin W of Ireland. *In:* MORTON, A. C. & PARSON, L. M. (eds) *Early Tertiary Volcanism and the Opening of the NE Atlantic*. Geological Society Special Publcations, **39**, 309-334.

TATE, M. P. & DOBSON, M. R. 1989. Late Permian to early Mesozoic rifting and sedimentation offshore NE Ireland. *Marine and Petroleum Geology*, **6**, 49-59.

THOMSON, K., GREEN, P. F., WHITHAM, A. G., PRICE, S. P. & UNDERHILL, J. R. 1999. New constrains on the thermal history of northeast Greenland from apatite fission track analysis. *Geological Society of America Bulletin*, **111**, 1054-1068.

TRUEBLOOD, S. & MORTON, N. 1991. Comparative sequence stratigraphy and structural styles of the Slyne Trough and Hebrides Basin. *Journal of the Geological Society, London*, **148**, 197-201.

TRUEBLOOD, S. 1992. Petroleum geology of the Slyne Trough and adjacent basins. *In:* PARNELL, J. (ed) *Basins on the North Atlantic Seaboard: Petroleum Geology, Sedimentology and Basin Evolution.* Geological Society, London, Special Publication, **62**, 315-326.

TURCOTTE, D. L. & SCHUBERT, G, 1982. Geodynamics; Applications of Continuum Physics to Geological Problems. John Wiley & Sons, New York, 450p.

UNDERHILL, J. R. 1991. Implications of Mesozoic-Recent basin development in the western Inner Moray Firth, UK. *Marine and Petroleum Geology*, **8**, 359-369.

VAIL, P. R. 1987. Seismic stratigraphy interpretation using sequence stratigraphy; Part 1, Seismic stratigraphy interpretation procedure. *In:* BALLY, A. W. (ed) *Atlas of seismic stratigraphy.* American Association of Petroleum Geologists, Studies in Geology, **27**, 1-10.

VAN WEERING, T. C. E, STOKER, M. S. SVAERDBORG, T., HENK DE HAAS, MCDONNELL, A. RITCHER, T. & STADNITSKAYA, A. 1999. Seismic stratigraphy and sedimentary processes along the SE Rockall Trough Margin. *In:* CROCKER, P. F. & O'LOUGHLIN, O. (eds) *Petroleum Exploration of Ireland's Offshore Basins*. Extended Abstracts. Petroleum Affairs Division, Department of Marine and Natural Resources, Dublin, Ireland, 100-102.

VROLIJK, P., DONELICK, R. A., QUENG, J. & CLOOS, M. 1990. Testing models of fission track annealing in apatite in a simple thermal setting; Site 800, Leg 129. *Proceedings of the Ocean Drilling Program*, **129**, 169-176.

WADDAMS, P. & CORDINGLEY, T. 1999. The regional geology and exploration potential of the northeast Rockall Basin. *In:* FLEET, A. J. & BOLDY, S. A. R. (eds) *Petroleum Geology of Northwest Europe: Proceedings of the 5th Conference*. Geological Society, London, 379-390.

WALSH, A., KNAG, G., MORRIS, M., QUINQUIS, H., TRICKER, P., BIRD, C. & BOWER, S. 1999. Petroleum geology of the Irish Rockall Trough – A frontier challenge. *In:* FLEET, A. J. & BOLDY, S. A. R. (eds) *Petroleum Geology of Northwest Europe: Proceedings of the 5th Conference*. Geological Society, London, 433-444.

WATSON, D. F. & PHILIP, G. M. 1985. A refinement of inverse distance weighted interpolation. *Geo-Processing*, **2**, 315-327.

WATTS, A. B. & RYAN, W. B. F. 1976. Flexure of the lithosphere and continental margin basins. *Tectonophysics*, **36**, 25-44.

WATTS, A. B., MCKERROW, W. S. & FIELDING, E. 2000. Lithospheric flexure, uplift, and landscape evolution in south-central England. *Journal of the Geological Society, London*, **157**, 1169-1177.

WATTS, A.B., 1989. Lithospheric flexure due to prograding sediment loads: implications for the origin of offlap/onlap patterns in sedimentary basins. *Basin Research*, **2**, 133-144.

WATTS, A.B., 1989. The elastic thickness of the lithosphere and the evolution of sedimentary basins. *Basin Research,* **4**, 169-178.

WEISSEL, J. K. & SEIDL, M. A. 1997. Influence of rock strength properties on escarpment retreat across passive continental margins. *Geology*, **25**, 631-634.

WEISSEL, J. K. & SEIDL, M. A. 1998. Inland propagation of erosional escarpments and river profile evolution across the Southeast Australia passive continental margin. *Geophysiscal Monograph*, **107**, 189-206.

WHEELER, D. A. 1979. The overall shape of longitudinal profiles of streams. *In:* PITTY, A. F. (ed) *Geographical Approaches to Fluvial Processes*. Norwich, GeoAbstracts, 241-260.

WHIPPLE, K. X. & TUCKER, G. E. 1999. Dynamics of the stream-power river incision model; implications for height limits of mountain ranges, landscape response timescales, and research needs. *Journal of Geophysical Research*, **104**, 17,661-17,674.

WHITE, N. & LOVELL, B. 1997. Measuring the pulse of a plume with the sedimentary record. *Nature*, **387**, 888-891.

WHITE, R. S. 1989. Initiation of the Iceland plume and opening of the North Atlantic. *In:* TANKARD, A. J. & BALKWILL, H. R. (eds) *Extensional tectonics and stratigraphy of the North Atlantic margins*. American Association of Petroleum Geologists Memoir, **46**, 149-154.

WILKINSON, G. C., BAZLEY, R. A. B. & BOULTER, M. C. 1980. The geology and palynology of the Oligocene Lough Neagh Clays, Northern Ireland. *Journal of the Geological Society, London*, **137**, 65-75.

WILLGOOSE, G. 1994. A statistic for testing the elevation characteristics of landscape simulation models. *Journal of Geophysical Research,* **99**, 13,987-13,996.

WILLSON, H. E., REID, R. E. H., PARNELL, J. & SMITH, R. A. 2001. Permian and Mesozoic. *In:* HOLLAND, C. H.. *The Geology of Ireland*. Dunedin Academic Press, Edinburgh, UK, 331-351.

WOOD, M. V., HALL, J. & DOODY, J. J. 1988. Distribution of early Tertiary lavas in the Rockall Trough. *In:* MORTON A. C. & PARSON, L. M. (eds) *Early Tertiary volcanism and the opening of the NE Atlantic*. Geological Society, Special Publication, **39**, 283-292.

WOOD, M. V., HALL, J. & VAN HOORN, B. 1987. Post-Mesozoic differential subsidence in the north-east Rockall Trough related to volcanicity and sedimentation. *In:* BROOKS, J. AND GLENNIE, K. (ed) *Petroleum Geology of Northwest Europe*, 677-685.

WRIGHT, J. & MILLER, K. 1996. Control of North Atlantic Deep Water circulation by the Greenland-Scotland Ridge. *Palaeoceanography*, **11**, 157-170.

YOUNG, E. M., MYERS, A. T. MUNSON, E. L. & CLONKIN, N. M. 1969. Mineralogy and geochemistry of fluorapatite from Cerro de Mercado, Durango, Mexico. *US Geol. Surv. Prof. Pap.*, **650-D**, 84-93.

YOUNG, R. & MCDOUGALL, I. 1993. Long-term landscape evolution; early Miocene and modern rivers in southern New South Wales, Australia. *Journal of Geology*, **101**, 35-49.

ZAPROWSKI, B. J., EVENSON, E. B, PAZZAGLIA, F. J. & EPSTEIN, J. B. 2001. Knickpoint propagation in the Black Hills and northern High Plains; a different perspective on the late Cenozoic exhumation of the Laramide Rocky Mountains. *Geology*, **29**, 547-550.

ZIEGLER, P. A. 1978. North-western Europe; tectonics and basin development. *In:* VAN LOON, A. J. (ed) *Key-notes of the MEGS-II. Geologie en Mijnbouw*, **57**, 589-626.

ZOBACK, M. L. 1992. First- and second-order patterns of stress in the lithosphere; the world stress map project. *Journal of Geophysical Research*, **97**, 11,703-11,728.